

STRUCTURAL AND FUNCTIONAL  
STUDIES OF PROLINE CATABOLIC ENZYMES

---

A Dissertation  
presented to  
the Faculty of the Graduate School  
at the University of Missouri-Columbia

---

In Partial Fulfillment  
Of the Requirements for the Degree

Doctor of Philosophy

---

By

TOMMI ANNA WHITE

Dr. John J. Tanner, Dissertation Supervisor

MAY 2007

The undersigned, appointed by the dean of the Graduate School, have examined  
the dissertation entitled

STRUCTURAL & FUNCTIONAL STUDIES OF BACTERIAL PROLINE  
CATABOLIC ENZYMES

presented by Tommi Anna White,

a candidate for the degree of doctor of philosophy,

and hereby certify that, in their opinion, it is worthy of acceptance.

---

Professor John J. Tanner

---

Professor Lesa Beamer

---

Professor Peter Tipton

---

Professor Michael Henzl

---

Professor Kent Gates

## **DEDICATION**

To the two most loving people, I dedicate the work contained in this dissertation to my husband, Frank Barhorst, and my mother, Margaret White.

## **ACKNOWLEDGEMENTS**

Many thanks to everyone who has shaped my abilities as a scientist, but first and foremost I must thank Jack Tanner, my advisor, for his guidance, patience, and instruction during the years of this work. I always felt comfortable going to him if an experiment wasn't working, and knew he could help me figure out something else to try. I thank him for letting me try new experiments and techniques, keeping me motivated, and inspiring me to do my best.

Graciously, I thank my supportive, thoughtful, patient, giving, and loving husband, Frank Barhorst. He has put up with my late hours and non-stop working for the last five years and still loves me somehow. Without him, life would not be bearable. Thanks for taking care of me, baby.

I must not forget my loving and proud parents, Margaret and Calvin White, who always told me to do my best and that was good enough. Thank you for all your love and support. I am indeed lucky to have you as not only as my parents, but also role models and best friends. Thanks for providing a warm, nurturing home where knowledge of all types was valued. I hope I can provide a similar environment for my children.

Thanks to the many members of the Tanner lab. It has been a wonderful place to work. I especially thank JJ (Jermaine Jenkins) for helping me keep my sanity on crazy days in the lab and all his help with my random questions, I do miss you. Collective thanks to each of the Tanner lab members: John Larson, for keeping me smiling especially when you danced, Min Zhang for patiently showing me the ropes and putting up with my cheesy American jokes, Season

(Prewitt) Kerns for her friendship, Jon Schuermann for giving me someone to laugh at (and with!), Christopher Bottoms for being a great teacher, Shorena Nadaraia for her craziness, Levi Felts for being himself, Zhonghui Ou (John Wayne) for her smiles, Li Ma for being a nice guy to sit next to, Joshua Pearson for his pink shirts and goofy ties, Dhiraj Srivastava for the quiet times, Harkewal (Hercules) Singh for his uplifting, positive attitude, Emily Arturo for her inspiring motivation (you will have no problems filling my shoes – actually I think you will quickly outgrow them!), and lastly Beth Ostrander, for her witty sarcasm, yet genuinely sweet demeanor - whatever you decide to specialize in, you will be my doctor. I will truly miss the conversations about our lives, helping troubleshooting each others problems, and the camaraderie felt when I worked with each of you.

Thanks to our collaborator at University of Nebraska-Lincoln, Don Becker, and his student, Navasona Krishnan, for teaching me new experiments on oxygen-reactive flavoenzymes. More thanks to Jay Nix of Advanced Light Source beamline 4.2.2 for help with data collection and processing, Mingyi Zhou for cloning TtPRODH, Beverly DaGue of the MU Proteomics Core for help with mass spectral analyses and Elizabeth Ostrander for TtPRODH mutagenesis and mutant crystallization.

I cannot forget to thank my many friends that I have made and professors I have had here at University of Missouri. Specifically I would like to thank the Biochemistry and Chemistry Departments faculty members, Biochemistry Graduate Student Organization, and the Griffiths Leadership Society for Women. These people and groups were instrumental in shaping my life. Thank you.

## TABLE OF CONTENTS

ACKNOWLEDGEMENTS.....	ii
LIST OF FIGURES .....	x
LIST OF TABLES .....	xv
LIST OF APPENDICES .....	xvi
ABSTRACT .....	xvii
<b>Chapter</b>	
<b>1. INTRODUCTION .....</b>	<b>1</b>
Proline – a unique amino acid.....	1
The enzymes of proline biosynthesis and catabolism.....	2
Importance of Proline Catabolism in Health and Disease .....	10
Bacterial Proline Catabolism.....	13
Structural Information for Proline Catabolic Proteins .....	15
Summary of Research in this Dissertation .....	16
References .....	18
<b>2. STRUCTURE AND KINETICS OF MONOFUNCTIONAL PROLINE     DEHYDROGENASE FROM <i>THERMUS THERMOPHILUS</i></b>	
Introduction.....	20
Materials and Methods.....	22
Cloning of TtPRODH .....	22
Native TtPRODH Expression and Purification.....	22
Dynamic Light Scattering.....	24
Native Crystallization and Attempted Molecular Replacement .....	25
Expression, Purification and Crystallization of Se-Met PRODH .....	26

Xray Diffraction Data Collection, Phasing and Refinement.....	28
PRODH Kinetic Characterization.....	29
UV-Visible Spectroscopy .....	30
Proline:O <sub>2</sub> Reactivity and Generation of Reactive Oxygen Species ...	31
Bioinformatics Analysis of the Bacterial PutA/PRODH Family.....	32
Tartrate Crystal Form .....	32
TtPRODH Mutagenesis .....	32
Results.....	33
Structure Determination.....	33
Overall Fold .....	34
FAD Conformation.....	37
Ligand-Free, Solvent-Exposed Active Site .....	40
MPD and Possible Electron Transfer Pathway .....	42
Crystal Soaking Experiments .....	44
Absorbance Spectroscopy and Steady-State Kinetics.....	45
Proline:O <sub>2</sub> Reactivity and Generation of Reactive Oxygen Species ...	47
Conserved Sequence-Structure Motifs of the PRODH Family .....	48
Discussion .....	51
New Subfamily of PRODH.....	51
FAD Conformation.....	53
Insights into Protein Motions Associated with Substrate Binding .....	55
Relationships Between Bacterial and Human PRODH.....	56
Obtaining the Solvent-Protected TtPRODH Active Site.....	59
References .....	62

### 3. MECHANISM-BASED INACTIVATION OF *THERMUS THERMOPHILUS* PROLINE DEHYDROGENASE BY *N*-PROPARGYLGLYCINE

Introduction .....	138
Materials and Methods.....	140
Crystallization .....	140
X-ray Diffraction Data Collection & Processing .....	141
Kinetic and Spectroscopic Characterization .....	142
Mass Spectrometry.....	143
Results.....	144
Structure of TtPRODH inactivated by <i>N</i> -propargylglycine .....	144
Spectral changes caused by inactivation.....	147
Kinetics of inactivation .....	148
Discussion .....	150
Inactivation of monoamine oxidase by propargylglycine compounds	150
Proposed mechanism of inactivation of TtPRODH by <i>N</i> -propargylglycine .....	153
Comparison to structures of other inactivated flavoenzymes .....	156
Potential applications of mechanism-based inactivators of PRODH	156
Stress response .....	156
Pesticide Development .....	157
Manipulation of proline catabolism in eukaryotic cells.....	158
Biophysical and structural studies of reduced PRODH and PutA	159
References .....	160
 <b>4. PRELIMINARY STUDIES OF INTERACTIONS BETWEEN     <i>T.THERMOPHLUS</i> PROLINE DEHYDROGENASE &amp; <math>\Delta^1</math>-PYRROLINE-     5-CARBOXYLATE DEHYDROGENASE</b>	
Introduction .....	192
Materials and Methods.....	195



Cloning .....	195
Expression and Purification .....	196
TtPRODH and TtP5CDH activity .....	197
Assessment of Intermediate P5C/GSA Channeling .....	197
Gel Filtration .....	198
Results .....	199
Analysis of separately expressed TtPRODH and TtP5CDH .....	199
Coexpression of TtPRODH and TtP5CDH .....	201
Enzymatic Activities of coexpressed TtPRODH and TtP5CDH .....	202
Gel filtration .....	203
Discussion .....	203
References .....	205
<b>5. ATTEMPTED STRUCTURE DETERMINATION OF <i>BRADYRHIZOBIUM JAPONICUM</i> PUTA: INHERENT CRYSTALLOGRAPHIC PATHOLOGY</b>	
Introduction .....	220
Crystal Pathology: Twinning, Pseudosymmetry and Anisotropy .....	221
Detection of Crystal Pathology .....	223
Materials and Methods .....	228
Crystals and Soaks .....	228
Data Collection and Processing .....	229
Molecular Replacement .....	229
Refinement .....	230
Crystal Pathology Detection .....	230
Merohedral Twinning .....	231
Results .....	231

BjPutA Mutant A310V .....	231
Crystal Reduction, Radical Scavenging and Merging Initial Data .....	231
Proline and Dithionite Reduction of BjPutA .....	232
Oxidized Diamonds .....	233
Spacegroup investigation for the Hexagonal Bipyramidal form .....	233
Analysis of Pathology Indicators.....	234
Cumulative Intensity Distribution .....	234
Perfect Twin Test .....	234
Partial Twin Test .....	234
L-function .....	234
Native Patterson.....	235
Parity Tests .....	235
Self Rotation Functions .....	235
Anisotropy Detection .....	235
Merohedral Twinning Refinements .....	236
Discussion .....	236
Exploration of BjPutA oxidation and reduction.....	236
Radical Scavenging and Merging Wedges of Initially-Collected Data.....	237
Proline & Dithionite Soaks .....	239
Spacegroup Investigation for the Hexagonal Bipyramidal Form .....	239
Examination of Intensity Distributions, Anisotropy and Twinning .....	240
Hexagonal Bipyramids .....	240
Diamonds .....	243
Pseudomerohedral twinning .....	244
Strategies for Structure Completion.....	246

References .....	248
VITA .....	288

## LIST OF FIGURES

FIGURE	PAGE
1. CHAPTER 1	
1.1. The amino acid L-proline.....	5
1.2. L-proline and L-proline analogs.....	6
1.3. Proline Biosynthesis: L-glutamic semialdehyde formation from glutamate .....	7
1.4. Proline Biosynthesis: Conversion of L-glutamic semialdehyde to L-proline.....	8
1.5. Domain composition of trifunctional and bifunctional Proline Utilization A proteins.....	14
2. CHAPTER 2	
2.1. Ni-NTA Affinity Purification of TtPRODH.....	66
2.2. Initial Crystals.....	67
2.3. Optimized Crystals .....	68
2.4. Selenomethionyl crystals .....	69
2.5. Experimental fluorescence spectra determined for selenomethionyl TtPRODH .....	70
2.6. Overall structure of TtPRODH.....	71
2.7. The solvent exposed hydrophobic patch (sticks).....	72
2.8. The solvent exposed hydrophobic patch (surface).....	73
2.9. Gel filtration of soluble aggregated TtPRODH.....	74
2.10. Gel filtration of TtPRODH upon addition of BOG.....	75
2.11. Superposition of TtPRODH and PutA86-669/THFA .....	76
2.12. Stereographic drawing of protein-FAD interactions in TtPRODH .....	77
2.13. Schematic of TtPRODH interactions with FAD .....	78

2.14.	Two views of FAD from TtPRODHD covered with experimental electron density map .....	79
2.15.	Superposition of the FAD cofactors from TtPRODHD and PutA86-669/THFA .....	80
2.16.	Comparison of active sites of TtPRODHD and PutA86-669/THFA (pyrophosphate and adenosine) .....	81
2.17.	Comparison of active sites of TtPRODHD and PutA86-669/THFA (proline-binding pocket) .....	82
2.18.	Space-filling representation of TtPRODHD.....	83
2.19.	Comparison of active site solvent exposure .....	84
2.20.	Locations of 2-methyl-2,4-pentanediol .....	85
2.21.	TtPRODHD electrostatic surface potential surrounding MPD site 1 .....	86
2.22.	Proposed electron transfer pathway for TtPRODHD catalysis.....	87
2.23.	Proline reduction of TtPRODHD .....	88
2.24.	High Salt Crystal form of TtPRODHD (oxidized).....	89
2.25.	High Salt Crystal form of TtPRODHD (reduced).....	90
2.26.	Potentiometric titration of TtPRODHD .....	91
2.27.	Steady-state parameter determination for L-proline (DCPIP).....	92
2.28.	Steady-state parameter determination for 3,4-dehydro-L-proline .....	93
2.29.	Determination of inhibition constant for L-THFA.....	94
2.30.	Determination of inhibition constant for mandelate .....	95
2.31.	Thermostability analysis of TtPRODHD.....	96
2.32.	TtPRODHD specific activity as a function of temperature.....	97
2.33.	Steady-state parameter determination for L-proline (o-AB).....	98
2.34.	Measuring P5C: o-aminobenzaldehyde complex formation .....	99
2.35.	Generation of hydrogen peroxide by TtPRODHD.....	100
2.36.	Unrooted phylogenetic tree .....	101

2.37.	Conserved motif locations in TtPRODH .....	102
2.38.	Archael L-proline dehydrogenase from <i>P. horikoshii</i> .....	103
3.	CHAPTER 3	
3.1.	Kinetic scheme for mechanism-based enzyme inactivation .....	162
3.2.	4-methylene-L-proline inactivation mechanism .....	163
3.3.	Crystals of inactivated TtPRODH .....	164
3.4.	TtPRODH inactivated monomer.....	165
3.5.	Superposition of oxidized TtPRODH and inactivated TtPRODH.....	166
3.6.	Two views of the modified flavin of inactivated TtPRODH .....	167
3.7.	Side view of the inactivated flavin of .....	168
3.8.	Views of TtPRODH FAD isoalloxazine .....	169
3.9.	Four views of inactivated FAD .....	170
3.10.	Electrospray Ionization-Time of Flight (apo).....	171
3.11.	Electrospray Ionization-Time of Flight (inactivated).....	172
3.12.	Active site changes beyond the flavocyanine adduct.....	173
3.13.	Residual active site electron density .....	174
3.14.	Spectral changes upon TtPRODH inactivation.....	175
3.15.	Time course of TtPRODH inactivation .....	176
3.16.	Spectra upon sodium dithionite addition to inactivated TtPRODH .....	177
3.17.	Theoretical Kitz and Wilson plot.....	178
3.18.	Theoretical Kitz and Wilson replot.....	179
3.19.	Kitz and Wilson plot and replot for TtPRODH inactivation (25 °C) .....	180
3.20.	Kitz and Wilson plot and replot for TtPRODH inactivation (4 °C) .....	181
3.21.	Possible flavin adducts.....	182
3.22.	Maycock's proposed reaction mechanism's .....	183

3.23.	Structure of monoamine oxidase.....	184
3.24.	Steps 1 and 2 of TtPRODH inactivation .....	185
3.25.	Schiff base formation with propynal and K99 .....	186
3.26.	Last step of TtPRODH inactivation – Michael addition.....	187
3.27.	Generic Schiff base reaction .....	188
3.28.	Comparison of isoalloxazine from inactivated TtPRODH and dithionite-reduced E. coli PutA PRODH domain .....	189
3.29.	Comparison of FAD from inactivated TtPRODH and dithionite-reduced E. coli PutA PRODH domain .....	190
4.	CHAPTER 4	
4.1.	Schematic diagram of proline catabolic enzymes .....	206
4.2.	Gel filtration profiles for TtPRODH and TtP5CDH .....	207
4.3.	Gel filtration profiles for mixtures of TtPRODH and TtP5CDH.....	208
4.4.	Gel filtration profiles for mixtures of TtPRODH and TtP5CDH in which the His tag of one protein has been cleaved .....	209
4.5.	Gel filtration profiles for separately expressed, but copurified samples of TtPRODH and TtP5CDH .....	210
4.6.	SDS-PAGE analysis of coexpressed His-TtP5CDH and untagged TtPRODH .....	211
4.7.	PRODH activity assay of coexpressed His-TtP5CDH and TtPRODH ..	212
4.8.	P5CDH activity assay of coexpressed His-TtP5CDH and TtPRODH..	213
4.9.	Gel filtration chromatogram of coexpressed His-TtP5CDH and TtPRODH .....	214
4.10.	Detection of P5C using the o-AB assay with coexpressed His-TtP5CDH and TtPRODH (no membranes nor NAD) .....	215
4.11.	Detection of P5C using the o-AB assay with coexpressed His-TtP5CDH and TtPRODH and membranes (no NAD).....	216
4.12.	Detection of P5C using the o-AB assay with coexpressed His-TtP5CDH and TtPRODH and NAD (no membranes).....	217

4.13.	Detection of P5C using the o-AB assay with coexpressed His-TtP5CDH and TtPRODH and NAD and membranes).....	218
5. CHAPTER 5		
5.1.	Twinned diffraction pattern from hexagonal crystal .....	250
5.2.	Example of expected cumulative intensity distribution .....	251
5.3.	Example of the Perfect Twin test.....	252
5.4.	Reduction of BjPutA with dithionite .....	253
5.5.	Cumulative intensity distribution (hexagonal bipyramids).....	254
5.6.	Cumulative intensity distribution (diamonds) .....	255
5.7.	SFCHECK output (hexagonal bipyramids).....	256
5.8.	SFCHECK output (diamonds) .....	258
5.9.	L-function output (hexagonal bipyramids) .....	260
5.10.	L-function output (diamonds).....	261
5.11.	Native Patterson (hexagonal bipyramids) .....	262
5.12.	Native Patterson (diamonds).....	264
5.13.	Self Rotation Function (hexagonal bipyramids).....	265
5.14.	Self Rotation Function (diamonds) .....	267
5.15.	Anisotropy (hexagonal bipyramids).....	268
5.16.	Anisotropy (diamonds) .....	270
5.17.	Location of the A310V mutation .....	272
5.18.	Radical Scavengers .....	273



## LIST OF TABLES

TABLE	PAGE
1. CHAPTER 1	
2. CHAPTER 2	
2.1. Data Collection and Refinement Statistics .....	104
2.2. Data Collection and Refinement Statistics for all TtPRODH structures	105
2.3. Structure determination using SOLVE/RESOLVE .....	106
2.4. Dynamic Light Scattering .....	107
2.5. Kinetic parameters using L-proline as the substrate .....	108
2.6. Conserved Sequence Motifs of PutA and PRODH .....	109
3. CHAPTER 3	
3.1. Data Collection and Refinement statistics for inactivated TtPRODH ....	191
4. CHAPTER 4	
4.1. PCR primers used for subcloning TtP5CDH and TtPRODH into pET-Duet1 .....	219
5. CHAPTER 5	
5.1. Expected intensity distribution values for normal and twinned crystals.	274
5.2. Merohedral twinning operators for various point groups .....	275
5.3. Processing statistics from merging initial data of ascorbate soaked hexagonal bipyramids .....	276
5.4. Simulated Annealing refinements using the first 5° of data from various data sets .....	277
5.5. Spacegroup investigation .....	278
5.6. Merohedral CNS least-squares twinning refinements (hexagonal bipyramids) .....	279

## LIST OF APPENDICES

APPENDIX	PAGE
1. CHAPTER 1	
2. CHAPTER 2	
2.1. Purification protocol for pK8AH TtPRODH in BL21(DE3)pLysS .....	110
2.2. Sequences used to generate Unrooted Phylogenetic tree.....	111
3. CHAPTER 3	
4. CHAPTER 4	
5. CHAPTER 5	
5.1. Data Set Summary of BjPutA.....	280
5.2. Indexing (hexagonal bipyramids) .....	281
5.3. Indexing (diamonds) .....	282
5.4. Data Processing statistics (hexagonal bipyramids).....	283
5.5. Data Processing statistics (diamonds).....	286

## ABSTRACT

Catabolism is the oxidation of organic nutrients into simple end molecules to extract energy. For proline, the catabolic pathway involves two enzymes, L-proline dehydrogenase (PRODH, EC 1.5.99.8) and L- $\Delta^1$ -pyrroline-5-carboxylate dehydrogenase (P5CDH, EC 1.5.1.12). Via the action of PRODH and P5CDH, proline can be utilized both as a carbon and nitrogen source. The conventional view of proline catabolism was that PRODH and P5CDH appear as separate enzymes in eukaryotes and as fused bifunctional enzymes (PutA) in bacteria. Analysis of genome sequence data, however, revealed a more complex situation for bacteria. The updated view is that PutAs are indeed restricted to bacteria, but monofunctional PRODHs and P5CDHs appear in both eukaryotes and bacteria. One of these newly discovered bacterial monofunctional PRODHs was chosen and characterized. This work resulted in kinetic and structural analysis of PRODH from *Thermus thermophilus*. *T. thermophilus* PRODH was also used for studying mechanism-based inactivation by *N*-propargylglycine. This work has also resulted in the first structure of a covalently modified PRODH as well as characterization of inactivation kinetics. Physical and functional interactions between monofunctional *T. thermophilus* PRODH and P5CDH utilizing coexpression have also been studied and preliminary results reported. Finally, the structure determination of *Bradyrhizobium japonicum* PutA from pseudomerohedrally twinned crystal is reported.

## INTRODUCTION

### **Proline - a unique amino acid**

L-proline is unique among the 20 naturally occurring amino acids (FIGURE 1.1). It is the only one in which the side chain is bonded to both the backbone N atom and the C<sub>α</sub> atom. Thus proline has a 5-membered ring that unites the side chain and main chain. Note also that proline is a secondary amine in contrast to the other amino acids, which have primary amino groups in the backbone.

Because of its unique structure, proline strongly influences local peptide conformation and protein folding energetics. For example, proline has low frequencies of occurrence in  $\alpha$ -helices and  $\beta$ -strands, and high frequency of occurrence in reverse turns. This is due, in part, to the fact that proline in a polypeptide chain does not have an N-H group that can donate  $i$  to  $i+4$  hydrogen bonds in  $\alpha$ -helices and interstrand hydrogen bonds in  $\beta$ -sheets. The 5-membered ring also imparts local rigidity to proline-containing polypeptides thereby decreasing the volume of available conformational space. Thus introduction of proline into proteins can increase thermal stability by lowering the conformational entropy of protein folding (1). Another unique feature of proline-containing polypeptides is that *cis* and *trans* peptide bond conformations are equally favorable for L-proline, whereas the *trans* conformation is favored for all other amino acids (2). Finally, L-proline and L-hydroxyproline (FIGURE 1.2) are largely responsible for the unique triple helical structure of collagen, which composes skin and bones.

Besides playing unique structural roles in proteins, L-proline protects organisms against various stresses. For example, plants accumulate proline under osmotic stress induced by drought, high salinity and freezing. In this context, proline is thought to serve as an osmolyte, which is a molecule that increases thermodynamic stability of folded proteins.

Proline also protects against oxidative stress. For example, it has been shown that proline and other pyrrolidine derivatives protect skin against UVA-induced photodamage by serving as effective quenchers of singlet oxygen, a reactive oxygen species (ROS) (3). Chen and Dickman found that proline prevents ROS-mediated apoptosis in fungus (4). Chen et al. subsequently showed that proline can protect yeast against oxidative stress (5). These studies suggest that proline may be a broad-based responder molecule during cellular stress and thus the enzymes that synthesize and degrade proline may be important in mediating the cellular stress response.

### **The enzymes of proline biosynthesis and catabolism**

Biosynthesis of proline from glutamate begins with the 2-step conversion of L-glutamate to L-glutamic semialdehyde via the intermediate L-glutamyl-5-phosphate (FIGURE 1.3). These two steps are catalyzed by the enzymes  $\gamma$ -glutamyl kinase ( $\gamma$ -GK, EC 2.7.2.11) and glutamate-5-semialdehyde dehydrogenase (GSAD, EC 1.2.1.41)(6). In eukaryotes,  $\gamma$ -GK and GSAD are fused into the bifunctional enzyme  $\Delta^1$ -pyrroline-5-carboxylate (P5C) synthetase (P5CS), whereas the two enzymes are separate molecules in bacteria. Proline is

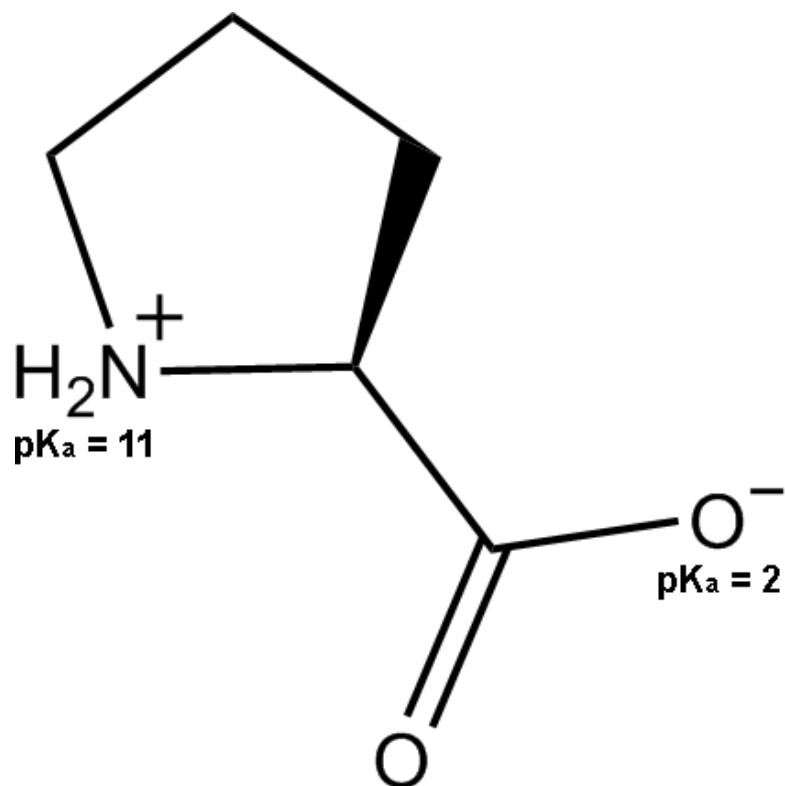
then produced from the action of  $\Delta^1$ -pyrroline-5-carboxylate reductase (P5CR, EC 1.5.1.2) following nonenzymatic ring closure of L-glutamic semialdehyde to P5C (FIGURE 1.4).

Catabolism is the oxidation of organic nutrients into simple end molecules to extract energy. For proline, the catabolic pathway involves two enzymes, L-proline dehydrogenase (PRODH, EC 1.5.99.8) and L- $\Delta^1$ -pyrroline-5-carboxylate dehydrogenase (P5CDH, EC 1.5.1.12) (SCHEME 1). PRODH is an FAD-dependent enzyme that catalyzes the oxidation of proline to P5C. As in proline biosynthesis, an equilibrium is established between P5C and its hydrolysis product L-glutamic semialdehyde. The latter molecule is the substrate for the second enzyme of proline catabolism, P5CDH, which catalyzes the oxidation of the semialdehyde to glutamate. P5CDH is an  $\text{NAD}^+$ -dependent enzyme having a catalytic Cys. As I elaborate in Chapter 2, PRODH and P5CDH are separate enzymes in eukaryotes and some bacteria, whereas the two enzymes are fused in other bacteria. The fused enzymes are known as Proline utilization A (PutA) and will be discussed in more detail below.

Via the action of PRODH and P5CDH, proline can be utilized both as a carbon and nitrogen source. In some organisms, like *Helicobacter* spp. and *Glossina morsitans*, it has been reported that L-proline is the preferred energy source (7,8). Electrons stored in the reduced  $\text{FADH}_2$  of PRODH can be transferred to quinone-like molecules in the membrane to participate in the electron transport chain to generate adenosine triphosphate (ATP) for energy. The product of PRODH catalysis, P5C, can be further catabolized to generate

glutamate which can enter tri-carboxylic cycle as  $\alpha$ -ketoglutarate or P5C can be converted to ornithine for entry into the urea cycle. In eukaryotes, PRODH and P5CDH are mitochondrial enzymes and P5C can also be shuttled out of the mitochondria into the cytosol for conversion back to L-proline. This shuttling of reducing equivalents into and out of the mitochondria is known as a proline cycling and it has been shown using human cancer cell lines and yeast that proline cycling contributes to the redox status of the cell (9,10).

FIGURE 1.1. The amino acid L-proline.



**L-proline**



FIGURE 1.2. L-proline and proline analogs. Reported substrates are in the top two rows, reported mechanism-based inactivators are in row three, and reported competitive inhibitors are in rows 4 and 5.

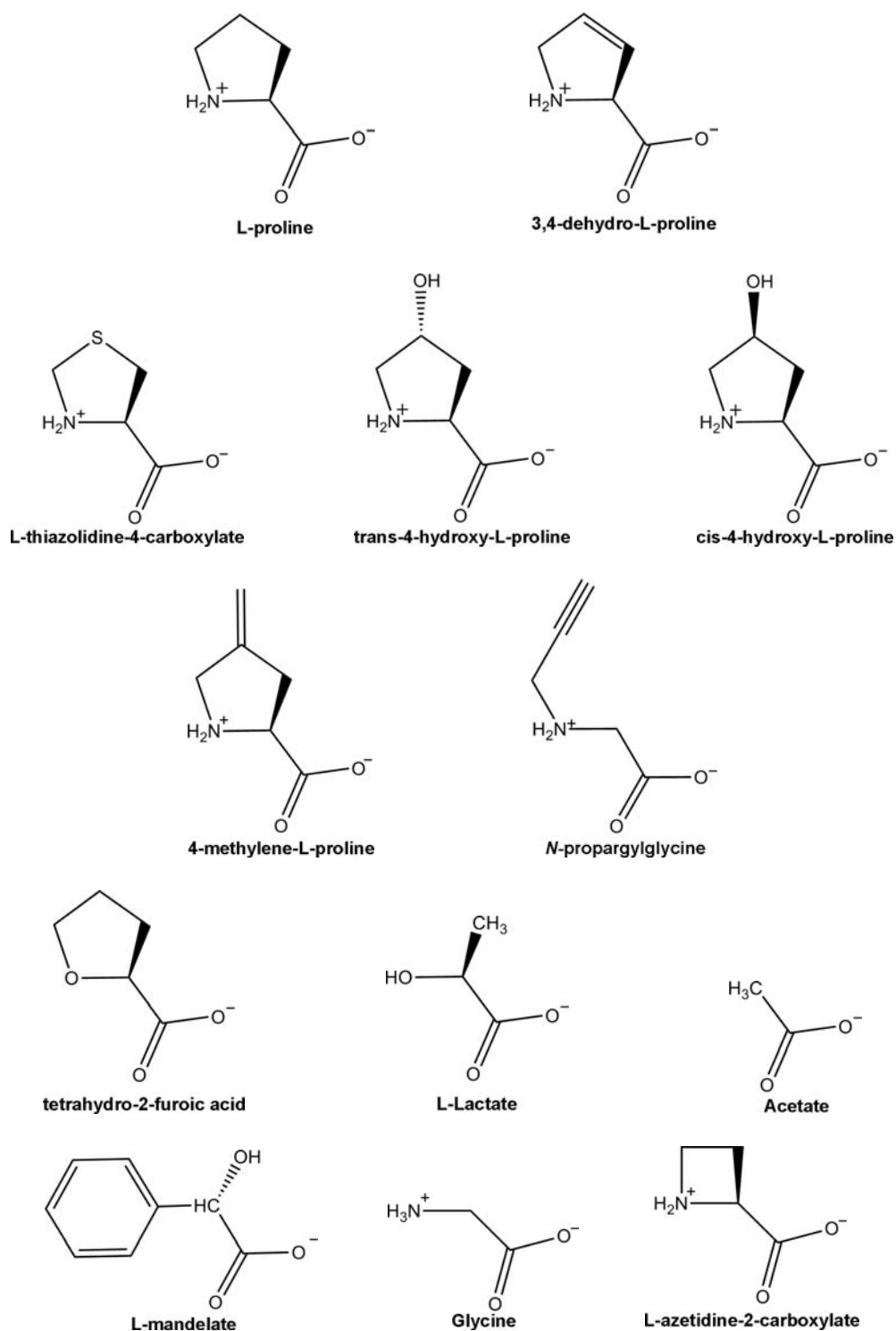


FIGURE 1.3. Proline Biosynthesis: L-glutamic semialdehyde formation from glutamate.  $\gamma$ -Glutamyl Kinase ( $\gamma$ -GK) converts glutamate to L-glutamyl-5-phosphate. Glutamic semi-aldehyde dehydrogenase (GSAD) catalyzes the next step of the reaction to form glutamic semialdehyde. In eukaryotes, these two enzymes are fused into the bifunctional enzyme  $\Delta^1$ -pyrroline-5-carboxylate synthetase (P5CS).

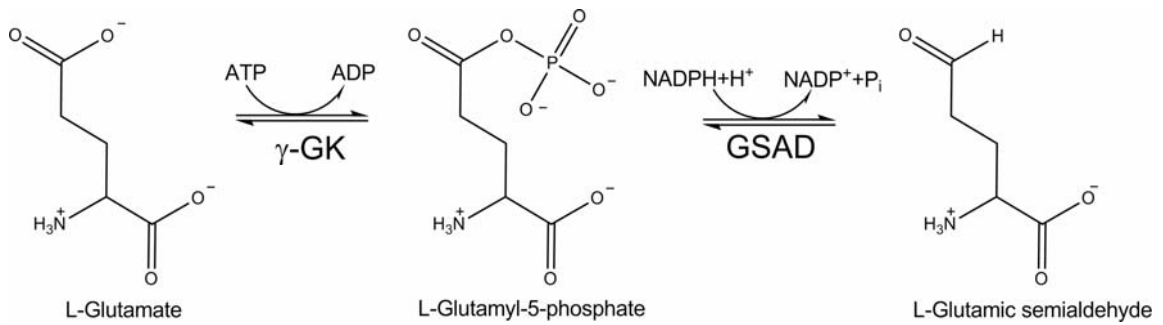
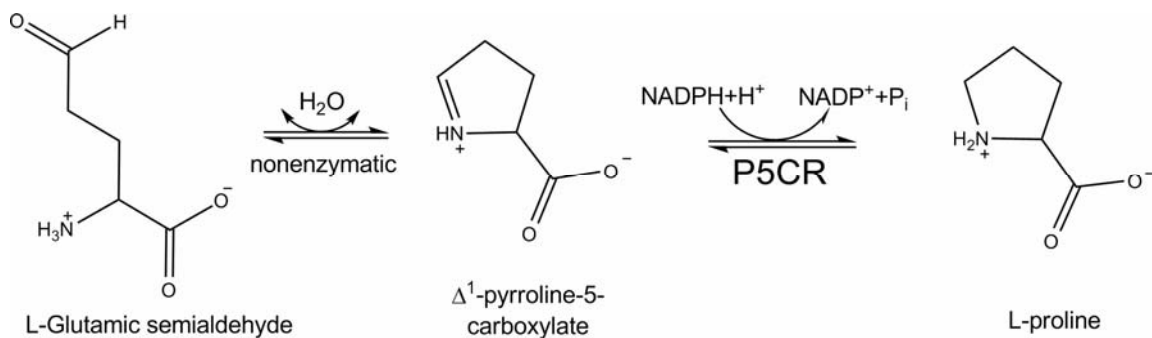
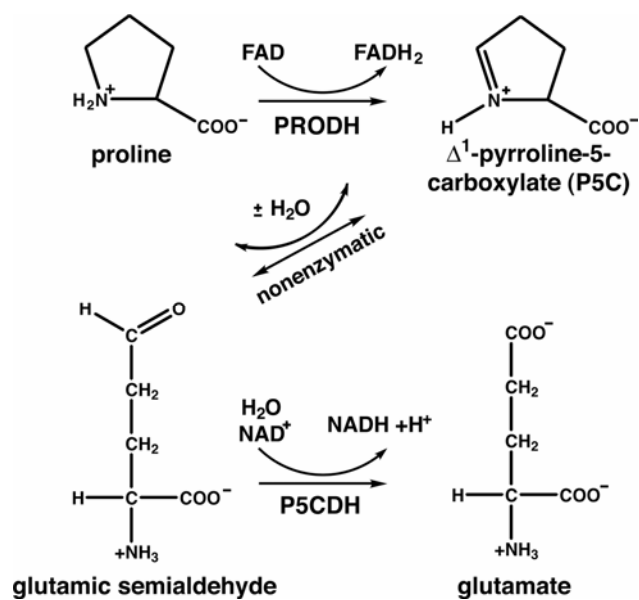


FIGURE 1.4. Proline Biosynthesis: Conversion of L-glutamic semialdehyde to L-proline. The final enzymatic step is catalyzed by  $\Delta^1$ -pyrroline-5-carboxylate reductase (P5CR).



SCHEME 1.1. Reactions catalyzed by L-proline dehydrogenase (PRODH) and L- $\Delta^1$ -pyrroline-5-carboxylate dehydrogenase (P5CDH).



### **Importance of Proline Catabolism in Health and Disease**

PRODH and P5CDH in eukaryotes are peripherally-associated inner mitochondrial membrane enzymes. These enzymes are synthesized in the cytoplasm and transported into the mitochondria where the mitochondrial-localization sequence is cleaved (11). Humans have two isozymes of PRODH, which share about 50% amino acid sequence identity (12). PRODH1 is encoded on chromosome 19, is expressed almost exclusively in liver and kidney, and catalyzes oxidation of L-hydroxyproline. PRODH2 is encoded on chromosome 22q11, is expressed more widely than PRODH1 (brain, heart, pancreas, kidney, liver) and specifically oxidizes L-proline. PRODH2 is also known as proline oxidase or POX, since it, as well as the yeast homolog, exhibits reactivity with molecular oxygen to produce superoxide (11,13). Eukaryotic PRODHs have been studied in a few organisms using mitochondrial extracts or by enzyme overexpression, but there have been no reported characterizations of soluble, purified eukaryotic PRODH.

Inborn defects in PRODH and P5CDH cause the metabolic disorders hyperprolinaemia I & II, respectively. Hyperprolinaemia I is an autosomal recessive disorder and is characterized by increased plasma proline levels. Efron reported in 1965 that hyperprolinaemia I maps to mutations in chromosome 22q11.2, which implicated PRODH2 rather than PRODH1. Interestingly, mutations in 22q11 are associated with a variety of disorders, including schizophrenia susceptibility, DiGeorge syndrome and velocardiofacial syndrome.

The link between defects in PRODH2 and brain disorders has been

examined in a variety of studies. For example, the PRODH gene knockout strain of *Drosophila melanogaster* (*slgA* mutant) exhibits sluggish movement in response to light, no detectable proline oxidase activity and elevated proline levels (14). The authors speculated that the defect in PRODH affected neural glutamate pools and also suggested the possibility that proline itself may be a neurotransmitter.

A PRODH-mutant mouse has been informative in characterizing links between PRODH and neuropsychological disorders. In 1976, a mouse displaying hyperprolinaemia I was bred (15). Further characterization of these mice, known as ProRE mice, revealed a truncation of the C-terminal end of PRODH2, resulting in a non-functional enzyme (16). The crystal structure of the *E. coli* PutA PRODH domain would later show that the truncated PRODH expressed by ProRE mice lacked helix 8, which contributes several residues to the active site (17). These mice exhibit decreased sensorimotor gating and altered neurochemistry (16). Sensorimotor gating is a neural filtering process, which allows focus to be maintained on a stimulus and it is one of the few neuropsychological attributes that can be assessed similarly in humans and rodents. Based on this work, PRODH2 was speculated to be involved in various psychiatric and behavioral disorders, including schizophrenia.

The relationship between defects in PRODH2 and schizophrenia was further studied with genetic linkage analysis performed by Karayiorgou's group at The Rockefeller University. Analysis of DNA from patients diagnosed with schizophrenia revealed several single nucleotide polymorphisms (SNPs) within

exons that could potentially underlie disease susceptibility (18). I simulated the Leu441Pro missense mutation identified by the Rockefeller group by creating the homologous Leu432Pro mutation of the *E. coli* PRODH domain of PutA. This mutant had a 5-fold lower  $k_{cat}$  and a severe decrease in thermostability compared to the native enzyme. This was the first demonstration that a schizophrenia-related mutation affects enzyme function (19). Valle's group subsequently determined the effect of several of the schizophrenia-associated SNPs on enzyme function using mitochondrial extracts. Four of the mutants, including Leu441Pro, showed greater than 30% decrease in activity compared to wildtype (20).

Human PRODH2 has also been implicated in apoptosis and cancer. Although it has been well documented that the p53 signaling cascade ends with damage to mitochondrial membranes, metabolic environment may play a role in expression of the cancer phenotype by alternative pathways or modulating known pathways. In a colorectal cancer cell line sensitive to p53, PRODH was shown by serial analysis of gene expression (SAGE) that the gene is upregulated (10-fold) prior to p53-mediated apoptosis. Only 14 other genes were upregulated to the same extent (21). This has been confirmed in various cancer cell lines including bladder, lung, ovarian and renal carcinomas, and colorectal cancer cell lines (13,22-25). By generation of reactive oxygen species, specifically superoxide radical, in a proline-dependent manner, various cancer cell lines undergo apoptosis (13). Proline-dependent PRODH apoptosis can be abrogated by overexpression of mitochondrial Mn-superoxide dismutase (24). This ROS

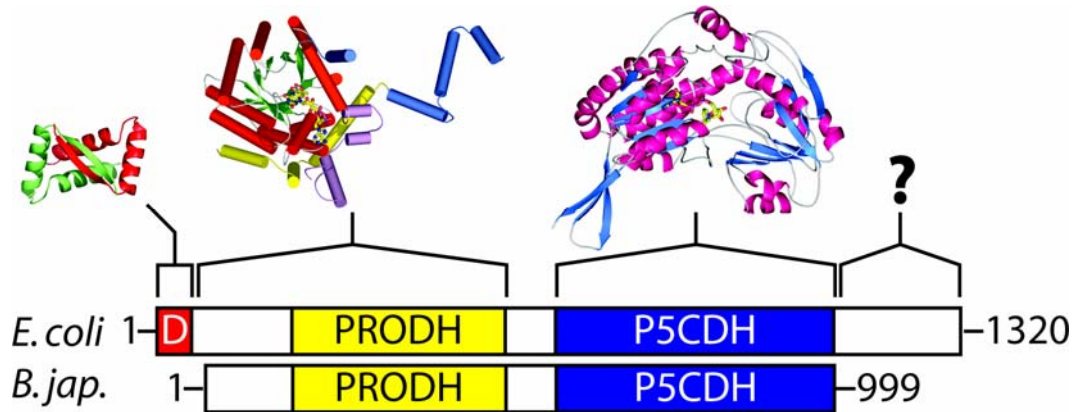
generation has been revealed to play roles in PRODH-mediated apoptosis, not only through intrinsic (mitochondrial) pathways, but also extrinsic pathways (26). TRAIL and DR5 are death receptors involved in extrinsic pathways and were reported to be activated by PRODH (26). Further mechanisms of regulation may involve the mTOR (mammalian target of rapamycin), which is similar to yeast regulation of proline catabolic enzymes (J. Phang, personal communication) (27).

### **Bacterial Proline Catabolism**

Early work on bacterial proline catabolic enzymes revealed that PRODH and P5CDH were combined into a single peripheral membrane associated polypeptide known as Proline utilization A (PutA). This early work focused on PutAs from *Escherichia coli* and *Salmonella typhimurium*, and the *E. coli* enzyme remains the best characterized PutA. In addition to having two enzymatic activities, PutAs from *E. coli* and *S. typhimurium* are autogenous transcriptional repressors. By binding to the 419 base-pair *put* intergenic region of DNA, PutAs repress divergent transcription of the genes *putA* and *putP* (encodes a sodium-proline symporter) (28). Thus, PutAs from *E. coli* and *S. typhimurium* are known as "trifunctional" PutA proteins. Upon reduction of the PutA flavin cofactor by L-proline, PutA gains affinity for the inner bacterial membrane, thereby relieving transcriptional repression (19). After oxidation of L-proline, the reduced cofactors of PRODH ( $\text{FADH}_2$ ) and P5CDH (NADH) transfer reducing equivalents to membrane electron acceptors (quinone and menaquinone) for entry into the electron transport chain to obtain energy by chemiosmotic phosphorylation.



FIGURE 1.5. Domain composition of trifunctional and bifunctional Proline Utilization A proteins. Trifunctional (*E. coli*) PutA is composed of a N-terminal autogenous transcriptional repression domain (red), a proline dehydrogenase catalytic domain (yellow), a  $\Delta^1$ -pyrroline-5-carboxylate dehydrogenase catalytic domain (blue), and a C-terminal domain of unknown function (?). Bifunctional (*B. japonicum*) PutA have similar catalytic domains (yellow and blue), but lack the autogenous transcriptional repression and C-terminal domains. Corresponding protein structures for each domain, if solved, are shown.



Not all PutAs serve as transcriptional repressors. One example of these "bifunctional" PutAs that has been studied in our lab is PutA from *Bradyrhizobium japonicum* (BjPutA). This protein has only 999 residues compared to over 1300 residues for trifunctional PutAs. Compared to the *E. coli* protein, BjPutA lacks the N-terminal DNA binding domain and a C-terminal 200 residue domain of unknown function. Characterization of BjPutA revealed that the protein is associated with the membrane independent of redox state, and there is no redox associated change in localization as with *E. coli* PutA.

Fusion of enzymes catalyzing sequential steps of a metabolic pathway, as in PutA, provides a kinetic advantage because the intermediate can be channeled between active sites (29,30). Indeed, Maloy's group reported kinetic data supporting substrate channeling for *Salmonella typhimurium* PutA (31). Becker's group has also obtained kinetic evidence for channeling in PutAs from *E. coli* and *B. japonicum* (D.F. Becker, personal communication).

Eisenberg and co-workers refer to such fused proteins as Rosetta Stone proteins because they decipher interactions between protein pairs (32). Thus, the Rosetta Stone hypothesis of protein evolution predicts that eukaryotic PRODH and P5CDH form physical and functional interactions. This hypothesis has not been tested for PRODH and P5CDH.

### **Structural Information for Proline Catabolic Proteins**

Our group has determined crystal structures of the PRODH and DNA-binding domains of *E. coli* PutA. The PRODH domain contains a unique  $\beta_8\alpha_8$

barrel in which the final helix of the barrel topology lies atop the C-terminal face of the barrel rather than alongside the barrel. Structures of the PRODH domain complexed with inhibitors acetate, L-lactate, and L-tetrahydro-2-furoic acid (THFA) provided insights into substrate recognition and showed that the carboxyl group is the minimal functional unit recognized by the enzyme. Most recently, the structure of the PRODH domain reduced by dithionite provided a glimpse of local conformational changes caused by reduction of the flavin. The structure of the DNA-binding domain of *E. coli* PutA was also recently determined. This work showed that the DNA-binding domain is a ribbon-helix-helix domain. A structure of the ribbon-helix-helix domain complexed with DNA has also recently been determined (J.J. Tanner, personal communication). Structure determination for full-length PutAs has been problematic, although progress on this front will be described the last chapter of this dissertation.

### **Summary of Research in This Dissertation**

When I started my research, the conventional view of proline catabolism was that PRODH and P5CDH appear as separate enzymes in eukaryotes and as fused bifunctional enzymes (PutA) in bacteria. My analysis of genome sequence data, however, revealed a more complex situation for bacteria. The updated view is that PutAs are indeed restricted to bacteria, but monofunctional PRODHs and P5CDHs appear in both eukaryotes and bacteria. These bioinformatics studies are described in Chapter 2. I then proceeded to characterize one of the newly discovered bacterial monofunctional PRODHs. This work resulted in

kinetic and structural analysis of PRODH from *Thermus thermophilus*, which is described in Chapter 2. I continued this line of research by studying mechanism-based inactivation of *T. thermophilus* PRODH by *N*-propargylglycine. This work has resulted in the first structure of a covalently modified PRODH, as well as characterization of inactivation kinetics (Chapter 3). Chapter 4 describes initial studies that attempt to test the Rosetta Stone hypothesis using PRODH and P5CDH from *T. thermophilus*. For this work I cloned both genes into the pET-Duet1 vector and obtained preliminary data suggesting that the two enzymes co-purify. This work will be continued by others in the future. Finally, Chapter 5 describes attempts to solve the structure of the full-length PutA from *B. japonicum* using data collected from twinned crystals.

## REFERENCES

1. Agah, S., Larson, J. D., and Henzl, M. T. (2003) *Biochemistry* **42**, 10886-10895
2. Pauling, L., Corey, R. B., and Branson, H. R. (1951) *Proc Natl Acad Sci U S A* **37**, 205-211
3. Wondrak, G. T., Jacobson, M. K., and Jacobson, E. L. (2005) *J Pharmacol Exp Ther* **312**, 482-491
4. Chen, C., and Dickman, M. B. (2005) *Proc Natl Acad Sci U S A* **102**, 3459-3464
5. Chen, C., Wanduragala, S., Becker, D. F., and Dickman, M. B. (2006) *Appl Environ Microbiol* **72**, 4001-4006
6. Hu, C. A., Lin, W. W., and Valle, D. (1996) *J Biol Chem* **271**, 9795-9800
7. Hoek, J. B., Pearson, D. J., and Olembo, N. K. (1976) *Biochem J* **160**, 253-262
8. Nagata, K., Nagata, Y., Sato, T., Fujino, M. A., Nakajima, K., and Tamura, T. (2003) *Microbiology* **149**, 2023-2030
9. Phang, J. M., Yeh, G. C., and Hagedorn, C. H. (1981) *Life Sci* **28**, 53-58
10. Brandriss, M. C., and Magasanik, B. (1981) *J Bacteriol* **145**, 1359-1364
11. Wang, S. S., and Brandriss, M. C. (1987) *Mol Cell Biol* **7**, 4431-4440
12. Phang, J. M., Hu, C. A., and Valle, D. (2001) in *Metabolic and molecular basis of inherited disease* (Scriver, C. R., A.L., B., Sly, W., and Valle, D., eds), McGraw Hiss, New York
13. Donald, S. P., Sun, X. Y., Hu, C. A., Yu, J., Mei, J. M., Valle, D., and Phang, J. M. (2001) *Cancer Res* **61**, 1810-1815
14. Hayward, D., Delaney, S., Campbell, H., Ghysen, A., Benzer, S., Kasprzak, A., Cotsell, J., Young, I., and Gabor Miklos, G. (1993) *PNAS* **90**, 2979-2983
15. Blake, R. L., Hall, J. G., and Russell, E. S. (1976) *Biochem Genet* **14**, 739-757
16. Gogos, J., Santha, M., Takacs, Z., Beck, K., V, L., Lucas, L., Nadler, J., and Karayiorgou, M. (1999) *Nature Genetics* **21**, 434-439
17. Lee, Y. H., Nadaraia, S., Gu, D., Becker, D. F., and Tanner, J. J. (2003) *Nature Structural Biology* **10**, 109-114
18. Liu, H., Heath, S., Sobin, C., Roos, J., BL, G., Blundell, M., Lenane, M., Robertson, B., Wijsman, E., Rapoport, J., Gogos, J., and Karayiorgou, M. (2002) *PNAS* **99**, 3717-3722
19. Zhang, M., White, T. A., Schuermann, J., Baban, B. A., Becker, D. F., and Tanner, J. J. (2004) *Biochemistry* **43**
20. Bender, U., S, A., G, S., A, W., and Valle, D. (2004) in *Proline Symposium*, Fort Deterich, MD
21. Polyak, K., Xia, Y., Zweier, J. L., Kinzler, K. W., and Vogelstein, B. (1997) *Nature* **389**, 300-305
22. Rivera, A., and Maxwell, S. A. (2005) *J Biol Chem* **280**, 29346-29354
23. Maxwell, S. A., and Rivera, A. (2003) *J Biol Chem* **278**, 9784-9789

24. Liu, Y., Borchert, G. L., Donald, S. P., Surazynski, A., Hu, C. A., Weydert, C. J., Oberley, L. W., and Phang, J. M. (2005) *Carcinogenesis* **26**, 1335-1342
25. Hu, C. A., Donald, S. P., Yu, J., Lin, W. W., Liu, Z., Steel, G., Obie, C., Valle, D., and Phang, J. M. (2006) *Mol Cell Biochem*
26. Liu, Y., Borchert, G. L., Surazynski, A., Hu, C. A., and Phang, J. M. (2006) *Oncogene* **25**, 5640-5647
27. Kuruvilla, F. G., Shamji, A. F., and Schreiber, S. L. (2001) *Proc Natl Acad Sci U S A* **98**, 7283-7288
28. Wood, J. M. (1981) *J Bacteriol* **146**, 895-901
29. Miles, E. W., Rhee, S., and Davies, D. R. (1999) *J Biol Chem* **274**, 12193-12196
30. Huang, X., Holden, H. M., and Raushel, F. M. (2001) *Annu Rev Biochem* **70**, 149-180
31. Surber, M. W., and Maloy, S. (1998) *Arch Biochem Biophys* **354**, 281-287
32. Marcotte, E. M., Pellegrini, M., Ng, H. L., Rice, D. W., Yeates, T. O., and Eisenberg, D. (1999) *Science* **285**, 751-753

## CHAPTER 2

### Structure and Kinetics of Monofunctional Proline Dehydrogenase from *Thermus thermophilus*

Portions of this work are reproduced from the following:

- *Acta Crystallographica* Section F © 2005 Volume 61 pages 737-739 by copyright permission of the International Union of Crystallography
- *Journal of Biological Chemistry* © 2007 in press

### INTRODUCTION

Oxidation of amino acids is a central part of energy metabolism. The oxidative pathway for proline consists of two enzymatic steps and an intervening nonenzymatic equilibrium (Scheme 2.1, (1,2)). The first enzymatic step transforms proline to  $\Delta^1$ -pyrroline-5-carboxylate (P5C), which is nonenzymatically hydrolyzed to glutamic semialdehyde. The semialdehyde is oxidized in the second enzymatic step to glutamate.

This 4-electron transformation of proline is common to all organisms, but the enzymes of proline catabolism differ widely among the three kingdoms of life. Amino acid sequence analysis shows that bacteria and eukaryotes share a common set of proline catabolic enzymes called proline dehydrogenase (PRODH) and P5C dehydrogenase (P5CDH). Studies of the bacterial enzymes have shown that PRODH is an FAD-dependent enzyme with a  $(\beta\alpha)_8$  barrel catalytic core (3,4) and that P5CDH is an  $\text{NAD}^+$ -dependent Rossmann fold enzyme featuring a nucleophilic Cys (5). These enzymes are unrelated in sequence and structure to hyperthermophilic archaeal proline catabolic enzymes, which appear in unique hetero-tetrameric and hetero-octameric complexes (6).

An intriguing aspect of proline catabolism in eukaryotes and bacteria is that PRODH and P5CDH are encoded on separate genes in some organisms, whereas the two genes are fused in other organisms. The traditional view has been that PRODH and P5CDH appear as separate enzymes in eukaryotes and fused bifunctional enzymes known as Proline utilization A (PutA) (7-15) in bacteria. Fusion of enzymes catalyzing sequential steps of a metabolic pathway provides a kinetic advantage because the intermediate can be channeled between active sites (16,17). Indeed, Maloy's group reported kinetic data supporting substrate channeling for *Salmonella typhimurium* PutA (18). Eisenberg and co-workers refer to fused proteins, such as PutA, as Rosetta Stone proteins because they decipher interactions between protein pairs (19). Thus, the Rosetta Stone hypothesis of protein evolution predicts that eukaryotic PRODH and P5CDH form physical and functional interactions.

As we elaborate in this paper, separate PRODH and P5CDH enzymes are not restricted to eukaryotes, but also appear in some bacteria. These bacterial monofunctional enzymes thus represent a new and unexplored group of enzymes. In addition, bacterial monofunctional PRODHs may serve as good models for understanding human PRODH, which has been difficult to purify for biochemical and biophysical study. Moreover, the bacterial enzymes are convenient systems for studying protein-protein interactions and intermolecular channeling. To begin exploring these questions, we previously reported the cloning, isolation and crystallization of the monofunctional PRODH from *Thermus*



*thermophilus* (TtPRODH) (20). Here we report the crystal structure and kinetic characterization of this enzyme.

## **MATERIALS AND METHODS**

### **Cloning of TtPRODH**

The *T. thermophilus* PRODH gene was cloned from genomic DNA purchased from American Type Culture Collection and introduced into the plasmid pKA8H between BamH I and Nde I sites. The pKA8H vector codes for an N-terminal 8x-His affinity tag and a tobacco etch virus protease site. Since the PRODH gene contains a BamH I site, digestion of the PCR product with BamH I was not possible. Therefore, the staggered reannealing method (21) was used with the following three primers:

Forward: 5'-CCTTGATCATATGAACCTGGACCTGGCTTACCGTTC-3',

Reverse 1: 5'-GATCCCTAGCCGGAACCAAGGCTCCTCAGG-3'

Reverse 2: 5'-CCTAGCCGGAACCAAGGCTCCTCAGG-3'

Two separate PCR amplification experiments were performed using the forward primer in conjunction with each of the two reverse primers. The two PCR products were purified, mixed in equimolar amounts, denatured at 96° C for 5 minutes, annealed by slow cooling and finally, digested with Nde I. The resulting PCR product was ligated into pKA8H, which had been digested with BamH I and Nde I. Sequencing confirmed that the gene had been successfully cloned into the vector.

### **Native TtPRODH Expression and Purification**

Unless otherwise stated, all chemicals were purchased from Fisher Scientific or Sigma Aldrich. PRODH was expressed in BL21(DE3)pLysS cells (Novagen) as follows. Small (10 mL) cultures were grown overnight in LB media and used to inoculate 1.5 L of LB media. Protein expression was induced with IPTG (0.5 mM) after the culture reached an optical density of  $OD_{600} = 0.6$ . Cells were harvested 3 hours after induction, resuspended in 50 mM  $NaH_2PO_4$ , 300 mM NaCl, 10 mM imidazole, 5% glycerol, pH 8.0 and frozen. Cells were thawed at 4° C and lysed by French press at 16,000 psi in the presence of five protease inhibitors (0.1 mM TPCK, 0.05 mM AEBSF, 0.1  $\mu$ M Pepstatin, 0.01 mM Leupeptin, 5  $\mu$ M E-64). The supernatant was collected after centrifugation at 15000 rpm for 30 minutes at 4°C, filtered through a 0.45  $\mu$ m filter (Millipore) and applied to 5 mL of Ni-NTA Superflow resin (Qiagen). The column was washed in two steps with the loading buffer supplemented with 50 mM imidazole followed by 75 mM imidazole. PRODH was eluted with 250 mM imidazole and dialyzed overnight in the dark at 4 °C into 50 mM Tris HCl, 50 mM NaCl, 0.5mM EDTA, 0.5 mM DTT and 5% glycerol, pH 8.0 (FIGURE 2.1). Prior to dialysis, flavin adenine dinucleotide (FAD), at a concentration of 0.1 mM, was added to the dialysis bag containing the eluted PRODH. Excess FAD was removed using a desalting column (Biorad P100). The protein was concentrated to 13 mg/mL using centrifugal concentrators. Protein concentration was determined using the Bradford Method with bovine serum albumin as the standard.

The purified protein exhibited the intense yellow color that is characteristic of flavoenzymes. The enzyme displayed PRODH activity as measured by an

assay described previously (3). The molecular mass as determined by MALDI-TOF mass spectrometry at the University of Missouri-Proteomics Center was  $37,968 \pm 3$  Da. This value was in good agreement with the theoretical mass predicted from the gene sequence (37,923 Da).

### **Dynamic light scattering**

Gel-filtration chromatography suggested that the protein exhibited a high degree of aggregation. For example, protein injected onto a Superdex-200 column eluted entirely in the void volume. The correlation between monodispersity and crystallizability has been well established (22,23), therefore; the protein was exposed to various solvent conditions in an attempt to identify solution conditions that promoted monodispersity. The monodispersity of each protein solution tested was assessed with a Protein Solutions DynaPro 99 Molecular Sizing Instrument. The parameters varied included pH, ionic strength, addition of Pro and Pro analogues and addition of various detergents, including n-octyl  $\beta$ -D-glucopyranoside (BOG). The protein concentration was in the range 1 – 3 mg/mL.

Only BOG had a significant effect on protein aggregation. When BOG was added to a final concentration of 20 mM, high molecular weight species was dramatically reduced. The protein/BOG solution was shown by dynamic light scattering to be reasonably monodisperse by analyzing polydispersity ( $C_p/R_h = 37\%$ ) with an apparent protein mass of 35 kDa. Based on these results, the purification procedure for both native and selenomethionine TtPROD<sub>H</sub> was modified by the addition of 20 mM BOG to the protein after the final dialysis step.

After overnight dialysis, excess detergent and FAD were removed using a desalting column (Biorad P100).

### **Native Crystallization and Attempted Molecular Replacement**

All crystallization experiments were performed at 295 K, using the sitting drop method of vapor diffusion, forming the drops with equal volumes of the reservoir and protein solutions. Commercially available crystal screens (Hampton Research and Decode Genetics) were used to identify initial crystallization conditions. Several conditions in the screens yielded crystals of various size and quantity. The precipitating agent 2-methyl-2, 4-pentanediol (MPD) was present in many of the positive conditions (FIGURE 2.2). After several rounds of optimization, the best crystals were grown with a reservoir containing 50 mM  $\text{MgCl}_2$ , 100 mM imidazole pH 7.5, 35 % MPD (FIGURE 2.3). Since the mother liquor provided cryoprotection, the crystals were picked up with Hampton mounting loops and frozen directly in liquid nitrogen.

The space group is  $P2_12_12_1$  with unit cell dimensions of  $a = 82.2 \text{ \AA}$ ,  $b = 89.6 \text{ \AA}$ , and  $c = 94.3 \text{ \AA}$ . There are two protein molecules per asymmetric unit, with 46 % solvent content and Matthews coefficient of  $2.3 \text{ \AA}^3 \text{ Da}^{-1}$  (24).

Molecular replacement calculations (high resolution limit =  $4 \text{ \AA}$ ) were performed with MOLREP (25) using the  $\beta_8\alpha_8$  barrel of the PRODH domain of *E. coli* PutA (3,4) as the search model (PDB code 1TIW). The top solution had R-factor = 0.57 and correlation coefficient = 0.23, which indicated that molecular replacement was not a suitable phasing method. Therefore, the structure of *T.*

*thermophilus* PRODH would be determined with multiwavelength anomalous dispersion phasing using a selenomethionyl derivative.

### **Expression, Purification and Crystallization of Se-Met TtPRODH**

A 10 mL overnight culture grown in LB media was pelleted, and the LB medium was removed. The cells were resuspended in 3 mL M9 media and diluted into 1.5 L of M9 media. The culture was then grown to an optical density of 0.5 (OD = 600 nm). Methionine production was inhibited for 30 minutes as described previously (26), followed by induction of protein expression by the addition of 0.5 mM IPTG. After 12 hours of induction at 22 °C with a shaking rate of 200 rpm, cells were harvested, resuspended in 50 mM NaH<sub>2</sub>PO<sub>4</sub> at pH 8.0, 300 mM NaCl, 10 mM imidazole, 1 mM DTT and 5% glycerol, and frozen.

Se-Met TtPRODH was purified using procedures described for purification of TtPRODH(20), except for the following modifications. As observed for native TtPRODH, the pellet obtained after centrifugation of lysed cells was bright yellow, indicating that a significant amount of Se-Met TtPRODH was bound to the cell debris in addition to Se-Met TtPRODH in the supernatant. Therefore, the enzyme was extracted from the pellet by resuspending the pellet in 20 mL of 20 mM n-octyl β-D-glucopyranoside, 50 mM NaH<sub>2</sub>PO<sub>4</sub>, 300 mM NaCl, 10 mM imidazole, 1 mM DTT, 5% glycerol, pH 8.0, followed by centrifugation. The detergent extraction step was repeated 1-2 times until no additional TtPRODH was liberated. The extracted protein was then purified using Ni-NTA chromatography as described previously (20).

Purified Se-Met TtPRODHD was dialyzed overnight in the dark into 4 L of 50 mM Tris-HCl pH 8.0, 50 mM NaCl, 0.5 mM EDTA, 5 mM DTT, 0.1 mM FAD and 5 % glycerol using 10000 MWCO dialysis tubing (Spectrum Spectra/Por). After dialysis, the enzyme was passed through a 12 mL Sephadex G-25 desalting column (GE Healthcare), to remove excess FAD, and then concentrated to 13 mg/mL using centrifugal concentrating devices (Amicon, Millipore). Molecular masses of Se-Met and native TtPRODHD obtained from MALDI-TOF mass spectrometry were  $38208 \pm 6$  Da and  $37968 \pm 3$ Da, respectively, which indicated 100 % incorporation of Se-Met into all 5 Met positions of the TtPRODHD polypeptide chain.

Se-Met TtPRODHD was crystallized using procedures described previously for native TtPRODHD (20). Briefly, crystals were grown at room temperature in sitting drops by mixing equal volumes of the enzyme (2  $\mu$ L) and reservoir (2  $\mu$ L) solutions (FIGURE 2.4). The enzyme solution contained 2 - 3 mg/mL Se-Met TtPRODHD and 20 mM of fresh n-octyl  $\beta$ -D thioglucopyranoside. The reservoir solution consisted of 100 mM imidazole pH = 7, 100 mM  $MgCl_2$ , 17% MPD and 5 mM DTT. The crystals typically appeared within one day after setup and grew to a maximum dimension of 0.2 mm. Crystals were prepared for cryogenic data collection by soaking in 100 mM imidazole pH = 7, 200 mM  $MgCl_2$  and 25 % MPD, then picked up with Hampton mounting loops and plunged into liquid nitrogen.

The space group is  $P2_12_12_1$  with unit cell dimensions of  $a = 82.1 \text{ \AA}$ ,  $b = 89.6 \text{ \AA}$ , and  $c = 94.3 \text{ \AA}$ . There are two protein molecules per asymmetric unit, with 46 % solvent content and Matthews coefficient of  $2.3 \text{ \AA}^3 \text{ Da}^{-1}$  (24).

### **X-ray Diffraction Data Collection, Phasing and Refinement**

Data were collected at Advanced Light Source beamline 4.2.2 using a NOIR-1 CCD detector. The structure was solved by single-wavelength anomalous diffraction (SAD) phasing, using data collected at the energy corresponding to the experimentally determined maximum of  $f''$  (FIGURE 2.5). The data set used for structure determination and refinement consisted of 180 frames with crystal-to-detector distance of 170 mm, oscillation range of  $1^\circ/\text{frame}$  and exposure time of 30 s/frame. Integration and scaling were performed with d\*TREK (27). Data collection and processing statistics for the experimentally determined TtPRODH structure are listed in Table 2.1. Data from other crystals, which were soaked in various inhibitors or substrates, are listed in Table 2.2

SOLVE (28) was used to identify a constellation of anomalous scattering centers, and the resulting SAD phases were improved with solvent flattening in RESOLVE (28). The partial chain trace from RESOLVE was used to determine the non-crystallographic symmetry (NCS) transformation relating the two molecules in the asymmetric unit. The RESOLVE phases were then improved with NCS averaging and solvent flattening in DM (29). The DM phases were input to ARP/wARP for automated model building (30). The model from ARP/wARP was improved with several rounds of model building in COOT, followed by refinement against the Se-Met peak data set with REFMAC5 (31).

Topology and parameter files for FAD were created using PRODRG (32) and the Libcheck module of CCP4i (33,34).

The final model includes residues 5-296 of TtPRODH chain A and residues 1-294 of TtPRODH chain B. In addition, 6 residues of the N-terminal affinity tag were built for chain B (residues -5 to 0). The C-terminal ends of the protein are disordered with residues 297-307 and 295-307 omitted in chains A and B, respectively. The model also includes 1 FAD cofactor per TtPRODH chain, 272 water molecules and 4 MPD molecules. See Table 2.1 for refinement statistics. Coordinates and structure factor amplitudes have been deposited in the Protein Data Bank (PDB, (35)) under accession number 2G37.

### **PRODH Kinetic Characterization**

TtPRODH was expressed in *E. coli* and purified as described previously (20). The purified enzyme was dialyzed into buffer containing 50 mM Tris-HCl, 50 mM NaCl, 0.5 mM EDTA, 0.5 mM DTT and 5% glycerol at pH 8.0 and stored at 4° C. PRODH activity was measured using the proline - dichlorophenolindophenol (DCPIP) oxidoreductase assay, as described previously for PutA proteins (11). One unit of PRODH activity is the quantity of enzyme that transfers electrons from 1  $\mu$ mol of proline to DCPIP per minute at 25°C. Steady-state kinetic parameters for L-proline were obtained using the DCPIP assay with proline as the variable substrate in the range of 0.1-100 mM. Three trials were performed for each proline concentration. The parameters  $K_m$  and  $V_{max}$  were obtained by fitting the data to the Michaelis-Menten equation, using Origin software. Kinetic constants for an alternative substrate, 3,4-



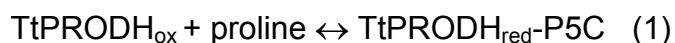
dehydro-L-proline, were determined similarly, with the substrate concentration varied in the range 3-500  $\mu$ M. Inhibition by L-tetrahydro-2-furoic acid (THFA), L-lactic acid and L-mandelic acid were examined by steady-state inhibition kinetic measurements, using proline as the variable substrate. Inhibition data were analyzed by the method of Dixon (36).

Thermostability was assessed by measuring PRODH activity as a function of incubation time at 90 °C. For this study, the enzyme was incubated in a water bath at 90 °C, and aliquots were removed at various time points and stored at 4 °C. After all of the aliquots were taken and cooled to 4 °C, activity assays were conducted at 25 °C in the presence of 25 mM proline.

### **UV-visible Spectroscopy**

Potentiometric titrations of TtPRODH were recorded at 20 °C in 50 mM potassium phosphate buffer (pH 7.5) containing 50 mM NaCl and 5 % glycerol using a three - electrode single compartment spectroelectrochemical cell as previously described (14,37). Measurements were made under a nitrogen atmosphere in a Belle Technology glove box. All potential values are reported versus the normal hydrogen electrode. Methyl viologen (20 mM) was used as a mediator dye, and pyocyanine (5 mM) and indigo disulfonate (3 mM) were used as indicator dyes. The UV-visible spectra in each experiment were recorded from 300-700 nm on a Cary 100 spectrophotometer. Corrected spectra of TtPRODH were obtained by subtracting the spectra of the dyes in the absence of protein measured under identical conditions. The reduction potential ( $E_m$ ) and  $n$  values were calculated by linear regression of a Nernst plot of the data.

TtPROD<sub>H</sub> was titrated with proline under aerobic conditions in the proline concentration range 0 - 160 mM. At each proline concentration, the absorbance spectrum was acquired after incubating the enzyme (56 mM) for 5 minutes with proline. The absorbance values at  $\lambda = 459$  nm were analyzed as previously described (11,38) to obtain an apparent equilibrium constant for the formation of a reduced enzyme-P5C complex (eq. 1).



### **Proline:O<sub>2</sub> Reactivity and Generation of Reactive Oxygen Species**

The rate of proline:O<sub>2</sub> activity was determined by monitoring the appearance of P5C as a function of proline concentration in the absence of an artificial electron acceptor. P5C was detected as the yellow dihydroquinazolinium complex with *o*-aminobenzaldehyde (*o*-AB) by monitoring absorbance at  $\lambda = 443$  nm ( $\epsilon = 2900 \text{ M}^{-1}\text{cm}^{-1}$ (39)). The assay mixture included 50 mM potassium phosphate buffer pH=7.5, 20  $\mu\text{g}$  of TtPROD<sub>H</sub>, 4 mM *o*-AB and 0.5 - 25 mM proline. The reaction was monitored for 15 minutes, and data from the 5-10 minute time period were used for rate calculations. One unit of proline:O<sub>2</sub> activity is defined as the amount of TtPROD<sub>H</sub> that generates 1  $\mu\text{mol}$  of P5C per minute at 25 °C.

Production of superoxide by TtPROD<sub>H</sub> was studied by measuring reduction of cytochrome *c* as described previously (40). Reduction of cytochrome *c* was indicated by an increase in absorbance at  $\lambda = 550$  nm. For

these assays, the L-proline concentration was 50 mM and the concentrations of cytochrome c and TtPRODH were 0.02 mg/mL each. Production of H<sub>2</sub>O<sub>2</sub> by TtPRODH (0.02 mg/mL) was measured using the Amplex Red H<sub>2</sub>O<sub>2</sub>/peroxidase assay kit (Molecular Probes – Invitrogen) and a standard curve obtained from solutions of known H<sub>2</sub>O<sub>2</sub> concentration.

### **Bioinformatics Analysis of the Bacterial PutA/PRODH Family**

Multiple sequence alignment calculations of PutA PRODH domains and bacterial monofunctional PRODHs were performed with ClustalW (41). The data set of sequences used for these calculations was obtained from the Protein Information Resource (PIR), using the Related Sequences tool with TtPRODH as the query sequence (see APPENDIX 2.2 for sequences). A total of 287 homologs of TtPRODH were identified.

### **Tartrate Crystal Form**

Another crystal form of TtPRODH was discovered when using 2 M sodium potassium tartrate, 100 mM Tris pH = 8.5, 0.5 % PEG 5000 MME, 4 % acetone (or 3% Isopropanol). These crystals grew as thin ovals with maximum dimension of 0.4mm. The space group was P2<sub>1</sub>2<sub>1</sub>2<sub>1</sub> and unit cell dimensions were a = 81.4 Å, b = 88.5 Å, c = 91.3 Å. Note that the cell dimensions are very similar to those of the MPD crystal form. These crystals diffracted to 2.3 Å and were reducible with proline.

### **TtPRODH Mutagenesis**

Site-directed mutagenesis to create the TtPRODHD double mutation R202A/E207A was performed with Stratagene Site-directed Mutagenesis Kit.

The following primers were used.

Forward: 5'-CCA GAC AAG GCC CTC ATT GAC GCC GCG TAC CTG-3'

Reverse: 5'-GGT CCA GGT ACG CGG CGT CAA TGA GGG CCT TG-3'

Mutations were confirmed with sequencing performed by the University of Missouri DNA core.

Crystals of TtPRODHD R202A/E207A were obtained in Crystal Screen 27 and Wizard II 5. Both conditions contained 0.1 M HEPES pH 7.5 an alcohol (20 % 1,4-butanediol or 20 % 2-propanol), and a salt (NaCl (0.2 M) or sodium citrate tribasic dihydrate (0.2 M)). These crystals exhibited the characteristic yellow color reminiscent of wildtype TtPRODHD, but they diffracted sufficiently well to obtain the unit cell dimensions. Those dimensions were similar to those of the MPD crystal form of native TtPRODHD.

## **RESULTS**

### **Structure Determination**

TtPRODHD contained 5 methionines that could be substituted with selenomethionine (Se-Met) for structure determination. This corresponds to 1.5 % Met. Note that the average occurrence of Met in proteins is 1.7 % (26). To utilize the anomalous selenium (Se) signal for structure determination, it must be strong enough to detect (42). This signal size decreases exponentially with protein molecular weight. Utilizing the following equation, one can determine the

estimated Bijvoet diffraction ratio (signal size) based on the number of anomalous scatterers in a protein:

$$\text{rms}(\Delta F_{+/-h}) / \text{rms}|F| = (N_A/2N_T)^{1/2} (2f''_A/Z_{\text{eff}})$$

where  $N_A$  is the number of anomalous scatters (5 for TtPRODH),  $N_T$  is the total number of non hydrogen atoms in the molecule (327 for TtPRODH) and  $Z_{\text{eff}}$  is the effective normal scattering at zero scattering angle (6.7 electrons for non-hydrogen atoms). Using a  $f''$  of 4 electrons, the estimated Bijvoet diffraction ratio for TtPRODH is 0.104. This ratio is well above the expected level of signal utilizing the K-edge absorption of selenium.

Several Se-Met SAD data sets were collected but only one readily, lead to automated structure determination using the SOLVE/RESOLVE programs (TABLE 2.3). Although all the data sets had good completeness, redundancy and resolution, the one that led to automated structure determination was distinguished by superior  $I/\sigma$  and  $R_{\text{merge}}$  (see X3 in TABLE 2.3)

### **Overall Fold**

The TtPRODH structure was determined at 2.0 Å resolution using Se-Met SAD phasing (TABLE 2.1). There are two protein chains in the asymmetric unit, labeled A and B, and 1 FAD cofactor bound to each protein (FIGURE 2.6). The structure reveals a distorted  $(\beta\alpha)_8$  barrel fold. The first strand of the barrel ( $\beta 1$ ) is preceded by 4  $\alpha$ -helices denoted  $\alpha A$ ,  $\alpha B$ ,  $\alpha C$  and  $\alpha 0$  (FIGURE 2.6, right side provides best view). The major distortion of the TtPRODH barrel from the classic

triosephosphate isomerase (TIM) barrel concerns the placement of  $\alpha 8$ . Helix  $\alpha 0$  packs against  $\beta 1$  thus occupying the location reserved for  $\alpha 8$  in the classic TIM barrel. Consequently, helix  $\alpha 8$  of TtPRODHDH is located above the carboxyl terminal face of the  $\beta$ -barrel rather than alongside the  $\beta$ -barrel as in the classic TIM structure.

The FAD cofactor of TtPRODHDH is bound at the carboxyl ends of the strands of the barrel (FIGURE 2.6). The *re* face of the isoalloxazine packs tightly against strands 4-6, while the *si* face opens to the substrate binding pocket and is available for hydride transfer from the substrate proline.

Helices A-C and 8 form a small domain above the carboxyl terminal face of the  $\beta$ -barrel (FIGURE 2.6, right side provides best view). Helices A and B form a right angle, as do helices B and C. Helix 8 fits into the cleft formed by helices A-C. These four helices pack together to form a solvent-exposed hydrophobic patch (FIGURE 2.7; FIGURE 2.8). The patch has a pronounced hole in the middle (FIGURE 2.8). Several hydrophobic side chains form the rim of the hole and line its sides, while the hydroxyl groups of Thr287 and Tyr283 form the bottom of the hole (FIGURE 2.7; FIGURE 2.8). If the Rosetta Stone hypothesis is true for TtPRODHDH and TtP5CDH, then the function of the hydrophobic patch may be to serve as a docking interface for P5CDH. The patch presents a concave hydrophobic surface to solvent (FIGURE 2.8), and thus it is tempting to speculate that this patch mates with a complementary convex surface of P5CDH. Involvement of this patch in interaction with P5CDH also makes sense for substrate channeling because the patch is close to the PRODHDH active site.

The pair of molecules chosen for the asymmetric unit corresponds to the largest interface in the crystal lattice, which buries 992 Å<sup>2</sup> of surface area. The two molecules interact primarily through the packing of α5 (residues 200-218) of one chain against α5 and α6 (residues 228-242) of the other chain (FIGURE 2.6). The orientation of the two molecules is such that the α5 helices form an angle of 50°. The interface has 4 intermolecular ion pairs (Lys213-Glu207, Arg230-Asp200) and 4 intermolecular hydrogen bonds (His210-His210, Tyr238-Glu170). Several hydrophobic side chains are also buried in the interface: Phe198, Leu203, Leu209, Leu214.

The significance of this interface is unclear at this time. It is not the one typically found in dimeric TIM, nor is it similar to the tetramer interface of archaeal TIMs (43). The classic TIM dimer interface involves loops 1-4 (43) and buries about 1500 Å<sup>2</sup> of surface area, which is 50 % larger than the TtPRODH interface. Analysis of detergent-solubilized TtPRODH by dynamic light scattering and gel filtration suggests the presence of apparent monomeric and dimeric species (FIGURES 2.9; FIGURE 2.10; TABLE 2.4). It is possible that the pair of proteins in the asymmetric unit represents the dimeric species observed in solution. However, it is also possible that this interface is an artifact of crystallization. An additional complicating factor in assessing the biological relevance of this interface is the possibility that TtPRODH interacts with TtP5CDH, as predicted by the Rosetta Stone hypothesis.

The TtPRODH structure is only the second PRODH structure solved to date, with the first being the PRODH domain of *E. coli* PutA (PutA86-669, PDB

code 1TIW (4,44)). Residues 263 - 561 of PutA form a distorted TIM barrel that is similar to that of TtPRODH (FIGURE 2.11). Within this catalytic core, the sequence identity between the two enzymes is 29 %, and the root-mean-square deviation for C<sub>α</sub> atoms is 1.7 Å for 243 aligned residues. Also, the general location of the FAD at the carboxyl-terminal tips of the strands is similar in the two structures. The major topological difference between the TtPRODH and the PutA86-669 barrels is an extra  $\alpha$ -helix that appears in PutA86-669 but is absent in TtPRODH. Residues 437-449 of PutA form an  $\alpha$ -helix ( $\alpha$ 5a in (FIGURE 2.11) that is replaced by a 5-residue loop in TtPRODH (residues 190-195). As discussed in the next section, this topological difference has a dramatic effect on FAD conformation.

### **FAD Conformation**

More than dozen residues interact with the FAD either through electrostatic or nonpolar interactions. Electrostatic interactions with the FAD are shown in (FIGURE 2.12; FIGURE 2.13). The interactions with the isoalloxazine in TtPRODH are also present in PutA86-669 structures (FIGURE 2.13). Accordingly, the positioning of the isoalloxazine within the barrel is similar in TtPRODH, and PutA86-669 (FIGURE 2.12). Surprisingly, the FAD conformations of the two enzymes are dramatically different (FIGURE 2.14; FIGURE 2.15). In TtPRODH, the adenosine is under the dimethyl benzene ring of the isoalloxazine (FIGURE 2.14). By contrast, in PutA86-669, the adenosine is below the pyrimidine ring of the isoalloxazine (FIGURE 2.15). The difference



is dramatic. When superimposed, the adenine groups of the two cofactors are separated by 13 Å (FIGURE 2.15).

Accordingly, the interactions involving the ribityl, pyrophosphate and adenosine groups are different in the two enzymes. For example, in TtPRODHD the ribityl 2'-OH is tucked under the pyrimidine ring of the isoalloxazine so that it forms hydrogen bonds with N1 of FAD (2.7 Å, (FIGURE 2.15) and the amine of Gly188 (FIGURE 2.12). Gly188 is located on the loop between  $\beta 5$  and  $\alpha 5$ , which passes below the pyrimidine ring (FIGURE 2.12). The 3'-OH of TtPRODHD is also directed toward this loop, but does not form hydrogen bonds with the loop. The 4'-OH is approximately trans to 3'-OH, and it forms a hydrogen bond to the pyrophosphate (3.0 Å, FIGURE 2.15). In contrast, in PutA86-669 the 2'-OH and 3'-OH groups are rotated approximately 90° from the corresponding groups of TtPRODHD (FIGURE 2.15). Moreover, the 4'-OH of PutA86-669 is rotated 180° from that of TtPRODHD and forms an intramolecular hydrogen bond with a ribose hydroxyl (FIGURE 2.15).

As noted above, the adenine bases of TtPRODHD and PutA86-669 are separated by 13 Å. This is due to different dihedral angle rotations of the pyrophosphate (FIGURE 2.15). In TtPRODHD, the adenine sits atop the N-terminal ends of  $\alpha 6$  and  $\alpha 7$  (FIGURE 2.6), right side provides best view). In contrast, the adenine of PutA86-669 packs against  $\alpha 5a$  and forms an intimate stacking interaction with Trp438 (FIGURE 2.11).

Three factors contribute to the strikingly different FAD conformations in TtPRODHD and PutA. First, Asp228 of TtPRODHD replaces Asn488 of PutA.

Although this seems like a conservative change, the structural ramifications are significant. Asn488 forms a hydrogen bond to the FAD pyrophosphate in PutA (FIGURE 2.16). Changing this residue to Asp not only eliminates the hydrogen bond but also creates electrostatic repulsion between the Asp228 carboxylate and the pyrophosphate. Apparently, this electrostatic clash is avoided in TtPRODHD by rotation of the pyrophosphate dihedral angle so that the adenosine half of the pyrophosphate faces away from Asp288 (FIGURE 2.16). Note that Asp288 forms an ion pair with Lys187, which, in turn, forms an ion pair with the pyrophosphate (FIGURE 2.16). It is concluded that Asp288 helps set up the FAD conformation in TtPRODHD by electrostatic repulsion with the pyrophosphate and electrostatic attraction to Lys187.

The other two factors contributing to the different FAD conformations are two helices that are present in PutA but absent in TtPRODHD. As noted in the previous section, PutA  $\alpha$ 5a is replaced by a short loop in TtPRODHD (FIGURE 2.16). Thus, TtPRODHD does not have a residue equivalent to PutA Trp438 for stacking against the adenine (FIGURE 2.16). In addition, PutA86-669 has extra secondary structural elements following  $\alpha$ 8, owing to its longer polypeptide length. These extra elements are presumably important for linking the PRODHD and P5CDH domains of PutA. One of these elements, a helix formed by PutA residues 565-570, is found to clash with the adenosine of TtPRODHD when the two structures are superimposed (clash distances  $< 1$  Å, (FIGURE 2.11). Thus, steric considerations prevent PutA86-669 from accommodating the FAD in the conformation observed in TtPRODHD.

The aforementioned analysis compared conformations of oxidized cofactors from TtPRODHD and PutA86-669. We recently reported the structure of dithionite-reduced PutA86-669 and showed that reduction of the FAD induces a 22° bend of the isoalloxazine and rotation of the 2'-OH by 90° so that it is tucked under the pyrimidine ring and forms a hydrogen bond to the FAD N1 (45). Thus, the conformations of the 2'-OH groups of oxidized TtPRODHD and reduced PutA86-669 are identical (FIGURE 2.15). Electron density maps show that the isoalloxazine ring in TtPRODHD is planar (FIGURE 2.14, right), as is the case for oxidized PutA86-669(4,44), so it is unlikely that TtPRODHD was reduced by exposure to X-rays during data collection. We conclude that the TtPRODHD structure presented here represents the conformation of the oxidized enzyme. Thus, in terms of the 2'-OH conformation, the oxidized cofactor of TtPRODHD resembles the reduced cofactor of PutA86-669 (FIGURE 2.15). This result has implications for understanding the differences in membrane association of *E. coli* PutA and TtPRODHD (see Discussion).

### **Ligand-Free, Solvent-Exposed Active Site**

It is significant that the TtPRODHD active site does not contain a bound proline analog because all PutA86-669 crystal structures solved to date have active site ligands bound, including acetate (PDB code 1TJ2), L-lactate (PDB code 1TJ0), THFA (PDB code 1TIW) and hyposulfite (PDB code 2FZM). Thus, the TtPRODHD structure provides the first view of a ligand-free PRODHD active site. Since the amino acid sequences of the proline binding pockets are identical in TtPRODHD and *E. coli* PutA, comparison of ligand-free TtPRODHD and inhibitor-

bound PutA86-669 possibly provides insights into conformational changes induced by the binding of proline. The following analysis refers to molecule A of the asymmetric unit but it also holds true for molecule B.

There are two major differences between TtPRODHD and PutA86-669 in the region of the proline-binding pocket. First,  $\alpha 8$  is shifted 3-4 Å away from the proline-binding pocket in TtPRODHD (FIGURE 2.11; FIGURE 2.17). The consequences of this conformational difference are significant because  $\alpha 8$  contributes two absolutely conserved Arg residues that participate directly in binding substrate. As shown in FIGURE 2.17, the two conserved Arg side chains of PutA86-669 (Arg555, Arg556) form ion pairs with the carboxyl group of THFA. Movement of  $\alpha 8$  in TtPRODHD pulls the analogous residues (Arg288, Arg289) out of the proline-binding pocket (FIGURE 2.17).

The second major difference between the proline binding pockets of TtPRODHD and PutA86-669 involves a conserved ion pair that is present in PutA86-669 but absent in TtPRODHD. As shown in FIGURE 2.17, Arg555 of PutA86-669 forms an ion pair with conserved Glu289. The analogous ion pair of TtPRODHD (Arg288-Glu65) is not observed because Glu65 is flipped out of the active site and points into the solvent. This difference is quite large, with the carboxyl groups of TtPRODHD Glu65 and PutA Glu289 separated by 10 Å. We note that Glu65 is free of crystal contacts in both molecules, thus the observed conformation of this residue is not likely an artifact of crystal packing.

Because of the conformational differences involving  $\alpha 8$  and Glu65 (Glu289), the active site of TtPRODHD is open and the FAD is solvent exposed,

sharply contrasting with the closed active site of PutA86-669/THFA, in which the FAD is buried (FIGURE 2.19). The solvent-accessible surface area (SASA) of the FAD in TtPRODH is 220 Å<sup>2</sup> for the A chain and 275 Å<sup>2</sup> for the B chain, based on analysis with the Ligand Protein Contacts server(46). For reference, the SASA of the isolated FAD is 963 Å<sup>2</sup>. By contrast, the FAD in PutA86-669/THFA is buried, with SASA of only 25 Å<sup>2</sup>. The THFA is also buried (0.0 Å<sup>2</sup> SASA). Exposure of the FAD in TtPRODH can be appreciated by viewing a space-filling model of the enzyme (FIGURE 2.18; FIGURE 2.19). It is evident from this view that almost the entire surface of the isoalloxazine *si* face is solvent exposed in TtPRODH. In particular, note that the hydride transfer acceptor atom of the flavin, N5, is open to solvent in TtPRODH. This atom is completely buried in PutA86-669/inhibitor complexes (FIGURE 2.19).

### **MPD and Possible Electron Transfer Pathway**

There are two MPD molecules bound to each TtPRODH, and the binding sites are in identical locations in the two proteins. Both sites are located on bottom face of the barrel, which is the face opposite from the FAD-binding site. Sites 1 and 3 are located in the N-terminal ends of the β-strands, while sites 2 and 4 have different interactions due to crystal packing (FIGURE 2.20)

MPD sites 1 & 3 (FIGURE 2.21) are equivalent and are located in the center of the bottom face of the β-barrel among the loops that connect strands with helices. The MPD molecule binds in a hole formed by Tyr95, Phe129, Tyr221, Asn182, Arg273 and Arg131. Tyr95 and Arg171 form the bottom of the hole, and the other side chains form the sides of the hole. The MPD in site 1

forms nonpolar contacts primarily with Phe129 and Tyr221 and hydrogen bonds with Asn182. The average B-factor for MPD in site 1 & 3 are 28 and 26 Å<sup>2</sup>, respectively.

MPD site 2 is bound near on the periphery of the barrel near  $\alpha$ 4 and  $\alpha$ 5 in chain B. This ligand is interacting in a crystal contact. This MPD molecule contacts side chains of Arg151, Glu152, Tyr179, and Pro178. It forms hydrogen bonds with water and Gly30 of a symmetry-related molecule. MPD site 2 has nonpolar interactions with Glu152 and Tyr 179. The average B-factor for MPD in site 2 is 17.5 Å<sup>2</sup>

MPD site 4 binds to chain A in the same location as MPD site 2 in chain B. Interestingly the crystal packing is different, and the B-factor of 40 Å<sup>2</sup> confirms that there are fewer interactions. There are the nonpolar interactions with Tyr 179, and MPD hydrogen bonds with water.

MPD has been shown to bind hydrophobic regions of proteins, reducing solvent-accessible areas, with implications in protein stability (47). We hypothesize that the N-terminal ends of the  $\beta$ -strands associating with MPD sites 1 & 3 may be a potential conduit for transferring electrons from the reduced flavin to electron acceptors in the membrane. The distance between MPD 1 and the flavin N5 is 12.5 Å. Arg184, which hydrogen bonds to the isoalloxazine N5, is hypothesized to play a role in this electron transfer. In inactivated TtPROD H (CHAPTER 3), Arg184 shows a movement of 0.5 Å upon flavin reduction. Dithionite-reduced EcPutA PROD H structures also show a movement of the homologous Arg431, which no longer forms a hydrogen bond with N5. With

R184 movement, there are charged residues that could form an electron transfer pathway, with conservation of these residues among most bacteria.

The proposed electron transfer pathway is Arg184, Gln252, Glu250 and Arg273 (FIGURE 2.22). Among the proposed residues in the electron transfer pathway, Arg184 is completely conserved among bacteria. Gln252 and Glu250 are present in most all bacteria, excepting of those contained in branch 2a (*Helicobacter*, *Campylobacter*, *Corynebacterium* and *Bacteroides*). Arg273 is highly conserved, although this residue has more variation than previous residues in the pathway. Besides the branch 2a bacteria, Arg273 is also not present in *Oceanobacillus* (Cys), *Staphylococcus* (Thr), *Halobacterium* (Phe), and *Jannaschia* (Gln). Two PutA enzymes from branch 2a member, *Helicobacter* sp., have been characterized and generate reactive oxygen species. Thus branch 2a PutAs may not have a need for an electron transport pathway (48).

Membrane association by SPR indicates that EcPutA prefers to bind neutral membranes (13). Perhaps MPD, which has been shown to bind hydrophobic regions, is binding to a potential location of membrane association on TtPRODH (FIGURE 2.22). Goals include the crystallization of TtPRODH in complex with quinone-like molecules, in order to gain insight into this association.

### **Crystal Soaking Experiments**

Addition of L-proline to a solution of TtPRODH causes a change from bright yellow to colorless indicating flavin reduction. Optical spectroscopy confirm that the characteristic flavin spectra disappears upon reduction with L-

proline (FIGURE 2.23). Interestingly, addition of solid proline to the MPD crystal form did not produce a corresponding color change. DCPIP assays were conducted in the presence of similar concentrations of MPD,  $\text{MgCl}_2$  and imidazole produced no change in TtPRODHD activity. It was thought that crystal packing interactions prevent closure of the active site, which is required for binding proline.

Other crystal forms were optimized, and mutagenesis was used to disrupt crystal packing (TABLE 2.2). The high-salt crystal form that could be reduced by proline (FIGURE 2.24; FIGURE 2.25). This crystal form had unit cell dimensions similar to those of the MPD form. Despite soaking with high concentrations of the isostructural analogs, L-THFA, and substrate, L-proline, the structure revealed in the same non-occupied, solvent-exposed active site. Mutagenesis to disrupt crystal packing between helices  $\alpha 5$  was also attempted (FIGURE 2.11). Double mutant Arg202Ala / Glu207Ala was created, purified and crystals optimized. Although the crystallization conditions were different and crystals were reducible with proline, the unit cell dimensions were similar to those of the MPD form. This mutagenized TtPRODHD crystal form was not pursued further.

### **Absorbance Spectroscopy and Steady-State Kinetics**

We performed biochemical analyses of TtPRODHD to understand how monofunctional PRODHDs differ from PutA PRODHD domains in terms of spectroscopic and steady-state kinetic properties. TtPRODHD displayed a flavin absorption spectrum similar to that of previously characterized PutAs (49), with maxima at 381 nm and 452 nm (FIGURE 2.26). Potentiometric titration of



TtPROD<sub>H</sub> yielded an  $E_m$  value of -75 mV for the bound FAD cofactor (FIGURE 2.26), which is similar to that previously reported for *E. coli* PutA ( $E_m$  = -77 mV, pH 7.5,(50)). No significant stabilization of semiquinone species was observed during the titration (FIGURE 2.26). Titration of TtPROD<sub>H</sub> with proline under aerobic conditions yielded an apparent equilibrium constant for the formation of TtPROD<sub>H</sub><sub>red</sub>-P5C (eq. 1) of 4.5 mM<sup>-1</sup> proline, which is about two-fold lower than the value of 9.5 mM<sup>-1</sup> for *E. coli* PutA (38).

The kinetic parameters of TtPROD<sub>H</sub> using proline as the substrate were estimated to be  $K_m$  = 27 mM,  $V_{max}$  = 20.5 U/mg and  $k_{cat}$  = 13 s<sup>-1</sup> (FIGURE 2.27)(TABLE 2.5). For reference, the corresponding values for PutAs from *E. coli* and *Helicobacter pylori* are listed in TABLE 2.5. Although, the  $K_m$  parameter of TtPROD<sub>H</sub> is 3 - 5 times lower than those of the PutAs, the  $k_{cat}$  value is comparable to the PutA values (TABLE 2.5). The kinetic parameters for TtPROD<sub>H</sub> more closely resemble those of PutA86-669 ( $K_m$  = 60 mM,  $k_{cat}$  = 17 s<sup>-1</sup>) than those of the PutAs.

Interestingly, 3,4-dehydro-L-proline was more efficiently oxidized than proline, with  $K_m$  = 4 mM,  $V_{max}$  = 119 U/mg and  $k_{cat}$  = 75 s<sup>-1</sup> (FIGURE 2.28). Analogous data for PutA are not available, although Wood reported, that in *E. coli* K12, PutA detoxifies 3,4-dehydro-L-proline by oxidation(51).

THFA and L-mandelic acid were identified as competitive inhibitors of TtPROD<sub>H</sub>, with  $K_i$  values of 1.0 mM and 2.4 mM, respectively (FIGURE 2.29; FIGURE 2.30). THFA is also a competitive inhibitor of PutA86-669, *E. coli* PutA and *H. pylori* PutA ( $K_i$  = 0.2 - 0.3 mM). Other proline analogs such as trans-4-

hydroxy-L-proline, cis-4-hydroxy-L-proline, L-azetidine-2-carboxylic acid and L-pipecolinic acid were neither inhibitors nor substrates of TtPRODH.

TtPRODH is highly thermostable, based on residual activity measurements, as expected for an enzyme from an extreme thermophile. TtPRODH exhibited over 85 % residual activity, after a 1-hour incubation at 90 °C, and over 60 % residual activity after 3 hours (FIGURE 2.31). The half-life estimated from these data was 257 +/- 6 min. For comparison, PutA86-669 exhibits a 50 % drop in activity after 2 hours at 45°C (44). The proline dehydrogenase activity of TtPRODH increased with increasing temperature, showing no maximum with current experimental capabilities (FIGURE 2.32).

### **Proline:O<sub>2</sub> Reactivity and Generation of Reactive Oxygen Species**

The solvent-exposed active site of TtPRODH suggested the possibility that the reduced enzyme would exhibit higher reactivity with molecular oxygen than PutA from *E. coli*. A chromogenic assay based on *o*-AB was used to measure the rate of oxygen reactivity. In this assay, P5C produced by oxidation of proline forms a complex with *o*-AB, which is monitored by absorbance at 443 nm. Detection of the *o*-AB:P5C complex over time indicates reactivity of the reduced FAD with O<sub>2</sub> during catalytic turnover with proline.

TtPRODH exhibited significant proline:O<sub>2</sub> reactivity with kinetic parameters of  $K_m = 1.3$  mM,  $V_{max} = 335$  mU/mg, and  $k_{cat} = 12.7$  min<sup>-1</sup> (TABLE 2.5) (FIGURE 2.33). Data from the *o*-AB assay are typically expressed as the ratio of the specific activity from the DCPIP assay to the specific activity from the *o*-AB assay, which indicates the preference of utilizing DCPIP over O<sub>2</sub> as the electron

acceptor. For TtPRODH, this ratio is 61. For comparison, the corresponding ratios for PutAs from *Helicobacter pylori* and *E. coli* are 16 and > 2500, respectively (TABLE 2.5). This reactivity was not increased upon addition of *E. coli* vesicles containing electron acceptors in the membranes (FIGURE 2.34).

Generation of ROS ( $O_2^-$ ,  $H_2O_2$ ) by TtPRODH was also studied. The production of superoxide was examined by monitoring the reduction of cytochrome c during the proline oxidation catalytic cycle. Reduction of cytochrome c was observed, which is consistent with generation of superoxide. Addition of superoxide dismutase to the assay (30 mg) eliminated the observed effect, which further implicates superoxide as the product of the proline: $O_2$  reaction. Since superoxide decomposes in water to  $H_2O_2$ , the generation of  $H_2O_2$  was also examined.  $H_2O_2$  was produced in a proline-dependent manner (FIGURE 2.35).

### **Conserved Sequence-Structure Motifs of the PRODH Family**

An intriguing aspect of proline catabolism is that PRODH and P5CDH are encoded on separate genes in some organisms, whereas the two genes are fused in other organisms (*putA*). The traditional view, which was developed prior to the whole genome sequence era, has been that PRODH and P5CDH appear as separate enzymes in eukaryotes and as fused bifunctional enzymes (PutA) in bacteria. Our analysis of genome sequence data, however, reveals a more complex situation for bacteria. The updated view is that PutAs are indeed restricted to bacteria, but monofunctional PRODHs and P5CDHs appear in both eukaryotes and bacteria.

The distribution of PutAs and monofunctional PRODHs in bacteria is depicted in the phylogenetic tree in FIGURE 2.36. Three main branches are evident. Branch 1 contains the best-characterized PutAs, including PutAs from *E. coli*, *Bradyrhizobium japonicum* and *S. typhimurium*. The organisms represented in branch 1 are primarily  $\alpha$ -,  $\beta$ -, and  $\gamma$ -proteobacteria. The PutAs in branch 1 of our data set have 999 - 1361 residues and the pairwise sequence identities are 38 - 99% with an average of 49 %.

Branch 2 contains PutAs from Gram-negative cyanobacteria,  $\delta$ - and  $\varepsilon$ -proteobacteria, and corynebacterium. The polypeptide length for branch 2 PutAs is 982-1294 and the pairwise sequence identity range is 23 - 73 % with an average identity of 38 %. Note that branch 2 is divided into two distinct groups, denoted 2A and 2B in FIGURE 2.36. PutAs from branch 2 have only recently been explored. For example, Krishnan and Becker showed that branch 2A PutAs from *Helicobacter pylori* and *Helicobacter hepaticus* appear to be unique among PutAs in that they exhibit oxygen reactivity and generate proline-dependent ROS (48).

Branch 3 consists entirely of monofunctional PRODHs. TtPRODH is the only enzyme of this branch to be purified and characterized. PRODHs of branch 3 have 279-333 amino acid residues, and the pairwise sequence identities for this group are 23 - 79 % with an average of 38 %. In some branch 3 organisms, the PRODH and P5CDH genes are very close together. For example, in *T. thermophilus*, only 15 bases separate the stop codon of the PRODH gene from the Met start codon of the P5CDH gene. In other organisms, the two genes are

quite far apart. For example, in *Staphylococcus aureus* subsp. *aureus* Mu50, the PRODH and P5CDH genes are separated by 800 kb. Interestingly, most of the organisms represented in branch 3 are Gram-positive bacteria. Counterexamples include *Thermus*, *Solibacter*, *Salinibacter*, and *Chlorobium*.

The availability of two PRODH structures (TtPRODH and PutA86-669) and many sequenced bacterial genomes allowed analysis of conserved sequence-structure motifs of the bacterial PutA/PRODH family. Nine conserved motifs were identified by mapping multiple sequence alignments onto the TtPRODH and PutA86-669 structures (TABLE 2.6). Each motif contains at least one residue that is identically conserved throughout the entire bacterial PutA/PRODH family (TABLE 2.6, bold letters) (FIGURE 2.37).

The TtPRODH and PutA86-669 structures show that the nine motifs cluster near the active site and that the identically conserved residues of the motifs have important roles in FAD binding and substrate recognition. Motifs 4-6 are primarily involved in FAD binding. For example, the conserved Gln of motif 4 forms a hydrogen bond to the FAD O2 (FIGURE 2.12, Gln163) while the Arg of motif 5 forms a hydrogen bond to the FAD N5 (FIGURE 2.12, Arg184). Also, the Lys and His of motifs 5 and 6 interact with the pyrophosphate (FIGURE 2.12, Lys187 and His227).

Motifs 1-3 and 7-9 are responsible for substrate recognition. For example, the Lys and Arg side chains of motifs 2 and 9 form ion pairs to the substrate carboxyl, as shown for the PutA86-669/THFA structure (FIGURE 2.17, PutA residues Lys329, Arg555, Arg556). The conserved Glu residues of motifs 1 and 9

play indirect roles in substrate recognition by providing stabilizing ion pairs to the two Arg residues of motif 9 when the substrate/product is bound (Arg555-Glu289 and Arg556-Glu559 in PutA, FIGURE 2.17). Size and shape complementarity are enforced by nonpolar contacts between the substrate and the Leu and Tyr side chains of motifs 7 – 9 (44). Finally, the conserved Asp of motif 3 (Asp133 of TtPRODH) plays a dual role in substrate recognition and FAD binding by forming stabilizing interactions with the Lys of motif 2 (substrate recognition, FIGURE 2.17), Tyr of motif 8 (substrate recognition, FIGURE 2.17) and the conserved Arg of motif 5 (FAD binding, FIGURE 2.17).

## **DISCUSSION**

### **New Subfamily of PRODH**

The genesis of this work was the realization, based on analysis of genome sequence data, that some bacteria lack putA genes and instead encode PRODH and P5CDH as separate monofunctional enzymes. This observation is significant because the traditional view of proline catabolism was that monofunctional enzymes are restricted to eukaryotes. Thus, bacterial monofunctional PRODHs represent a new subfamily of proline catabolic enzyme. Moreover, isolation of recombinant eukaryotic PRODHs in sufficient quantity and purity for biophysical study has been problematic (our unpublished results) and therefore the bacterial homologs are potentially attractive model systems for understanding human PRODH. We thus set out to characterize a bacterial monofunctional PRODH in order to establish paradigms for this new subfamily,

compare its structure and biochemical properties to those of PutAs, and set the stage for probing protein-protein interactions between monofunctional PRODH and P5CDH.

One major result of this work is that monofunctional PRODHs and PutAs share a common catalytic core consisting of a unique TIM barrel (FIGURE 2.11). The PutA/PRODH barrel is distinguished from other TIM barrels by placement of  $\alpha 8$  above the barrel. This distortion is functionally significant because  $\alpha 8$  contributes conserved motif 9 to the active site (TABLE 2.6). Observation of this structural distortion of the classic TIM barrel fold in enzymes from two branches of the bacterial PutA/PRODH family suggests that it is a defining structural signature of this family.

Interestingly, the TIM barrel catalytic core, FAD conformations, and proline binding pocket described here for the PutA/PRODH family bear no resemblance to those of PRODHs from the hyperthermophilic archaeon *Pyrococcus horikoshii* (PDH1 and PDH2) (FIGURE 2.38). For example, PDH1 from *P. horikoshii* is an  $(\alpha\beta)_4$  hetero-octameric complex with the  $\beta$ -subunit binding an FAD cofactor and exhibiting PRODH activity(6). The FAD-binding domain of PDH1 consists of a Rossmann dinucleotide-binding fold similar to that of monomeric sarcosine oxidase, which is a member of the glutathione reductase family (6). As expected for a Rossmann fold protein, the FAD of PDH1 is highly extended, and the pyrophosphate interacts with a glycine-rich loop and associated conserved water molecule (52). Thus, the protein-FAD interactions in PDH1 are quite different from those described here. Furthermore, proline binds on the *re* face of the FAD

in PDH1, in contrast to PutA and TtPRODH which bind proline on the *si* face. Thus, the PutA/PRODH and PDH1 families represent two distinctly different solutions to the problem of catalyzing the oxidation of proline by a flavoenzyme.

### **FAD Conformation**

Although the catalytic cores of TtPRODH and PutA86-669 are similar in overall fold, the FAD conformations are surprisingly different. This difference is attributed to an Asp/Asn sequence difference (FIGURE 2.16) and two helices present in PutA86-669 but absent in TtPRODH (FIGURE 2.11; FIGURE 2.16). Based on amino acid sequence alignments, the Asn-pyrophosphate hydrogen bond,  $\alpha$ 5a, and the 560s helix are present in all PutAs and missing in all bacterial monofunctional enzymes. Interestingly, the stacking Trp of  $\alpha$ 5a is present in most, but not all, PutAs. For example, branch 2A enzymes have Met or Leu in place of the stacking Trp, but these residues could also provide a nonpolar interaction with the FAD adenine. We therefore predict that all PutAs have the FAD conformation observed in PutA86-669 and that all bacterial monofunctional PRODHs have the FAD conformation observed in TtPRODH. It is concluded that the FAD conformation is the major structural difference between PutAs and bacterial monofunctional PRODHs.

The different FAD conformations in PutA and monofunctional PRODHs presumably reflect different structural and functional requirements. For example, we suggest that the difference in position of the ribityl 2'-OH reflects the different membrane association requirements of *E. coli* PutA and TtPRODH. *E. coli* PutA is membrane-associated only when the FAD is in the reduced state. In the



oxidized state, it remains in the cytoplasm and represses transcription of the *putA* and *putP* (encodes a proline transporter) genes (15,53,54). We recently showed that reduction of FAD in PutA86-669 triggers rupture of the hydrogen bond between the ribityl 2'-OH and Arg556, causing rotation of the 2'-OH so that it is tucked below, and hydrogen bonded to, the FAD N1 (45). We further showed that the 2'-OH-Arg556 hydrogen bond is a structural constraint that prevents oxidized PutA from binding the membrane(45). Interestingly, we find here that the 2'-OH of oxidized TtPRODH is tucked below the FAD N1, that is, locked in the membrane-binding position (FIGURE 2.14; FIGURE 2.15). This makes sense because TtPRODH does not have a repressor function and is presumably membrane-associated in both the oxidized and reduced states.

A larger question is how come the global FAD conformations of PutAs and monofunctional PRODHs differ so much, with the adenosine moieties of the two cofactors separated by 13 Å. It is possible that the particular FAD conformation found in PutA is necessary for coordinating the two catalytic functions of PutA, i.e., substrate channeling. Monofunctional PRODH and P5CDH may interact and exhibit intermolecular substrate channeling according to the Rosetta Stone hypothesis. We note that this occurs for tryptophan synthase, in which indole is channeled between separate  $\alpha$  and  $\beta$  subunits (16),(17). Presumably, the FAD conformation in TtPRODH is the one required for docking of TtPRODH with TtP5CDH. Observation of different FAD conformations in TtPRODH and PutA86-669 may indicate that the protein-protein interface between TtPRODH and TtP5CDH differs substantially from the PRODH:P5CDH domain interface in

PutA. Clearly, structures of full-length PutAs, other monofunctional PRODHs, and a monofunctional PRODH:P5CDH complex would address how come PutAs and monofunctional PRODHs require such different FAD conformations.

### **Insights into Protein Motions Associated with Substrate Binding**

Structural information on the ligand-free form of the PutA PRODH domain has been elusive due to the propensity of PutA86-669 to crystallize only in PEGs contaminated with either L-lactate or acetate (44), which are both competitive inhibitors. These structures showed that the inhibitor is buried, which raised the question of how proline enters the active site and how P5C is released. Clearly protein motion is required, but the nature of this motion is unknown.

TtPRODH crystallized in MPD, which allowed us to determine the first structure of a PRODH in the ligand-free state. Although a structure of ligand-bound TtPRODH is not known, structural and biochemical data suggest that the active site of PutA86-669 complexed with THFA is a good model for the proline bound conformation of TtPRODH. For example, all residues that contact THFA in PutA86-669 are identically conserved in TtPRODH, including Arg288, Arg289, Lys99, Tyr285, Leu254, Tyr275, Asp133 and Tyr190 (TtPRODH residue numbering). Moreover, the steady state kinetics parameters for TtPRODH are similar to those of PutA86-669. In particular, the  $K_m$  for proline is 27 mM, which compares favorably with the value of 60 mM for PutA86-669. Furthermore, THFA is a competitive inhibitor of TtPRODH with  $K_i = 1$  mM, which is similar to the value of  $K_i = 0.2$  mM for PutA86-669. These data strongly suggest that TtPRODH and PutA86-669 bind the substrate proline similarly. Thus,

comparison of ligand-free TtPRODHD with PutA86-669/THFA provides clues about those parts of the TtPRODHD active site move in response to substrate binding and product release.

Our analysis suggests that, prior to substrate binding, the enzyme adopts an open state in which  $\alpha 8$  is shifted away from the FAD and the conserved ion-pair between the first Arg of motif 9 and Glu of motif 1 is broken (Arg289-Glu65). Upon binding substrate,  $\alpha 8$  moves closer to the proline binding pocket to enable ion-pair formation between proline and the two Arg residues of motif 9, as well as formation of the ion-pair between motifs 1 and 9. The proline-binding pocket displays perfect charge balance when a carboxyl-containing molecule is bound in the active site (proline, P5C, THFA), (FIGURE 2.17). There are four Arg/Lys (motifs 2, 5, 9), two Glu (motifs 1, 9), one Asp (motif 3), and the substrate/inhibitor carboxyl in the pocket. In the absence of substrate/product, the binding pocket has one excess positive charge, necessitating movement to alleviate electrostatic repulsion. The TtPRODHD structure suggests that the major conformational adjustment involves  $\alpha 8$  and the Glu of motif 1.

Interestingly, there is a glycine residue in the loop connecting  $\beta 8$  and  $\alpha 8$  (FIGURE 2.6, Gly279). This residue is identically conserved throughout the entire bacterial PutA/PRODHD family except for branch 2A PutAs. In *E. coli* PutA, for example, the conserved glycine is Gly544. We suggest that this conserved Gly serves as a flexible hinge between  $\beta 8$  and  $\alpha 8$ , allowing  $\alpha 8$  to shift in response to substrate binding.

### **Relationships Between Bacterial and Human PRODHD**

Humans have two isozymes of PRODH, which share about 50% amino acid sequence identity (55). PRODH1 is encoded on chromosome 19, is expressed almost exclusively in liver and kidney, and catalyzes oxidation of L-hydroxyproline. PRODH2 is encoded on chromosome 22q11, is expressed more widely than PRODH1 (brain, heart, pancreas, kidney, liver), and specifically oxidizes L-proline.

PRODH2 is part of the p53 signaling pathway with the PRODH2 gene identified as a p53 inducible gene (56). Up-regulation of PRODH2 and proline oxidation in lung, renal, and colon carcinoma cells has been shown to generate ROS and induce cell death by mitochondrial dependent processes (57-62). Perturbation of mitochondrial membranes by ROS causes the release of cytochrome c into the cytosol and subsequent activation of the intrinsic caspase pathway. Because the p53-apoptosis pathway involves ROS, PRODH2 appears to play a role in p53-mediated apoptosis by modulating the cellular redox environment. Indeed, antisense repression of PRODH2 prevents p53-induced apoptosis(62). Thus, PRODH2 is a pro-apoptotic protein that helps reduce carcinogenesis in humans by serving as a ROS generator. Accordingly, PRODH2 is often referred to as proline oxidase in the literature.

Bacterial monofunctional PRODHs are potentially attractive model systems for understanding the structure and biochemical function of human PRODHs. Although the sequence identity between TtPRODH and human PRODH1/2 is less than 20 %, conserved motifs 3-9 are clearly present in the sequences of both human PRODH1 and PRODH2. Considering residues within

10 Å of the active site, there is 45 % sequence conservation between human PRODH1/2 and TtPRODH. These data strongly suggest that the human enzymes have the  $(\beta\alpha)_8$  catalytic core and active site structure common to TtPRODH and PutA86-669. On the other hand, human PRODH1 and PRODH2 have 536 and 600 residues, respectively, compared to only 307 for TtPRODH. Thus, the human enzymes clearly have additional structural elements not found in TtPRODH.

Interestingly, analysis of human PRODH1/2 amino acid sequences suggests that the conformation of FAD in human PRODH1/2 is similar to that of PutA rather than TtPRODH. Both human enzymes have Asn at the position equivalent to *E. coli* PutA Asn488. Furthermore, sequence alignments suggest that the human enzymes have the equivalent of PutA  $\alpha 5a$  and that Leu replaces the stacking Trp. We note that Leu is also present at this position in some branch 2A PutAs. Thus, the FAD conformation observed in *E. coli* PutA is probably present in the human enzymes and the conformation observed in TtPRODH seems to be a unique signature of bacterial monofunctional enzymes. Production of proline-dependent superoxide is central to the role of PRODH2 in p53-mediated apoptosis (61,63). It is therefore highly significant that we observed reactivity of TtPRODH with molecular oxygen resulting in superoxide generation.

Reactivity of a FAD-dependent dehydrogenase with molecular oxygen implies that the reduced FAD is accessible to solvent. *E. coli* PutA is essentially nonreactive with molecular oxygen(48), suggesting that the FAD remains

sequestered even after the active site opens to release P5C. On the other hand, *H. pylori* PutA reacts strongly with molecular oxygen indicating that O<sub>2</sub> has access to the reduced cofactor (48). Krishnan and Becker have suggested that Asn291 of *H. pylori* PutA, which is replaced by the bulkier Tyr437 in *E. coli* PutA, may account for the differences in O<sub>2</sub> reactivity of these two PutAs (48). This particular Tyr is part of conserved motif 5 (TABLE 2.6, Tyr437 in *E. coli* PutA). It forms a water-mediated hydrogen bond to the O atom of the THFA ring (FIGURE 2.17) and is in position to protect the active site from bulk solvent by virtue of its location on the edge of the proline-binding site (see Tyr190 in FIGURE 2.18). Tyrosine, being larger than Asn, may afford more protection of the active site from solvent. Interestingly, human PRODH2 and TtPRODH - both ROS generators - have Tyr at this position (Tyr446 in PRODH2 and Tyr190 in TtPRODH, FIGURE 2.11). Thus, the Asn hypothesis, which may explain the difference in O<sub>2</sub> reactivity between *E. coli* and *H. pylori* PutAs, does not explain the O<sub>2</sub> reactivity of TtPRODH and human PRODH2. The TtPRODH structure shows that  $\alpha 8$  is important for protecting the FAD from solvent and that there is sufficient flexibility in the  $\beta 8$ - $\alpha 8$  loop to allow movement of  $\alpha 8$  away from the proline binding pocket resulting in exposure of the isoalloxazine. These results suggest that movement of  $\alpha 8$  may contribute to O<sub>2</sub> reactivity of PRODHs.

### **Obtaining the solvent-protected TtPRODH active site**

Crystal packing of TtPRODH in the P<sub>2</sub><sub>1</sub>2<sub>1</sub>2<sub>1</sub> lattice must be highly favorable. Attempts to disrupt this crystal lattice were unsuccessful. Chapter 3 discusses results obtained with a mechanism-based inactivator of TtPRODH. It

was hypothesized that a covalently-attached inhibitor would induce TtPRODHD to pack in a different crystal lattice. Unfortunately, no other crystal forms were discovered. However, the structure of the inactivated TtPRODHD was solved using the MPD crystal form (see Chapter 3).

Strategies for obtaining a solvent-protected TtPRODHD active site are important because it remains unresolved whether or not the accessibility of the TtPRODHD active site results from crystal-packing. Perhaps lysine methylation would result in a different crystal form (64). This procedure methylates surface lysines turning primary amines into tertiary methylated amines which changes the surface potential. It is reported to be a “rescue strategy” for obtaining crystals when other methods are not fruitful. Another strategy would be relocating the His-tag to the C-terminal end of the protein. This strategy was attempted in Don Becker’s lab, our collaborator. C-terminally his-tagged TtPRODHD was reported precipitate after affinity chromatography (N. Krishnan, personal communication). A final strategy is homolog screening. For example, we cloned, expressed and purified *B. subtilis* PRODHD. The enzyme was highly aggregated in solution which could be relieved by adding BOG, similar to TtPRODHD. Unfortunately, no crystals were obtained with initial crystal screening. These screens were attempted again with the presence of 10 mM THFA, and again no crystals were obtained. There are plenty of other homologs to crystallize, although soluble aggregation may be a potential issue with bacterial PRODHD, as it was seen in two of these enzymes already. Until a bacterial PRODHD with a solvent-protected

active site is crystallized, questions about induced-fit substrate binding remain unanswered.



## REFERENCES

1. Adams, E., and Frank, L. (1980) *Annu Rev Biochem* **49**, 1005-1061
2. Phang, J. M. (1985) *Curr Top Cell Regul* **25**, 91-132
3. Zhang, M., White, T. A., Schuermann, J., Baban, B. A., Becker, D. F., and Tanner, J. J. (2004) *Biochemistry* **43**
4. Lee, Y. H., Nadaraia, S., Gu, D., Becker, D. F., and Tanner, J. J. (2003) *Nature Structural Biology* **10**, 109-114
5. Inagaki, E., and Tahirov, T. H. (2004) *to be published*
6. Tsuge, H., Kawakami, R., Sakuraba, H., Ago, H., Miyano, M., Aki, K., Katunuma, N., and Ohshima, T. (2005) *J Biol Chem* **280**, 31045-31049
7. Menzel, R., and Roth, J. (1981) *J Biol Chem* **256**, 9762-9766
8. Brown, E., and Wood, J. (1992) *Journal of Biological Chemistry* **267**, 13086-13092
9. Muro-Pastor, A. M., and Maloy, S. (1995) *Journal of Biological Chemistry* **270**, 9819-9827
10. Muro-Pastor, A. M., Ostrovsky, P., and Maloy, S. (1997) *J Bacteriol* **179**, 2788-2791
11. Becker, D. F., and Thomas, E. A. (2001) *Biochemistry* **40**, 4714-4721
12. Zhu, W., and Becker, D. F. (2003) *Biochemistry* **42**, 5469-5477
13. Zhang, W., Zhou, Y., and Becker, D. F. (2004) *Biochemistry* **43**, 13165-13174
14. Krishnan, N., and Becker, D. F. (2005) *Biochemistry* **44**, 9130-9139
15. Larson, J. D., Jenkins, J. L., Schuermann, J. P., Zhou, Y., Becker, D. F., and Tanner, J. J. (2006) *Protein Sci* **15**, 2630-2641
16. Miles, E. W., Rhee, S., and Davies, D. R. (1999) *J Biol Chem* **274**, 12193-12196
17. Huang, X., Holden, H. M., and Raushel, F. M. (2001) *Annu Rev Biochem* **70**, 149-180
18. Surber, M. W., and Maloy, S. (1998) *Arch Biochem Biophys* **354**, 281-287
19. Marcotte, E. M., Pellegrini, M., Ng, H. L., Rice, D. W., Yeates, T. O., and Eisenberg, D. (1999) *Science* **285**, 751-753
20. White, T. A., and Tanner, J. J. (2005) *Acta Crystallography* **F61**, 737-739
21. Ailenberg, M., and Silverman, M. (1996) *Biochem Mol Biol Int* **39**, 771-779
22. Ferre-D'Amare, A. R., and Burley, S. K. (1994) *Structure* **2**, 357-359
23. D'Arcy, A., Banner, D. W., Janes, W., Winkler, F. K., Loetscher, H., Schonfeld, H. J., Zulauf, M., Gentz, R., and Lesslauer, W. (1993) *J Mol Biol* **229**, 555-557
24. Matthews, B. W. (1968) *J Mol Biol* **33**, 491-497
25. Vagin, A., and Teplyakov, A. (1997) *Journal of Applied Crystallography* **30**, 1022-1025
26. Doubleie, S. (1997) *Methods Enzymol* **276**, 523-530
27. Pflugrath, J. (1999) *Acta Crystallography* **D55**, 1718-1725
28. Terwilliger, T. C. (2003) *Methods Enzymol* **374**, 22-37
29. Cowtan, K., and Main, P. (1998) *Acta Crystallogr D Biol Crystallogr* **54 ( Pt 4)**, 487-493

30. Morris, R. J., Perrakis, A., and Lamzin, V. S. (2002) *Acta Crystallographica* **D58**, 968-975
31. Winn, M. D., Murshudov, G. N., and Papiz, M. Z. (2003) *Methods Enzymol* **374**, 300-321
32. van Aalten, D. M., Bywater, R., Findlay, J. B., Hendlich, M., Hooft, R. W., and Vriend, G. (1996) *J Comput Aided Mol Des* **10**, 255-262
33. Potterton, E., Briggs, P., Turkenburg, M., and Dodson, E. (2003) *Acta Crystallogr D Biol Crystallogr* **59**, 1131-1137
34. 4, C. C. P. N. (1994) *Acta Crystallography* **D50**, 760-763
35. Berman, H. M., Bhat, T. N., Bourne, P. E., Feng, Z., Gilliland, G., Weissig, H., and Westbrook, J. (2000) *Nat Struct Biol* **7 Suppl**, 957-959
36. Dixon, M. (1953) *Biochemistry Journal* **55**, 170-171
37. Stankovich, M. T. (1980) *Anal Biochem* **109**, 295-308
38. Brown, E., and Wood, J. (1993) *Journal of Biological Chemistry* **268**, 8972-8979
39. Mezl, V. A., and Knox, W. E. (1976) *Anal Biochem* **74**, 430-440
40. Tarpey, M. M., and Fridovich, I. (2001) *Circ Res* **89**, 224-236
41. Thompson, J. D., Higgins, D. G., and Gibson, T. J. (1994) *Nucleic Acids Res* **22**, 4673-4680
42. Hendrickson, W., and Ogata, C. (1997) *Methods Enzymol* **276**, 494-523
43. Walden, H., Bell, G. S., Russell, R. J., Siebers, B., Hensel, R., and Taylor, G. L. (2001) *J Mol Biol* **306**, 745-757
44. Zhang, M. (2004) in *Chemistry*, pp. 36-54, University of Missouri, Columbia
45. Zhang, W., Zhang, M., Zhu, W., Zhou, Y., Wanduragala, S., Rewinkel, D., Tanner, J. J., and Becker, D. F. (2007) *Biochemistry* **46**, 483-491
46. Sobolev, V., Sorokine, A., Prilusky, J., Abola, E. E., and Edelman, M. (1999) *Bioinformatics* **15**, 327-332
47. Anand, K., Pal, D., and Hilgenfeld, R. (2002) *Acta Crystallogr D Biol Crystallogr* **58**, 1722-1728
48. Krishnan, N., and Becker, D. F. (2006) *J Bacteriol* **188**, 1227-1235
49. Vinod, M. P., Bellur, P., and Becker, D. F. (2002) *Biochemistry* **41**, 6525-6532
50. Zhu, W., Gincherman, Y., Docherty, P., Spilling, C. D., and Becker, D. F. (2002) *Arch Biochem Biophys* **408**, 131-136
51. Wood, J. M. (1981) *J Bacteriol* **146**, 895-901
52. Bottoms, C. A., Smith, P. E., and Tanner, J. J. (2002) *Protein Sci* **11**, 2125-2137
53. Chen, C. C., and Wilson, T. H. (1986) *J Biol Chem* **261**, 2599-2604
54. Gu, D., Zhou, Y., Kallhoff, V., Baban, B., Tanner, J. J., and Becker, D. F. (2004) *J Biol Chem*
55. Phang, J. M., Hu, C. A., and Valle, D. (2001) in *Metabolic and molecular basis of inherited disease* (Scriver, C. R., A.L., B., Sly, W., and Valle, D., eds), McGraw Hiss, New York
56. Polyak, K., Xia, Y., Zweier, J. L., Kinzler, K. W., and Vogelstein, B. (1997) *Nature* **389**, 300-305

57. Hu, C. A., Donald, S. P., Yu, J., Lin, W. W., Liu, Z., Steel, G., Obie, C., Valle, D., and Phang, J. M. (2006) *Mol Cell Biochem*
58. Rivera, A., and Maxwell, S. A. (2005) *J Biol Chem* **280**, 29346-29354
59. Pandhare, J., Cooper, S. K., and Phang, J. M. (2006) *J Biol Chem* **281**, 2044-2052
60. Maxwell, S. A., and Davis, G. E. (2000) *PNAS* **97**, 13009-13014
61. Liu, Y., Borchert, G. L., Donald, S. P., Surazynski, A., Hu, C. A., Weydert, C. J., Oberley, L. W., and Phang, J. M. (2005) *Carcinogenesis* **26**, 1335-1342
62. Maxwell, S. A., and Rivera, A. (2003) *J Biol Chem* **278**, 9784-9789
63. Donald, S. P., Sun, X. Y., Hu, C. A., Yu, J., Mei, J. M., Valle, D., and Phang, J. M. (2001) *Cancer Res* **61**, 1810-1815
64. Walter, T. S., Meier, C., Assenberg, R., Au, K. F., Ren, J., Verma, A., Nettleship, J. E., Owens, R. J., Stuart, D. I., and Grimes, J. M. (2006) *Structure* **14**, 1617-1622

# SCHEME 2.1. Proline Catabolism

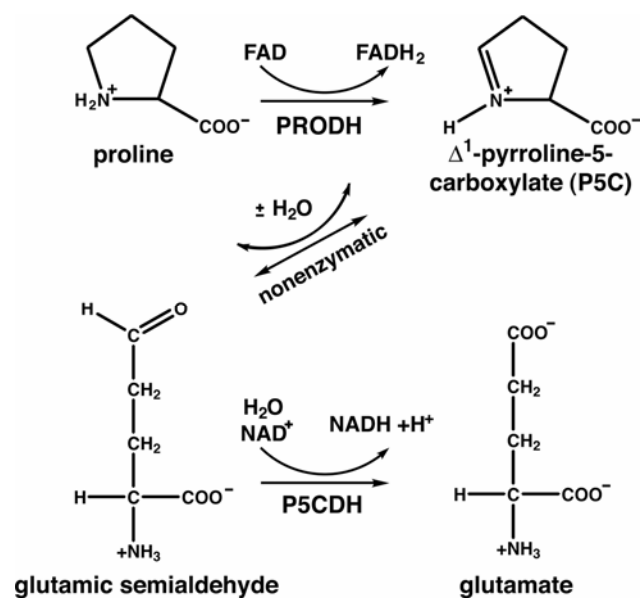


FIGURE 2.1. Ni-NTA Affinity Purification of TtPRODHD. Lanes correspond to the following: 1) Marker (Biorad Precision Plus). 2) 14  $\mu$ L pre-IPTG sample (1 mL of OD<sub>600</sub> = 0.6 cells were pelleted and resuspended in 1 mL H<sub>2</sub>O). 3) 14  $\mu$ L Post-IPTG sample (300  $\mu$ L of induced cells were pelleted and resuspended in 1 mL H<sub>2</sub>O). 4) 2  $\mu$ L Cell free extract. 5) 2  $\mu$ L pellet. 6) 2  $\mu$ L flowthrough. 7) 14  $\mu$ L wash 50 mM imidazole. 8) 14  $\mu$ L wash 75 mM imidazole. 9) 14  $\mu$ L elution 1. 10) 14  $\mu$ L elution 2. 11) 14  $\mu$ L elution 3 12) 14  $\mu$ L elution 4.

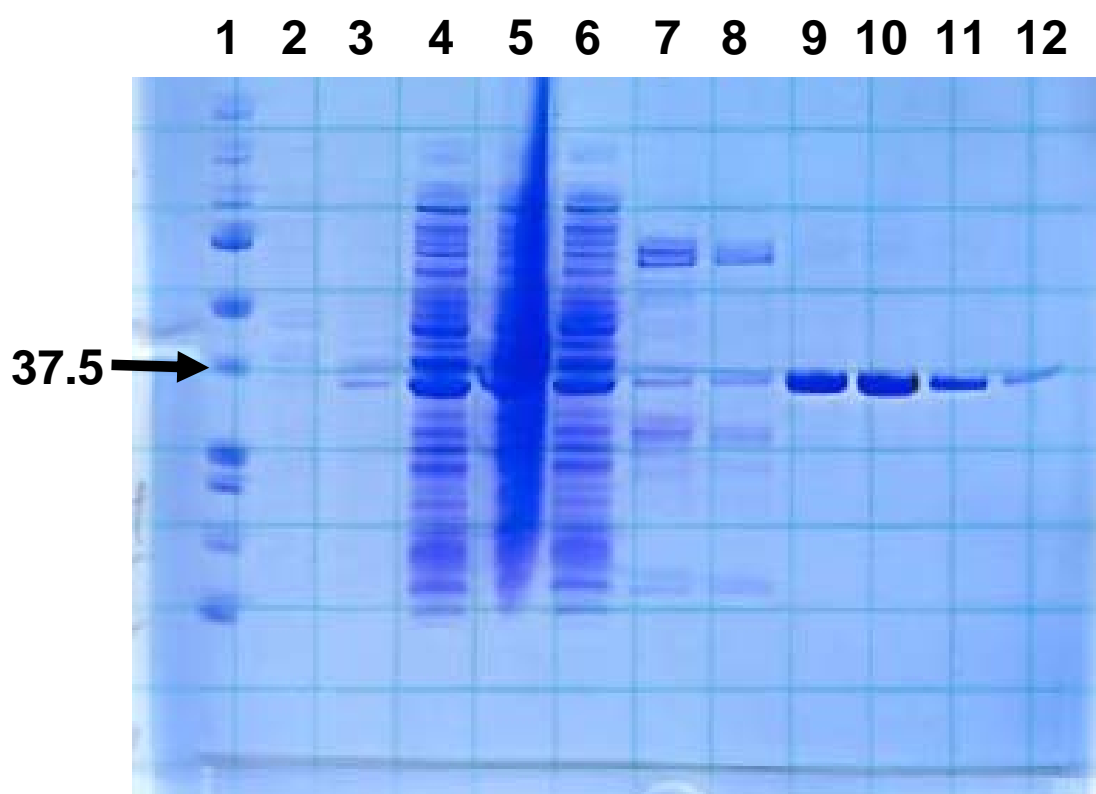


FIGURE 2.2. Initial crystals obtained from crystal screen condition Wizard 4 (35% 2-methyl-2,4-pentanediol, 100 mM Imidazole pH = 8, 200 mM  $\text{MgCl}_2$ ).

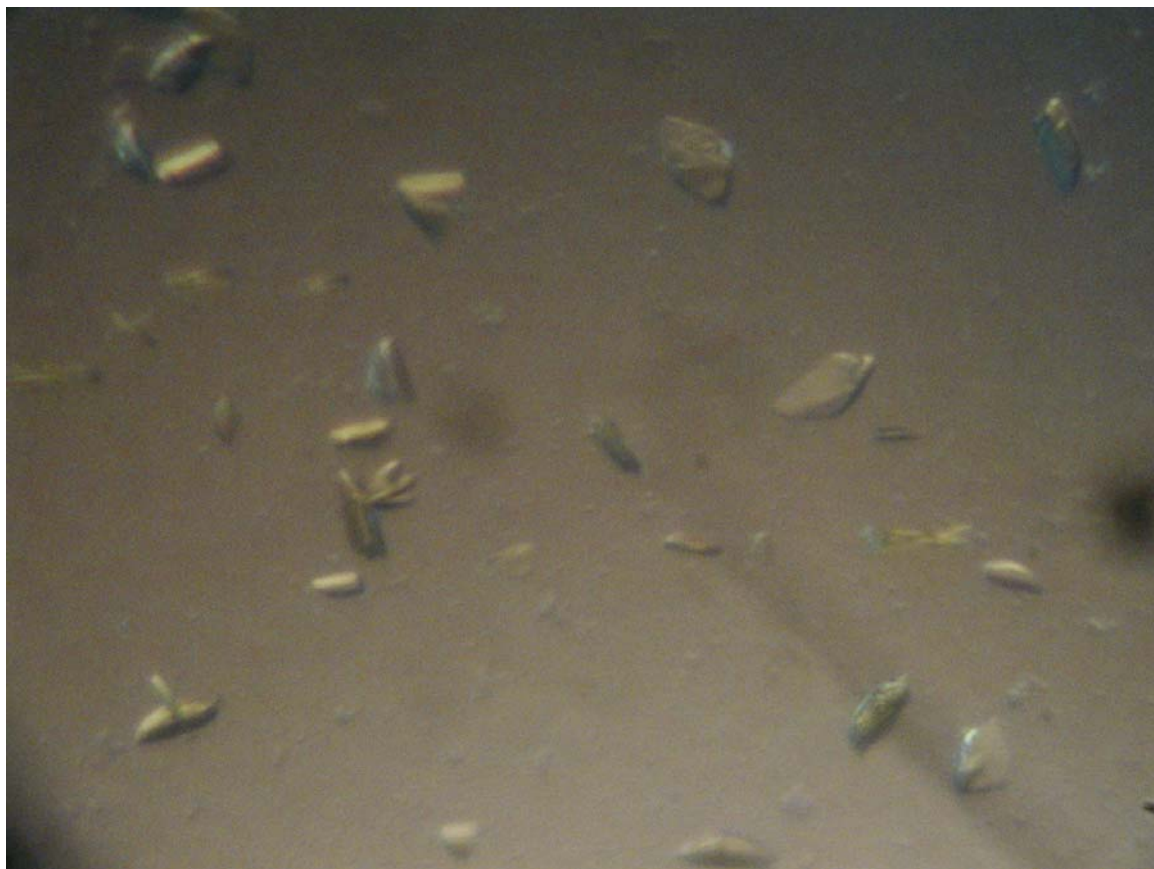


FIGURE 2.3. Optimized TtPRODH MPD crystals which diffract to 2.3 Å (50 mM  $\text{MgCl}_2$ , 100 mM imidazole pH = 7.5, 35 % MPD).

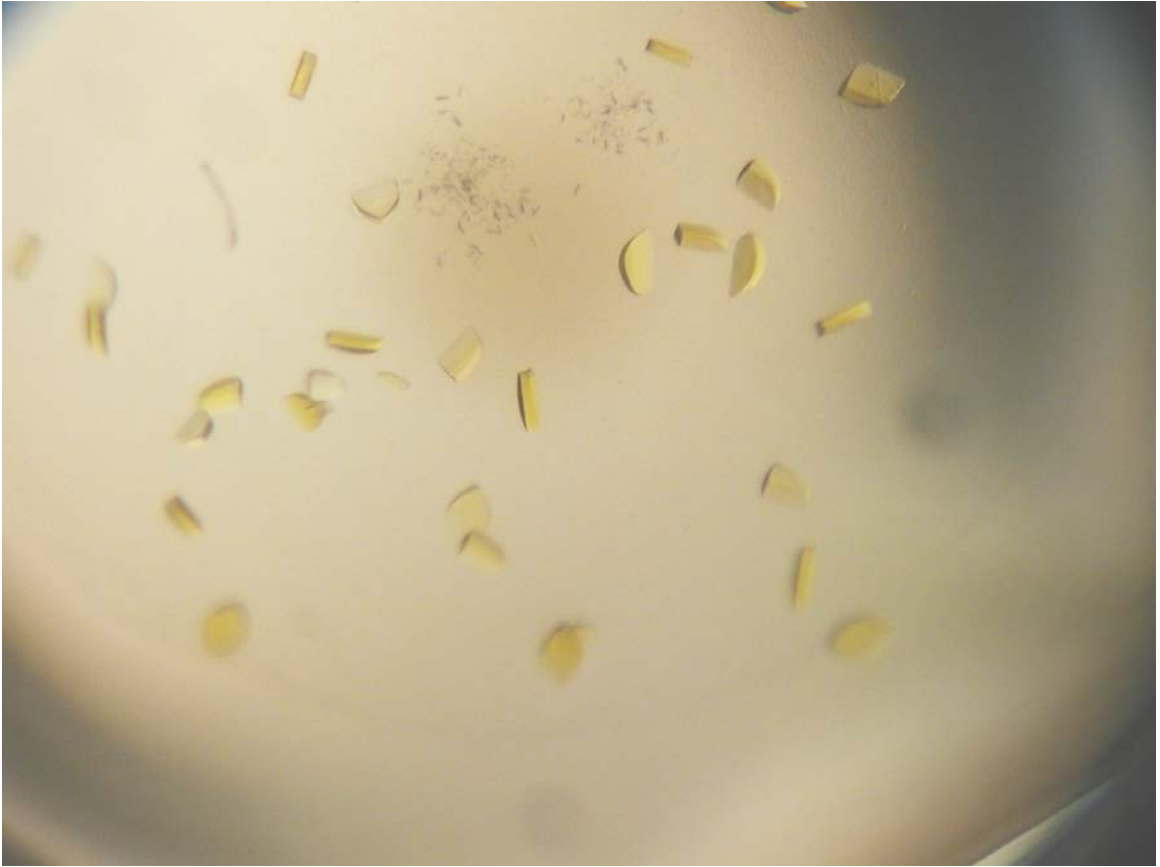
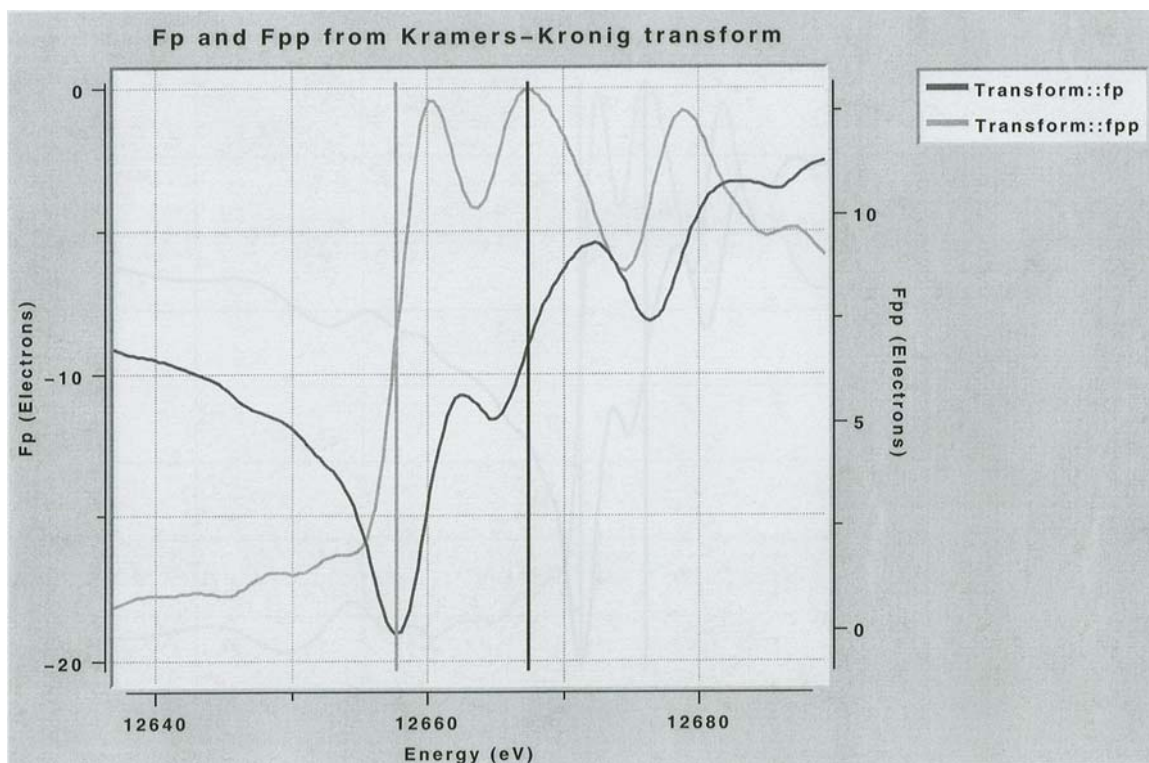


FIGURE 2.4. Selenomethionyl crystals used for structure determination which diffracted to 2 Å (100 mM imidazole pH = 7.0, 100mM MgCl<sub>2</sub>, 17% MPD, 5 mM Dithiothreitol in reservoir and fresh 20 mM N-octyl β-D thioglucopyranoside was added to 3 mg/mL protein).





FIGURE 2.5. Experimental fluorescence spectra determined for selenomethionyl TtPRODHD to utilize the anomalous signal at the peak wavelength of 12666 eV for singlewavelength anomalous diffraction.



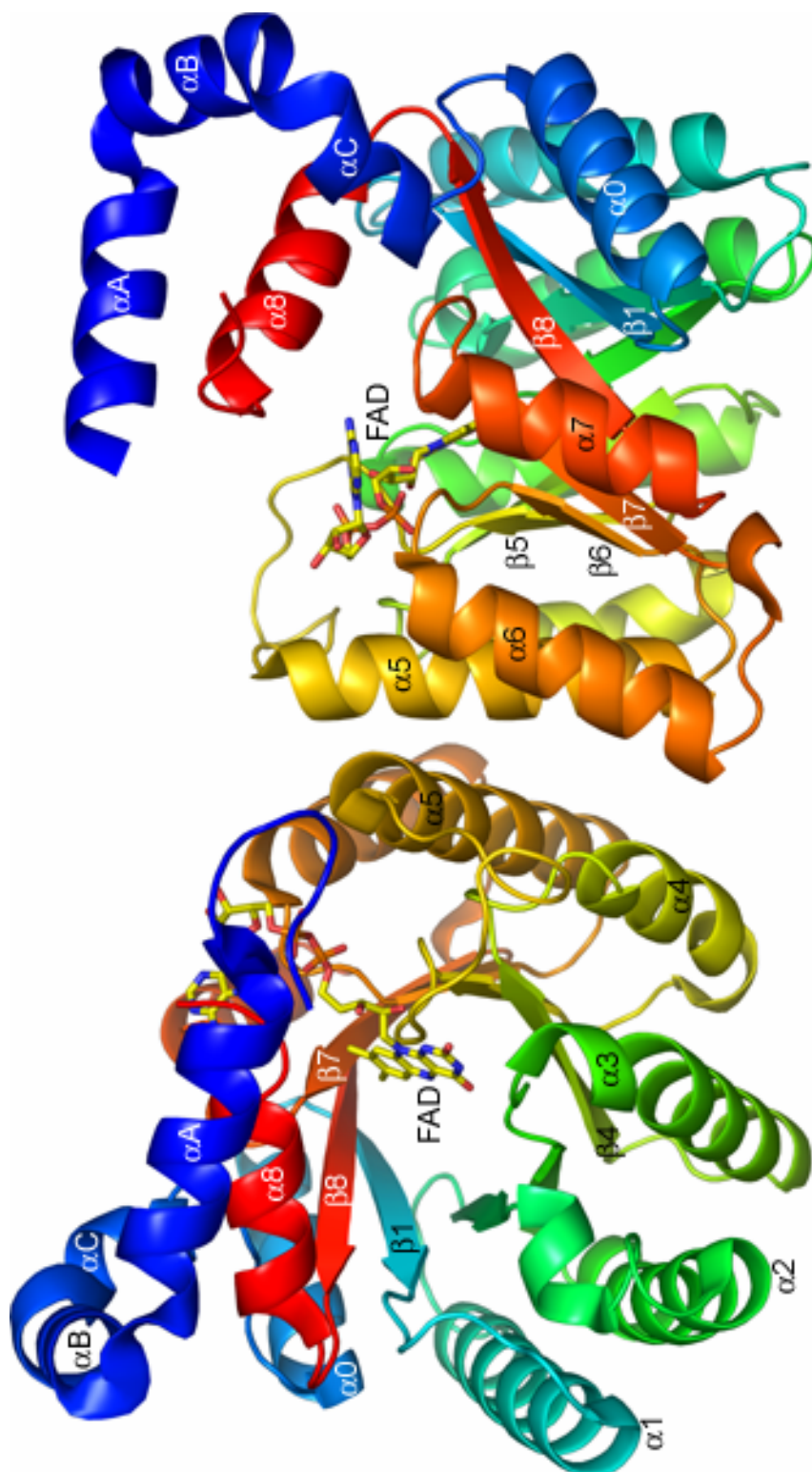


Figure 2.6. Overall structure of TtPRODH. Ribbon drawing of the two TtPRODH molecules in the asymmetric unit. The protein chains are colored in the rainbow scheme, with dark blue at the N-terminus and red at the C-terminus. Selected  $\alpha$ -helices and  $\beta$ -strands are labeled. The FADs are drawn as stick models in yellow. The glycine hinge between  $\beta 8$  and  $\alpha 8$  is noted (Gly279).

FIGURE 2.7. The solvent exposed hydrophobic patch formed by  $\alpha$ -helices A, B, C and 8. The orientation is similar to that of the right hand protein in FIGURE 2.6. Hydrophobic side chains of the patch are colored green.

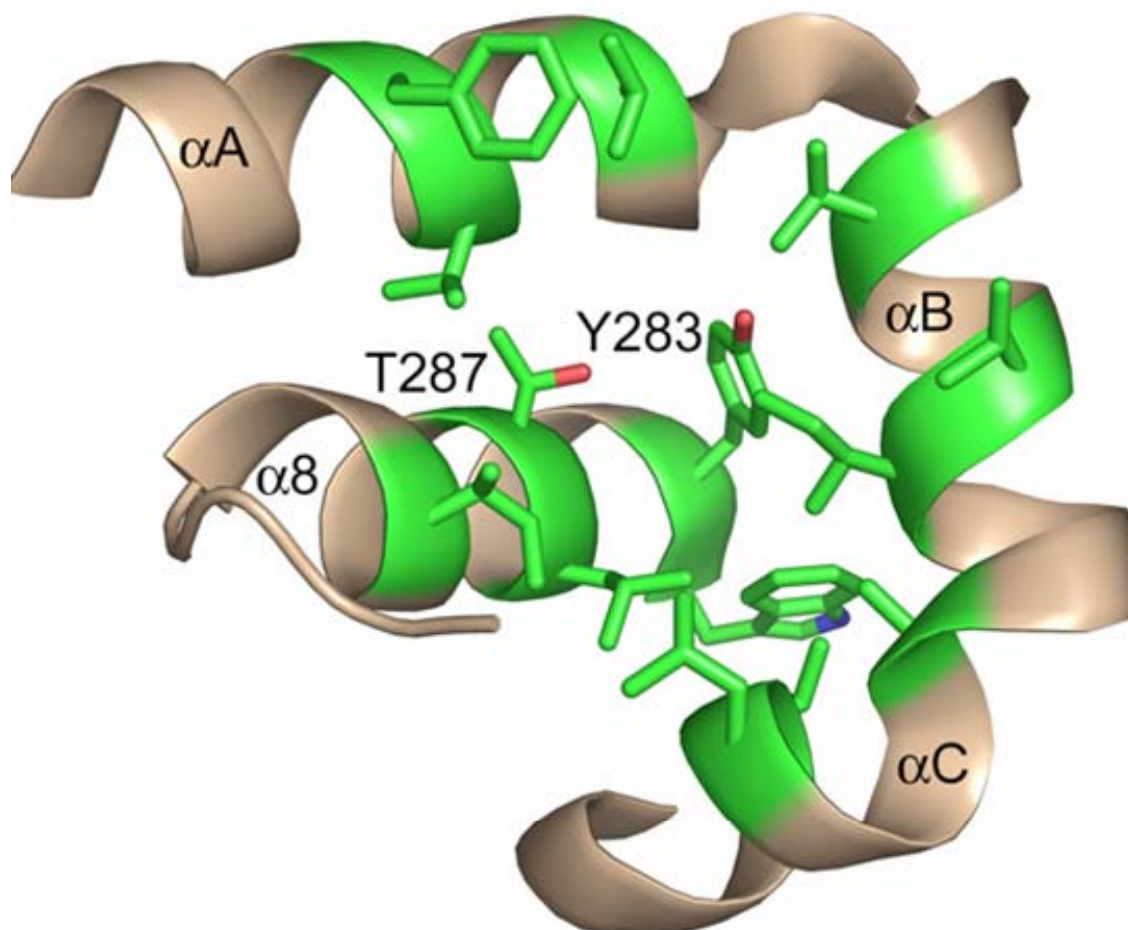
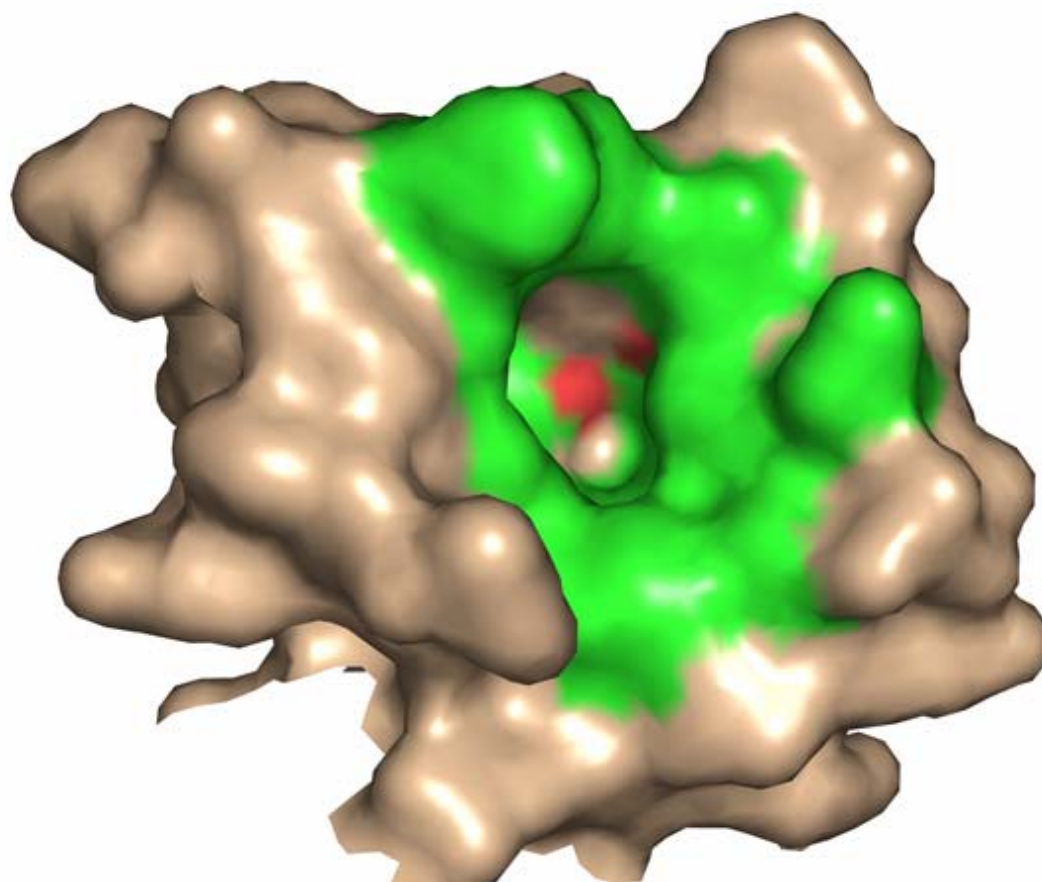


FIGURE 2.8. Surface representation of the hydrophobic patch. The orientation is identical to that of FIGURE 2.7.



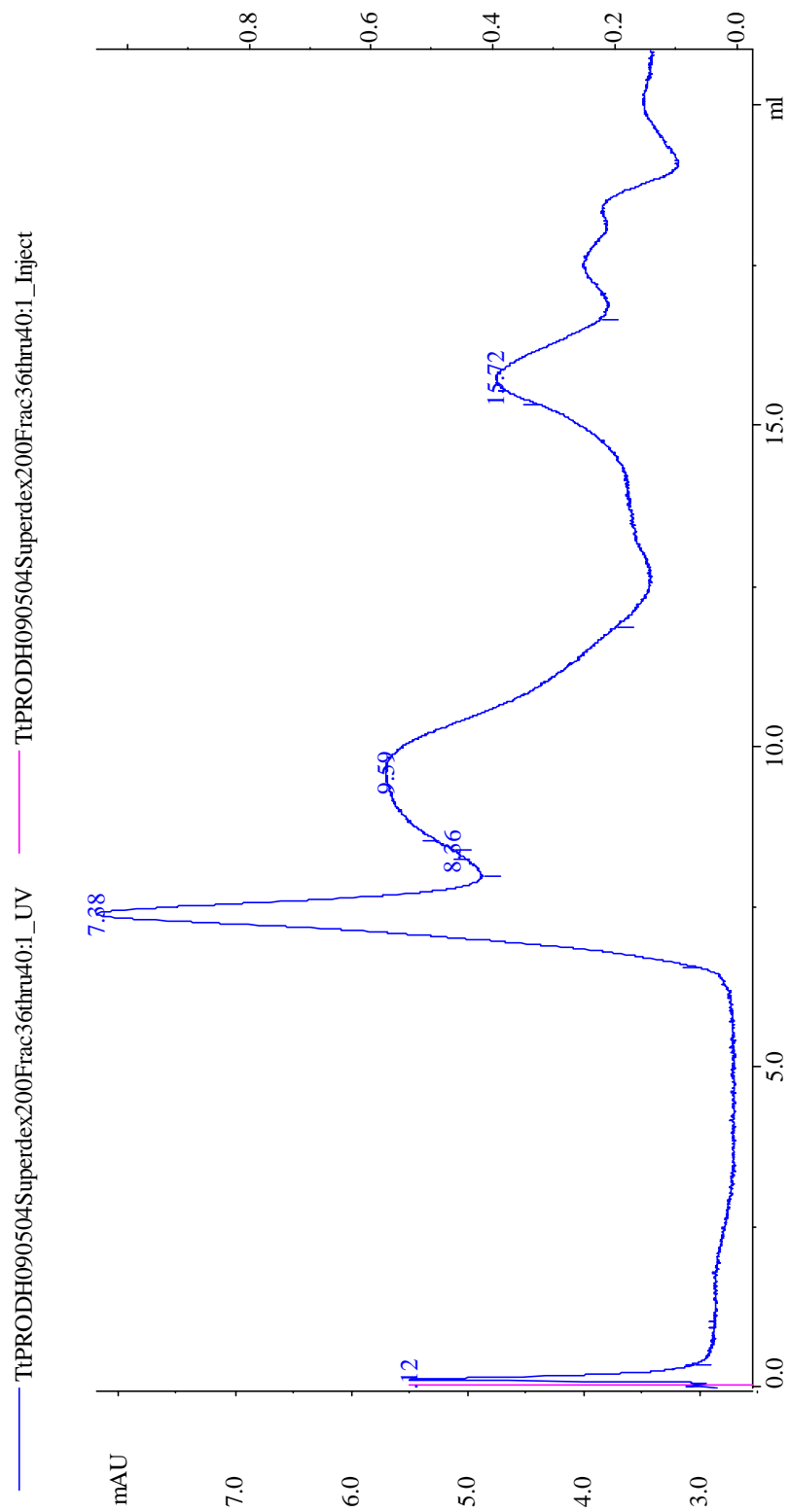


FIGURE 2.9. Gel filtration profile of soluble aggregated TtPRODH in 50 mM Tris pH 8, 50 mM NaCl, 0.5 mM EDTA, 0.5 mM DTT, and 5 % glycerol.

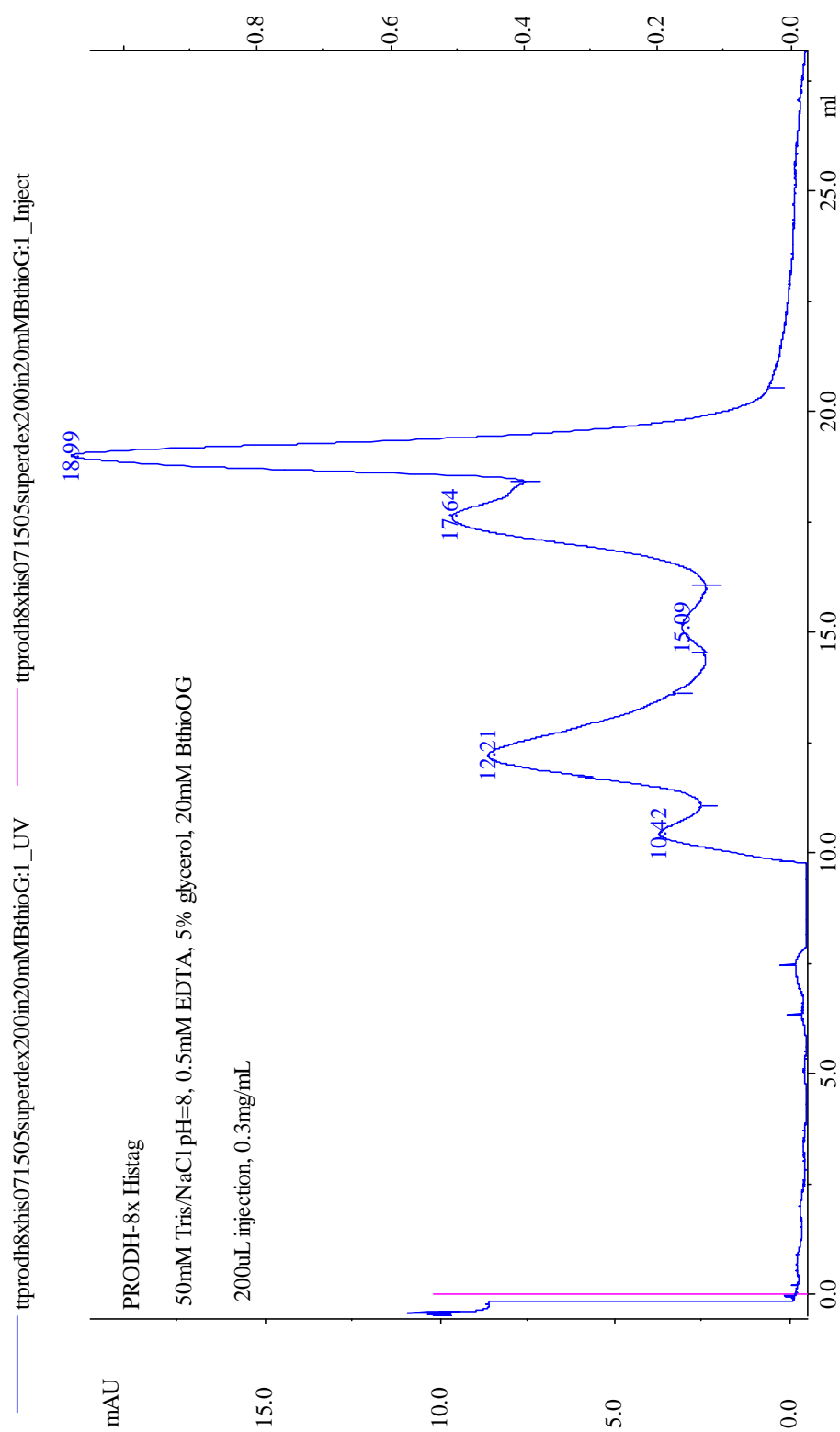


FIGURE 2.10. Gel filtration profile of TtPRODH upon addition of 20 mM n-octyl- $\beta$ -glucopyranoside in 50 mM Tris pH 8, 50 mM NaCl, 0.5 mM EDTA, 0.5 mM DTT, and 5 % glycerol.



FIGURE 2.11. Superposition of TtPRODHD (blue) and PutA86-669/THFA (white, PDB code 1TIW). The FAD cofactors of TtPRODHD and PutA86-669 are colored yellow and green, respectively. Glu65 of TtPRODHD is drawn in stick mode. Trp438 of PutA86-669, which stacks against the FAD adenine, is also drawn. The dashed lines indicate the Glu289-Arg555 ion pair in PutA86-669.

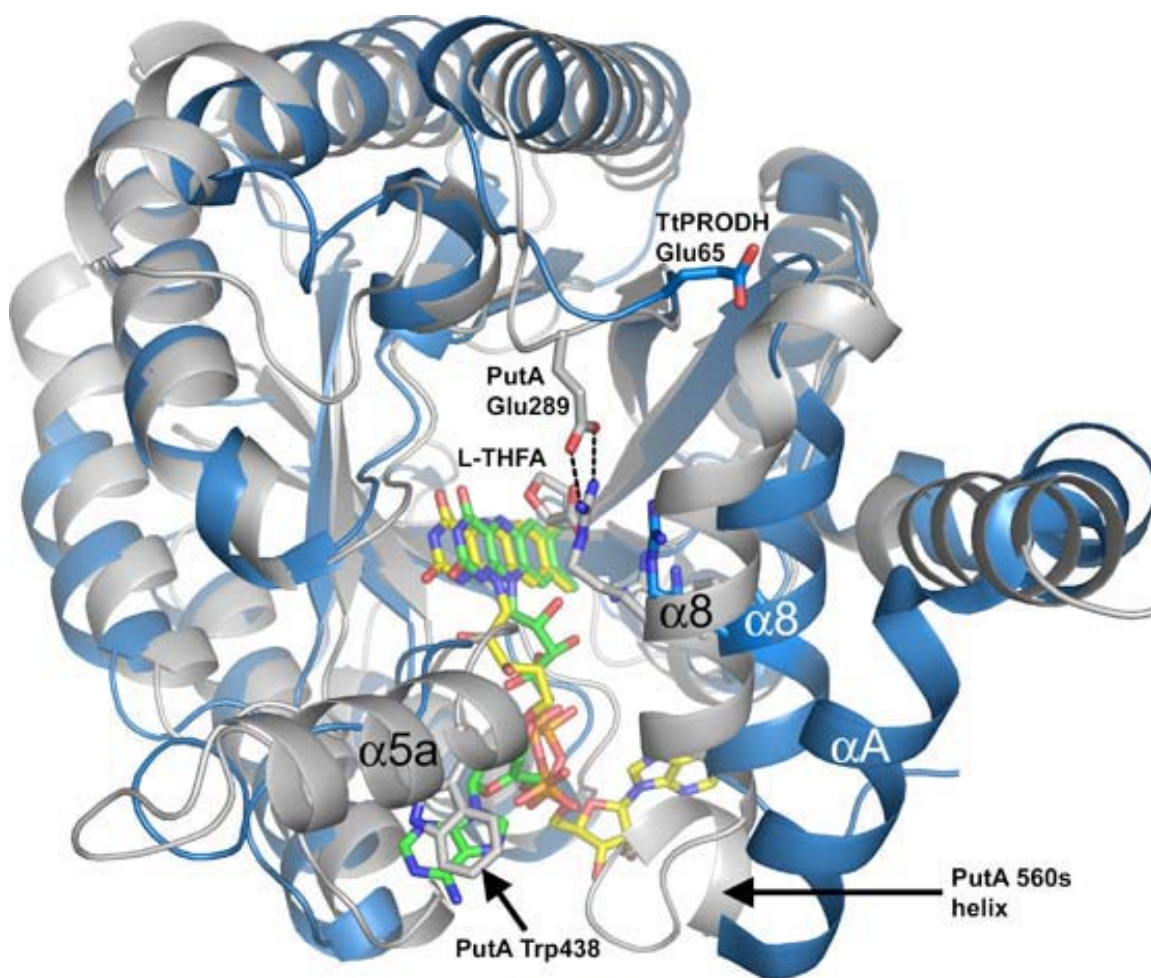


FIGURE 2.12. Stereographic drawing of protein-FAD interactions in TtPRODHD. The dotted lines indicate hydrogen bonds and ion pairs. The FAD is colored yellow. Residues interacting with FAD are colored green. Strands  $\beta 4$  and  $\beta 6$  are indicated.

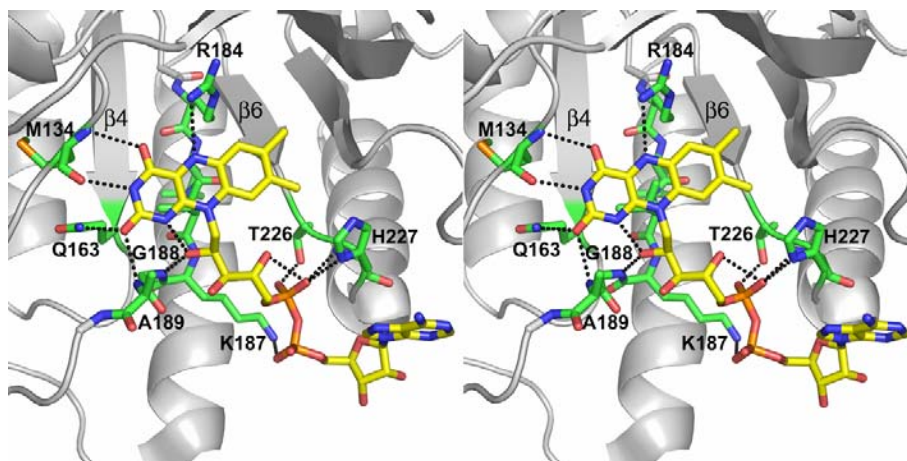




FIGURE 2.13. Schematic of TtPROD<sub>H</sub> interactions with FAD. Bacterial PutA/PROD<sub>H</sub> completely conserved interactions are boxed with the corresponding motif listed.

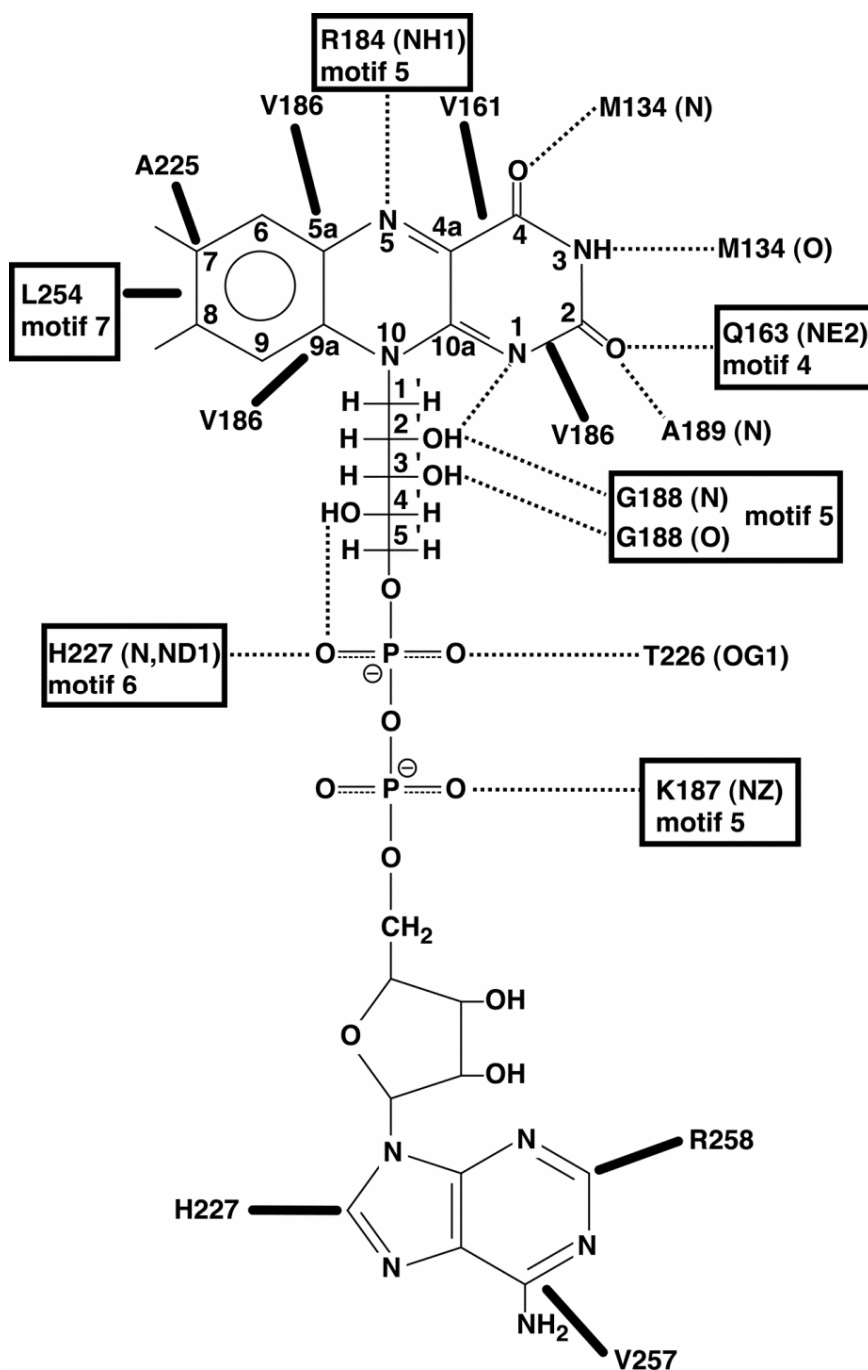


FIGURE 2.14. Two views of the FAD from TtPRODHD covered by an experimental electron density map ( $1\sigma$ ). The map was calculated using  $|F_{\text{obs}}|$  and experimental phases after density modification.

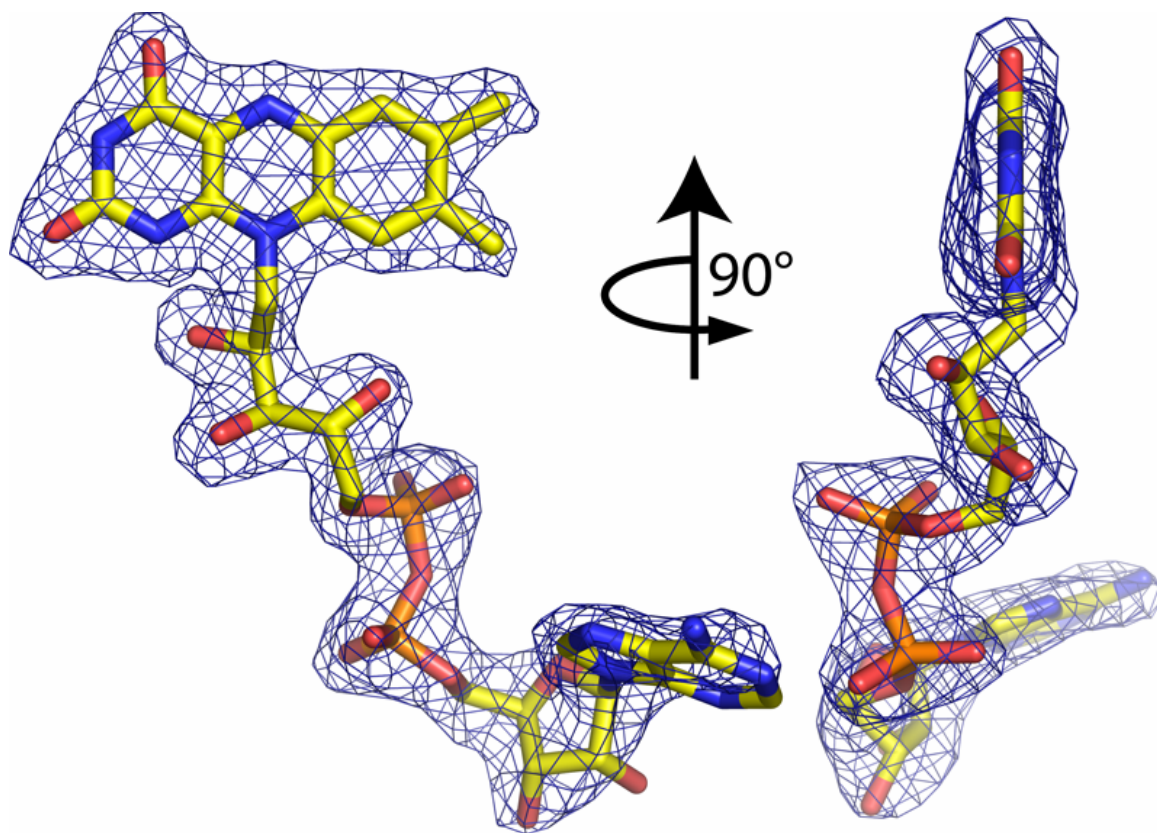


FIGURE 2.15. Superposition of the FAD cofactors from TtPRODHD (yellow C atoms, orange P atoms), PutA86-669/THFA (green C atoms, cyan P atoms) and dithionite-reduced PutA86-669 (white C atoms, cyan P atoms). The 2'-OH and 4'-OH groups of TtPRODHD are indicated. Note that the 2'-OH groups of TtPRODHD and dithionite-reduced PutA86-669 superimpose nearly perfectly, whereas the 2'-OH group of PutA86-669/THFA points toward the viewer. The orange dotted lines denote hydrogen bonds in the TtPRODHD cofactor. The black dotted lines denote hydrogen bonds in the PutA86-669 cofactors. The 3'-OH hydrogen bond to the ribose is present in both PutA86-669 structures but only one dotted line is drawn for clarity.

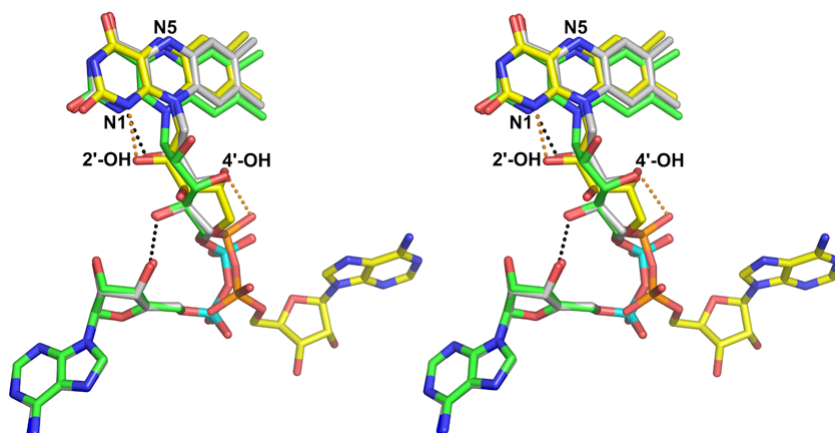


FIGURE 2.16. Comparison of the active sites of TtPRODHD (yellow) and PutA86-669/THFA (white). This stereoview emphasizes differences between the two enzymes in interactions with the pyrophosphate and adenosine moieties. Residues are labelled as TtPRODHD/PutA86-669. The orange and black dotted lines denote hydrogen bonds in TtPRODHD and PutA86-669, respectively.

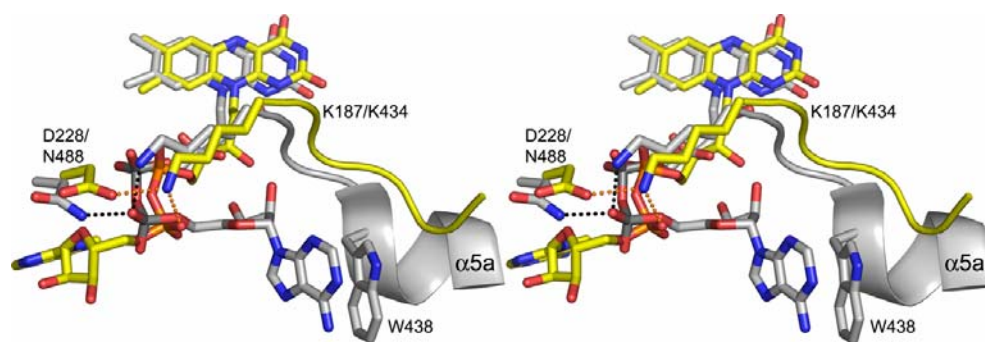


FIGURE 2.17. Comparison of the active sites of TtPRODHD (yellow) and PutA86-669/THFA (white). This stereoview shows differences between the two enzymes in the proline-binding pocket. The inhibitor THFA is shown in green. Residues are labelled as TtPRODHD/PutA86-669. The orange and black dotted lines denote hydrogen bonds in TtPRODHD and PutA86-669, respectively. For clarity, Y275/Y540, which form hydrogen bonds with D133/D370, are not labeled.

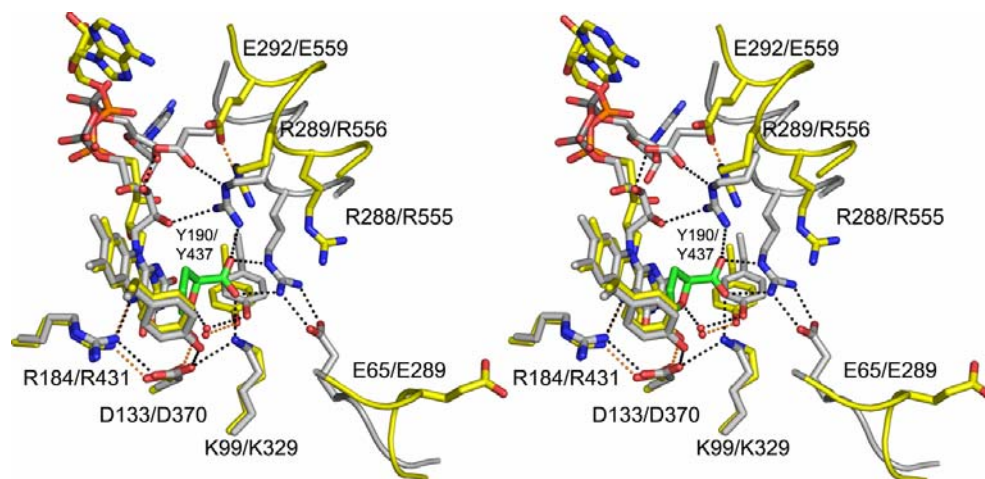


FIGURE 2.18. Space-filling representation of TtPRODHD emphasizing solvent exposure of the FAD (yellow). Helix  $\alpha 8$  is colored magenta. Tyr190 is shown in green. The orientation is similar to that of FIGURE 2.11.

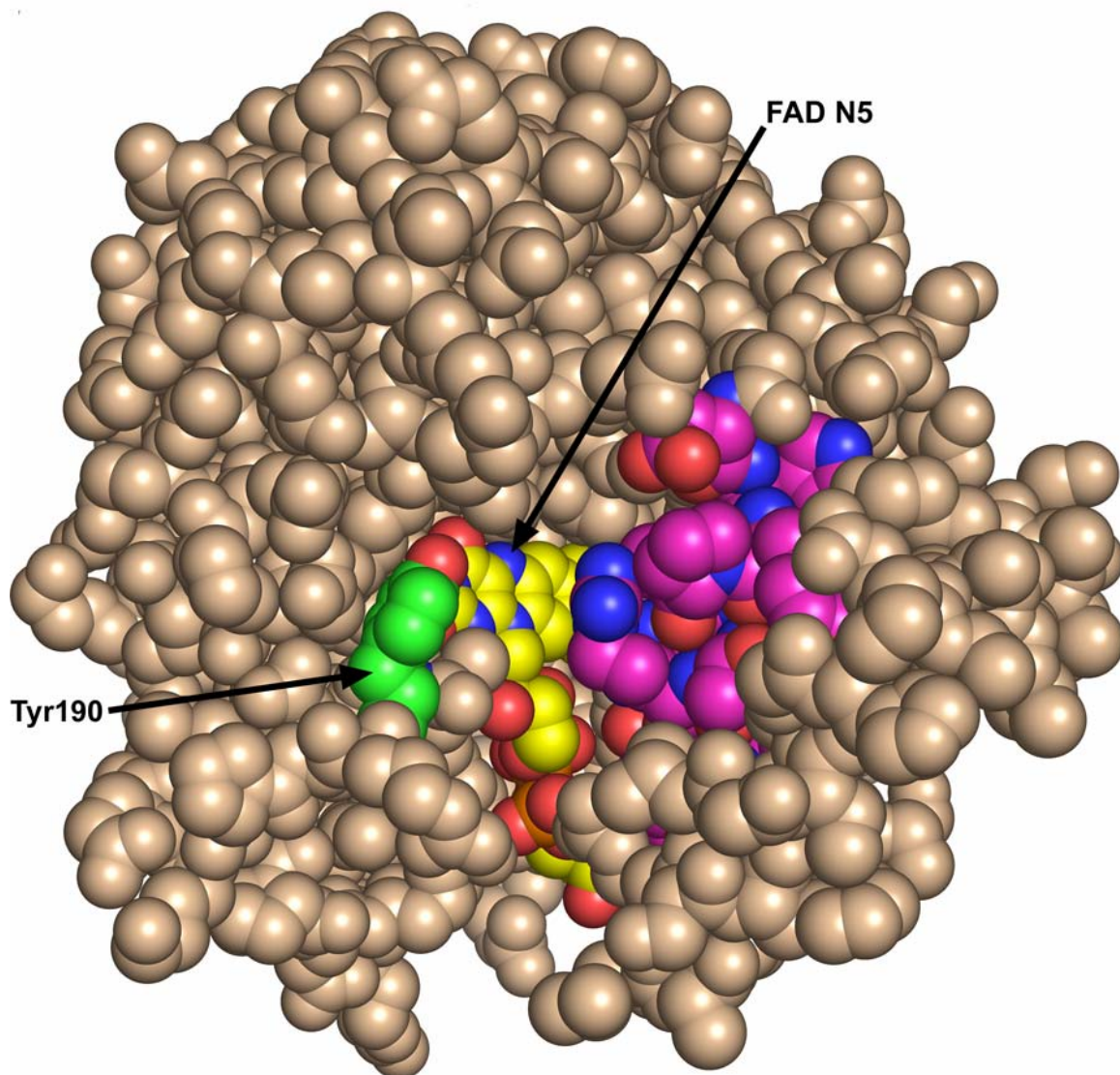




FIGURE 2.19. Comparison of active site solvent exposure in TtPRODH (top) and EcPutA (bottom) PRODH. These two structures were superimposed and then surface rendered with FAD in yellow CPK spheres.

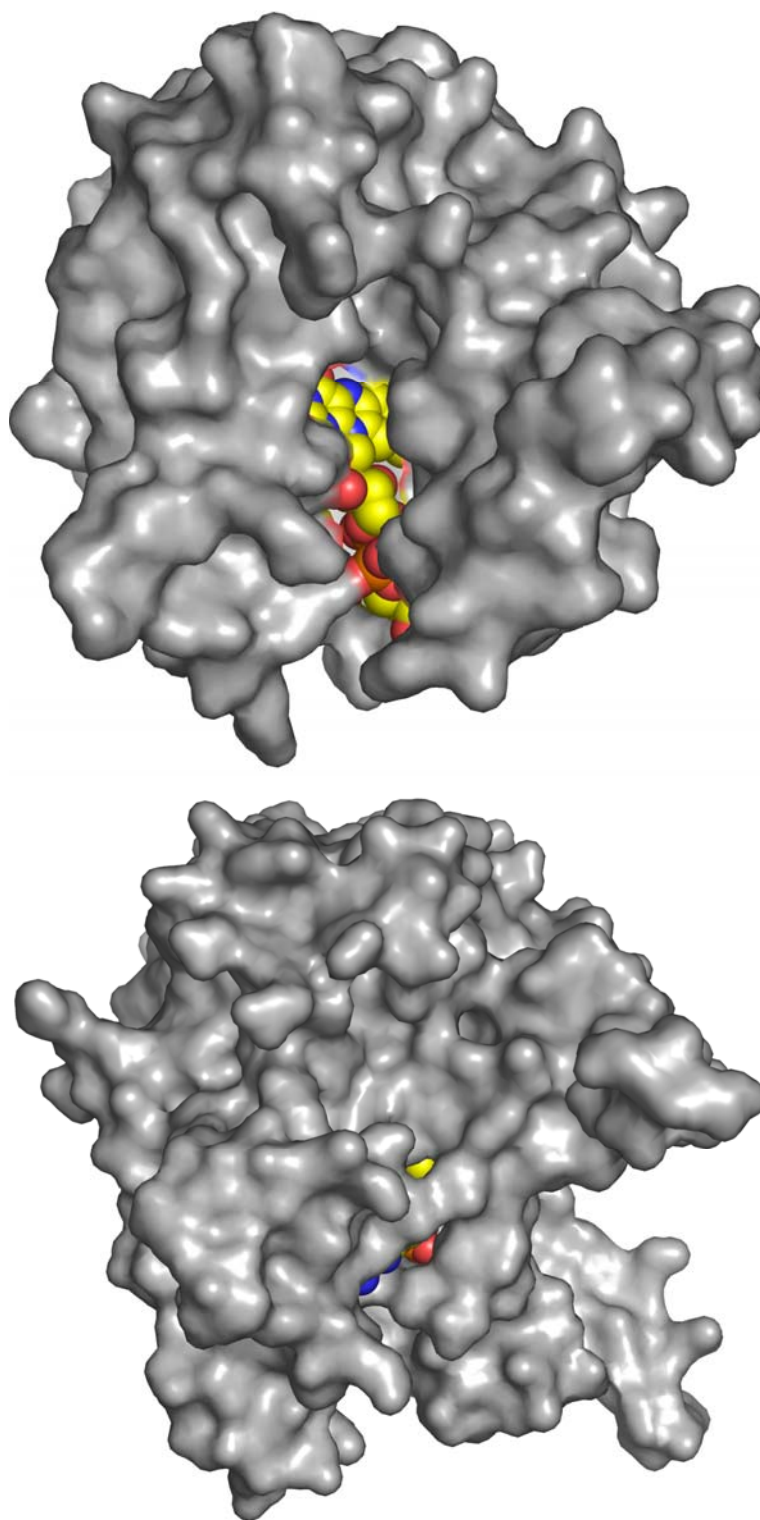


FIGURE 2.20. Locations of 2-methyl-2,4-pentanediol (MPD) in TtPRODH chain A while viewing the electrostatic surface potential. These MPD molecules occur in the same location in chain B. MPD 3 binds the N-terminal ends of the strands and is shown here on the right in yellow CPK sticks. MPD 4 is shown on the left in yellow CPK sticks.

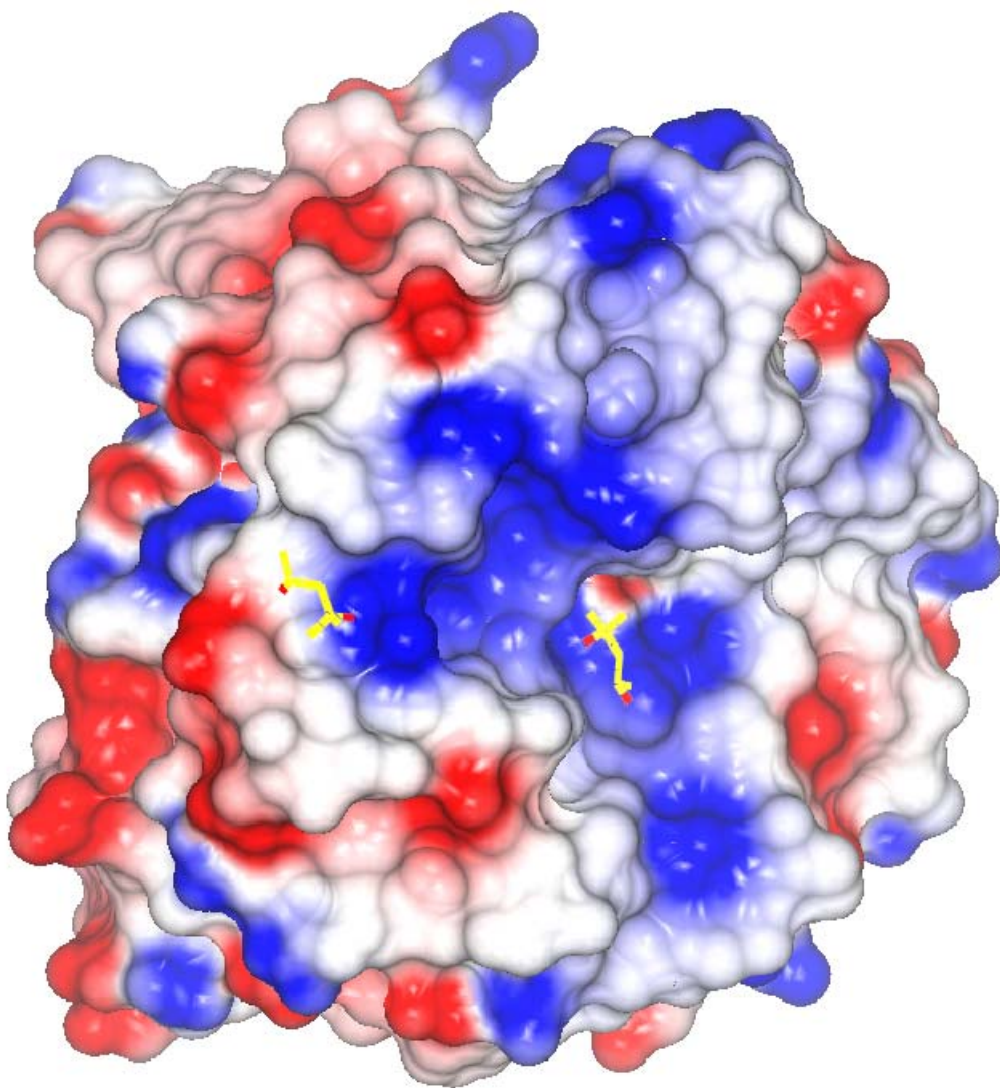




FIGURE 2.21. TtPRODHD electrostatic surface potential surrounding MPD site 1. Blue surface indicates areas of positive potential and red areas indicate areas of negative potential. MPD in site 1 is shown in yellow.

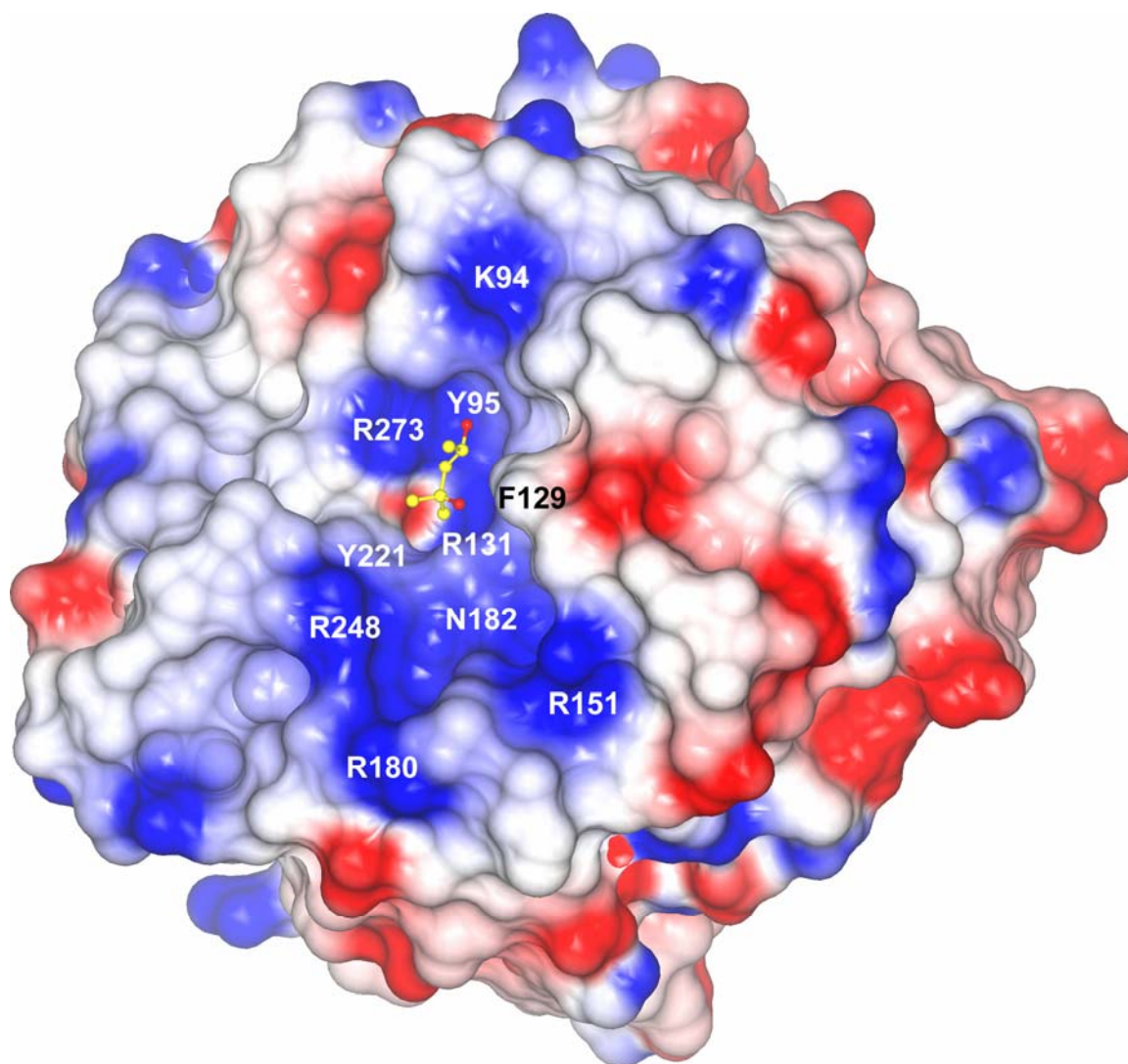


FIGURE 2.22. Proposed electron transfer pathway for TtPRODHD catalyzed oxidation of proline. To transfer electrons from reduced FADH<sub>2</sub> to electron acceptors in the membrane, the enzyme could utilize charged residues such as conserved R184, Q252, E250 and R273. R184 is shown in light orange CPK sticks, Q252 is shown in light green CPK sticks, E250 is shown in teal CPK sticks and R273 is shown in salmon CPK sticks. FAD and MPD are shown in yellow and green CPK spheres, respectively. For clarity, some of the ( $\beta\alpha$ )<sub>8</sub> barrel has been removed.

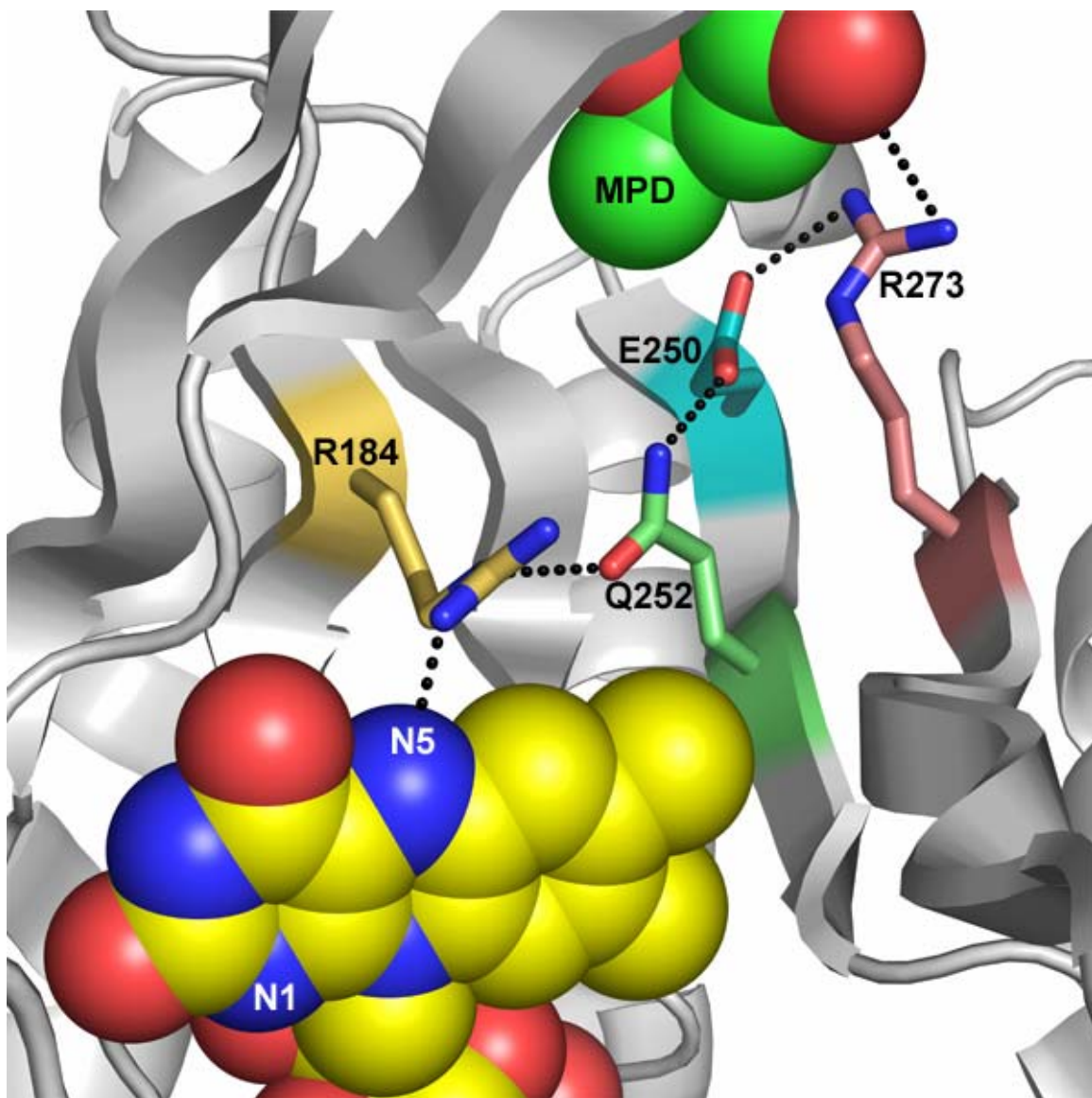


FIGURE 2.23. Proline reduction of TtPROD<sub>H</sub>. Red line is oxidized TtPROD<sub>H</sub>. Purple line is reduced with 500 mM L-proline after 1min. Maroon line is the same reduced TtPROD<sub>H</sub> sample after 16 hours.

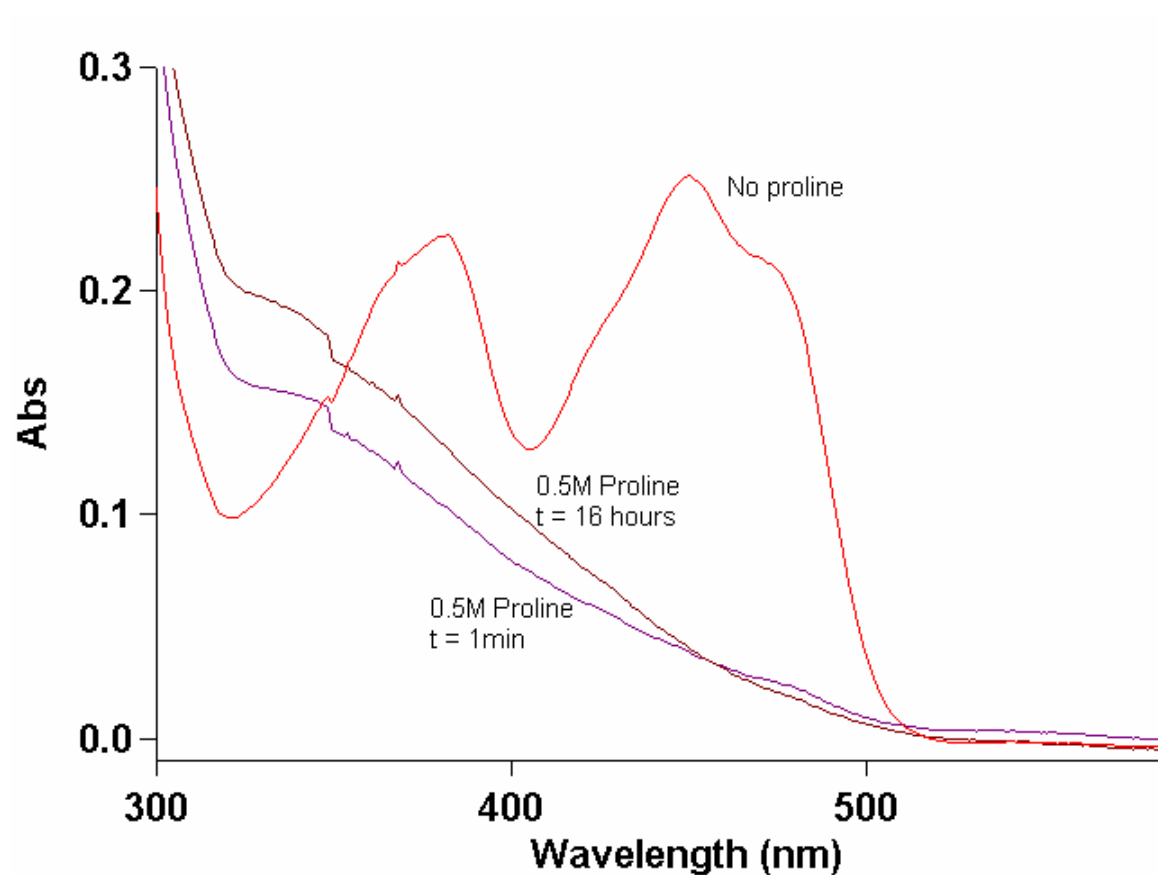


FIGURE 2.24. High salt crystal form of TtPROD<sub>H</sub> (2 M Na K Tartrate, 100 mM Tris pH = 8.5, 0.5 % PEG 5000 MME, 4 % acetone (or 3% isopropanol) in reservoir and fresh 20 mM N-octyl  $\beta$ -D thioglucopyranoside was added to the 3 mg/mL protein).

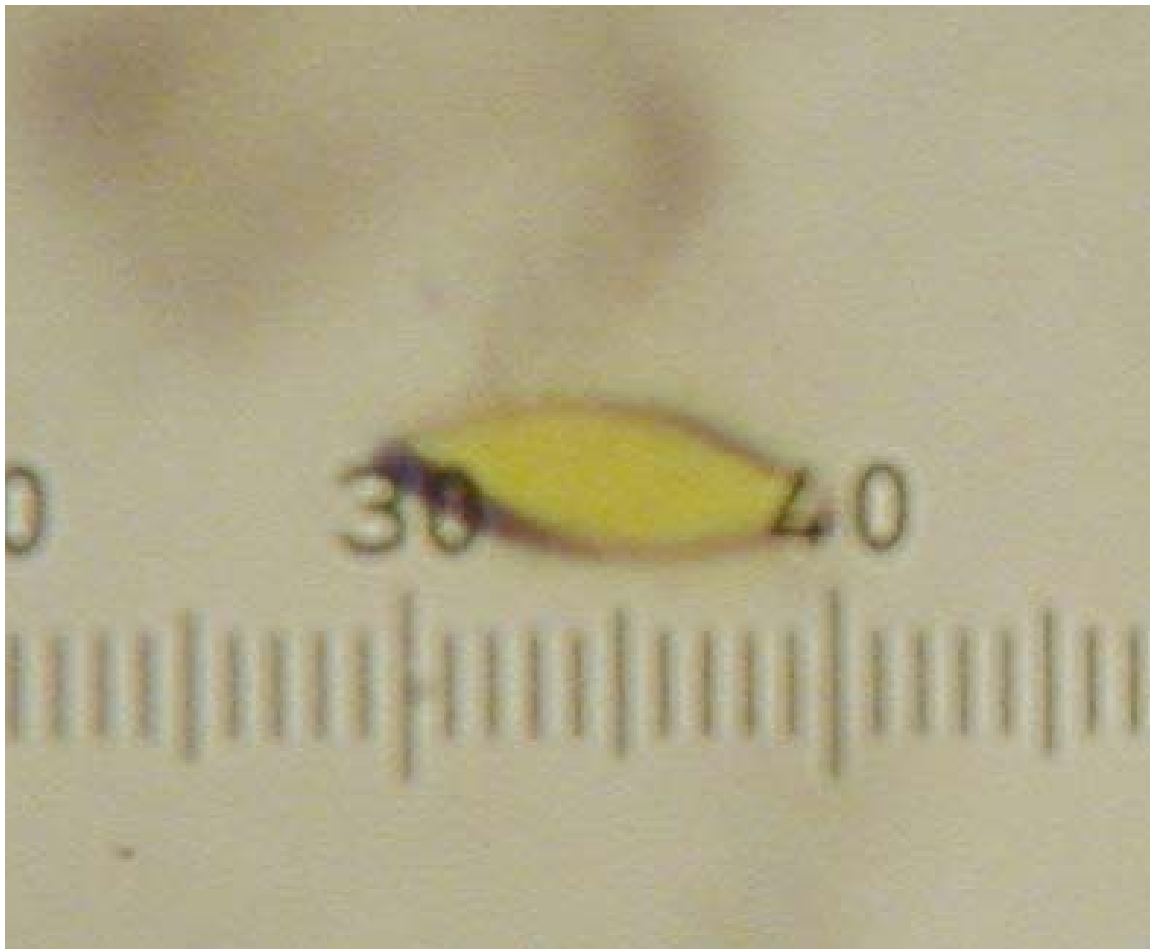


FIGURE 2.25. High salt crystal form of TtPRODH reduced with L-proline (s). (2 M Na K tartrate, 100 mM Tris pH = 8.5, 0.5 % PEG 5000 MME, 4 % acetone (or 3% isopropanol) in reservoir and fresh 20 mM N-octyl  $\beta$ -D thioglucopyranoside was added to the 3 mg/mL protein).

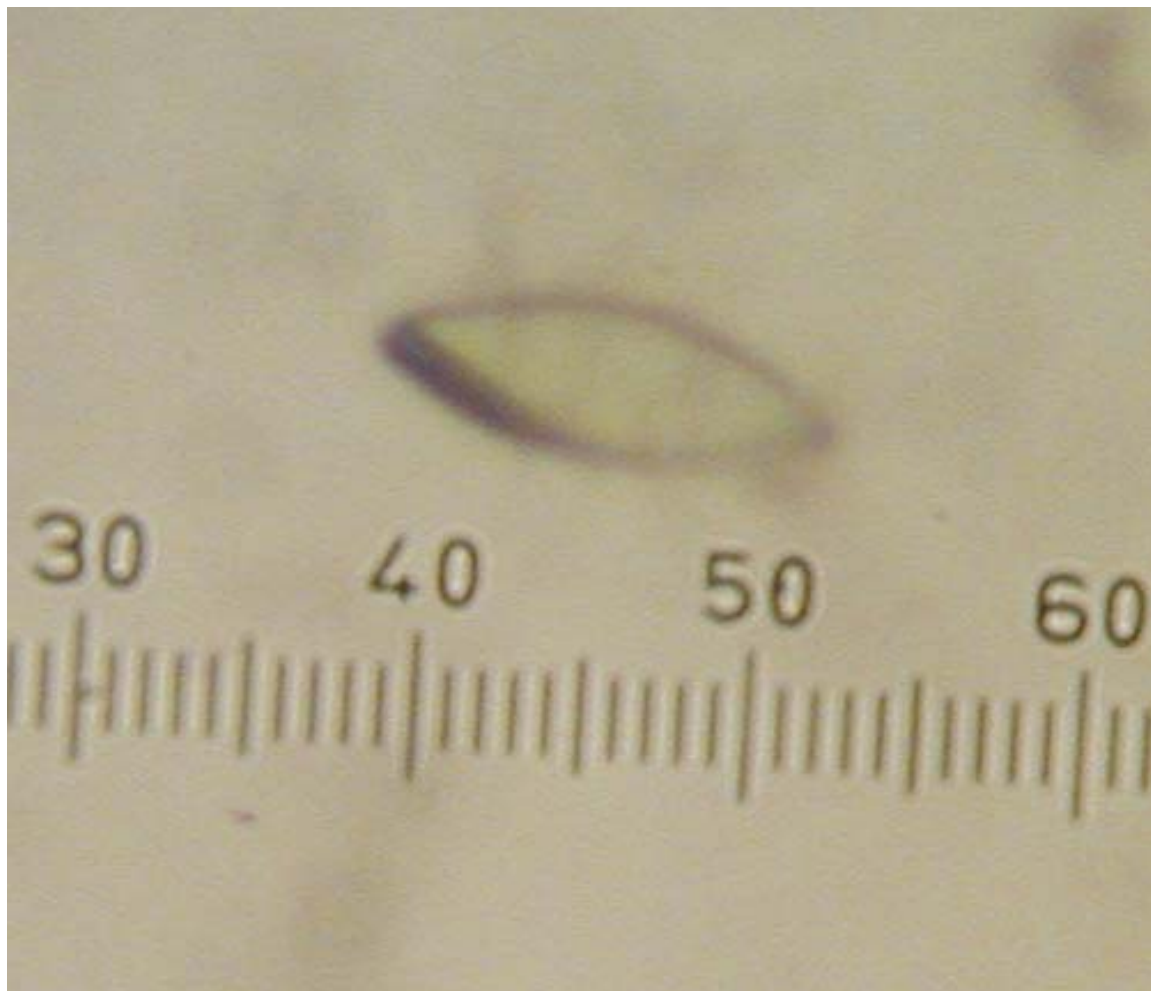


FIGURE 2.26. Potentiometric titration of TtPRODH (25 mM) at 20 °C (pH 7.5). Curves 1-11 correspond to fully oxidized, -0.041 V, -0.050 V, -0.063 V, -0.071 V, -0.08 V, -0.092 V, -0.098 V, -0.111 V, -0.118 V, and fully reduced, respectively. The inset is a Nernst plot of the potentiometric data, which yielded a midpoint potential of  $E_m = -0.075$  V with slope of 35 mV.

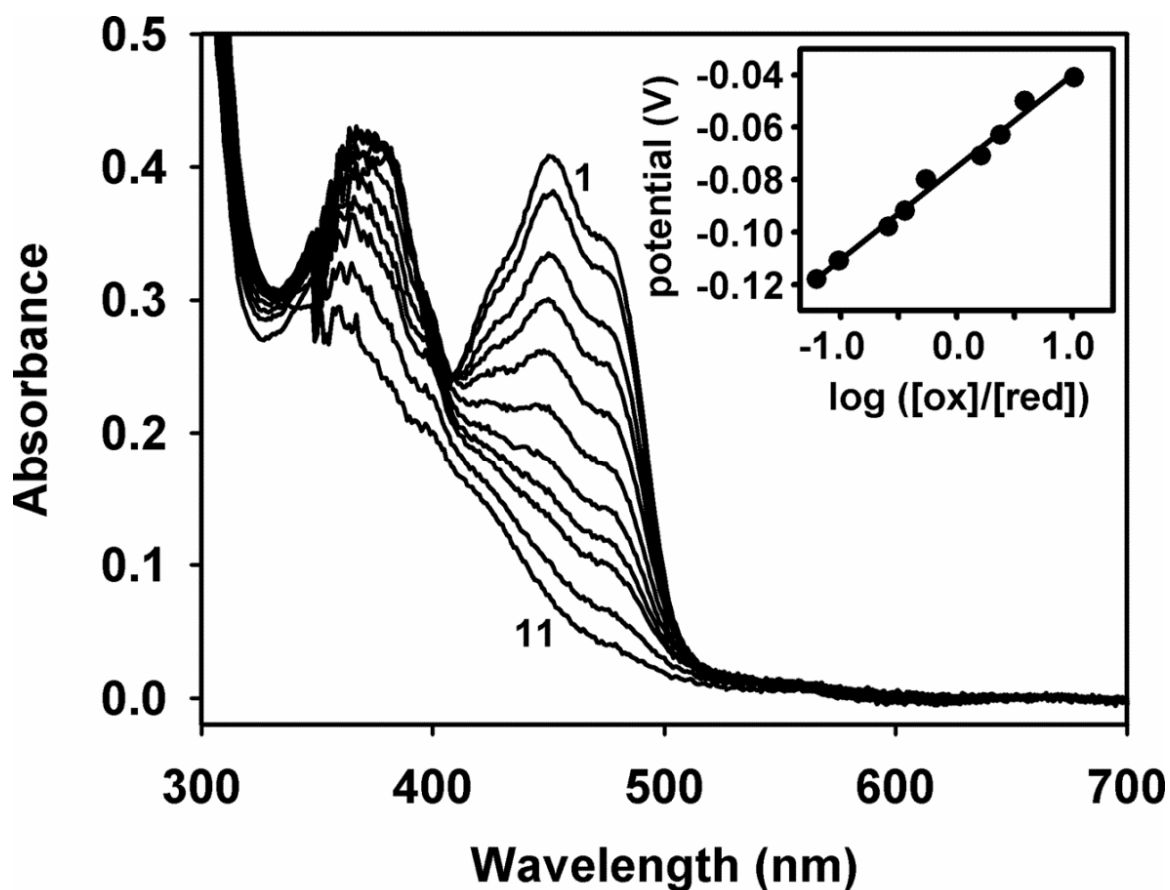


FIGURE 2.27. Steady-state kinetic parameter determination at 25°C for TtPRODH catalysis of L-proline using DCPIP assay. Plot generated with Origin 7.0.

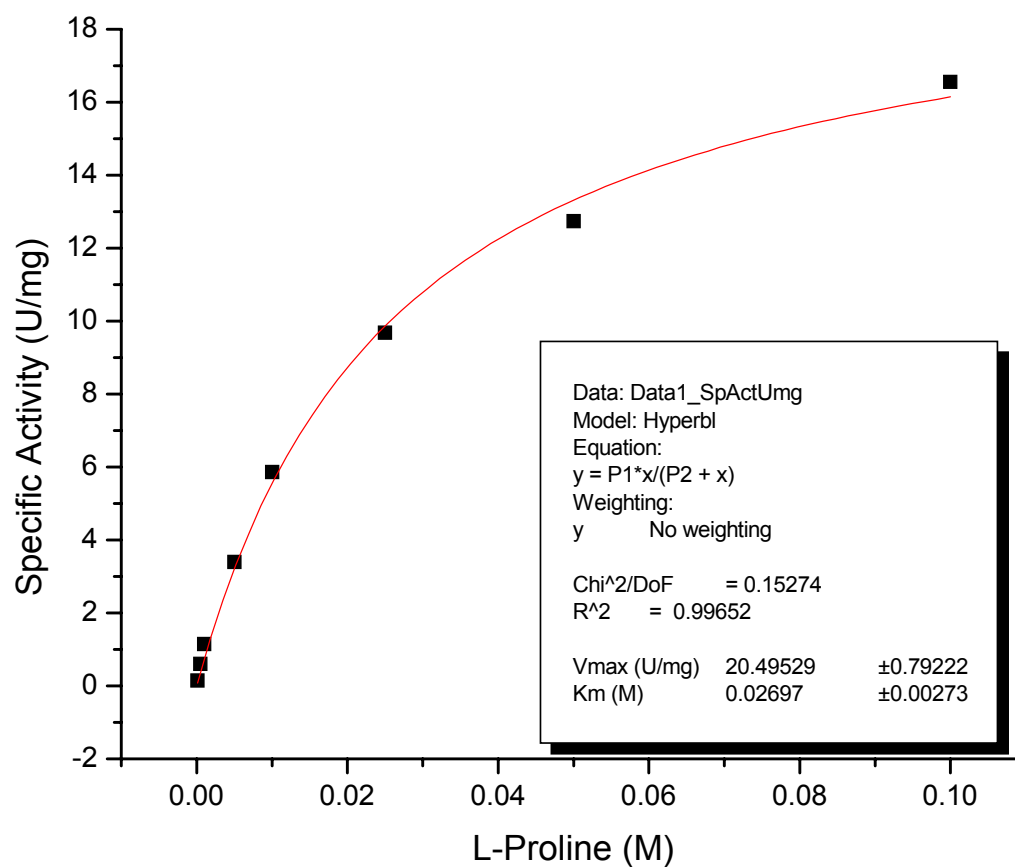


FIGURE 2.28. Steady-state kinetic parameter determination at 25°C for TtPRODHD catalysis of 3,4-dehydro-L-proline using DCPIP assay. Plot generated with Origin 7.0.

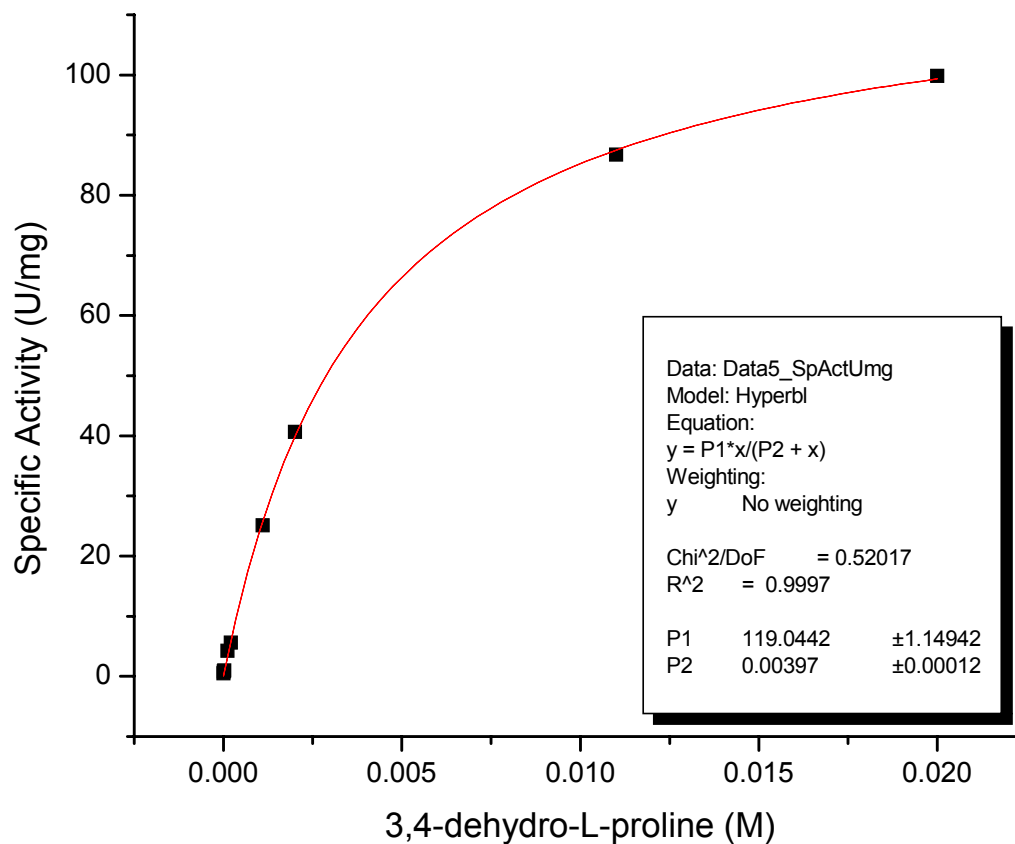




FIGURE 2.29. Determination of inhibition constant for L-Tetrahydrofuroic Acid. at 25°C using DCPIP assay. Plot generated with Origin 7.0

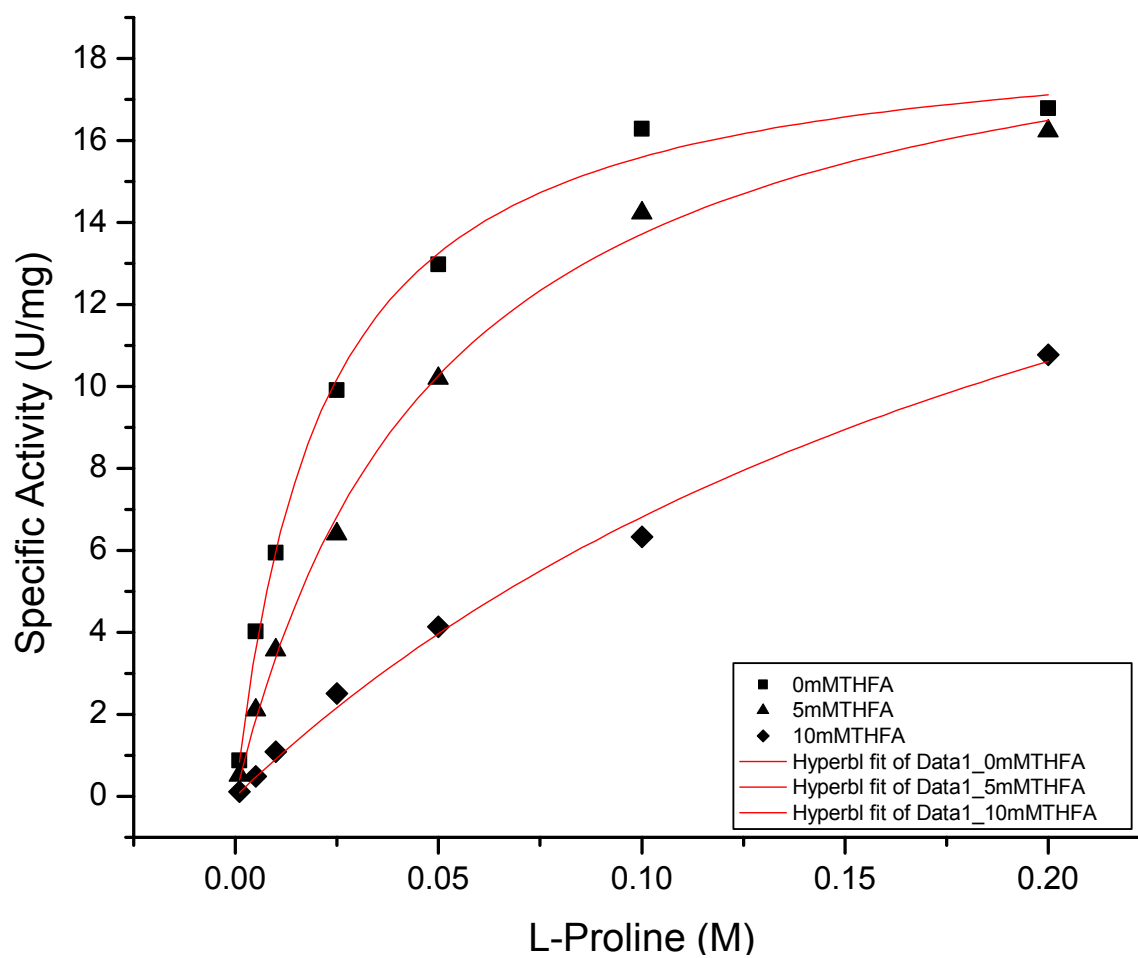


FIGURE 2.30. Determination of inhibition Constant of mandelate at 25°C using DCPIP assay. Plot generated with Origin 7.0.

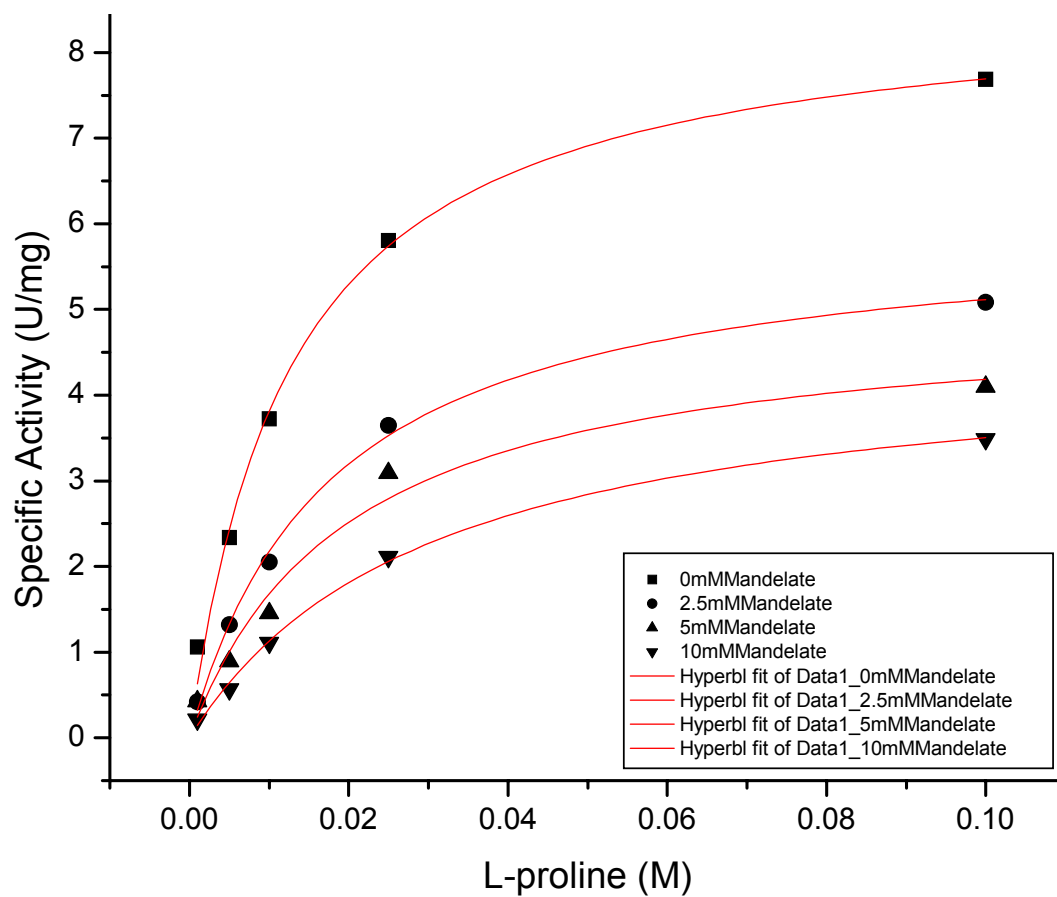


FIGURE 2.31. Thermostability analysis of TtPROD<sub>H</sub>. The percent activity remaining after incubation of the enzyme at 90 °C is plotted as a function of incubation time.

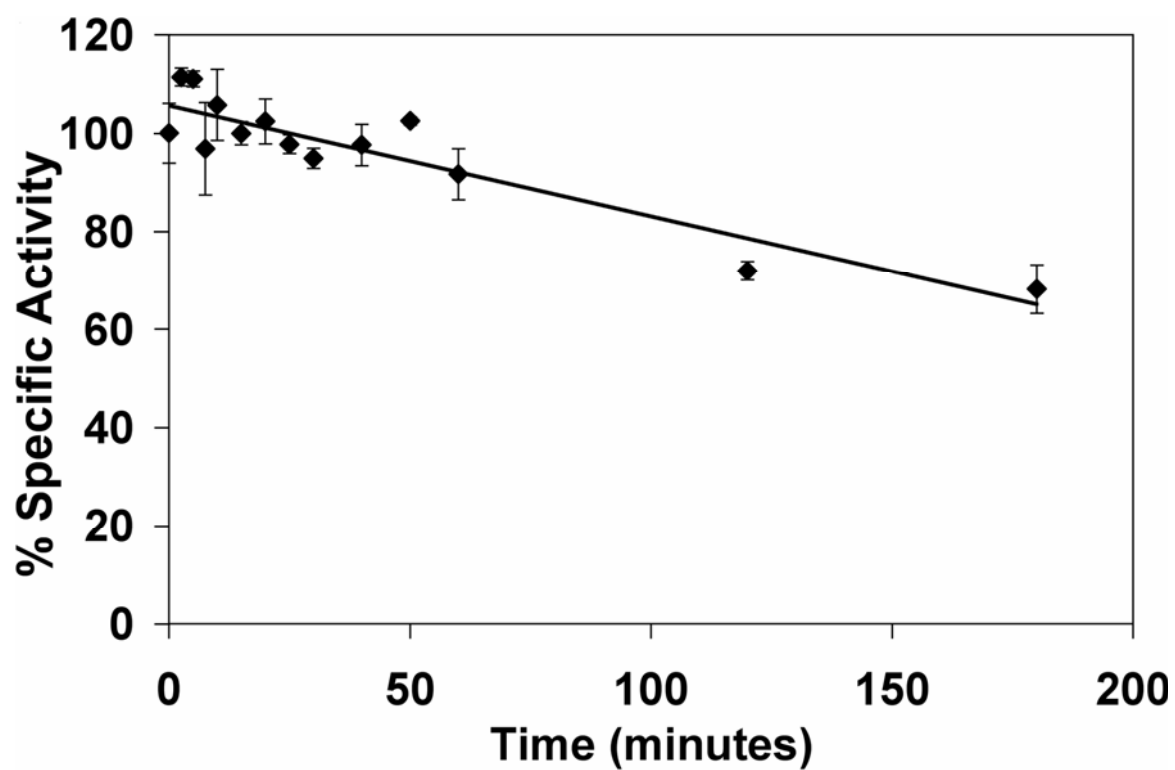


FIGURE 2.32. TtPRODHD specific activity as a function of temperature using the DCPIP assay. Assay conditions were equilibrated to the temperature indicated before assaying for TtPRODHD activity.

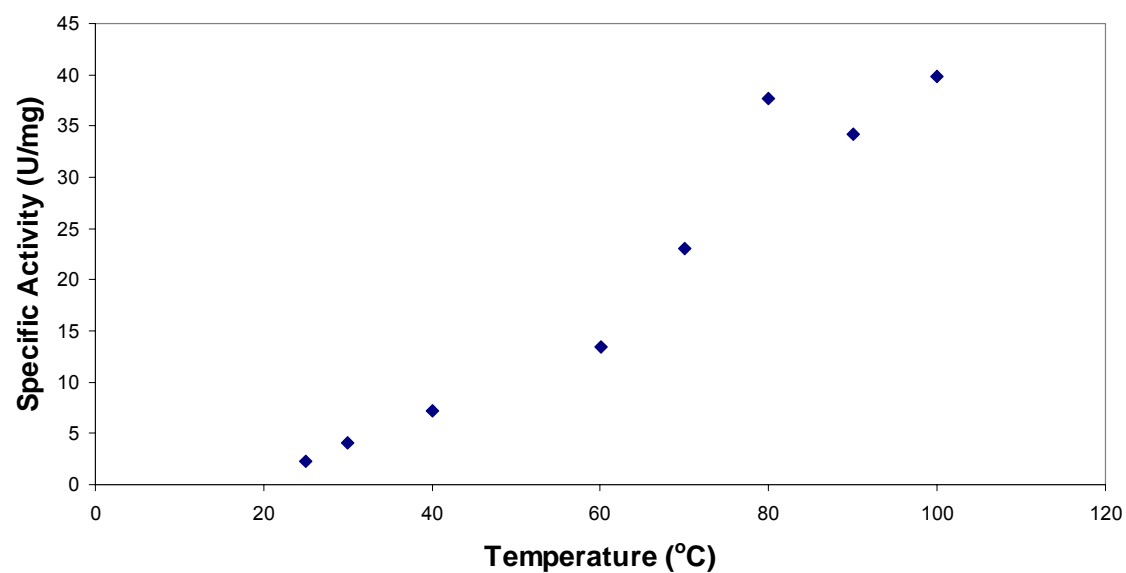


FIGURE 2.33. Steady-state kinetic parameter determination at 25°C for TtPRODH oxygen reactivity utilizing *o*-aminobenzaldehyde. Plot generated with Origin 7.0.

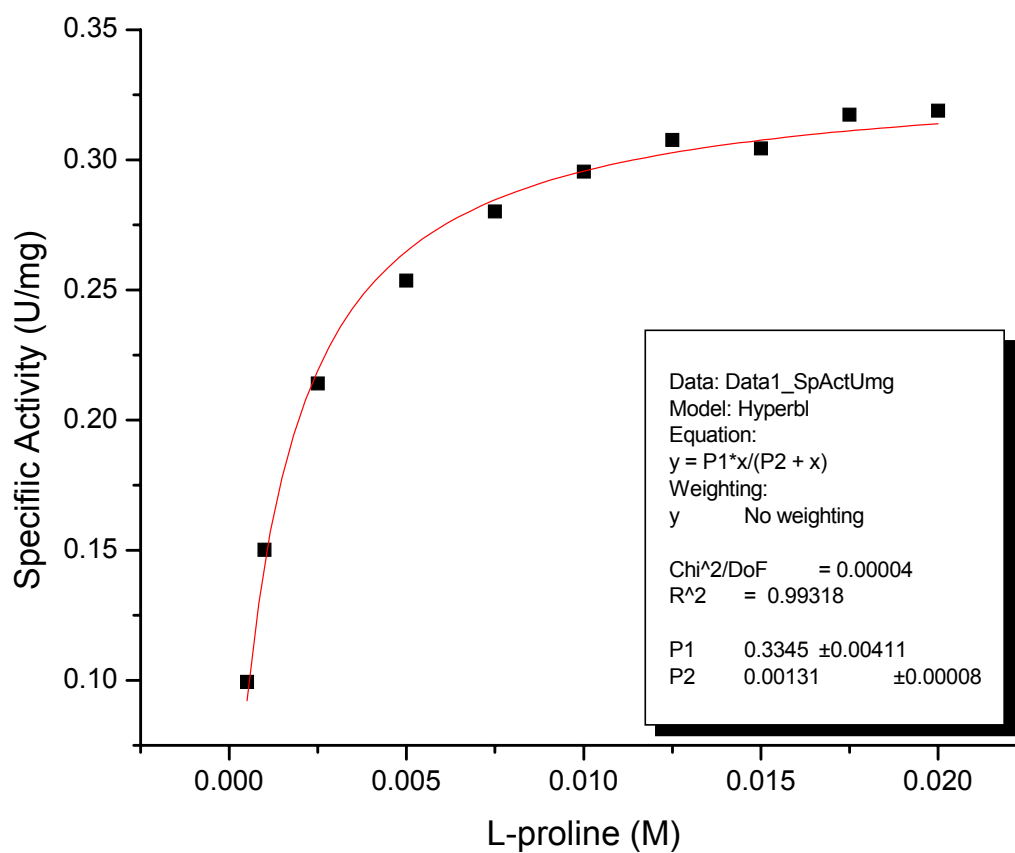


FIGURE 2.34. Measuring P5C:o-aminobenzaldehyde complex formation at 443 nm. The diamonds indicate complex formation in the absence of *E. coli* membrane vesicles. The squares indicate complex formation in the presence of *E. coli* membrane vesicles.

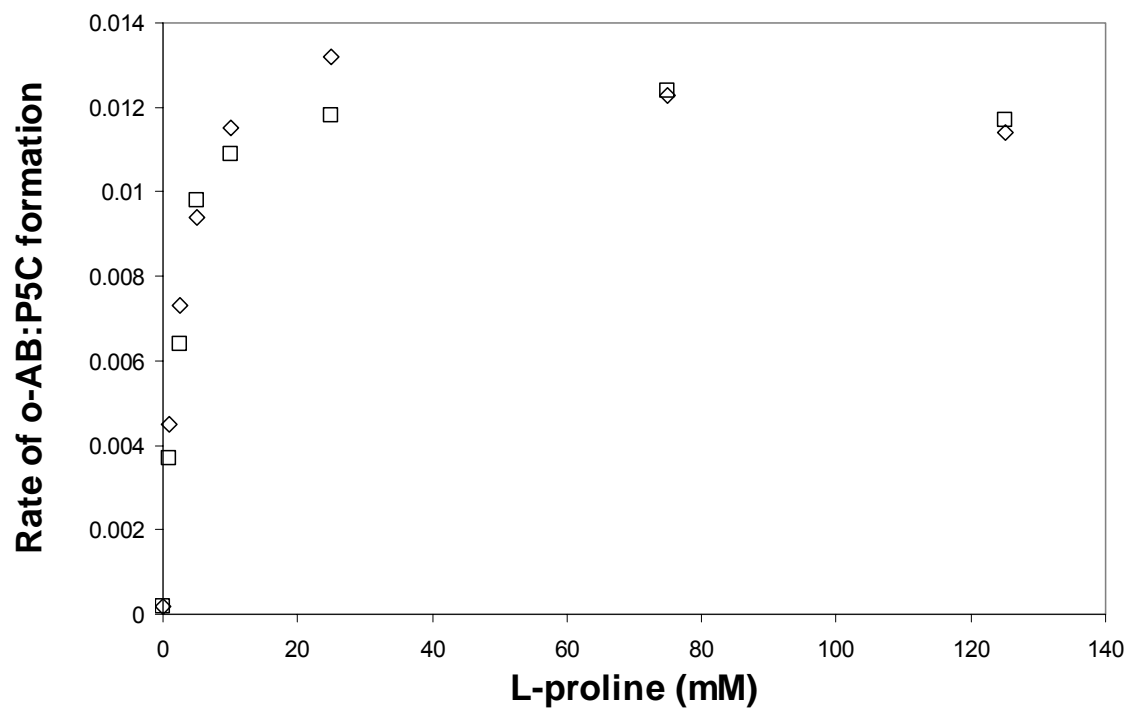


FIGURE 2.35. Generation of hydrogen peroxide by TtPRODH. Production of  $\text{H}_2\text{O}_2$  was measured using the Amplex Red  $\text{H}_2\text{O}_2$ /peroxidase assay kit as described in the text.

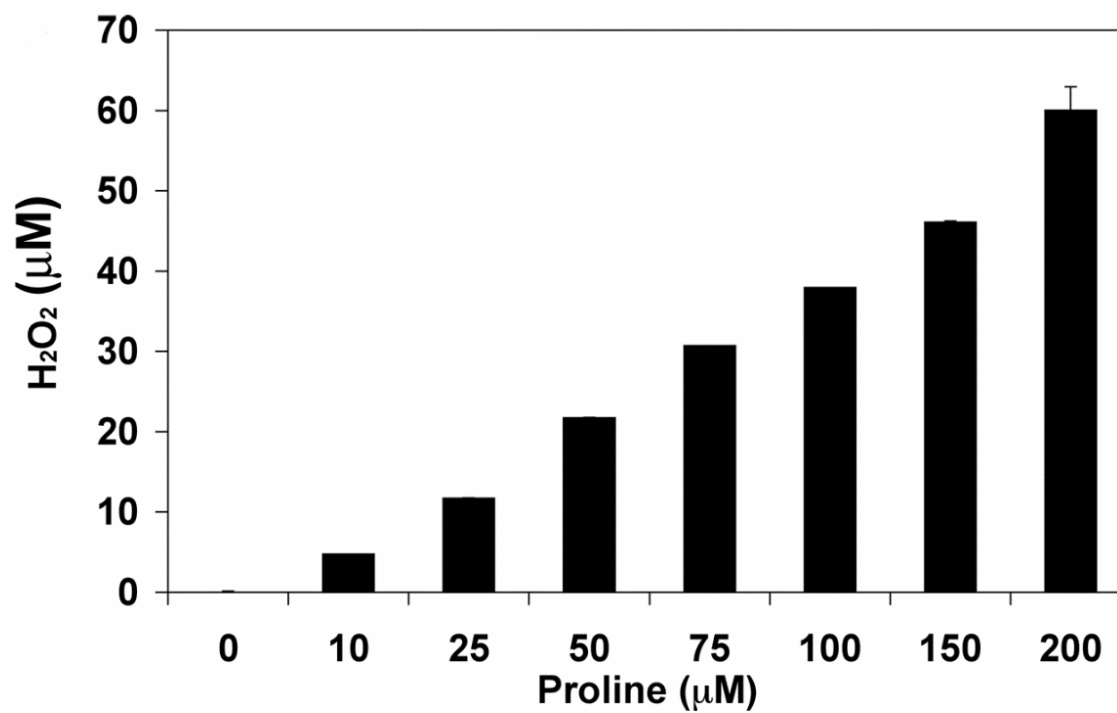


FIGURE 2.36. Unrooted phylogenetic tree representing the bacterial PutA/PRODH family generated with ClustalW.

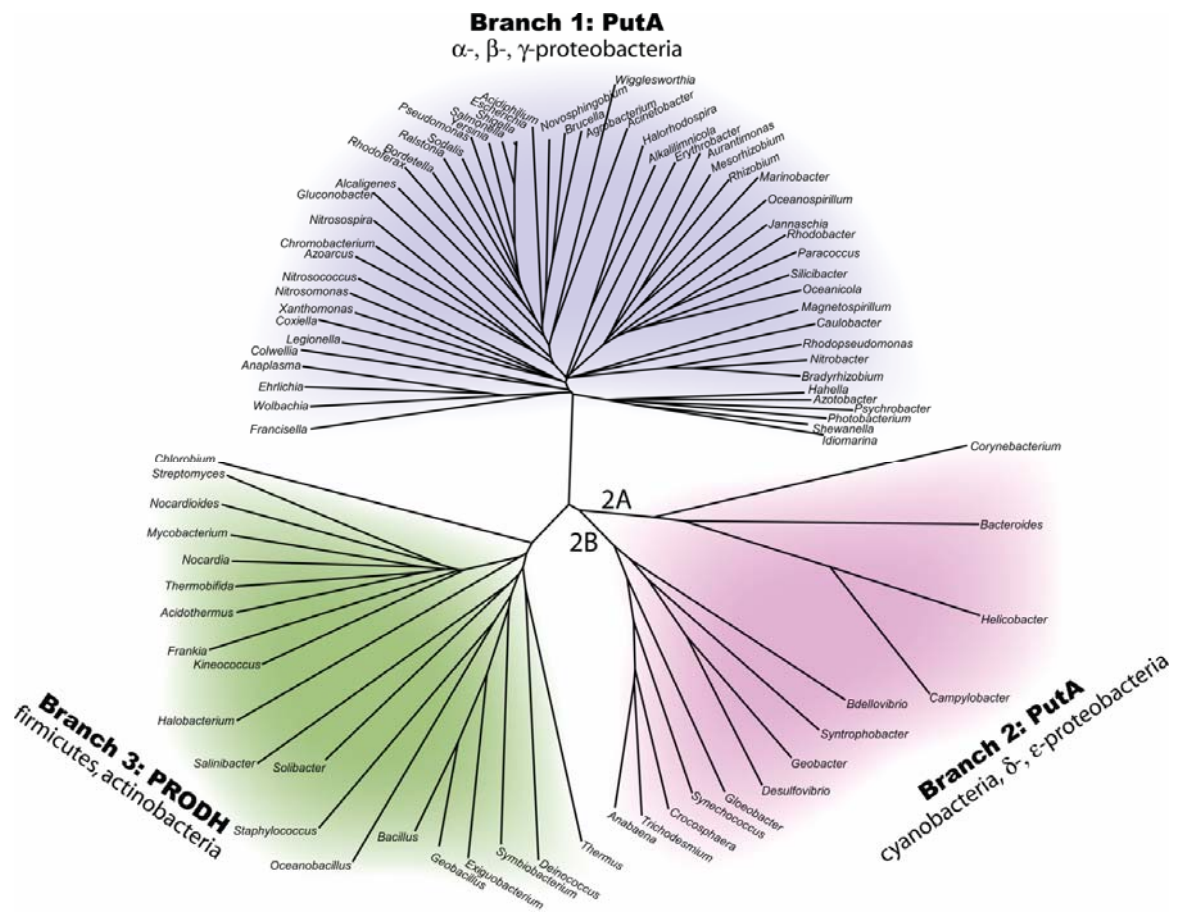




FIGURE 2.37. Conserved motif locations in TtPROD<sub>H</sub>. Each number corresponds to the conserved motif and each motifs conserved residues are highlighted in a different color.

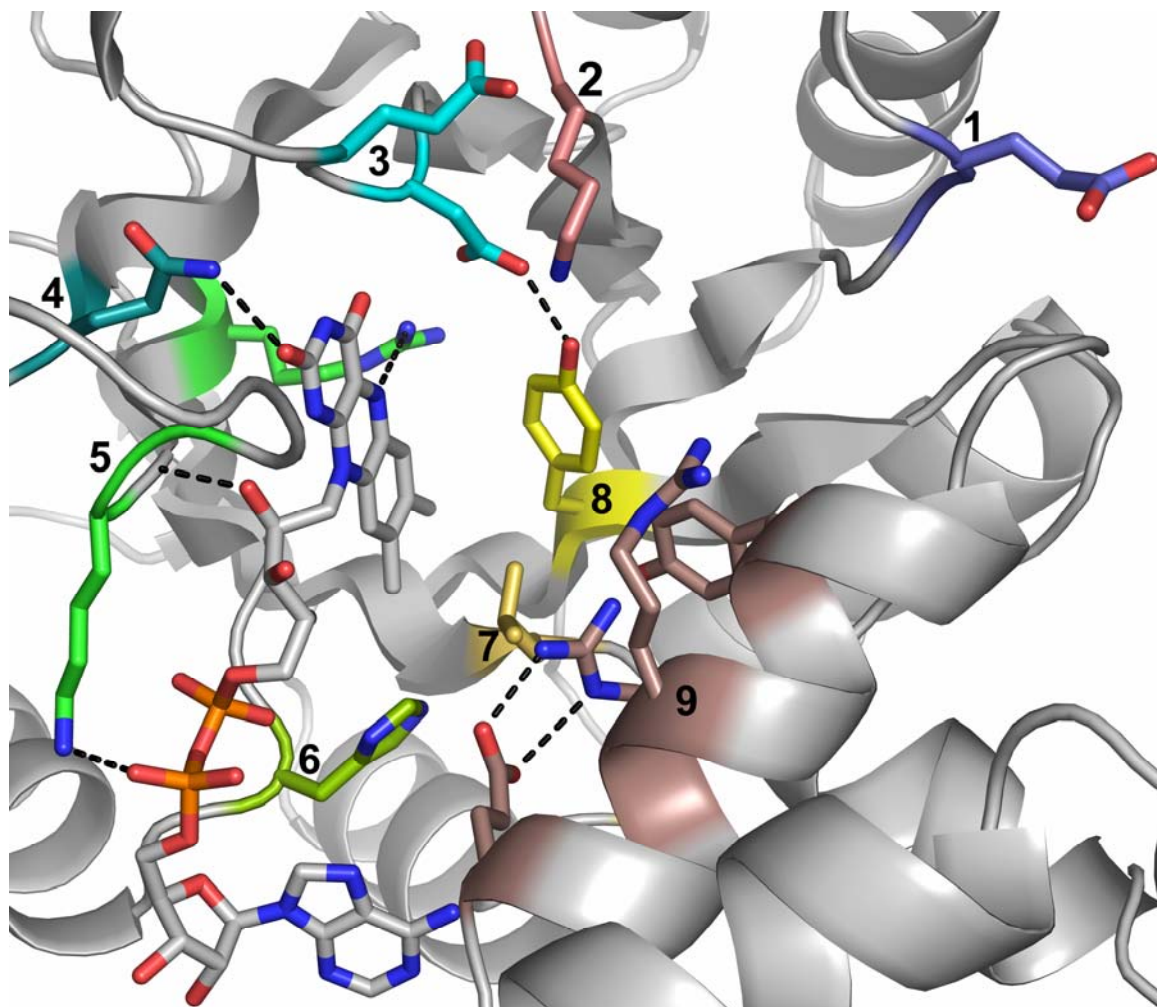


FIGURE 2.38. Archaeal L-proline dehydrogenase from *P. horikoshii*. FAD is shown in yellow CPK spheres, FMN is shown in green CPK spheres, and ATP is shown in magenta CPK spheres. This heterooctameric complex ( $\beta\alpha$ )<sub>4</sub> has two domains. The  $\beta$  domain (left) has proline dehydrogenase activity, contains FAD and has a monomeric sarcosine oxidase fold. The  $\alpha$  domain has a unique fold with ATP-bound (right). FMN is bound at the interface of the two domains.

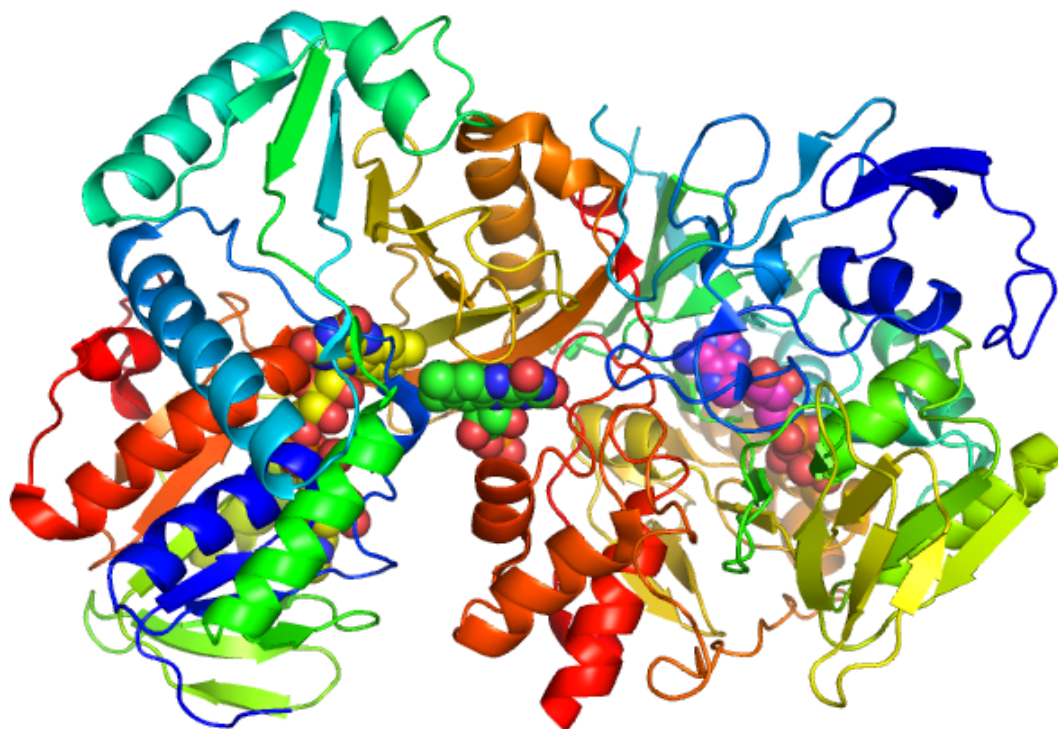


TABLE 2.1. Data Collection and Refinement Statistics<sup>a</sup>

Wavelength (Å)	0.97932
Diffraction resolution (Å)	47.16-2.00
No. of observations	292071
No. of unique reflections	46775
Redundancy	6.24 (3.12)
Completeness (%)	98.0 (86.3)
$R_{merge}$	0.079 (0.399)
Average $I/\sigma$	13.6 (3.0)
Wilson B-factor (Å <sup>2</sup> )	16
PDB accession code	2G37
No. of protein chains	2
No. of protein residues	592
No. of protein atoms	5184
No. of water molecules	272
$R_{cryst}$	0.190 (0.242)
$R_{free}^b$	0.231 (0.362)
RMSD <sup>c</sup>	
Bond lengths (Å)	0.014
Bond angles (deg.)	1.5
Ramachandran plot <sup>d</sup>	
Favored (%)	94.4
Allowed (%)	5.4
Generously allowed (%)	0.2
Average B-factors (Å <sup>2</sup> )	
Protein	16
Water	16
FAD	17

<sup>a</sup>Values for the outer resolution shell of data are given in parenthesis.

<sup>b</sup>5% random  $R_{free}$  test set.

<sup>c</sup>Compared to the Engh and Huber parameters (57).

<sup>d</sup>The Ramachandran plot was generated with PROCHECK (58).

**Table 2.2. Data Collection and Refinement Statistics of *Thermus thermophilus* Proline Dehydrogenase Structures**

I		II		III		IV		V
Name	Oxidized-Jan	THFA-March		Oxidized-Jun	THFA-Jun		Reduced-June	
Soaks	nothing	THFA		Nothing	THFA		Proline	
Precipitating Agent	2-methyl-2,4-pentanediol	2-methyl-2,4-pentanediol		Sodium Potassium Tartrate	Sodium Potassium Tartrate		Sodium Potassium Tartrate	
Wavelength (Å)	0.97932	0.9791		1.12718	1.12718		1.12718	
space group	$P2_12_12_1$	$P2_12_12_1$		$P2_12_12_1$	$P2_12_12_1$		$P2_12_12_1$	
<i>a</i>	82.0669	82.0637		81.3705	81.917		81.5625	
<i>b</i>	89.5896	89.8929		88.5231	88.7067		88.423	
<i>c</i>	94.3157	94.79		91.2553	92.267		91.9451	
diffraction resolution (Å)	47.16-2.00	39.42-1.80		45.63-2.30	40.93-2.20		45-97-2.30	
outer shell	2.07 - 2.00	1.86 - 1.80		2.38 - 2.30	2.28 - 2.20		2.38 - 2.30	
no. of observations	292071	397654		208978	120951		105038	
no. of unique reflections	46775	64955		29833	34545		29153	
redundancy	6.24 (3.12)	6.12 (2.94)		7.00 (6.89)	3.5 (3.38)		3.60 (3.65)	
completeness (%)	98.0 (86.3)	99.0 (92.3)		99.5 (98.4)	99.1 (99.3)		96.4 (94.7)	
mean $I/\sigma_I$	13.6 (3.0)	14 (2.9)		14.5 (4.4)	12.8 (3.2)		10.2 (3.1)	
$R_{merge}$	0.079 (0.399)	0.074 (0.230)		0.076 (0.410)	0.045 (0.301)		0.067 (0.370)	
$R_{cyst}$	0.190	0.210		0.253	0.231		0.253	
$R_{free}$	0.231	0.244		0.307	0.280		0.312	
no. of protein residues	592	594		540	554		537	
no. protein atoms	5184	4901		4384	4403		4465	
no. of water	272	279		89	97		61	
RMSD bond lengths (Å)	0.14	0.15		0.14	0.13		0.14	
RMSD bond angles (Å)	1.5	1.7		1.6	1.6		1.7	

Values for the outer resolution shell of data are given in parenthesis

Table 2.3. Data collection statistics for Se-Met SAD data sets.

	thfa x4s1	thfa x4s2	thfa x1s1	x3
Resolution Limit	2.2	2.2	2.7	2
Exposure (sec)	35	35	35	35
Redundancy	7.2	13.26	7.16	6.24
Completeness	99.8	99.9	100	98
Average I/ $\sigma$ <sup>a</sup>	10.9 (21.4)	11.8 (22.6)	8.6 (15.0)	13.6 (28.9)
R <sub>merge</sub> <sup>a</sup>	0.111 (0.054)	0.134 (0.068)	0.166 (0.078)	0.079 (0.043)
Se Sites found	-	-	-	7/10
SOLVE score	-	-	-	0.24
Solve FOM	-	-	-	24.77
Residues built	-	-	-	73%

<sup>a</sup> Parenthesis show values for low resolution bin

TABLE 2.4. Dynamic Light Scattering results for TtPRODHD in 20 mM n-octyl- $\beta$ -D glucopyranoside and various controls.

TtPRODHD with 20 mM BGD						
	D (E-9cm <sup>2</sup> /s)	R (nm)	MW (kDa)	Polyd (nm)	%Polyd	Polyd Index
Regu I Peak 1	1.44E+04	0.1341	0.02209	0.01935	14.4	0.02
Regu I Peak 2	750.7	2.867	37.21	1.068	37.3	0.14
Regu I Peak 3	0.3244	5853	3.99E+09	0	0	0
Buffer						
	D (E-9cm <sup>2</sup> /s)	R (nm)	MW (kDa)	Polyd (nm)	%Polyd	Polyd Index
Regu I Peak 1	2.38E+04	0.08361	0.007021	0.0187	22.4	0.05
Regu I Peak 2	5.488	392.4	5.67E+06	149.6	38.1	0.15
Buffer with 48 mM BGD						
	D (E-9cm <sup>2</sup> /s)	R (nm)	MW (kDa)	Polyd (nm)	%Polyd	Polyd Index
Regu I Peak 1	2.84E+04	0.06697	0.004099	0	0	0
Regu I Peak 2	879.2	2.341	22.76	0.6927	29.6	0.09
Regu I Peak 3	46.78	42.68	2.61E+04	9.423	22.1	0.05
Regu I Peak 4	0.3244	5853	3.99E+09	0	0	0
BSA (1 mg/mL)						
	D (E-9cm <sup>2</sup> /s)	R (nm)	MW (kDa)	Polyd (nm)	%Polyd	Polyd Index
Regu I Peak 1	2.86E+04	0.07343	0.005125	0	0	0
Regu I Peak 2	601	3.553	62.63	0.4881	13.7	0.02
Regu I Peak 3	0.3272	6418	4.99E+09	0	0	0

TABLE 2.5. Kinetic parameters using L-proline as the substrate

	TtPRODH	<i>E. coli</i> PutA <sup>a</sup>	<i>H. pylori</i> PutA <sup>b</sup>
proline:DCPIP assay			
$K_m$ (mM)	27	100	146
$V_{max}$ (U/mg of protein)	20.5	5	3.6
$k_{cat}$ (s <sup>-1</sup> )	13	12	8
$k_{cat}/K_m$ (s <sup>-1</sup> M <sup>-1</sup> )	481	122	56
$K_i$ for THFA (mM)	1.0	0.2	0.35
proline:O <sub>2</sub> assay			
$K_m$ (mM)	1.3	ND	150
$V_{max}$ (mU/mg of protein)	335	< 2	230
$k_{cat}$ (min <sup>-1</sup> )	12.7	<0.3	31
DCPIP/O <sub>2</sub> activity ratio	61	> 2500	16

<sup>a</sup>Data obtained from Zhu et al. (42) and Krishnan and Becker (44).

<sup>b</sup>Data obtained from Krishnan and Becker (44).

Table 2.6. Conserved Sequence Motifs of PutAs and Bacterial Monofunctional PRODHs<sup>a</sup>

Motif	Branch 1 <sup>b</sup>	Branch 2 <sup>c</sup>	Branch 3 <sup>d</sup>
1	s-y-D-m-L- <b>G-E</b> (288, 289)	v-d-l-l- <b>G-E</b> (146, 147)	l-d-X-l- <b>G-E</b> (64, 65)
2	i-S-i/v- <b>K-l-S</b> (329)	s-i/v- <b>K-X-t/s</b> (177)	S-i/v/l- <b>K-X-s/t</b> (99)
3	i- <b>D-A-E-E</b> (370, 372)	<b>D-M-E</b> (224, 226)	<b>D-m-E</b> (133, 135)
4	G-X-v-v- <b>Q-a-y-q-k-R</b> (404)	g-i-v- <b>Q-A-Y-l-x-d</b> (254)	G-X-v-l- <b>Q-a-y-L</b> (163)
5	<b>R-L-v-K-G-A-Y-W-D-x-E-i-k</b> (431, 434, 435)	<b>R-l-V-K-G-a-y-w-d</b> (285, 288, 289)	<b>R-l-v-K-G-a-Y-X-E-p</b> (184, 187, 188)
6	F-a-t- <b>H-N</b> (487)	i-a-s- <b>H-N</b> (342)	i-a-t- <b>H-D</b> (227)
7	E-f-Q-r- <b>L-h-G-M-g-e</b> (513, 515)	e-f-q-v- <b>L-y-G-M-a</b> (371, 373)	E-f-Q-m- <b>L-y-G-i-r</b> (254, 256)
8	i- <b>Y-a-P-v-G</b> (540)	l- <b>Y-x-y-P-g</b> (391)	v- <b>Y-v-p-y-G</b> (275)
9	L-L-a- <b>Y-L-v-R-R-l-l-E-N-G</b> (552, 555, 556, 559)	<b>Y-L-v-R-R-l-l-E-N</b> (406, 409, 410, 413)	<b>Y-f-m-R-R-l-a-E</b> (285, 288, 289, 292)

<sup>a</sup>Letters in bold indicated amino acid residues that are identically conserved throughout the entire family of bacterial PutAs and PRODHs. Upper case letters denote residues that are identically conserved within a branch of the family. Lower case letters indicate amino acid residues that are highly, but not identically, conserved within a branch.

<sup>b</sup>Numbers in parenthesis refer to *E. coli* PutA residue numbers.

<sup>c</sup>Numbers in parenthesis refer to *H. pylori* PutA residue numbers.

<sup>d</sup>Numbers in parenthesis refer to TtPRODH residue numbers.



## APPENDIX 2.1. Purification protocol for pKA8H TtPRODHD in BL21(DE3)pLysS

- Large scale purification (6 L)
  - 6 L LB media
  - 100 mg/mL Ampicillin
  - 34 mg/mL Chloramphenicol
- Using 10 mL overnight cultures add to 1.5 L media
- Grow to  $OD_{600} = 0.6$
- Induce with 0.5 M IPTG for 3 hours.
- Harvest by centrifuging at 7000 rpm for 10 min at 4 °C
- Resuspend harvested cell pellet in 50 mL:
  - 50 mM  $NaH_2PO_4$ , 300 mM NaCl, 10 mM Imidazole, 5% glycerol, pH = 8
- Freeze at -20 °C overnight (or longer)
- Thaw
- Add protease inhibitors (AEBSF, TPCK, E-64, Leupeptin and Pepstatin)
- French Press at 16000 psi (2 passes)
- Centrifuge, collect supernatant, extract pellet with 20 mM BOG
- Filter with a 0.45  $\mu$ m filter
- Affinity Chromatography
  - Wash with 3 column volumes of 50 mM Imidazole and another wash with 3 column volumes of 75 mM for Imidazole
  - Nickel-NTA resin and elute with Imidazole 300 mM
- Dialyze into following buffer overnight
  - 50mM Tris, 50 mM NaCl, 0.5mM EDTA, 0.5 mM DTT, 5% glycerol, pH = 8.0
  - Add 0.1 mM FAD to protein pre-dialysis
- Post dialysis - add 20 mM N-octyl  $\beta$ -D glucopyranoside
- Concentrate to 13 mg/mL
- Desalt to remove excess FAD and detergent

## APPENDIX 2.2. Sequences used to generate Unrooted Phylogenetic tree.

```
>Hahella Q2SL11 Q2SL11_HAHCH De
MFKASSVLSPIQAVSLDSLWTAITQNYAVDEAAYLEELMALATPGTEELRAITQGATKL
IEDVRAQDDSVHMDALLQEYSLDTQEGVLLMCLAEALMRIPDKATADALIRDKMSAAQW
DKHMGKSESTLVNASTWGLLLTGKVVKLDRNIDGTPANVLKRLINKCGEPVIRGAMNQAM
KIMGKQFVLGRDISEALQNGRKYRDKGYSYSFDMLGEEAALTAEDAERYFQSYIKAIETVG
ADQYDTRPGASSISIKLSALHPRYEQAHQDRVLTEMYEKVLLLVRARERNVSLTIDAE
MDRLELSRLFEKLYRSPDSRGWGEFGLVVQAYSKRALPVLWCWLTALAAEQGDRIPLVRLV
KGAYWDSEIKLCQQRGLPSYPVYTRKESTDVSYLACARFLFSEYARNHIYPQFATHNAHT
VASVQALAEKNDRPFQRLHGMGDALYNALLAKQKRTVRIYAPVGAHKDLLPYLVRRLL
ENGANSFFVHRLVDAETPIDSLVQHPVHELTRYSSLANHRIPLPAQIFGNRINSMGVNLF
VENQYSPLEKQLRAWDQHQWKACPVINGEHRTLSAPNPVLSPYDQSQSAGTVYWSQSDNV
DDALSAAYVGFEKWNNTPEVEKRAQSLEKLADLMEAGMPELMALCCREAGKTLQDSIDEVR
EAVDFCRYAAEQARKHFSKPNVLPGPTGESNELYLEGKGVFVCISPWNFPLAIFIGQVTA
ALAAGNAVIKPAEQTSLIAARAIDMMLEAGVAKEAIQFLPGDGAQLGPQLLSDNRVCGV
AFTGSTQTAHIINRSLAARDGAIATLIAETGGQNAMIVDSTALPEQVVKDVVQSAFASAG
QRCSALRVLFVQKDIADGILELLSGALKELKVDHPKHLSTDVGPVIDAEAQAGLLKHIEE
MKANSRWNAEAILPGDHNKGFFVTPSAFEIGSINELSKEHFGPILHIVRYAAEDLDKVID
SINDTGFGTLTGIHSRNETTAAYIEKRVKVGNTYINRNQIGAVVGVPFGGHLSGTGPK
AGGPHYLLRFANERTRTINTTAVGGNATLLSLGVEHI
>Shewanella Q3QL02 Q3QL02_9GAMM
MFKASEVLAGRYDNANLDELFSLSIQNYIVDEEAYLKELIALVPSSDEEIARITSRAHDL
VAKVRQYEKKGLMVGIDAFLLQYSLETQEGIIILMCLAEALLRIPDAETADALIADKLSGA
KWDEHMSKSDSVLVNASTWGLMLTGKIVQLDKNLDGTPSNLLSRLVNLGEPVIRQAMYA
AMKIMGKQFVLGRTIEEGLKNAAEKRKLGYTHSYDMLGEAALTMKDADKYRDYANAIQA
LGTAKFDESEAPRTISIKLSALHPRYEVANEDRVMTELYATLIKLI EQARSLNVGIQID
AEVDRLELSLKLFFKLYQSDAAKGWLLGIVVQAYSKRALPVLMWLTRLAKEQGDEIPL
RLVKGAYWDSELKWAQQAGEAGYPLFTRKAATDVSYLACARYLLSEATRGVIYPQFASHN
AQTVAAITAMVGDRKFQRLHGMGQELYDITVLAEEAVPTVRIYAPIGAHKDLLPYLVRR
LLENGANTSFFVHKLVDPKTPIESLVTHPLKTLQGYKTLANNKIVKPADIFGAERKNSKGL
NMNIISESEPFFAALEKFKDTQWSAGPLVNGETLSGEVRDVVSPYNTTLKVGQVAFANEA
TIEQAIAGADKAFASWCRTPVETRANALQKLADLLEENREELIALCTREAGKSIQDGIDE
VREAVDFCRYAVQAKKMMSKPELLPGPTGELNELFLQGRGVFVCISPWNFPLAIFLGQV
AAALATGNTVIKPAEQTCLIGFRAVQLAHEAGIPKDVLLQFLPGTGAVVGAKLTSDEIRIG
GVCFTGSTTTAKVINRALAGRDGAIIPLIAETGGQNAMVVDSTSQPEQVVDVSSAFTS
AGQRCSALRVLYLQEDIAERVLDVLKGAMDELTLGNPGSVKTDVGPVIDAAKANLNAHI
DHIKQVGRILHQLSLPEGTENGHFVAPTAVEIDSIVLTKENFGPILHVRYKAAGLQKV
IDINSTGFGTLTGIHSRNEGHAEVADKVNNGVNYINRNQIGAVVGVPFGGQGLSGTG
PKAGGPHYLTRFVTEKTRTNNTAIGGNATLLSLGDAD
>Aurantimonas Q1YLD6 Q1YLD6_9RH
MTPETTAALRGTDGDRDAVRQRYGEDEAIVVKDLAARISLSETDRAAISAGADIVRRVRR
ETSPSMMESFLAEYGLSTEAGVGLMCLAEALLRVPDAETVDELIQDKIEPSDWGAHLGHS
SSSLVNASTWALMLTGRILDDDDPSRPAAALRGLVRRVGEPPVRRRAVAQSMRLLGRQFVLG
QTIEEGMRNARERERQGYTYSYDMLGEAARTEADALRYLKSYSDAIASIAKAAKGDVRSN
PGISVKLSALHPRYETTHRDVTMATLVPRALELARQAAKANIGFNIDAEQDRLDLSLDI
IEAVLSDESILKGWDGFGVVVQAYGRRAPVIEYLDTLARRLDRRIMVRLVKGAYWDEIK
LAQEMGTHTFPVFTRKVNTDLSYMACAQMLLDRRDRIYPQFATHNAHTCAAILKMAGNDR
DSFEFQRLHGMGESLHDIVHRQNDTRCRIYAPVGAHRDLLAYLVRRLLENGANSFFVNQI
VNEAIAPENIARDPLSEVEALGEAIANPTIRTPAELFAPERRNSKGFRVNEPASITPLIE
ARQAFADAVWTARPMLADDLPVSGEGRAATSPADPGRRVGTVHEASVKDVHRAAAAEEAG
FAAWSAVPVAERATTLRAIADLYEANIAELTVIATREAGKTLADGIAEIREAVDFLRYA
DEAERLEVEEPPGTGRGIFVCISPWNFPLAIFTGQIAAALAAGNAVLAKPAEQTPLIATRA
VELMREAGLPAAALQLLPDGPVNGVGLLTSRRRIAGVCFTGSTEVAQIIHKALANAGPD
AVLIAETGGLNAMIVDSTALTEQAVRDILIASFQSAGQRCSALRMLYVQEDARDRLHML
```

EGAMDALVVGDPWRIDTDVSPVIDADARDDIAGYIASRKAAGQALKTLVPVQDGLYAAPS  
 VVSVGGIDDLEREVFGPVLHVATFKAREIDGVVDAINARGYGLTFGLHTRIDDRVQQIVE  
 RIQVGNITYVNRNQIGAIVGSQPFGGEGLSGTGPKAGGPFYVARFRRTEPAEDLPAPAPPD  
 IPAATVAEAIARLDARNWAARGDRVAVLRRALSGKGGIIRRACSAVGAFDPGPFITLPGPT  
 GESNRLSLYPRGTVLCLGPTAEIALAQAVQALSAGCAVIVAPGAAALAGPVIAAGAPLA  
 VFDGTLAPGDLEHLDGIDVVAAGRSDWTWALRNALAARKGAIIPLETAIIGPSRYVVER  
 HLCIDTTAAGGNASLLAAAE  
 >Rhodobacter Q52711 Q52711\_RHOC  
 MTDLSALGPKAKFAPEAEVLQALVAQAALPQPQLDRIAARGADLVARIRAEAKPSLMEHF  
 LAQYGLSTREGVALMCLAEAMLRVPDTATIDALIEDKIAPSDWGKHLGTAASSLVNASTW  
 ALMLTGKVLDDGAGGIAGTLRGAMRRLGEPVIRAAVGQAMREMGRQFVLGETIEKALERA  
 EKREAEGYTFSYDMLGEAALTAADAERYRLAYAQAITAIGKAATRGSIANPGISIKLSA  
 LHPRYEVAQEARVMAELVPVVRDLARAAARAGIALHIDAEEQDRLALSLRVMAAVIADPE  
 TAGWEGFGAVVQAYGKRAGAAIDALAAMARAAGRRINIRLVKGAYWDAEMKRAQVEGHPG  
 FPLFTSKTGTDVAYICLAAKLFGLNDCIYPQFATHNAHTVAAVLEMAAGRPFQRLHGM  
 GARLHDIVLRETGGRCRIYAPVGAHRDLLAYLVRRLLENGANSSFVNQIVNESVPPAEVA  
 ACPFAALPTARAPRGLLAPADLFGAGRVNAQGFDLSDPEVLARIEAARDVTLPDAAPIVA  
 GPVSGTLRPVRNPATGAVVAQVTEADAATVALALDAAQVWSAPAATRAAVLCRAADLYEE  
 NFGPIFAALAQEAGKTLGDAVSELREAVDFLRYYAAEGAADTRPPRGAVVAISPWNFPLA  
 IFTGQVAAALMAGNAVLAKPAEQTPIIAALAVRLLHQAGVPETALQLLPGDGPTVGAALT  
 RDPVAGVVFSTGSETAQIIARAMAAHLAPGTPLIAETGGLNAMVVDSTALPEQAVRDVV  
 ASAFRSAGQRC SALRCLYVQDDIAPHILIGMLKGAMEELVSGD PARLSTDVGPVIDAEAKA  
 GIETYLAANKARILHRSTAPEGGHFVAPALLQVGGIADLEREIFGPVLHLATFAAEDLPA  
 VIAAINARGYGLTFGLHSRIDARVETVAETIRAGNIYVNRNQIGAVVGSQPFGGEGLSGT  
 GPKAGGPLYLNRFYAPEPVVAVGGWTEAATPILPEARETQLDEIFLPGPTGELNRLTRHQ  
 RGPILCLGPGAEAAASAQAAAVVALGGQAVQASGAVSPKALETTLTLAGVLWWGAAEMGRA  
 YAQALAVRPGPLVPLITAKPDLAHVAHERHLCVDTTAAGGNAALLAG  
 >Azotobacter Q4J680 Q4J680\_AZOV  
 MFKASRVLQGNVLDTSAGEFFPFI SAN YCVDEAAWLNELLPLADPGEAGIAAIRERAGAL  
 IEAVRRRGNVLEVTL DALLREYSLDTQEGMLMCLAEALLRVPDPATAEALIRDKLSAAQW  
 AQHLGHSNLLVNFAAWGLLMTGRLVSPSSDGRPKKVIGRLLQRSGEVPVIRAALNQAMK  
 LMGNQFVLGRNIAEALRNARRARERGYGHSFDMLEGEAALTEAAAERFLT DYRLAIEALGR  
 EPQVGGGPRPSISIKLSALHPRYEAQRRRVLAE L FASVRELAELARSLNVGITIDAE EA  
 DRLELSLELF EKLLCDPAIRGWGEFGLVVQAYS KRALPVLVWLTLLGRELDTRIPVRLVK  
 GAYWDSEIKQCQVQGLEGPVVFTRKEGTDTSYLACARYLLGEHCRGVLYPQFATHNAHTV  
 SCILAMAETHPPHDFEFQRLYGMGDALYDCLLERQQVQVRIYAPVGEHRELLPYLVRRL  
 ENGANS SFVHRLVDPRIPVEALIGHPVEQLRRC SGLANPRIPLPVDI HGAGRKN SRGINL  
 NVRSQWEPFERALRVQLEHRWQAAPLVDGQVLAGEVHEVRSPQDLDRVVGTVWFAGAE LV  
 DRAMARLAAAWPRWNATPMERRAAIFGR LADLLEEHRTELVALCILEAGKTIQDSLDEVR  
 EAVDFCRYYAQQARLT LKRT ELRGPTGERNELFYEGRGLFVCISPWNFPLAIYLGQIVAA  
 LVAGNCVLAKPAEQTSLIAARALELLFAAGLPKEAIAFLPGDGPALGAACCADPHLAGVC  
 FTGSTETARLINRRLAWRDGPLVTLIAETGGQNMIVDSTALPEQVVKDALHSAFTSAGQ  
 RCSALRVLYLQNEIAGPVIELLRGAMAELRVGLPQRRD TDVGPLIDTQARQALLEHVDLL  
 KGEERLLAEAGLAPALNGHFLAPLAFEIGGIGELRKEHFGPILHVVRYYAAEDLEQVVA AI  
 NASGYGLTLGVHSRNEATARRIEALTRVGNLYVNRNQIGAVVGVQPFGGCGLSGTGPKAG  
 GPNYLLRFVHERSTAINTA AVGGNASLLSLTERE  
 >Chromobacterium Q7NXT8 Q7NXT8\_  
 MQFESFAHQQSALRDAITAAYRRDERECVQALLPQAAMSPEQVASVQDLARRLVTEVRRE  
 RTRSSGVDALMHEFSLDSSEGIALMCLAEALLRIPDRETADKLIRDKISRGDWKAHLGNS  
 SSLFVNAAAWGLLV TGKLVSSH SANGLSAAMTRLIAKGGEPLIRKGVDMAMRMLGKQFVT  
 GETIEEALANGREREARGYRFSYDMLGEAAMTEADAQRYLKDYVTAIHAIGKESNGRGIY  
 DGPGISVKLSAIHPYARLKHERMMTELLPRLKALFLLAKQYNI GLNIDAE EADRLEISM  
 DLVEALANDADLNGFEGIGIVVQAYQKRC PFVIDFLIDLARRTGHRFMVRLVKGAYWDAE  
 IKRAQVDGLPGYPVYTRKVYTDVSYLACAKLLAAQDAIYPQFATHNAYSLSAIYNLAAG  
 KDYEFQCLHGMGETLYDQVVGKDKLGKACRIYAPVGSSETLLAYLVRRLLENGANSSFVN  
 RIVDENVSIDELVTD PVAEAAGFSGMPHSKIPLPEALYGEGRNSKGLDLSSEHVLATLQ  
 LGLQASEQQRWAAF PMLGDGDVTDGELQEVRNPADHSDVVGK VIEASAADVERALALSAG

IAAWAATPVAERAASIRRMADLMEAHMPALMGLAVREAGKTLNNAIAEVREAVDFCRY  
AAQIVSEFDNASHRPLGPVVCISPWNFPLAIFIGEVVASLAAGNTVLAKPAEQTSLIAAY  
AVRLLHEAGIPRAALQFLPGRGEVVGAAALTGDARIQGVIFTGSTEV AQIINRTLAKRQDD  
PVLVAETGGMNAMIVDSSALPEQVVTDLSSAFDSAGQRC SALRVLYLQNDIADKVIAMI  
KGAMDELTIGNPAKLTTDVG PVIDAE AQAGLLAHIA RMKNSARAMHQTKLSAACEQGT  
FVAPTLFEIDNLSELKREVF GPVLHVLRYAASDL DKVVAEINATGYGLTHGIHSRIDET  
IADICGKIKVGNIIYVNRNIVGAVVGVPFGGEGKSGTGPKAGGPYYLYRLTRA AWQPK  
LA AVPAAADLSALDALAAAAKAQSLALDGAIAAARKESPLTHSVALPGPTGENNLLS  
FAGRGRIGCVADDAQALAEQLAAAF AAGNRAVLADNELGRKFASALNGHVSLAADVLEAD  
VDVAVLYAGAKAE EARRELAARDGALVPLILRGENGYNVHRLVVERALSVNTTAAGG  
NASLMSMTE >Silicibacter Q5LP42 Q5LP42\_SIL  
MTHALRTHIDSQTYADQSALLDQLVAQAALSEVDRAAICAAAAGLVRDIRSSTAPGL  
MEVFLAEYGLSTDEGIALMCLAEALLRVPDADTIDALIEDK IAPSDWGKHLGHSSSLV  
NASTWALMLTGKVLDERKASPVGALRGAIKRLGEPVIRTAVSRAMKEMGRQFVLGETI  
QSAMKRASGMEAKGYTYSYDMLGEARTEADAARYHLSYSRAIAAIAEACTHGDIRAN  
PGISVKLSALHPRYELAQDARVMDLVPRLRALALLAKAAGMGLNVDAAEADRLSLSLQ  
VIEAVMAEPALKGWDGFGIVVQAYGPRAGLVIDTLYEMAQRHDKLMVRLVKGAYWDTE  
VKRAQVEGVDGFPVFTQKSATDVSYIANARKLLSMTDRIYPQFATHNAHTVAAILHMA  
KDGPYEFQRLHGMGETLHNLVLTANKTRCRIYAPVGAHRDLLAYLVRRLLENGANSS  
FVNQIVDENVPPEVVAADPFETVKAPAKPLKRGPELFAPERPNMSGFDLGHQPTLDAI  
DAARDPFRSHRWQAGPLLAE EASPEAAEAVVNPADPHDVPGSVAPASADAELSLARAQ  
PWQAPAAERA AVLNRAADLYEAHYGELFALLHREAGKTLPDVAELREAVDFLRYYAAN  
IPDAASAGIFTCISPWNFPLAIFSGQIAAALATGNAVLAKPAPQTPLIAHRAVQLLHEAG  
VPRDALQLLPGGPAVGAA LTSDPRVSGVAFTGSTATAQKIRAAMAANMRPGTPLIAET  
GGLNAMIVDSTALPEQAVQAVIESAFQSAGQRC SALRCLYLQEDIAEDVLTMLKGAM  
DALNLGNPWALSTDSGPVIDEAA RKIITDHVAGARAEGRVLKELALPPEGTFVAPT  
LIKVAGIGALEREIFGPVLHVATFRSNELDQVIAAINATGYGLTFGLQTRIDDRVQHV  
TEAVHAGNIYVNRNQIGAIVGSQPFGGEGLSGTGPKAGGPNYMARFCAPDRQQAADWA  
APMATLPRATGTPAPVRVQSLPGPTGESNRLSEMARPPLLCLGPTAATVATQAQAVEAL  
GGTAIRATGALAAEALETVEGISGVIWWGDE ETARAYELALSRRSGPILPLIPGLPDG  
ARVLAERHVCVDTTAAGGNAALLGGMG >Coxiella Q83DR6 Q83DR6\_COXBU P  
MTDTHLLFFEKAI AQNAIRPSLNKTYRMDETT CVNHLLKTI AFTPRLEAAVSRLAKEL  
VTVAVREQESEKGGIEGFM MQYDLSTEEGILLMCLAEALLRVPDKETENLLIRDKLTS  
AEWNKYVGASESSFVN FATWGLALSGKILKKEKDQG FKNVWRNLVRRSGEPVIRKAVRE  
AMKLMS EHFVLGRTIEEAVKRSQSAIKEGFRHSYDMLGEVARTQEDADRYDSYHRAIS  
VLGKSHPTKSVHEAPGISVKLSALYPRYDFKKRELAVPFLIERVKELALHAKEQKIGMT  
IDAEADR LDISLDIFEALFTDEAFENWQGLGLAVQAYQKRAFYLIDWLIDLAQRQKRRI  
PVRLVKGAYWDTEIKLAQMEGLSGYPVFTRKVNTDISYIACAQKMLNAQDAIYPQFATH  
NAYSVAAILNLMDHHYDNYEFEFQQLQGMGKALHHYIVTKLKLPCR VYAPVGYHEDLL  
PYLVRRLLENGANSSFVNRIADKTVPVDQLIESPVKKIEAFGDIPNPKIPLPKGIFKTR  
TNSSGIDLSNFAELMPLNEEIIHHALEKEWEAAPFLQEIKNGKPVFDPTDNRRQIGVIE  
LANESDVEKAIQAGHSAFPNWDQKGISARATILRK MADLLEKHKAE LMAVVVREGGRTLQ  
NALSEVREATDFCRYAEQAEQHLSDKALPGYTGESNTLRMNGRGII LCISPWNFP IAI  
FTGQIAAALVTGNAVIAKPSGQTPLTGALVTRLFHEAGVPKEILQLMPGSGKTVGQAL  
IEDTKISGVIFTGSDATARHIQKT LAARPGPIVPFVAETSGINAMIADSTALPEQLVND  
VIVSAFDSAGQRC SALRI LYIQEDIAADVIKMLKGAMAEIKMGDPLLLSTDVG PVI  
DANAQKTLQKHQALMQEAKLIYKVDLPRETDFGT FVAPQAYELPNLGLITEEVFGPILH  
VIRYKRENLNKVIEEINGLGYGLTFGIQSRIDETVDYIQQRINAGNIYVNRNTVGAVVG  
VPFGGSWLSGTGPKAGGPHYLP RFCIESTLTINTTAAGGNASLMAMED >Oceanicola  
Q2CBQ1 Q2CBQ1\_9RHOBMPRDVQAPALDEIAAATYAPEAETVAALAAAADLPEQARAE  
IGRRAAGLVTDIRKASRPG LMEVFLAEYGLSTDEGIALMCLAEALLRVPDAETIDALIE  
DKIAPSDWGRHLGRSSSLVNASTWALMLTG RVLDDDRPAPFRALRGAVRRLGEPVIRT  
AVGRAMREMGRQFVLGEDIDRAMARA AKMEAKGYTYSYDMLGEARTEADAQRYLEDYAR  
AITAISRAATHDDVAENPGISVKLSALHPRYEEPRRAQVLEELVPRLRRLCRLAAEANM  
GLNIDAAEADRLLLLSLDVIAETLIDPALADWQGGFIVVQAYGQ RAGAVIDWADLAARQ  
NRRIMVRLVKGAYWDTEIKRAQVLGLDGFVPVFTEKAATDVSYIANARKLLGLTDRLY  
PQFATHNAHTMAAVLHMAEGLPRAAW

EFQRLHGMGETLHNLLEEREGTRHRIYAPVGAHEDLLAYLVRRLLENGANSSFVNQIVDE  
DVPAEVVAADPFAALGNPPPLRRGPDLFPDRGNAAGWDITHRPTLAALDAARAPFRRHAW  
TPASSGQKYADATAATGAPLEVNPADPDDRVGTVATASKEGAARAHAAARPWSAPAAER  
AAALRRAAAAYEAHAPELFAILHREAGKSLDDAIGEVREAVDFLHYAANATDAPGTRGT  
WVCVSPWNFPLAIFTGQLTAALAMGNAVLAKPAEQTPLIAARAVELLHEAGVPAEALQLV  
PGDGATGAALIADARTRGVAFTGSTDTALKIRASMAKHCAPGTPLIAETGGLNAMIVDST  
ALPEHAVRDILASAFQSAGQRC SALRCLYVQEDIAERLTTMLTGAMDTLTLGDPWDIATD  
VGPVIDTEARDGIEAYVEAARAEGRLVHEIAAPGRGTFIAPVLIRVRGIEDLPFEVFGPV  
LHLATFAADEVEGVI ERINARGYGLTFGLHTRIDDRVQEVVERIAVGNAYVNRNQIGAIV  
GSQPFGGEGLSGTGPKAGGPDYLP RFAPAPAPAGGGAWDADDSPTRLARALAAAPAPEPV  
ETIDLPGPTGESNRLTLLPRGPLLCLGPSAATARAQAEAVRALGGQAVEAEGRIDPAWLT  
DLDGLAGVLWWGDADEARALEQALAKREGPIVALITGAPDRAHACHERHVCIDTTAAGGN  
AQLLAEVAAR

>Magnetospirillum Q2W4B4 Q2W4B4

MIFTAPLPAPDPERQAIHRAAGTSEADLVSGLSAGIPLLEDEARRRIVNRAVNLDVGARRN  
RRTLGLDGLLNEYRLSTREGVVLMLCLAEALLRIPDDHTVDLLIKDKIASADWDGHLGHSP  
SVFVNASTWALVLGDRLLHLEEDGRAVLGRMAGRLGEAVRRALRHAMGLMGRQFVLGRT  
IAEALDNARAWEARGYRHSFMDLGEAARCEQAAQDYLRAYAGAI EALGRHAKGAGPIAGP  
GLSVKLSALHPRFEMAQRQ RVLGELVPRRLDLCHRARDAGIGLTIDAE EADRLDISLDVM  
EAALADPALDGDWDFGMVQAYQKRARPVIAWAGALAARRQQLMIRLVKGAYWDGEVKR  
AQERGLGGFPVFTTKEATDVSYLACAADLLARPDLFYPQFATHNAHTAAVMENTGGAGD  
WEFQRLHGMGEALYAQLVPEFP CRTYAPVGS HQELLPYLVRRLLENGANSSFVSRLADEE  
IPAHVVAADPLAALGRITPQLVAEPSALFGPSRRNSGGLDLSSPAVLAQLDLALAAVATP  
ERSAPIVDGRERENQAAKPVLD PADHRRVVGEVVDASPADVEAALASARAAFPWDDLGG  
EARASILERAADRLEADRARFMALAI REAGKTIPDALSEVREAVDFLRFYAAEARARFSQ  
PVRLPGPVGESNELMLGGRGVFACISPWNFPLAIFVGVQVAAALAAGNAVVAKPAPQTPLM  
AAA VRL LHQAGVPPQALHLVPGGPAIGEALT VNPLVDAIAFTGSTATARHINRLRAAMD  
GPLAPLIAETGGLNAMIVDSSALPEQVVADCLESAFRSAGQRC SALRVAFIQREAWTRI Q  
PLLAGAMAELSLGDPALLSTDVGPVIDEASRRRLLAHGRLRHAGRMIGQSACPPDCRVG  
TFFAPMAHQLDNLDLLQSEVFGPILHVIPWEAGRLEQVLDCAATSYGLTLGIHSRIDAT  
IAQVIARARIGNIYVNRMTIGAVVGSQPFGGGLSGTGAKAGGPNTLIRYGVVERCLSVNT  
AAAGGDVALMAGPQRHGTK

>Mesorhizobium Q3WRH9 Q3WRH9\_9R

MPALDALRDEIRKHYLADEDVLLRRLIESADLSPARREAI SAKAAELVRVRAGSTRHLM  
ESFLAEYGLSTSEGVALMCLAEALLRVPDAETMDDL IADKIAPHDWSAHSGESASIFVNA  
STWALMLTGRVLDDEGN GIEATLRGMVRR LGEPVIRA AVAAAMREMGEQFVLGRTIAEAI  
KRGRAMTAKGYTYSYDMLGEARTEADARRYFQAYRNAIAALKGEAKSEDIRANPGISVK  
LSAIHPRYEATQRERVMPVVTERRLLLLAQDARAARMGLNIDAE EADRLDLSLDVIERVLA  
DPSLEGWDGFGIVVQAYGRRAPFVIDWLYALAE RLDRRIMVRLVKGAYWDTEIKRAQVMG  
LSSYPVFTRKVNTDISYIACARKLLSLTDRIYPQFATHNAHTVAAILAMAENRNAFEFQR  
LHGMGEALHDI IKRREGTRCRIYAPVGAHEDLLAYLVRRLLENGANSSFVHQIVDEEVS  
EEIARDPFALAEAAAGSAPNPAIPLPALIFGRQRINAKGWDITDETALREIETARRPFQAP  
HRWEGRPITRARGQGEARIIVNPARTSEIVGT VFDASPGQVSESVRLAVAAQPGWAATPV  
TERAEILRRIADLYEAHAGEFFALCAREAGKTL PDGIAELREAVDFLRYYANEAQAEEG  
TGARGVIACISPWNFPLAIFTGQIAAALVTGN AVVAKPAEQTCL IATRAVALMHEAGVPE  
DVLHLLPGDGPSVGAPLTADPRIAGVCFTGSTEVARI ERQLAKTAAPDAMLIAETGGLN  
AMIVDSTALPEQAVRDILASAFQSAGQRC SALRILYIQKDVEARVTAMLRGAMQALTVDG  
PWQVPTDVGPVIDDEALSGISGYCEEMERKGRLLARIERPEGGRFVAPAAFQVSGIEEME  
REVFGPVLHVATFEAEDLGHVISAVNAKG YGLTFGLHTRIDARVQEVVDGIHAGNIYVNR  
NQIGAVVGSQPFGGEGLSGTGPKAGGPHYLRFRFRGKAGPDLAPADAPAIAAEELVRAMP  
DAQKSGWADRTDRIVALRRALRGRWADVLASAAALDLGPVDLPGPTGEANTLQLAPGRV  
LCLGADADALAAQVIQALAAAGNAVLAVAKDAPAILQPLTRAGFPLAAFHGNVAPQTLETL  
ALDLVAATGERQWLTAVRTALSAREGRIVPLVTEL VYPAAYAHERSVCVDTTAAAGGNASL  
LAAA

>Psychrobacter Q1QBN4 Q1QBN4\_PS

MNPVEQFTPQEPILFNPIDLLSPEYIAQSSTELHTRISPLYSVDEERWLTQLLPLAKPTD  
AERDSAATQTRQLVEHVRNDGKAVKMVDSL LLEYS LDTQEGVLLMSLAEALIRVPDNYTA

DALIHDKMSVADWKKHLKNDNGFMVNASTWGMMTGRVVSIDSDDTTASGFLDRMTKKMGE  
PVIRSAMQKAMRIMGHQFVLGETIEGANKNSQPYRNKGYTYSFMDLGEAAITHKDAEKYF  
NDYLHAIKATASVKVKEGMPKPSVSIKLSALHPRYEATQEEQVMGLLRQRCLLLLIEAARE  
VNVDSLIDAEADRLEISLKLFESELYRDNLTDWDGLGLVVQGYSKRAIAILSWLARLAT  
EVGDRIIPVRLVKGAYWDTEIKLAQQKGLSGYPVWTRKEGTDATYLAACARFLLSEHLRGLI  
WPQFATHNAHTLASIMTMSSHRDFEFQRLHGMGDALYDHILQAYQIPVRIYAPVGAHKDL  
LPYLVRRLLENGANSSFVHQLLDKSYPIDKLTVHPYDKLLTNATLHNPDIPLPLAIYGAR  
RASFGPNIFVESQWIPFKAAIDTHIKTWSATSVINGNAVNDNTVDGDTHQLDKQAICAP  
WNHEVIAGEVVYANATIAQQAIAAAVAGQGEWQAVAATKRAAILRKIADLYEENYAEELMA  
LCQVEAGKTLQDSIDEIKEAVDFCRFYADEAERLDDVIYEFTDLAGKPSRQVYKARGTFI  
CISPWNFPLAIYTGQVVAALAAGNTVVAKPAEQTSLIAHFQAQLMYQAGVPVEALQLVIG  
AGDVGAALTAADNIAGVIFTGSTQTAQRINQSLNAHAQVSGELPVFIAETGGQNMIMDS  
TALPEQVVRDAVLSAFGSAGQRCRILCVQEEMADDLIELLQGNMAELIVGNPLYATT  
DVGPVIDIDAKRGLEAHIERMRAEPTATILAQTPMSDSSEVSQDQATFVLPTAIEVKSID  
VIGGEHFGPILHVLRYEARLDNLKIDAINATGFGLTLGIHSRIENTVEHIERRAFVGNTRY  
INRNQIGAVVNVQPFGGCGLSGTGPKAGGPHYVARLMSLTTEQLANEQVALIDNTAATST  
QTIIA

>Rhodoferax Q21UN0 Q21UN0\_RHOFD

MATVTGLIKVDETLRSRIKDAATLQGRTSHWLIKQAVLQYVEGIERGHRPQVATAGATSS  
VEAVEIDDADDLTLPASPALFPQPFLDWAQNVLPQTEMRAAITAAWHRPEPECLPMLVQ  
LAHVTDPVQVRAIAEVGTRLVDGLRSNKDSGGVEALVQEFSLSSQEGVALMCMAEALLRI  
PDNATRDALIRDKISHGDWHSHLGNSPSMFVNAAVWGLMLTGKLTATASEKSMASALTRM  
IGKGGEPLIRQGVHRAMKLMGEQFVTGQTI SEALANSRALEKKGFYSYDMLGEAATTEL  
DAERYVASYEQSIRAIGMASNGRGIFEGPGISVKLSALHTRYSAQRDRVMGELLPRLTK  
LALLARQYDIGINIDAEESDRLELSLDLLESLCFDPRLKGNWNGIGFVVQAYLKRCPYVID  
HVIDLARRSGRRLMIRLVKGAYWDAEIKRAQLDGLDGYPVYTRKVHTDVSYLACARKLLA  
APDAVYPQFATHNAQTVASIYQMAGNNYYAGQYEFQCLHGMGEPLYEQVTGTVDAGKLGR  
PCRIYAPVGTHTLLAYLVRRLLENGSNSSFVNRIGDPKVRVEDLVADPVLEAQAI ELEA  
QGLGAPHPKIALPRQLFAALGAQSRNLSSGLNLANEQQLASLAAGLLRSTQGNAAAAATV  
AGMAHVNPQTAAADLQAVCNPADTRDQVGVWRPATVAEVELAVNRAARATQIWQVTPPQ  
ERAACLKRAADLLEQRTQSILGLIVREAGKSLPNAISEIREAVDFLRYYAAQVEATFDNQ  
TQRPLGVVLCISPWNFPLAIFAGQVAAALASGNCVLAKPAEQTPLVADLMVKILHEAGVP  
MDAVQLVPGTGEVVGAAALVANRQVAGVMFTGSTEVARLIAQTLSQLSRQGRICIPLIAET  
GGQNAMVVDSSALAEQVVGDLSSAFDSAGQRCRSLRLLCIQEDVAERVIGMIKDAMREW  
VMGNPDRMHTDVGPVIDEDARAQIEQHIERMRSDGQPVTRMARDESGAQGHFVMPTLIEI  
DRIERLQREVFGPVLHVLRYRRDDLDAVLDAINATGYGLTFGVHSRIDETIAQVTQKVQA  
GNIYVNRNVIGAVVGVQPFGGMGLSGTGPKAGGPLYVYRLLQEDDAQSNPGLAALAASPA  
SRVLVPGSFDRQLAAHPALQALQRLMASLQGPTLAAAQALGSFDAQGAAACEAYRACS  
VLGQAFMLPGPTGESNRYQLLPRGAVWAVPQTALGLLHQLAAALASGNACWIETPASDSV  
VARMLNTLPPEVLRVQQRSDQLRGEPHLSAMLFEGDGDALQALSPRVAQQPGAIVRIE  
SLSPAQLAAGACYDLSALMHEQSISTNTAAAGGNAQLMTMD

>Bordetella Q2KZJ2 Q2KZJ2\_BORA1

MASTTLGVKVDDALRDLKAAAQKLQCTPHWLHKQALVAYLEKIERGHLPPEMAHLGSGE  
DGAEEDAGGQAGATPPFYEFQDVQPQSVLRAAITAAYRRPEPECVPLLLGQARMPHLEK  
IHMAAKLVQTLRAKRTGGGVEGLIQEFSLSSQEGVALMCLAEALLRIPDRATRDALIRD  
KVSRGDWKSHMGGQSFLFVNAATWGLMITGKLVAVSSEQSLSKALTRLIGKGGEPLVRKG  
VNMAMRMMGEQFVSGQTI SEALANNRKMESRGFRYSYDMLGEAATTAQDAERYNAAYEQA  
IHAIGKAAAGRGYIEGPGISIKLSALHPRYSRAQRERVMSELLPRVKKLAILARQYDIGL  
NIDAEADRLEISLDLLEALCFTPELEGWNGIGFVIQAYQKRAPFVIDYVIDLARRSGHR  
IMVRLVKGAYWDSEIKRAQVDGLEGYPVYTRKLYTDVAYLACARKLLAVPEAVYPQFATH  
NAYTLAAIYHLAGQNYYPGQYEFQCLHGMGEPLYDEVVGPLAQGKLNRPRIYAPVGTHE  
TLLAYLVRRLLENGANTSFNLIIGDSSIPVEQLVADPVEAAARIVPLGAPHDKIPLPREL  
YGHARANSAGLDLSNEHRLGSLSAALLASAGMPWRAAPMLGESEFVWDESRAQDVLPAD  
QRDGVGRLIEADSHDVEAALRAAANTAPIWQATPVAERAQCLRRAAQLLEEQMOTLLGLI  
VREAGKTLPNIAIAEVREAVDFLRYYADQAEREFDNDTHRPLGSLVCISPWNFPLAIFTGQ  
VAAALAAGNTVLAKPAEQTPLIAAQAVAILRAAGVPAGAVQLLPKGGETVGAQLVAHASV  
RGVMFTGSTEVARLIARNLADRLDDRGTIPLIAETGGQNAMVVDSSALSEQVVFVVLSS

AFDSAGQRCSSALRVLCVQEDNADHVLTMRLGAMRELRMGNPDRLSTDVGPVIDAEARQNI  
LRHIESMRAAGHEIVQIEGGAECRFGTFVPPTLIEINDIAELKREVFGPVLHVVRYPARD  
LDRVIESINGTGYGLTFGVHTRIDETVARVTESVQAGNIYVNRNIVGAVVGVQPFGEHL  
SGTGPKAGGPLYLYRLLSMRPAGLPPGLEQOMPLTLTLPGPTGETNTYRVEPRGAVYCVA  
ATAAGARAQWAAAQATGNLAWFADTPAARELLATLESAAREGQVALLEDAEVDAAADFQAV  
LFEGDGDALKALNQRIARREGPILAVHGLSPDELAAGASYVAERLLNERSCSVNTAAAGG  
NASLMTIG

>Rhodopseudomonas Q6N9G9 Q6N9G9

MPSDPPLAEFTAAYAPDDAALAAELLTTATLTPDREAQIDAIATDLITAIRGSEHGLRGV  
EAMLREFALSTKEGLALMVLAEALLRVPDAATADAFIEDKLGQGDFAHHRIKSDAVLVNA  
SAWALGLSARLVHAGETPQGTLAALTRRIGAPAVRAATRQAMRLIGNHFVLGETIDAALA  
RAQPYAREGSRYSDMLGEGARTAADAERYYSYADAITAIGRRAGNAALPARPGISVKL  
SALHPRFEAISRDVMRELTPRLLELAQLAKSHDLAFTVDAEEADRLELSLEVFAACFAD  
PSLKGWDGYGLAVQAYQKRAATVIDHVAELARAFDRRMLRLVKGAYWDTEIKRTQERGL  
ADYPVFTRKAMTDLNLYLHCARKLLALRPLLFPQFASHNALTVAITILAEAGDGDGYEFQRL  
HGMGEALYGRLLADHPQAVCRIYAPVGGHRDLLAYLVRRLLENGANSSFVAQAGDSDVP  
TELLARPATLIGHPENARNSAIPLPRDLYQQRINSRGIEFGDRSALAALLGDI EGARRP  
LPTVASTSPEQAAATVTAARKGFESWSRTSGDHRAAILQRAGDLLEQRRGELIALLODEG  
GKTLDDGVAEVREAVDYCRYYASEGRRLFGEPQALPGPTGERNTLALRGRGVFVAISPWN  
FPLAIFLGQITAGLMAGNAVAKPAEQTPVIAEVAVRLLHEAGVPPAALHLVQGDGRIGA  
ALVEQRDIAGVVFTGSTEVARAINRTLAAKDGPVPLIAETGGINAMIVDATALPEQVAD  
DVIAAFRSAGQRCSSALRLLCVQDDVADRVIAMIAGAARELTIGDPRDPATHVGPVIDAE  
AKTRLDTHIATMKRQAQLHFAGTAPASGNFVAPHIFELNRASELTEEVFGPILHVVRYPKA  
AQFDDLLDDIATTGYALTGLVQSRIDDTIARVIARLPTGNVYVNRNIIGAVVGVQPFGG  
GLSGTGPKAGGPHYLPRFALEQTVSINTAAAGGNAALLTGSE

>Gluconobacter Q5FP43 Q5FP43\_GL

MIIGLRPSVSVSEAESMSTFVPSYPVRSRLRQAIAADMRRPEAECILPLIEQATLTETEQQ  
NTFDVARHLTRTLRTQRRPGGVEALVQEFSLSSAEGVSLMCLAEALLRIPDAATRDALIR  
DRIGTGDWLSHVGGKKSVMFVNAASWGLMLTGKLTNDTDEGLAAALFRLVGRGGQPLVRR  
LDIAMRMMGEQFVIGETIEEARKVSTEPEERGFKYSYDMLGEAAMTEADALRYRRDYERA  
IDVIGQTARGANVYEKAGISIKLSALHPRYAFQAQRERVLKELGQTLKDLVIQARRYDIGI  
NIDAEESERLDSLIEDLCHCELDGWNIGIVVQAYGRRAPKVL DYLDLGRSSGHR  
LMIRLVKGAYWDSEIKKAQVEGQTDFFVYTRKCYTDVSYIACAKKLLAARDVVPQFATH  
NARTLATIYTLAGLNFQIGDYEFCQLHGMGETLYNEVVGPKLNRPCRVPYAPVGSSETLL  
AYLVRRLLENGANSSFVNQIGDESLPIETLIADPVALAKAVQPPGASHPAIALPKDLFVP  
ERTNSRGLDLTDEHTVTALAEAVCASEKQTTLEDLSCSGETQEIRNPANHLDRIGSVRFGT  
EEDVRKAIDAAESEGAWAALSADARSTKLDRAADLLEEHQSELMALLVREAGKSYANAL  
SEVREAVDFLRYAVQARETAQAGSSAPLGVVACISPWNFPLAIFLGQISVALAAGNTVV  
AKPAEETPFIALRAVALLREAGVPENALRLVPGAGETGAALVADPRISGVMFTGSTAVAG  
LIASLTLSRTGADGQPVFPVAETGGQNAMIVDSSALTEQVQVADVLVS AFDSAGQRCSSALR  
VLCVQEDCADRVLTMLRGAVEELRVGNPAELHTDVGPVISAEAQSGIQTYIDASRAQNRA  
VWSLPLPDTTSTNGTFIAPTIIIEIDSLADLKGEVFGPVLHVLRFEASGFEALINAINQSGY  
GLTFGLHTRIESRMAHVTSRIEAGNLYVNRNMVGAVVGSQPFGEKLSGTGPKAGGPLIL  
RRLMSTAPAHTDWNQELPEPARLFLSWLMRTSFPLYQTIVDAMQHGMC GTTRELPGPVG  
ETNLYQLLPRGAVLCVASDRETMLRAVGLALSGGNTAFVQGPVNASDWDVSDLPDALALHI  
RRTQGGRVAGCRTILASPEEKQMAEQTRAALS RSGMIVQLYMLDAKSPIRPEWVLQEKVV  
STNTTAAGGNASLMTIG

>Alcaligenes Q6QHN6 Q6QHN6\_ALCD

MQISQKHSTVMDIHSKFDPASRFRGFASGQPAASELRERITAACRTAEPVAVSALLAMAK  
MEPEVARKANQLSMQIAQRLRERKNSAGRAGIVQGLLQEYALSSQEGVALMCLAEALLRI  
PDMATR DALIRDKIARGHWQEHAGRSPSLFINAATWGLFLTGKLVSTYSESSLTLLTRL  
IAKGGEPLIRKGVDMAMRMMGEQFVTGETIKEALDHARGLEAQGFYSYDMLGEAAMTAE  
DADRYRQSYERAIIHAIGEASNGRGVYEGPGISIKLSALHPRYSRAQYGRVMDELYPVVRS  
LALLARRYDIGLNIDAEADRLELSLDLLEKLCFEPALAGWNGIGLVIQAYQKRCLFVID  
HVIELAQRSRHRMLIRLVKGAYWDSEIKRAQVEGQDGFVYTRKVYTDVSYLACARKLLV  
APAEIYPQFATHNAHTMAAIYNLAEPANYQPGQYEFQCLHGMGEPLYEQVVGSLADGKLG  
RPCRIYAPVGTHETLLAYLVRRLLENGANTS FVNRIADPSIPLEALVEDPVAVERMAQE

EGEAGRPHPCIPSPSALYGQARRNSHGLDLSNEQTLRGLEPILVDSARTGWTAEPLLGES  
AEAEP TAWKPVLNPADHRDVVGKVRASEEQQIEAALRSATGFAPQWAATSAGDRAFLER  
AADLLQDQLPYLLGLLCREAGKSYANGVAEVREAI DFLRFYAAHARTDFDDPAHKPLGPV  
VCISPWNFLAI FVGQVSAALAAGNPVLAKPAEQ TSLIAAEATRLMHTAGVPRAALQLIP  
GRGSVVGARMVADARVQGVMTGSTAVARQLQRTMAERLGPTGAPVPLIAETGGQNAMIV  
DSSALVEQVVADVMASAFDSAGQRC SALRVLCVQDDVADRLLHMLRGAMAE SNGVDPSSL  
CTDVGPVIDLAARTTIESHIELMQSRGRRVNRAGRAAEVLEGGTFVLPTMIELESISEL  
EREVFGPVLHVVR YARQDLDTMLAQISATGYGLTMGIHSRIDETIGRVVSSAKVGNVYVN  
RNMVGAVVGVPFGGEGLSGTGPKAGGPLYMYRLLAESPHDVLVRAAERGLPGSVADGSV  
TQASEPF EALLSWIETHRERPLTARCRLKRTAGSGQMRVLVGPTGERNTYSLQPRVAAL  
CLAEDEDSLLFQLAGALVGCRAIWPSNTDTQALRATLPLDVQAEIALARDWAAPTVEFD  
VALYQGSREGLLAASARLAERQGPITSLWRFP TDSGKVPLEALVVEQAVSTNTAAAGGNA  
SLMTIS

>Paracoccus Q3P751 Q3P751\_PARDE

MNRVNPTVRSDVFSQAQKFADEAELL SGLVAQAGLDDAQRAAITRRAADLVRRIRDEAKP  
TMMEHFLAEYGLSTREGVALMCLAEAMLRVPDRMTIDALIEDKIAPSDWGKHLGEASSSL  
VNASTWALMLTGKVLDDDQAGIAGTLRRAVRRLGEPVIRTAVGRAMKEMGRQFVLGQTIE  
AALERA AKREAQGFTYSYDMLGEAAMTGADAARYDRAYSDAIAAIAKACTRGSVEDNPGI  
SIKLSALHPRYEVAQESRVMTELVPVVLKLARQAKAAGMGMNIDAEQDRLVLSLKVIEA  
VLSDP SLAGWDGFGVVVQAYGKRAGQVIDWLYETATRLDRRIMVRLVKGAYWDTEIKRAQ  
VEGFPGFPLFTSKVATDVSYIANARKLIGYADRIYPQFATHNAQTVAAIL EMAGETRFEF  
QRLHGMGERLHDIVLRDHNGRCRIYAPVGAHRDLLAYLVRRLLENGANSSFVHQIVDES  
SPEEVARDPFAALAEARPPLGLITPDALFGASRRNSTGFDLTDEETLARIYTARDVAIPD  
AMPLTVSEPTGKMQDVLNPATGEK IARVMMVDADTAARA IADARIWDASAAERA AVLRRRA  
ADLYEDHYGPIFGILGREAGKSLADAVAE LREAVDFLRYAAEAGEASPGAPRGIVGAISP  
WNFPLAIFTGQIAAALMAGNAVI AKPAEPTVIAAYAIGLLHQAGVPKAAQLLP GAGRV  
VGTALSSDPRVSGLVFTGSTGTAQT IARTMAANLAPGTPLIAETGGLNAMVVDSTALPEQ  
AVRDIVNSAFRSAGQRC SALRCLYVQEDVAPHLVEMIKGAMDELRLGDPWDLTTDVGPVI  
DPGAQKEIADYIAANANRVLHKLAA PSRGWFIPTMLKVSGIADLERE IFGPVLHVATFR  
GDQLDQMIADINARGFGLTFGLHTRIDSRVQEVSDAIHVGN IYVNRNQIGAVVGSQPFGG  
EGLSGTGPKAGGPRYVPRFFAPAAPS AVPGTWQGE GDEARLRGALADASPKKIDERLMPG  
PTGELNRLTAHARPPVLCLGPGAEAVAAQVA AVQALGGQAVGADGALPPEALTRLPQLST  
VLWWGDEAQGRAHAQALAA REGEIVQLITAMPDLAHIAHERHLCVDTTAAGGNAALLAG

>Sodalis Q2NTK7 Q2NTK7\_SODGM Pr

MGTTTGMVKLDDEARERIKQAARQLDRTPHWLIKQAI FHYLDALEQGATPGLPLPAAEAD  
DTLKVVSDEPRQPFIDLAEQILPQSITRAAVTA AWRRPETEAVPWLLEQARHPAPMAETI  
QTLAGKLANQLRHQKRSGGRAGIVQDLLQEFSLSSQEGIALMCLAEALLRIPDKATRDAL  
IRDKISNGNWQTHLGRSQSLFVNAATWGLLFTGKLVATHNEASLSRSLNRIIGKS GEPLI  
RKGVD MAMRLMGEQFVTGEHIG EALANahrleQQGFRYSYDMLGEAALTEEDAQAYLLSY  
QQAIHAIGKASSGRGIYEGPGISIKLSALHPRYCRAQYERVMAELYPRLLRLTLARQYD  
IGLNIDAE EADRLEISLDLLARLCFEPALAGWNGIGFVIQAYQKRC PQVIDELIDLAKRS  
QRRLMIRLVKGAYWDSEIKRAQIEGLEDYPVFTRKVYTDLSYLACARKLLSVPHYIYPQF  
ATHNAHTLAAIYHFAGQNYYPGQYEFQCLHGMGEPLYEQVVGKVAEGKLNRP CRIYAPVG  
SHETLLAYLVRRLLENGANTS FVNRIADSAVPLEQLIADPVQEV TQLAVREGRAGLPHPK  
IPLPRDLYGAQRRNSAGLDLANEHR LASLSAALLNVEHQTWQAAPVVVTEIGDGA VQKVL  
NPADHRDVVGECRQASSEEVAHALAAAVHHGSLWSATPPADRAAVLKEAANRLETDMQPL  
IGLLVREAGKSFSNAVAEVREAVDFLRYYACQIAQDFDNDNYRPLGPVVCISPWNFLAI  
FLGQIAAALAGNTVLAKPAEQ TPLIAARAVALMLEAGVPLGVLQLLPGAGETVGAALVA  
DPRVRGVMFTGSTQVARLLQTTLAARLD PQGRPIPLIAETGGLNAMLVDSSALTEQVIID  
VVTSAFDSAGQRC SALRLLCIQEDVAERTLRMLRGAMAEYTLGNPERLATDIGPVIDSSA  
KAAIDSHITAMRERGYTVWQTPAAEAAGDIQGT FVPLTLIELDSIEALTQEVFGPVLHV  
RYQRRELD SIIDQINGSGYGLTLGLHTRIDETIQRVTERAHVGNCYINRNIVGAVVGVP  
FGGEGLSGTGPKAGGPLYLYCLLSQRRDDALLPSLQALDAVHAPDFTRREILQQAHPALV  
AWMETHQPTLVAQCRHLGEISQAGSVRLLTGPTGEQNSYRLLPREHILCLADQDPDLLLQ  
LAAITSIGARALWAESPQSRRLFTTLPDSVRQRITLLADWTQEDVRLDAVLFHGDSQLR  
NLAQTL SKRPGPLITVQGNARGDQIALERLLIERAISVNTAAAGGNASLMTIG

>Francisella Q2A415 Q2A415\_FRAT



MNDLLNHSGEYPISKEIMNIYKYWLIDEKEAMTKLVEKAHMSSVQKAQVRERAYGLVEKV  
RKNRLKKSIGIDAFMIEYDLSSEEGVVLMLCLAEALLRVPDKYITIDLLIKDKLTSAAWKNHV  
GMEKHLFVNAATWSLMLTGKILKDPHRSYRKVFQNFLKKTSEPVIQAMKQAMKIVGKQY  
VLGETIEEALKVSEAKVARGYSYSDMLGEAAMTMDDAEYYSQYLHAIHELAKYATNTE  
IKKNPGISIKLSALHPRYEVAKHQVRVHTELYPKLLKLTQLAKDYNVGMNIDAEETERLQI  
SLELVERLAHEPSLEGFNGIGIVVQAYQKRAPYVLDYLANLAKKTNRRFMIRLVKGAYWD  
AEIKHAQEQGLAGYPVFTRKYHTDVSQACVKQLFENHQYIYPQFATHNAQTVAVVFELA  
NGNRDFEFQCLHGMGDALYDNNVGKEGYEDIPCRIYAPVGGHKHLLAYLVRRLLENGANS  
SFVNRIVDENLPIEELIEDPVKKAIDHGCQHPNIPYPKDIVSPRLNSQGHNTNDFAVLA  
DMYKQIEKYTHKNYKAKPIVSGIDLDKTITESTVINPNTNEVIGSVINADAKIAKRALKN  
AQSAFEWSNTPATKRADILEKFADLLEQDTNKFIAIAMIEAGKTLANAIDEVREAVDFC  
RYAAQARKEFNPIELPALSDHLKQIEFTGRGAMVCISPNWFLAIFLGQITAVLAAGN  
TVVAKPAEQTPIIAYKAVKLLFKAGLPKNVLQFTPGDGATVGSALVKSVPVCKGVIFTGST  
EVAAIINQTLANKSSEIVPFIAETGGQNAMIVDSSSLPEQVTADVIRSAFDSAGQRCAL  
RILCLQEDIADNYIKMIVGAMKELKIGDSKYIDTDVGPVIDKEAADNLNAYIEEKKSQFK  
LIYQSQPNQDTQKGTFFVMPTAFEIDKISDLGREQFGPILHILRFKANQLDKLINDINATG  
YGLTAGVHSRINEVMNYVKNNLKAGNIYVNRNIVGAVVGVQPFQGGQKSGTGPKAGGPYY  
MHRLANEKLSGVGAVEEIIYNPEKIAEYEQTNKLIKDKYITITNIVAGEKAKKDKYTNLKA  
ANGKTIGKKYVASVNTVDNAIEIASKEVEIWNHVNAEQRAATIEKFLELLEKERYLIASS  
LVVESNISVEDAHIQIDKTIQQVAYYCLQAKKEFAHPQLLPGPTGEIDELSLKGRGVVVS  
MCSSDLLIRFVGQTAAALLAGNTVVAKPAYTGNLTAYNIVKLMLKAGIDSKVLHLVLS  
DEEITSALLFNSKVALVSFSGSVSAVKQVHQALVLRGAIIPFVAESIAKNGKCTSLAIE  
TASPLYLRRFVVEKTVSVDTTASGGNASLMSLEE  
>Wigglesworthia Q8D2C0 Q8D2C0\_W  
MDTRILGIKLDNKLSHRIENISSRLNRTPHWIIKQAIFLHLLDLEKKSKSSEKLIENKNE  
IQDYQDKINEKIIIFKPFEEFAQQILPQSYLRFNTTNAWSTPEKEIVPKLLELSKCEEETE  
KKIHLSKYLAQGLREKSKKYNREQMVQDLLREFPLSSKEGIALMCLAEALLRIPDVNTR  
NSLIKDKIKNKDWKSHFGSNKGLFINSVWGLCITNNLIKRRHKEKNLSSYLNKVIQKIGE  
PIVGKAINVAMKLMGKQFVVGENIQQALKNTNILEKKGFSYSDMLGEAALTEEDAQKYM  
TSYENAIHCIGKSSLGKGIYKGPISIKLSAIHPRYSRNKYEKVMSELYPRLRSLTLLAR  
HYDIGMNI DAEEANRLEISIDLLDKLCCEPSLFGWSGIGFVVQAYQKRCMYVIEELIDIA  
KRTKRRMLMRLVKGAYWDSEIKNAQIEGIEDYPVFTRKAYTDISYLACAKKLLSESNIY  
PQFATHNAHTVSSIIYHFAGENYYSQYEFQCLHGMGEQLYEKVVGNAIDKKLDRPCRIYA  
PVGTHKTLAYLVRRILENGANNSFINRISDNNVSIKLVLSPIKESISISKKENVEIGT  
SHPNIPLPKNLYGNRENHGFNSNENVLAKLSSDLLKNSDKFWKVTPIIHSLDKGSI  
SKIINPANKKDIIGECQSSTLKDVESALESSVKGIELWSSKEPLERSKILYDISNIEKN  
TNIFINLLVRESGKTFPNAVSEIREAVDFLRYYSNQIKPFNNKTHIPLGCVLCISPNWFP  
LAIFLGQISAALASGNAVIKPAEQTPIVAYEAIKLMIDSGIPSESLQFLPGSGKIIIGNS  
LSKDHRHIGVMFTGSTQVARLLQLNLSDRLSKGRPVPLIAETGGLNAMIVDSSALTEQVV  
SDIIVSAFDSAGQRCALRLLCIQEDVSEKTLNMIKGAIDSYTVGNPEYFSTDIGPVIDK  
NAKINIDQHILNMKKSNHVSQSEMSYDTKQDLGNFVLPTLIELDDIDQIKEEVFGPVLH  
IVKFKEEEMNNIFEKINSSGYGLTIGIHSRIEENIEKVTTSTKVGNYVNRNIVGAVVGV  
QPFQGGELSGTGPKAGGPLYLYRLLSDRKEKNILSSLEELDKNKKVDLTRCEKIQESCVS  
LIEWISVNYPDLEKYCNFYFISQSQSGSSRVLQGPTGEKNITYLLLPRERILCLSNENDLL  
IQLAAVTSIGGKAILSHNPITQKIFSILPQSVLKNVILIPNWKREDSMFDIVLFHGDELQ  
LKEVLEILSKKRGPVINVHSHKNGDKKIFLEKLLIERTISLNTTAAGGNTTLLSMV  
>Photobacterium Q6LFT6 Q6LFT6\_P  
MFNAADVLQPSFIERPLNEIWTLISPLYSVDESLWLEQLLPLAEPDIERKHTTDDKAAEL  
IQVRADKNAIQIMIDALLLEYSLDTKEGILLMCLAEALMRIPDAATADALIRDKLSVADW  
KSHLKNSDSLFVNASTWGLMLTGKVVTMDAKEDGKPSHVINRLVNKMSEPVIQAMNQAM  
KIMGHQFVLGRTISEAMKNGKSNRDKGFTYSFDMLEAALTAQDAQYFKDYIMAVESVG  
RDEYASQKGSNQSPDPTVSIKLSALHPRYDVANEARVLDEMYESVLTLLSRARELNVGI  
TIDAEAEADRLELSLKLFEKLYRSDAVKGWGRFGIVVQSYSKRALPVLAWLAALSKAQGDI  
IPLRLVKGAYWDSLEKLSQQSGFSDYPVFTRKESTDSAYLACARFLLSEHLRGVIYPQFA  
SHNAHTISAIVAMTDHRDFEFQRLHGMGDALYNHAMDYQANVRIYAPVGSKDLLPYLV  
RRLLENGANSSFVHRLVDANCPISLTHEPVDTLRSRPSLNNSLIPLPPQIFGESRKNSA  
SINIDIESEWTFPNAAIQAFSQHQWQAGPIVNGVTLDGEQHAITAPYNRSESVGQVAFSS

ASQVAQAIDVASEAYPAWSQVAASERGECLQRLADLLELHTGELVALCHREAGKTIQDSI  
DEIREAVDFCRFYGEQASSELASAKSIKSFQDSTKQLTQYQGRGVFACISPNWFPLAIFLG  
QVSAALAAGNTTVAKPAEQTSLIAYRAIELMLEAGIPAGAIQLLPGTGAEVGATLTDDVR  
IAGVAFTGSTETAQRINRSLVARDCEAVPFIAETGGQNAMIVDSTALPEQVVRDVVRSF  
ASAGQRCSSALRVLFVQADIADRIITLIKAMAELSVGRPELHSTDVGPVIDIAAKEKLLT  
HIESLKNQSTLVAQTQLSDECKLGDFVAPTAFEINSIDILKNENFGPILHIVRFKANEID  
QVVDQINHTGFGTLGLVHSRNERITYCRIEQRARVGNCYINRDQVGAVVGVPFGGQGLSG  
TGPKAGGPHYLYRFTKDVLSA

>Pseudomonas Q9R9T7 Q9R9T7\_PSEP

MATTTLGVKLDPTRETLKAAQSIDRTPHWLIKQAFNYLEKLEGGATLTTELNGHASNP  
ADDAGEVQADHSHQCFLEFAESILPQSVLRSAITAAYRRPEQEVVPMLEQARLSAPLAD  
ATNKLASIAEKLRNQKSVGGRAGIVQGLLQEFSLSSQERRGVCLAEALLRIPDKGTRDA  
LIRDKISTGNWQPHLGNSPSLFFVNAATWGLLLTGKLVSTHNETGLTSSLTRIIGKSGEPM  
IRKGVDMAMRLMGEQFVTGETIAEALANASRFEAKGFRYSYDMLGEAALTEHDAQYKYLAS  
YEQAIHSIGKASHGRGIYEGPGISIKLSALHPRYSRAQYERVMEEELYPRLLSLTLLAKQY  
DIGLNIDAEAEADRLELSLDLLERLCFEPFLAGWNGIGFVIQAYQKRCPYLINYFFDLAKR  
TPHRLIIRLLKGAYWDSEIKRAQVEGLEGYPVYTRKVYTDVSYVACARKLLAVPEAIYPQ  
FATHNAHTLSAIYHIAQNYYPGQYEFQCLHGMGEPLYEQVVGKIADGKLNRPGRVYAPV  
GTHETLLAYLVRRLLENGANTSFVNRIADHSISIQELVADRWPASIAWVPRKGSIGLPH  
RIPLPRDLYGTERAKLAGIEMANEHRLGLLSCAMVATAHKQWEAAPLLACAARESAAAPV  
LNPADHRNVVGHVQEATVAKFDNAIHCALNPAPIWQATPPAERAAILERTADLMEAEIHP  
LMGLLIREAGKTFPNAIAELREAVDFLRYAVQALNDFSNDAHRPLGPVVCISPNWFPLA  
IFTGQVAAALAAGNPVLAKPAEQTPLIAAQAVRLLLEAGIPEGVLQLLPGRGETVGAGLV  
GDERVKGVMTFGSTEVARLLQNRVAGRLDNQGRPIPLIAETGGQNAMIVDSSALTEQVVI  
DVVSSAFDSAGQRCSSALRVLCLEDSADRVIEMLKGAMAESRLGCPDR LAVDIGPVIDAE  
AKAGIEKHIQGMREKGRPVYQVAIADAAEIKRGTFFVMPTLIELDSFDELKREIFGPVLHV  
VRYNRRNLQDLIEQINNSGYGLTLGVHTRIDETIAKVETATPATCRHRNIVGAVVGVP  
FGGEGLSGTGPKAGGPLYLYRLLSTRPADAIGRHFQQQDGEGETPDRTLHEQLVKPLHGLK  
AWAENNLADLAALCSQFASQSQSGIARLLPGPTGERNSYTIIPREHVLCLADNETDLA  
QFAAVLAVGSSAVVVDGEPGKALRARLPRELQAKVKLVADWNKDEVAFDAVIHHGSDQL  
RGVCQQVAKRAGAI VGVHGLSSGDHQIALERLVIERAVSVNTAAAGGNASLMTIG

>Erythrobacter Q2N7F6 Q2N7F6\_9S

MSKIAPLNRLHFR TAYRQEENACVAERLKQAAPVSARHEEAQALAVRLIEDARSRKASGI  
DAFLHTYGLATEEGIALMCLAEALLRVPDHETADALIRDKLGDIDWGEHLGESSSTFVNA  
ATFSLMLTGEVLERPEEHQRGMGKTLKRTVNRLGEPVIRKATLQAMRILGGQFVYGRITIG  
EALKRAKPERAKGLTHSFMDLGEAAMTFEDAERYRRAYERAIERLAGETDGTIQSSPGIS  
VKLSALYPKYDIFHQDAAVEALVPMLRDLAIKARDANMHFNIDAEAEERLEISLDI IERL  
AADDALFTKADGTRWDGFLAIQAYQKRAAPLCDWIVKLARRHRRFMVRLVKGAYWDE  
IKLSQVGGYEDFPVFTRKVATDVSYLACA AKLLEAPDAIYPAFATHNAYTVGAVKALAGH  
TEFEFQRLHGMGEELFEALAAQEGNRKTPVRIYAPVGVHKDLLAYLVRRLLENGANS SFV  
NRMADA EVP AVELANDPVEELALLEPKRNPDIPLPADIFPGRNRSIGVDLADPLVRDPLL  
QRLEALESRHWHYAGPTFPSEDAGEEAPINAPQDLTHEVGTRRDSTEEEVRAAITQAEFIQ  
PGWNALGGEKRAVLLEAAADLFEDHMEFLSLCRREAGKTVLDGVLEVREAVDFLRYAT  
EARRQFSAPIMLPGPTGEENRLHLAGRGVFATISPNWFPLAIFIGPAAAAMAAGNTVIAK  
PAEQTPLIAALAVKLCHEAGIPEEVFQLLPGAGDVGQMITGDPRIAGVAFTGSTETAQAI  
NRSLAAREGP IATFIAETGGQNAMIVDSSALPEQVARDVVASAFQSAGQRCSSAQRMLYIQ  
DDVYDDMLAMIRGAFAALQIGDPTDFAIDVGPVIDPDAKAALERHVARRKKAGRTVWRRK  
LPRGTANGCFVAPTI IELDSILDKRENFGPILHVARYKADGLNRVIADINSTGYGLTLG  
LHSRIEATRRYVEARARVGNFYVNRNQIGAVVESQPFGEGLSGTGPKAGGPHYVARFAT  
ERVVCIDTTAAGGNATLLAS

>Wolbachia Q73IQ2 Q73IQ2\_WOLPM

MISSIQEPNELRKRLQGFYRTDEKSYIRYLVEKAELSADSKNRIYNIQVIEKIKHNKL  
SIVDSFMQQYSLSNDEGIALMCLAESLLRIPDDYTIDEI IKDKIANQEWNKYLGHSSSLF  
VNASTWSLMIGSSILRDNEGDSKFYYAISKLLKNLGEPIIRKAVKQAMSMLGNHFVVGET  
IEEALRYAKLDDNSKFLYSFMDLGETAHTAEDAEEYFNSYMHSIKAIGESTEINDCFKSH  
GVS IKLSALHPRYEFQFDNIAEELRAKLLLECHEAKKYNISLCIDAEETERLEMSLILF  
EQLRLDESLSEWEGLGLAVQAYQKRALSVDLDFVEDVAIRSKHKIMVRLVKGAYWDSEIKR

TQELGLNDYSVFTRKSYTDVSYFVCAQKLLSKPNSFYPCFGTHNVYTFASIMELADKNHP  
GFEFQRLHGMADKLDYDAMSELATNVSCRVPVGEHSDLLPYLIRRLLENGANSSSFVNQ  
ISDPNVKIDELISDPLEKAINFNYPHPGIPLPDILGPERKNSLGMDISDSVIVSQFAD  
DIKGFSEKKWQIGPIIDGKALFDNAEFIEVVNPAHLENVIGEVSATSDQALNALEIAHS  
AFAKWQNVSAEERAKCLEKAADLLEERMKELIYILIVEAGKILSDAIAEVREIDFLRYY  
AMIAKNELSDWKKLPGPTEGDNFIFFEGRGVFLCISPWNFPLAIFIGQVSAALAAGNAVL  
AKPAEQTPIIAYEAVKILHEAGIPKNVLHLIPGDGGYLKILVDPDNRIAGVAFTGSTQTA  
QIINKMLANRDGPVPLIAETGGLNAMIVDSSALLEQVAMDALLSAFRSSGQRCSALRVL  
FIQEDIAEKQIKMICGAAQELKIGDPIQLSTDIGPIIDKASIDMLTQHTQKMEDEDSNL  
LFKVPMDTNSHNGYFFPPYIYEIQKISQLKQEVFGPIILHIIRFNKSQLNEVIDINSTGY  
GLTFSLQSRISQSIETISKKISVGNVYINRNQIGAAVGIQPFGGRLSGTGPKAGGPHYL  
QRFSTEKVVSNTTAFGGNTTLMCLD

>Nitrosomonas Q3NDK3 Q3NDK3\_9PR

MRIHPARAAMAHLYLCDETEAVNALIPRARLSAMERAATEALARDLVQRMQRWRGGLN  
MFLHQYALSTEEGVALMCLAEALLRVPDAETQDRLIRDKIGSVHWEKHLGQSSSLFVNAS  
TWALMLTGRVVRLGEGRSWNTNIFSRMVQSRGKPVIRQAMSAAMRIMGRQFVLGCTIEEA  
LRRGTEAARRGYRFSFDMLGEAAVTREDAERYARVYAGATAAITSHEARKEAQHGDIFAR  
NSISVKLSALHPRLEYVKAERVLAELPQLMPLCQAACKARIGFTIDAEADRLDLQLDI  
FEALSRTRELAGEGLGLAVQTYQKRAVIDWLAIAAREHKRRIPVRLVKGAYWDSEIK  
RAQELGIDGFPVFTRKASTDVSYLACARMLLADRSAFFPMFATHNAHTLAAVKVLGNRS  
DYEFQRLHGMGEELYDQAVGADHSGVQCRIYAPVGPHKDLLAYLVRRLLENGASTSFVNR  
FADNKMPIASIIADPVDQIEAMSAKPHPHIPLPKNLFTDRKNSRGLLI SDPAQARLLLLNA  
VAAAIEHGFEARPLIGGEPYPGEGA AVFDPALHSRQVGTVLNATPDMVTRAASTAAAQG  
AWDRLGGVRRAEILERAADLFERDMAVLIALCVREAGKTVSNALADVREADIDFLRYAGI  
ARADFAEPKVMGPPTGERNELSLHGRGVFAAISPNWFPVAIFTGQVASALAAGNSVLAKP  
AERTSLAAYTAIQLMHEAGVPGEVLHFLPGSGRVIGTAMVRHPATTGVVFTGGTDTGHVI  
NRMLAERAGPIVPFIAETGGLNALIADSTALPEQLVRDVLTSAFDSAGQRCSALRVFLQ  
EDIAERVISLIRGAMAE LRIGDPMKLDTDIGPVIDGNSLAKLEAHAKRMSREAGFIAEAP  
LSDETR DGFFFA PRAYEIDAISRIEREVF GPILHVIRFKATRLDKVCEAINATGYGLTLG  
VHTRI QETVDFIRARVRIGNLYVNRNQIGAVGVQPFGGEGLSGTGPKAGGSHYLHRFAV  
ERTVCINTAATGGNTALLSLDEVACRGRDS

>Brucella Q578K6 Q578K6\_BRUAB P

MTDNIPVSKVAVFQNFAPPPIREQSALRQAITAAYRRPEAECVSALAEQATLPEETRQQIR  
STARKLIEALRAKHKG TGVEGLVHEYSLS SQEGVALMCLAEALLRIPDMATRDALIRDKI  
SNGDWKSHIGGGRSLFVNAATWGLVVTGKLTNTVNDRLGSAALTRLIARC GEPVIRRGVD  
MAMRMMGEQFVTGETIDEALKRAKELEERGFRYSYDMLGEAATTAADAERYYKDYETAIH  
AIGRASAGRGIIYDGP GISIKLSALHPRYTRAQSERVMGELLPKVKALAAIAKSYNIGLNI  
DAEEADRLELSL DLLQSLCEDPDLAGWDGIGFVVQAYGKRCPLVLD FII DLARRTKRRVM  
VRLVKGAYWDAEIKRAQVDGLEDFPVYTRKVHTDVSYIACARKLLAATDVIFPQFATHNA  
QTLATIIYHLAGPDFKTGKFEFQCLHGMGEPLYDEVVGPEKLGRPARIYAPVGPHETLLAY  
LVRRLLENGANSSSFVNRIGDKNVSVD ELIADPVEVVRSM AVVGARHDQIALPENLYGARR  
NSAGFDLSNEVT LAELSKTLKETAGRAWTAEPQVAGAKVKGVSRPVLNPGDRNDVVGTVT  
EIAEADVAKAMKAAQTATTSWSAVAPAERAACLERAADIMQRDMPALLGLVMREAGKSMP  
NAIAEVREIDFLRY YAEQTRRTLGVGHKALGPVVCISPWNFPLAIFTGQIAALVAGNP  
VLAKPAEETPLIAAEGVRILHEGGIPADALQLLPDGGRIGAAALVAAPETCGVMFTGSTEV  
ARLIQAQLASRLLPNGKPVPLIAETGGQNAMIVDSSALAEQVVF DVIA SAFDSAGQRCSA  
LRVLCLEQEDVADRILTMLKGALRELSIGRTDQLKVDIGPVITDEAKNTIEKHIIQAMRDLG  
RKVEQLPLGPETQNGTFVAPTII EIESLRDLKREVFGPVLHVVR YKRDDMESLIDDINST  
GYGLTFGLHRLDETIANVADRIRVGNIIYINRNIIGAVGVQPFGGRLSGTGPKAGGPL  
YLGRLVETAPIPPRHASVHTDAALKDFARWLGNRGMNDLAQAARDTGSASALGLELELPG  
PVGERNLYALHPRGRVLLVPQTEIGLYRQLTAVLATGNTAVIDEACGLRAVLKDLPETVA  
ARAIWTGDWQADAPFAGALIEGDSARIKEVNSRIAALPGPLVLTQAASPEDLAANQDAYC  
LNWLLLEEVSTSINTTAAGGNASLMAIG

>Escherichia coli P09546 PUTA\_E

MGTTTTMGVKLDDATRERIKSAATRDRTPHWLIKQAFISYLEQLENSDTLPPELPALLSGA  
ANESDEAPTPAEEPHQPF LDFAEQILPQSVSRAAITAAYRRPETEAVSMLLEQARLPQPV  
AEQAHKLAYQLADKLNRNQKNASGRAGMVQGLLQEFSLSSQEGVALMCLAEALLRIPDKAT

RDALIRDKISNGNWQSHIGRSPSLFVNAATWGLLFTGKLVSTHNEASLSRSLNRIIGKSG  
 EPLIRKGVDMAMRLMGEQFVTGETIAEALANARKLEEKGFYSYDMLGEAALTAADAQAY  
 MVSYYQAIHAIGKASNGRGIYEGPGISIKLSALHPRYSRAQYDRVMEELYPRKSLTLLA  
 RQYDIGINIDAEESDRLEISLDLLEKLCFEPELAGWNGIGFVIQAYQKRCPLVIDYLIDL  
 ATRSRRLMIRLVKGAYWDSEIKRAQMDGLEGPVYTRKVYTDVSYLACAKKLLAVPNLI  
 YPQFATHNAHTLAAYQLAGQNYYPGQYEFQCLHGMGEPLYEQVTGKVADGKLNRPRIY  
 APVGTHETLLAYLVRRLENGANTSFVNRIADTSLPLDELVADPVTAVEKLAQQEGQTGL  
 PHPKIPLPRDLYGHGRDNSAGLDLANEHLASLSSALLNSALQKWQALPMLQEPVAAGEM  
 SPVINPAEPKDIVGYVREATPREVEQALESAVNNAPIWFATPPAERAAILHRAAVLMESQ  
 MQQLIGILVREAGKTFNSAIAEVREAVDFLHYYAGQVRDDFANETHRPLGPVVCISPWNF  
 PLAIFTGQIAAALAAGNSVLAKPAEQTPLIAAQGIAILLEAGVPPGVVQLLPGRGETVGA  
 QLTGDDRVRGVMFTGSTEVATLLQRNIASRLDAQGRPIPLIAETGGMNAMIVDSALTEQ  
 VVVDVLASAFDSAGQRC SALRVLCQDEIADHTLKMRLGAMAECRMGNPGRLLTTDIGPVI  
 DSEAKANIERHIQTMRSKGRPVFQAVRENSEDAREWQSGTFVAPTILIEDDFAELQKEVF  
 GPVLHVVRYNRNQLPELIEQINASGYGLTLGVHTRIDETIAQVTGSAHVGNLYVNRNMVG  
 AVVGVPFPGGEGLSGTGPKAGGPLYLYRLLANRPESALAVTLARQDAKYPVDAQLKAALT  
 QPLNALREWAANRPQLALCTQYGELAQAGTQRLPGPTGERNTWTLLPREVLICADDE  
 QDALTQLAAVLAVGSQVLWPDDALHRQLVKALPSAVSERIQLAKAENITAQPFDAVIFHG  
 DSDQLRALCEAQAARDGTIVSVQGFARGESNILLERLYIERSLSVNTAAAGGNASLMTIG  
 >Nitrobacter Q3SN37 Q3SN37\_NITW  
 MSPQPPPPFSVPYAPDDRTIAKQLLTGARLAPEQETRIDQTARRLIDAIRQNDDPLGGVE  
 DMLREFALSTKEGLALMVLAELLRVPDAETADRFIEDRLGQGDFIHHETRSSAFLVNAS  
 AWALGLSARVIQPGETPQGTIGRLAKRLGPVPAIRAATRQAMRLMGSHFVLGETIEAALER  
 THTHSAGCSRYSFDMLGEGARTAADADRYFDSYAAAIEAIGRGAGDNPLPDRPGISVKLS  
 ALHPRYEAVSRGRVMAELVPRAIDLARRARALDLAFTVDAEEADRLELSLDVVAIAVDR  
 SLAGWSGFLAVQAYQKRAGAVIDYIDDLAQALNRRMMVRLVKGAYWDTEIKRAQERGLE  
 GYPVFTTRKAMTDLNYLACARKLLALRPRLFPQFATHNALTVATLLELTGGESGFQRLH  
 GMGEALYAALCKDRHAIACRIYAPVGSRRDLLAYLVRLIENGANS SFVATASDPDVPPE  
 TLLRRPADIIIGSADNAGHARIPLPRDLFQPERINSRGIEFGERA AVNRLVTDVATERVSA  
 VPVNYSGPNDVNRAVTTARDGFSTWSRAPATERAAALERAADLLEQRSARFIAWLQREGG  
 KTLDDCVSEVREAADFCRYAAEGRKLFQDAQPLPGPTGERNTLRLRGRGVFAAISPWNF  
 PLAIFMGQVTAALMAGNAVVAKP AEQTPRIAVEAVRLLHEAGIPVKALHLIQGDGHIGAA  
 LVAHRDIAGVVFTGSTEVARSINRVLAGKDGPVPLIAETGGINAMIADATALPEQVADD  
 VATSAFRSAGQRC SALRLLFVQEDVADRIIEMIVGAARELKIGDPSDPATHVGVVIDDDA  
 RKRLDAHIARMTREARVHFAGPAPSSGSFVAPHIFELDDARHLTEEVFGPILHIVRYSSS  
 ALDGVLEAIADSGYGLTLGIHSRIDDTVEAVVDRLQVGNVYVNRNMIGAVVGVPFGGHG  
 LSGTGPKAGGPHYLTRFATEQTVTVNTAAAGGNAALMTGEG  
 >Caulobacter Q9AA07 Q9AA07\_CAUC  
 MTDWDSLDAGKYRDEAAVIADLLAAKPLSSEDRAAVRAEAEALVRGARRSVRKQGVVESF  
 LQEFSLGTREGLALMCLAEALLRTPDDDDTRDKLIAEKIGSADWASHLGGSDSLFVNASTW  
 GLMLTGKIVEPDETARNDMPGFIKKLAGRLGEPVIRA AVGQAIRIMGEQFVLGRTIEAAI  
 KRAAAEGDMCSFDMLGEGARTAADAARYEKAYADAIETVGKLSNGAGPEAGHGVSVKLSA  
 LCPRYEATHEDRVWEELYPRTLRLAKIAARHNLNFTIDAEADRLALSLKLLDKLCREPE  
 LGDWTGLGLAVQAYQKRCGEVIARLKALSEETGRRLMVRLVKGAYWDSEIKRAQVAGRPD  
 YPVFTTKPATDLSYLVNAKALIEAAPHLYAQFATHNAHTLA AVVRMAKNTGVKIEHQRLH  
 GMGEALYKAADDLYDGITL RAYAPVGGHEDLLPYLVRRLENGANTS FVHALLDERVPVE  
 KVVTDPIDTVEAHPDRHAKIPTPINVYGERRVNSAGLDLSVKADRERLSA AVAAQDGVTLS  
 SAGPLVGGKVAGGAPLPIAPANDQKTGVGVSEAQSAQIDEAFKLARAAQPAWDRAGGV  
 ARAQVLRAKMGDALEANI ERLIALLSREAGKTLSDGIAEVREAVDFCRYYAMLAEDQFGEA  
 EILKGPVGETNSRLLAGRGVFCISPWNFPLAIFTGQIAAALAAGNAVLAKPAEQTPLIA  
 FEAVKLYHAAGLDPRLLALLPGRGETVGAALTSHELDLGVAFTGGTDTAWRINQTLAARQ  
 GPIVPFIAETGGLNGMFVDTTAQREQVIDDVIVSAFGSAGQRC SALRLLFLPHDTADHII  
 EGLKGAMDALVLGDPALAVTDVGPVIDAEAKDALDKHLVRLKSDAKVLHALAAPAGGTFF  
 APVLA EIPTADFLEREVFGPVLHVVRYPENLEKVAGALAARRYGLTLGIHSRIESFAAD  
 VQRLVPAGNAYVNRSM TGAVVGVPFPGGEGLSGTGPKAGGPHALLRFAVERALSVNITAQ  
 GGDPA LLNL  
 >Rhizobium Q98L65 Q98L65\_RHILO

MTAGPLPDARSTGPMPLDTIRQQIRANYLPDEDEAVKRLAEATGLSAADRDAISARAAD  
LVRVRGSSDPRLMEVFLSAYGLSTKEGVALMCLAEALLRVPDTETMDDLIADKIAPHDW  
SAHSGGSSSIFVNASTWALMLTGRVLDEGEGGIEGTLRSMVRRLGEPVIRKAVAAAMREM  
GEQFVLGRTIAEAVKRGRPMTQKGYLYSFDMLGEAARTEADALRYHKAYADAISSLDAGS  
NGPDIRQNHGISVKLSALHPRYEVAQKEEMLPVMAERLLSLALAAHRSRMGLNIDAEED  
RLDLSLDVIERVLAEPELAGWNGFGVVVQAYGPRAAFVIDWLYALARKYDRTIMVRLVKG  
AYWDTEIKRAQTLGLAGYPVFTRKANTDVSYMACAKKLLGMTDRIYPQFATHNAHTVAAI  
LSMATNRDSFEFQRLHGMGEALHETVRQAEGTRCRIYAPVGAHSDLLAYLVRRLLENGAN  
SSFVHQLTDEDVEPEDDIARDPLETVESQGPANPAIARPSQIFGAGRNSRGFDITDTVT  
LAAIDKARAAAFAGPDRWHAKPITRAAGYGKPHPVNPAKPDEVVGTVEHAAKQVAIAVR  
IAVEAQPAWAKRPVGERAAILNRAADLYEANAVEFFALATREAGKSLADGVAEVREAVDF  
LRYAAEAANAETGTQARGAIVCISPWNFPLAIFTGQIAAALVTGNSVIAPAEQTPLIA  
FRAVELLREAGVPEDIIQLLPGDGPSVGGPLTADPRIAGVCFTGSTEVAKLIEKQLAETA  
APDAMLIAETGGLNAMIVDSTALPEQAVRDILASAFQSAGQRC SALRVLYVQKDVEKKML  
DMLKGAMEALNIGDPWRISTDVGPVIDDEAQASIRDYCTRKGLEGRLIAKLEAPKDGRFV  
APHVFRVKGIEEMEREVEFGPVLHVASFDADEIDAVIAAINRKGYGLTFGLHTRIEGRVQH  
FVDGIHAGNIYVNRNQIGAVVGSQPFGEGLSGTGPKAGGPHYLRRFRKGPEAGTEVGE  
HKVTATELADNLPDPALGGWSTRPDRIAILRKHLRGKGAAGAAAAIDFGQVDLPGPTG  
EANTLSLSPRGRVLCGPDAETLLAQTIQALAAGNAVLAVAPGAPAAALSALTGKGLPLAA  
IDGRPDPEARALRVDVAFSGTPEAARIVRQVIADRTGPIVPLVSEVLNPAAYAHRAV  
CVDTTAAGGNASLLAAA

>Halorhodospira Q2CQE2 Q2CQE2\_E

MSAFVHPEPEQLLPAERRALAAAYRIDEPTRSRALLEEADCDPATRSRIQERARGLVHGM  
IRAQRRQSSLTALLHEYDLSSSEGVALMCLAEALLRIPDAPTADQLIHDKLTGGWSSHL  
GRDRLLVNAATLGLALTGRILDTRDAERWFGDRLHTAIARRGAPLIRRAVRRSMGLLGE  
TFVLGRDIPEAQRARKLEAKGYRYSYDMLGEAARTEADAEHFFQAYCRGIEHFGRSADP  
DAPMDARAEVSVKLSALDPRFEPGQEERVQATVIRLQALCRRAREAGIALCVDAEEAAR  
IDLTLDVLEAVMADPELADWDGLGIAVQAYQKRAPEWIDWLAERAGHYRRRLRIRLVKGA  
YWDTEIKDSQIQGLDDYPVFTRKAASDVCFACARRMLRHPQQIYPQFATHNAHTVAAM  
ELADEQPFQRLHGMADDLYDQLVDARPGRGVPVRIYAPVGQHEALLPYLVRRLLENGA  
NSSFVNRIHEGDEVLEIADPVEHLRSRTTLRHPHLPLPSGIFGPERVNSRGIDFSNRQET  
AALAAAMTTAAEPAREARPIINGQGATEADGTWAEVCSPTDTAQHVGRVLWAGHEHLEQA  
LASAAAAPRWAATPVDERARALERLADLYEAHTAELMTLCTLEGKTLKDGIAEVREAV  
DFCRYAVQARRLMGEPTPLPGPTGETNALQLHGRGTYLCISPWNPLAIFTGQITAALA  
AGNAVIAPAEQTPLIAHRAVELMHQAGIPGDVLHLLPGEGRIGPPLVADRRIDGVAFT  
GSVATAQQIHRTLAERDGPVPLIAETGGLNALIVDSSALPEQAVVDVLRSAFFSAGQRC  
SALRLLCIQEDIAEPFLAMLRGAMDALRVGDPRWLATDVGPVIDSDARARLEAHHEAMAA  
AGRVVHRTPLGQAGERGHFVPPSLYRLDAIEDLQEEFFGPMLHYTTWRAGELDSVERIN  
AAGYGLTFGVHSRIDSHREMATRSIRAGNAYVNRDIVGAVVGSQPFGEGLSGTGFKAGG  
PNYLLRFVNERNVTENTAAAGGNASLFALGEDDEA

>Marinobacter Q36JQ3 Q36JQ3\_MAR

MSLQQSVAPELNDIRQAIRANYLADEHEVIHRLIAEAQLSDETRKAI SARAAELVRDVRN  
SARPTIMEKFLAEYGLTTKEGVALMCLAEALLRVPDNLTIQDLIEDKITSNGWGAHVGA  
KSGMINSATLALLMTSNLLKDSEQSVGDTLRKLVKRLGEPVVRTVAGQAMKEMGRQFVL  
GRTIEEAQDRGKSQEERGYTYSYDMLGEAARTDADAQRYYYQAYS DAIDSISKRC KG DVRT  
NPGISVKLSALLARYEYGHKERVNMELMPRALKLARKAAAAANMGFNIDAEEQDRLDLSLD  
VIEAILSDPELKDWDQGFVVVQAFGKRASQTLDWLYALSEKLD RRIMVRLVKGAYWDAEI  
KRAQVMGLSDFPVFTRKACSDVAYLAGARKLLGMTDRIYPQFATHNAHSVAVLEAKDL  
SRDKFEFQRLHGMGESLHDQVLED SGVPCRIYAPVGAHKDLLAYLVRRLLENGANSSFVN  
QIVDTSITPEEIAKDPIDVVVGLGHNLSKAIHVPSKIFGEQRRNSKGWDITDPVTVAEI  
DEGRNRYKSHQWKGGPILAVDSVSDEVVEVRNPANPDDL VGHI TYTSEADISSALGAAQE  
GFKQWSAVPAEERAAMIRRVGDLYEENVHEL FALT TREAGKSLLDVAEIREAVDFAMFY  
ANEGIRYKNDGEARGVMCCISPWNFPLAIFTGQILANLAAGNAVVAKP AEQTSLLAFRAV  
ELMHQAGIPRAAIQLLPGTGATVGSGLTSDARVTGVCFTGSTATAQRINKAMTEHMEPDA  
PLVAETGGLNAMIVDSTALPEQVVRDVLASSFQSAGQRC SALRMLYVQKDIADNLLLEMLY  
GAMEELGIGDPWQLSTDVG PVIDENARKKITDHCQKFEQQGKLLKKNVPEKGLFVSPAV  
LQVSGIEELEEEIFGPVLHVATFEAKDIDKVIDAVNAKGYGLTFGIHSRVDRRIEHIASR

IKVGNTYVNRNQIGAIVGSQPFGGEGLSGTGPKAGGPQYVRRFLRGEVVEKPAQSSDKVL  
SADKAQKLIDKLAKVEVPEAEGRQALLVPFFGKVPAPLDEGYEDMPGPTGEQNHLSCHGR  
GLVLCCLGPDAESAVEQAGTALSQGNKVVIAPGAEKALADAIKAGLPVVASDGMLDPDAL  
SHLTGFEAVVSVAEKPLLKQYRMALSKRDGALLPVITEHKLDQRYVIERHLCIDTTAAGG  
NASLIASAE

>Yersinia Q8ZF67 Q8ZF67\_YERPE B

MANTTMGVKLDEATRDRIKSAAQRIDRTPHWLIKQAIIFYNLEKLESNSELPELATTSSLS  
LQDTEDAIPQLTENTHQPFLDFAEHVLPQSVTRAAITAAYRRPETEAIPMLLEQARLPAD  
LAQATHKLAYSIAEKLNRNQSAGHGRAGMVQGLLQEFSLSSQEGVALMCLAEALLRIPDKP  
TRDALIRDKISNGNWHSHLGRSPSMFVNAATWGLLFTGRLVSTHNEAKLSGSLNRIIGKG  
GEPLIRKGVDMAMRLMGEQFVTGETISEALANARKLEDKGFYSYDMLGEAALTEADAQA  
YLLSYQQAIHAIGKASNGRGIYEGPGISIKLSALHPRYSRAQYERVMDELYPRLLSLTLQ  
ARQYDIGINIDAEADRLEISLDLLERLCFEPQLAGWNGIGFVIQAYQKRCPSTIDAVID  
MAQSRRRRLMIRLVKGAYWDSEIKRAQIDGLEGPVYTRKVYTDVSYLACARKLLAVPNL  
IYPQFATHNAHTLSAIYHLAGQNYYPGQYEFQCLHGMGEPLYEQVVGKVAEGKLNRPRI  
YAPVGTHETLLAYLVRRLLENGANTSFVNRIADATLPLDELVADPVSAREAMAAEAGQLG  
LPHPRIPLPRELFGKDRANSSGVDLANEHRLASLSSALLASASQVWRAEPVIDAEQDNGD  
ALPVINPAEPADVVGYVREATEGEVSRLDAAARAGAIWFATPPAERAAILIRAAELMEN  
QMOTLMGILVREAGKTFSSNAIAEVREAVDFLHYAGIVRDNFANDSHRPLGPVVCISPWN  
FPLAIFTGQVAAALAAGNSVLAKPAEQTPLIAAQAVERILLDAGIPQGVLLPGRGDSVG  
ALLVNDARVRVMTGTSTEVATILQRSIAGRLDPQGRPTPLIAETGGLNAMIVDSSALTE  
QVVTDVVASAFDSAGQRCALRILCIQDDVAEHTLQMLRGAMAECRMGNPERLSTDIGPV  
IDAEAKTGIERHIQAMRAKGRKVYQAARTNSLDEKEWQRGTFIKPTLIELDSFDELQKEV  
FGPVLVHVRVFRQRLNELVDQINASGYGLTLGIHTRIDETIARVTEKAKVGNLYVNRNMV  
GAVVGVPFPGGEGLSGTGPKAGGPLYLYRLLSSRPDDALANTLAHQDGEQQQNVAGREAL  
LTAHRAFTQWATEQQHDSLATLCQRYASLAQGGTVRLLPGPTGERNTYALLPRERVLCIA  
DTESDTLTQLAAVLATGSQVLWPENDVQKALLPQLPTEVQSRITLTHDWQTANITFDAVI  
YHGDADQLRTLCEQVAQIDGPIVSVQGFARGETNILLERLLIEHSLSVNTAAAGGNASLM  
TIG

>Shigella Q3Z3A0 Q3Z3A0\_SHISS P

MGTTTMGVKLDDATRERIKSAAATRIDRTPHWLIKQAIIFYNLEQLENSDTLPELPALLSGA  
ANESDEAPTPAEAPHQPFLDFAEQILPQSVSRAAITAAYRRPETEAVSMLLEQARLPQPV  
AEQAHKLAYQLADKLNRNQNASGRAGMVQGLLQEFSLSSQEGVALMCLAEALLRIPDKAT  
RDALIRDKISNGNWQSHIGRSPSLFVNAATWGLLFTGKLVSTHNEASLSRLNRIIGKSG  
EPLIRKGVDMAMRLMGEQFVTGETIAEALANARKLEEKGFYSYDMLGEAALTAADAQAY  
MVSYYQAIHAIGKASNGRGIYEGPGISIKLSALHPRYSRAQYDRVMEELYPRKSLTLLA  
RQYDIGINIDAEADRLEISLDLLENLCFEPQLAGWNGIGFVIQAYQKRCPLVIDYLVDL  
ATRSRRRLMIRLVKGAYWDSEIKRAQMDGLEGPVYTRKVYTDVSYLACAKKLLAVPNLI  
YPQFATHNAHTLAAIYQLAGQNYYPGQYEFQCLHGMGEPLYEQVTGKVADGKLNRPRIY  
APVGTHETLLAYLVRRLLENGANTSFVNRIADTSLPLDELVADPVTAVEKLAQQEGQTGL  
PHPKIPLPRDLYGHGRDNSAGLDLANEHRLASLSSALLNSALQKWQALPMLQPVAAAGEM  
SPVINPAEPKDIVGFVREATPREVEQALESAVNNAPIWFATPPAERAAILHRAAVLMESQ  
MQQLIGILVREAGKTFSSNAIAEVREAVDFLHYAGQVRDDFANETHRPLGPVVCISPWNF  
PLAIFTGQIAAALAAGNSVLAKPAEQTPLIAAQGIAILLEAGVPPGVVQLLPGQGETVGA  
QLTGDDRVRGVMFTGTSTEVATLLQRNIASRLDAQGRPIPLIAETGGMNAMIVDSSALTEQ  
VVVDVLASAFDSAGQRCALRVLCLODEIADHTLKMRLGAMAECRMGNPGRLTDDIGPVI  
DSEAKANIERHIQTMRSKGRPVFQAVRENSEDAREWQSGTFVAPTLIELDDFAELHKEVF  
GPVLHVVRYNRNLPELIEQINASGYGLTLGVHTRIDETIAQVTGSAHVGNLYVNRNMV  
AVVGVPFPGGEGLSGTGPKAGGPLYLYRLLANRPESALAVTLARQDAEYPVDAQLKAALT  
QPLNALREWAANRPQLALCTQYGELAQAGTQRLLPPTGERNTWTLLPRERVLCIADDE  
QDALTLAAVLAVGSQVLWPDDALHRQLVKALPSAVSERIQLAKAENITAQPFDAVIFHG  
DSDQLRALCEAVAARDGAIVSVQGFARGESNILLERLYIERSLSVNTAAAGGNASLMTIG

>Colwellia Q47VW3 Q47VW3\_COLP3

MLFTGSLITDCPIRQKIREFYRIDENVAVDHILPAAEVNVSARSRAWERARKMVLKIRQD  
QEGNGAIDSLNNEYSLSSEEGVVLMLAEALLRVPDKHTQDELIRDKISQGWSSHLGAS  
DSLNVNASSWGLLLTGSMVNYADKRKKEQFGLLKKTVGRLGEPVIRKSMNYAMKVMGKQF  
VMGETIKAATERAATKEQQGYVSYDMLGEGARTMADANMYLKAYQDAINAIGEVAVASG

KNDPRKVPGISIKLSAIHPRYEFSSHKERMTEIVPKLKALCLQAKQYNIGLTVDAEESER  
LDISLDIIEAVFSDSELGDWQGFQIALQAYQKRAIHVVDWLRDLTLRTERKMMVRLVKGA  
YWDTEIKNAQKDGLNHFVFTKSSSTDVSYHACANKLLEYRDTIYPQFATHNAYTAATIV  
ELAGDDKAGFEFQCLHGMGDSLYDQIVKEESIQCRIYAPVGHEDLLAYLVRRLLENGAN  
SSFVNAIVDEDQPVESLLEDPEKTRQLKAKYNNQIIMPIDLYRGEGEKGRDNSKGLDLT  
DINEIIPKAALDNWFDHLLNKNNEVPDGANAVMNPANRSEIIGFHHASHGDMLLMIDK  
AETAFTWSKTPAVDRAALLCRIGDILERHIDELIAMCIKEAGKVAQDGIDEVREAVDFC  
RYAARAIELSSDERLEARGVVLICISPNWFPLAIFLGQVAAAIAATGNTVLAKPAEQTGLI  
ALRAIELMKSIVGLPENVVQAVIARGSAVGNIIIPDSRIQTVMTGTSTETGTRISQTLSDR  
GGDQVPLIAETGGQNCMIVDSTALPEQVVDVIVSSGFQSAQGRCSALRVLFQEDIADNV  
ITMLQGALAEHLIGNPAKLSTDIGPVIDQKALDALNAHAEMYKSHGKLLYQCEFSDEVD  
EDGHFFFAPRLYEIDDISVLKQEVFGPCVHIVRFKGNIEISVVDKINGTGFGLTMGIHTR  
IEHRAINLAKLSRAGNIYINRNMIGAIVGVQPFGGRLSGTGPKAGGPNYLTRLVKEKAT  
PDERDFNFSANKTITLSGDAENHQANHLMDKANWAEKEWRSTELNTRISCVRQLLAKIA  
HVEIVDDLAEDLNHTLVLARSQIDIEKRLKPKQQLPGPTGESNIIYLENRGNIICYADE  
NVSFHFVWQSIIVTSLATGNTVIAVVSDFYQEALEFRDKFVATGAGKDVQVAKQCHLEA  
MLAHPALSGVVVDSCGEIKHYISEKLALRHGAILPVITSEYFDTMIQRLVTEKTISIDTT  
ASGGNTSLMTLVEED

>Ralstonia Q46VY6 Q46VY6\_RALEJ

MATTTLVGKLDDASRDRLKRVASIDRTPHWLIKQAIIFTYLEQIERGHLPHAMAGGAGE  
ADGADGAEMSHADGAPQPFLEFAQSIQPSVLRAAITSAYRRPETDCVPVLLQARLPQQ  
QAEAAIKMAKKLATALREQVGTGREGLVQGLIQEFSLSQEGVALMCLAEALLRIPDKP  
TRDALIRDKISGANWQSHLGQSPSLFVNAATWGLLLTGKLVATHTESGLSKALTRIIGKG  
GEPLIRKGVDMAMRLMGEQFVTGETISEALANARKYEAQGFRYSYDMLGEAAMTEEDAQR  
YLASYEQAIHAIGQASRGRGIYEGPGISIKLSALHPRYSRAQHERVINELYERLKSLLTLL  
ARQYDIGINIDAEADRLEISLDLLERLCFEPELAGWNGIGFVVQGYQKRCPFVIDYLID  
LARRSRHRLMIRLVKGAYWDSEIKRAQVEGLEGPVYTRKVYTDVSYVACARKLLSVPDA  
IYPQFATHNAHTLSAIYQIAGHSYYPGQYEFQCLHGMGEPLYDQVVGPIADGKFNRPCRI  
YAPVGTHTETLLAYLVRRLLENGANTSFVNRIADDTISLDELVADPVAVVETMHRDEGTLG  
LPHPKIPSPRGLYKGSRANSAGIDLANEHLASLSSALLAGTSERVVADPMLGTVEVPRAA  
DAITTPVLNPAHDRDVVGQVTEASQADVDAALQAAANAAPIWQATPPDVRASALERAADL  
MEAQMQLSMGIIIMREAGKTFNSAIAEVREAVDFLRYYAAEVRRSFDNETHRPLGPVVCIS  
PWNFPLAIFTGQVAAALAAGNTVLAKPAEQTPLIAAAAVRILREAGVPAGAVQLLPGRGE  
TVGAALVGDAVKGVMFTGSTEVARILQRNIAGRLDAAGRPIPLIAETGGQNAMIVDSSA  
LAEQVVGDVVNSAFDSAGQRCALRVLCQEDVADRVLAMLKGAMNELTMANPDRLSTDV  
GPVIDEEARGNIVRHIDAMRAKGRRVHQADPNAPQGASCRHGTFFVPPTLIELDSIDELKR  
EVFGPVLHVVRFPRAALDTMIGQINGTNYGLTMGIHTRIDETIAQIVQHAEVGNLYVNRN  
IVGAVVGVQPFQGEALSGTGPKAGGPLYLHRLLSVCPQDAVRSVRHAEASGNPPAAPER  
PVAAQALKDWAKTEMPEVAAACDRFAEASAAGISVTLRGPTGERNTYSLLPRHHVLCCLAA  
QEQLDAIQLAAVLAVGSQAVMAENPVSRGLFARLPKGVQSRVRIVSDWTSPEPAFDAVIH  
HGSDQRLRTVCEQVAARPGPIIGVQGLAQGEPNIALERLLIERSLSVNTAAAGGNASLMT  
IG

>Salmonella Q57QN1 Q57QN1\_SALCH

MGTTTGMVKLDDATRERIKMAASRIDRTPHWLIKQAIFSYLDKLENSDTLPPELPALFAGA  
ANESEEPVAPQDEPHQPFLEFAEQILPQSVSRAAITAARRPETDAVSMLMEQARLSPPV  
AEQAHKLAYQLAEKLRNQKSASGRAGMVQGLLQEFSLSSQEGVALMCLAEALLRIPDKAT  
RDALIRDKISNGNWQSHIGRSPSLFVNAATWGLLFTGRLVSTHNEANLSRSLNRIIGKSG  
EPLIRKGVDMAMRLMGEQFVTGETIAQALANARKLEEKGFYSYDMLGEAALTAADAQAY  
MVSYYQAIHAIGKASNGRGIYEGPGISIKLSALHPRYSRAQYDRVMEELYPRKLSLTLA  
RQYDIGLNIDAEADRLELSLDLLEKLCFEPELAGWNGIGFVIQAYQKRCPLVIDYLVDL  
ASRSRRRLMIRLVKGAYWDSEIKRAQMEGLEGPVYTRKVYTDVSYLACAKKLLAVPNLI  
YYPQFATHNAHTLAAIYHLAGQNYYPGQYEFQCLHGMGEPLYEQVTGKVADGKLNRPCRIY  
APVGTHTETLLAYLVRRLLENGANTSFVNRIADATLPLDELVADPVEAVEKLAQQEQAGI  
PHPKIPLPRDLYGEGRINSAGLDLANEHLASLSSALLSNAMQKWQAKPVLEQPVADGEM  
TPVINPAEPKDIVGWGREATESEVEQALQNAVNPVWFATPPQERAAILQRAAVLMEDQ  
MQQLIGLLVREAGKTFNSAIAEVREAVDFLHYAGQVRDDFDNETHRPLGPVVCISPNWF  
PLAIFTGQIAAALAAGNSVLAKPAEQTSLIAAQGIAILLEAGVPPGVVQLLPGRGETVGA

QLTADARVRGVMFTGSTEVATLLQARNIATRLDAQGRPIPLIAETGGMNAMIVDSSALTEQ  
 VVVDVLASAFDSAGQRC SALRVLC LQDDIAEHTLKMRLGAMAECRMGNPGRLTDDIGPVI  
 DSEAKANIERHIQTMRAGRPV FQAARENNDDAQEWQTGT FVMPTLIELENFAELEKEVF  
 GPVLHVVRYNRNQLAELIEQINASGYGLTLGVHTRIDETIAQVTGSAHVGNLYVNRNMVG  
 AVVGVQPFGGEGLSGTGPKAGGPLYLYRLLAHRPPNALNTTLTRQDARYPVDAQLKTTLL  
 APLTALTQWAADRPALQ TICRQFADLAQAGTQRLLPGPTGERNTWTLLPRERVLCLADDE  
 QDALTLA AVLAVGSQALWSDDAFHRDLAKRLPAAVAARVQFAKAETLMAQPFDAVIFHG  
 DSDKLRTVCEAVAAREGAIVSVQGFARGESNILLERLYIERSLSVNTAAAGGNASLMTIG  
 >Xanthomonas Q4UPS6 Q4UPS6\_XANC  
 MNAQPDTFASSHLARPLLAPELPAAPGALRAAITAAWLKDETEHVRELLEQARLPAAEQ  
 KVQALAADLVTRVRARAQDQGAIEAFMRQYDLGSEEGVLLMCVAEALLRIPDQDTADKLI  
 RDKLGEADWKKHVGSGDSVLVNSTWGLMLTGKLVQLNDLTRADVPGAFKRLIGRVGEPV  
 IRLAVRQAMKIMGHQFVMGRTIGEALARSRKGDNANYRYSFDMLGEGALTMKDAQRYLQA  
 YRDAIHAIGRSGSFVGTDFVFAAPSISIKLSALYPRYEHAKRARVMAELVPGVLELAQLAK  
 SYGIGYTVDAEEADRLELSLDII EATFSDPSLDGWEGLAVQAYQKRTPYTIDFLADLA  
 RRVGRRIPVRLVKGAYWDAEIKRAQIDGHPGYPVFTRKQNTDVSYLACARRMFAHSDALY  
 PMFATHNAQTIAAVRAISAGKTYEHQKLHGMGDDLYAEVIPADRLGLPCR VYAPVGSHE  
 LLPYLVRRLLENGANSSFVNRTIDEDVAIEDLIRDPVEAVSSFASIPHPKIPLPADLLRS  
 QNQNRKNSMGANLANDNDLRQLADQLTAAIKPWKAAPLVPGAVITTPSEAVFNPADRRET  
 VGHWQPADPATVQKALASAAAQPAWNRTPAASRATILEHAADLLEARMPEFMAICVKEA  
 GKTLPDVAEVEAVDFLRYYAAQARAQFGAPERLPGPTGESNELQLHGRGVFVCISPWN  
 FPLAIFLGQVAAALAAGNTVIAKPAEQTNLVGFAAVKLLHEAGVPEAAVQFLPGDGATVG  
 AALTNDPRVAGVAFTGSTDTARIINRTLAARDAAGVLI AETGGQNAFIADSSSLPEAVV  
 KDAISSAFISAGQRC SAARVLFVQDDIADKVMTMLAGAMGELKIGDPALLSTDVGPVIDA  
 DALKILEEHASRMDSEARLIGTTTTLDSATAHGSFFAPRAYELKSLAQLQREIFGPVLHII  
 RWKADQLDSVIDQINATGYGLTLGVHSRIDETIDRITSRVAVGNVYVNRNQIGAVVGVQP  
 FGGQGLSGTGPKAGGPHYLLRFATEKVVTVNTTAAGGNASLLTLGD  
 >Jannaschia Q28LK1 Q28LK1\_JANSC  
 MSDLSHFRQAIASAHLEDDALALDRLRSAHDIAPPVRKAASTRAARLVASIRAEDRGGLM  
 EVFLAEYGLSTAEG LALMRLAEALLRVPDDATVDALIEDKIVPAQWSGHRGKSKSGLVNA  
 STLALMLTGRVLSDEDGAGIAGTLKGAVKRLGEPVIRKATRRAMKEMGNQFVLGQTIAEA  
 MKRGRDRAAQGYTYSYDMLGEAAVTADEARIFYASYADSIAYLAKQATHDDIRQNPGISV  
 KLSALHPRYEEAQDRDRLSELVPRVLELAQA AKAARMGFNIDAEADRLDLSLDVIEAVL  
 RDESLAGWDGFGVVVQAYGKRCAPVIDWLYALAEIHDRRIMVRLVKGAYWDTEIKRAQVA  
 GLPGFPVYTAKAATDVSYLCCARQLLDRTDRIYPQFATHNAHTVAATIEMAEDPLAFEFQ  
 RLHGMGEALHEQVRAANMTRCQIYAPVGAHRDLLAYLVRRLLENGANSSFVHKIMDEDT  
 PEAVAEDPFLTLSHPATPVTLPGDLYAPERPNSHGIDLTPASLAALDAARAPFREATWQ  
 AGCGMGETQEVNRPADPSDLVG YVTLSTAGDAQTAIETAQAWDAANRTDVLNRAADLYET  
 HAPELFALLAREAGKTLPDCEAELREAVDFLRYYAARIDDLTDPALGRVTCISPWNFPLA  
 IFTGQISAAALAAGNAVLAKPAEATPLIAARAVALLEAGVPKTA LQLLPGEGGTVGAALT  
 SDPRIDGVAFTGSTATAQVIHRAMASNLAAPSAPLIAETGGGLNAMIVDSTALPEQAVKD  
 VMSAFRSAGQRC SALRCLYVQKDIAPAFKALY GAMDELSLGDWPLANDIGPVIDARAQA  
 GIAAHIATARADGRILHEGTAPVLGTFIAPT AIRVTSIADMSEEIFGPVLHVATFKSSDL  
 DRVIDDINATGYGLTFGIHSRIDDR IADVTGRIMAGNLYVNRNQIGAIVGSQPFGGQGLS  
 GTGPKAGGPSYVPRFCRTPLGEGTPGTPADIEGAHDLHVALPADRTLTTQDLPGPTGET  
 NRLTTHPRGRVLC LGPGSAAARDQASAATATGCAPVLAPDLPAAALTDLRAFDVAVIYWG  
 DAAARAYRKVLADRDGPILPLIMDADPKPRLILERHTCIDTTAAGGNAALLAAVA  
 >Idiomarina Q5QY28 Q5QY28\_IDILO  
 MFKASEVLSKQHQAEDLKS LQQAITDNYIVDEDEYMR ELLPLVPADDDTVSAVTERAAKL  
 VEQVREQADNGVDAFLQEYSLDTKEGII LMC LAEALLRIPDAYTADALI QDKLSGGDWQ  
 KHMGSASWL VNSGTWGLAL TNSVTNPTGKAMETPRGA FRRLVRKL GKPIIRKATY TAMQ  
 IMGKQFVLGR TIEEALKE SRDNRDKGYTHAYDMLGEAALTMKDADY YKQYVNSIKTITK  
 EEFNNPDAPRPTISIKLSALHPRYEASNH ERLTELATTLTEL VKLAKEADVGTIDAE  
 EADRHELSMELFEKVYRSGVCKGWPRFGLV VQAYSKRALPTLCWITALAKECGDEIPVRLV  
 KGAYWDNEIKWTQENGLLGYPVFTRKSHSDISYLACARYLLSDDTDGAIYPQFATHNAQT  
 FMAIQQMNETHQRRIEYQRLHGMGDSLYDTIMEQNPGMVVRIYAPVGPHKDLLPYLVRRL  
 LENGANSSFVHKLLDADTPVNDLVEHPMKTASGYEKYANSKIPLPSEMYGDR TNSLGLNM



NIHSQADDFIAAVQQYRDKQWQGGPIVDGKTIETDHHVSITSPQETSKQVGSIIYWGDKKL  
SEQALKSANAAYKSWRKVPTDERAECLEKFADLMEANRNELIALCSVEAGKGLQDGIDEV  
REAVDFCRYANQARELMGGPIQLPGPTGEDNELFVEGRGTFICISPWNFPLAIFVGQVA  
AALVTGNSVIAKPAEQTGLIAYRAVQLALEAGIPGNVLHFMPSGSGAEVGSYLTQSQEDIGG  
VCFTGSTYTAQAINRALAARTGPIVPLVAETGGQNAMMVDSTALPEQVVTDIVASAFQSA  
GQRCSALRVLFVQDDVADRVLDLLRGAMEELQVGDPLLHETDVGPIVIGIAKTNLEQHIS  
DIQQAGRLIARAPLPDYAMGGTFVAPTAIEIDSISQLVKENFGPILHVIRFKTSEIDEVI  
ESINNTGFGLTFGIHSRNETFAHDVASRIDVGNVYINRNQIGAIVGVQPFGGGRGMSGTGP  
KAGGPHYLTRFITEKTRSDNITAVGGNATLLSLDD

>Oceanospirillum Q2BPW3 Q2BPW3\_

MSITIEQSRHAIRNSYLADEAAVITGLINNSGLDETERQSSISASAADLVRKVRSESSPSM  
MEKFLAEYGLTTKEGVALMCLAEALLRVPDSLITDALIEDKVVSGNWKGHLGQSASSLVN  
SSTWALLITGKLLKDDDEAKGIGSTVKGMIKRLGEPVVRTAVAQAMKELGRQFVLGRDINE  
ATKRAKKLEKQGYSSYDMLGEAARTDADAIRYHQAYSQAISELTPACTSNDIRTNPGIS  
VKLSALHARYELGQKTRVMQELVDRTLTLALQAKDANMGFNIDAEADRLDLSLDVIEAV  
LADKRLADWDGFGIVVQAFGPRAAHVLDWLYATAQRLDRRIMVRLVKGAYWDAEIKRAQV  
LGLDGFVPVTRKVNSDLSYMCCAELMQMTDRIYPQFATHNAHSAAAILFMAKKHNVDNF  
EFQRLHGMGESLHDTVLSNNTRCRIYAPVGAHRDLLAYLVRRLLENGANSSFVNQIVDT  
RITPEEIAKDPFSQVLESQDQISNNYIPKPAEIFGDKRLNAKGWDITDHVTLEQLEPARE  
AFQTTQWHAKPMIAGDATSSDTSEVRNPANPEDLVGMVTEANPADIESAIAAAELGFQRW  
SKTAPSERAACLRRVADLFEANAPELFALASREAGKTLDDAVGEIREAVDFARYYANEAE  
KHAESEARGVITCISPWNFPLAIFAGQVLAGLASGNTVIKPADQTPMAARAVALMHEA  
GIPNDVIQLLPGSGINVGAPLTSDPRI SAVCFTGSTLTAQRINKVMAENMAPDAPLVAET  
GGMNAMIVDSTALPEQVVRDVLMSFQSAGQRCSALRVLYVQEDIADNLLLEMLYGAMDEL  
RMGNPWLLSTDIGPVIDSNAQAKIEAHCEKFAAKGKLLKLLNTPEGGTFVAPTVLKVEGI  
EEIEEIEIFGPVLHVATFAAKDLQVVDINSKGYGLTFGLHTRVDNRVERIINQIKVGNI  
YVNRNQIGAIVGSQPFGGEGLSGTGPKAGGPHYVKRFTRSAISQGTDPASGQSVNTETLE  
QLIQQLDLTTQGLKADPEQLQKVFIAGIASLKPVPTEATEMPGPTGELNLLSETGRGVVL  
CLGPDAESAVKQAATALFQGNVVIQAQGIADLLKQCADAKLPVQGMVGQLTAEAITAH  
GFAAVSCNASHDVLKTIHQALAAAREGALLPLITELDQPERFVMERHLCIDTTAAGGNASL  
IATAG

>Alkalilimnicola Q34YB6 Q34YB6\_

MSHFVHPQPDALLHPERAVLAAYRADEAKVTSVMLERAALGETANRRIQAHARSLVMGM  
ISAQKGEFGVDALLHEYDLSSSEEGIVLMCLAEALLRVPDRYTADKLIHDKLTASHWETHL  
GRDRPLFVNAATWGLLLTERIIDTDDRDRWLGGVLHMMVARAGEPVIRTAVRRAMGLLAD  
TFVLGRDIDEALKRAHPNERKGYRYSYDMLGEAARTDADAQAYFEAYRNAIHRVGKAVDP  
QARIRDRAGVSVKLSALDPRYEPGQEARVMGTVLPRLLQLCELARDYNIALCVDAEESWR  
LDLSLDVIEAVLAEPGLADWEGFLAIQAYQKRCYALVGWLEAQAARQNRALMVRLVKGA  
YWDTEIKETQVQGLRDYPVFTKRAATDVAYLACARRLLSECPHLYPQFATHNAHTVAAM  
ELAGRQPYEFQRLHGMGEALYEQLLGRAGGPDIPCRIYAPVGSHEELLAYLVRRLLENGA  
NSSFVNRIHEGDVEALVADPASSLRARESLRHPRIPLPRDLYGEQRLNSIGLDFSDRH  
EMLVWLAEMEAASEHAWRAAPLIDQVKAGAGEAVHCPADRERQVGRVWSEHADVEHALEA  
AVAGRETWANTRAETRARALEQIAELYEAHGAELMALCTREAGKGLKDGIAEVREAADFC  
RYAHQARRLFGQATVLPGPPTGERNELRLHPRGTFLCISPWNFPLAIFTGQVTAALAAGN  
TVVAKPAEQASLIAHQAVALMHRAGIPETALHLLPGDGGEIGPHLVADPRISGVAFTGGT  
DTARRIQQGLAQREGPIVPLIAETGGLNAMVVDSSALPEQVVVDIIRSAFHSAGQRCSAL  
RLLCVQEDIADLLAMLKGAMDALTVGDPHWLATDVGPVIDPAARDGLLAHERMVSAGR  
LLHQAPLRPECERGSFVAPALYRLDRIDQLGREHFGPLLHWVTWRAGELDALVDRINGLG  
YGLTLGVHSRVDETA AAVNRRARVGNAYVNRDMVGAVVGSQPFGGEGLSGTGFKAGGPHY  
LLRFAAERVVTVNTAAAGGNASLFAMGEDD

>Acinetobacter Q6FBR9 Q6FBR9\_AC

MSLEFGMNMMDNDPQMDTAKPHFGYISEFKEKTELEQHINDAWRRPEPETVETLLQAASI  
SDELNHKIYELAFELANGLRERKTSSGKAGIVQGLLQEFSLSSQEGIALMCLAEALLRIP  
DAATRDLLIRDKINQGNWKDHVGQSSLMFVNAAAWGLMLTGKLMETPKQGSLSGLLTSIL  
ARSGRGVIRKAVDVAMRMGEQFVTGETIEEALDNAKSHKGFYSYDMLGEAALTTHD  
AERYFNDYTQAIHAIGQASNGKGVYDGPGISIKLSALHPRYQRSQIARVHDELYGKVFNL  
ALLSKKYDIGLNIDAEADRLEISLELLERLCFEPELADWKIGFVIQAYQKRCFYVVDY

VVDLAKRSKKRLMIRLVKGAYWDSEIKKAQIDGMHDYPVFTRKVHTDLSYIACAKKLLAA  
PEQIYPQFATHNAQSLATIYELADPGKYYAGQYEFQCLHGMGEPLYEQVVGSRSDKKLGI  
PCRIYAPVGNHETLLAYLVRRLLENGANTS FVNRIADQNLKIEDLIQSPFDEIAINAQRE  
GQAGLKHPAIPLPNLYGSLRQNSKGFDLANDATLTALNETAQQLEHKVWESRPLLAQTV  
DQIDVSPQALLNPAVHLDIVGYVQEATLEQVDVALESATQAQQAWANTEKNHRAATLKKA  
ANLMESRMQELMVLLCREAGKTYANAISEVREAVDFLRYYATQIESLKPTAQIEPLGTVL  
CISPWNFPLAIFTGQIAAALGAGNCVIAKPAEQTPLIAAQA VHLHEAGIPKSVLQLLPG  
RGETVGAKLSSDQRIQGVMTGSTEVAKILQKTVAKRLSPSGHPIPLIAETGGQNAMIVD  
SSALTEQVVIDVLNSAFDSAGQRC SALRILCVQEDNSKTLVTMLKGAMQQLIMGNPFLK  
TDIGPVIDLEAKQTIDQHIQKMRSGYPVYQLIFNHEAASQAQLSQGTFTPTLIELPNL  
DDLEREVFGPVLHVITYKHGEIKQLLQHINAKGYGLTMGLHTRIDETINTVVQHAEVGNL  
YINRNIVGAVVGVPFGGEGLSGTGPKAGGPLYLYRLMASCTEKAIQTPFGIPAENVAVP  
LTQLSLFREFSAWIKKQYP AHQLPNVPLNVGHAFDLQGPTGETNRYMMLPRKRILAIAS  
NELELCHQMLAIFAVNSQVALLESNPSLQKFGQDLPTVVRQAIIEIRGVEHGDFDAVLHH  
GSTEELQVLQTQIANRQGPIVGITHLQNSEQVIPLERLVIEHAISVNTAAAGGNASLMTM  
SE

>Novosphingobium Q2GAH2 Q2GAH2\_

MTQTAPFAAFAPRHSVPSDLRRAITAATRAERECMVMLLPEATLPQATRASQAALARKL  
VEALRAKPRGNGVEQLVQEYALSTHEGVALMCLAEALLRIPDNDTRDDLIRDKIAGGDWL  
AHLGGDRSLFVNAATWGLVVTGKLASSVDDTGLGAALTRLIARAGEPVIRRGVDLAMRMM  
GEQFVTGETIDEALKRARPLEDRGFYSYDMLGEAAMTASDAARYHADYQAAIHAIGKAA  
ARRGVYEGPGISIKLSALHPRYARAQQDRVFAELLPRLKALAYLALRYDIGLNIDAEED  
RLELSLDLLEELAMDPELAGWNGLG FVVQAYGKRCPFVIDWIVDLARRSGRRIMVRLVKG  
AYWDAEIKRAQVDGQSGFPVYTRKAHTDVAYIACARRLLAATDVVFPQFATHNAQTLATI  
HEMAGPDFAVGRYEFQCLHGMGEPLYDEVVGKDKLDRPCRIYAPVGTHETLLAYLVRRL  
ENGANS SFVNRIANPDVPVDEIVADPVAQVAADADPGAPHPLIALPAALYPDRRNSSGLD  
LADESTLAALTDRFQAI SAHSRHAHPSADLPHVNPRPVLNPNANHRDVGHVSEAAPAAAG  
MAASLAAASRWSATPVAARAMILERAADAMQAAMPELIALIVREAGKSVSNAIAEVREAV  
DFLRYYASQAPAMSGSRPLGVALCISPWNFPLAIFTGQVAAALMAGNPVLAKPAEETPLI  
ASEAVRI LHEAGVPDDALVFLPGDGAIGAALVAPEIAAVLFTGSTEVGRLIQRQLATRL  
SAEGRPIPLIAETGGQNAMIVDSSALAEQVVADVIASAFDSAGQRC SALRVLCQEDVAD  
HVLAMLRGALAEELTVGPTDRLSADIGPVIAAEAREAIEAHVARMEAAGCPVHRLPLGTAT  
NEGTFVAPTIIELSAPDLLTREVFGPVLHVIRFRRADMDAMVERINAWGYGLTFGLHTRL  
DETVARVTAKAHAGNIYVNRNVIGAVVGVPFGGHGLSGTGPKAGGPLYLRRLVASAPAA  
PALELTERELPGPVGERNIYALRPVGRVLVAAQSPERLAALTSRVERLGGTPIAADDGWQ  
AQGPFARALVEGDAAFILSFQQAVAALDGP IAPVLASADDDTMLVAEVSLSINTTAAGGN  
ASLMAMA

>Legionella Q5X4L5 Q5X4L5\_LEGPA

MLEKQSIHLPEGLRAAINKAYRMDLSLITELSEQAALDPQQMMAIKTSATKLVQSVRSE  
RKKSTGIDSFLT EYALSSDEGIALMCLAEALLRVPDNATIDNLIKDKLAGGDWGAHRGQS  
ESFFVNATTWALMLTGKVLTP EKAENTLT KALLKLVNRSSEAVVRKAVDKAMRIMSKQFV  
MGRTINEALARAKKKEDRGYRYSYDMLGEAALTSADAARYFEAYKEAII SIGEKADKHSD  
VYRRPGISIKLSALHPRYSEFQYERVMAELPPKLLALSRLAKDYGIALTIDAEESERLDL  
SLDVIEKVFTDES LQGWNGFGLAVQSYQKRAFVYLDWVAALARSKQRRIMVRLIKGAYWD  
SEIKKTQM QGFSEYPVFTRKVFTDVSFQACAKKILTM TDAIYPQFATHNAYS VAMILNLV  
GGYRDFEFQCLHGMGNELYEQIVPANCYGIPCRIYAPVGSHEDLLPYLVRRLLENGANS  
FVNRIVDDKAPISELVEDPVAKSRLLDKINKNIPLPEDIFLPVRKNSKGFDFTNRLERA  
LLQQELAKIESKEWQASPMIAGRKLSSDLLQVTMSPQQPAYAIGSVQQATLDDVEVALNQ  
AKLAFESWSKKAVEERASCLNRFADLLQANMSELMVLT CREAGKTWSDGIAEVREAI DFC  
RYYAKKAQELMSSPQRFNGYTGELNELSLHPRGTILCISPWNFPLAIFTGQVVAGLVTGN  
CVIAKPAEQTPLIAAYAVKLMHQAGIPEGVIQLIPGAGETIGAALVADKRIKAVLFTGST  
DTANLINRTLATRGGEIIPLIAETGGQNAMIVDSSALLEQVVVDVTSAFGSAGQRC SAL  
RVLYVQEEVYPRTVELLKGAMAELVVGDPQWLSTDVGPVIDKEALSILKNHVENMRKHHE  
ILYQCTVDDEALSGYFMPPTAIAIDSISALEKEVFGPILHVIQFKRKDLDKVINQINQ TG  
YGLTLGIHSRINETVDYIRQRVHAGNCYVNRNMIGAVVGLQPFGGEGLSGTGPKAGGPNY  
LIRLCHERTYTVDTTAAGGNASLMSIPEEG

>Azoarcus Q5P8F4 Q5P8F4\_AZOSE B

MREAVQPCKNLVHPSHARRARSRAQVTAGCVRERQPSPIALSGVLLAMKPEIPDPATAA  
LPAAARSELRRRIDTAWRTPEPECVPPLIRAARIDAALQARIRAQARELVAGLRATRTHS  
SGVDALMKEFSLSSQEGVALMCLAEALLRVPDSATADRLIRDKLAHRDWHAGLHSPSLF  
VNAATWGLLVGTGRLVGTSSAQGLSSALTRMLARGGEPLIRRGMDLAMRLLGEQFVTGRNI  
AEALERSAAARRRGYRSFDFMLGEAAMTAADAQRYLAGYEQAIHAIGKASAGRGVVDGDG  
ISVKLSALHPRYVWSQRGRVLAELLPRKSLCMLARHYDLGLNIDAEADRLELSLDLLE  
ALALDDELQGLGFWVQAYQKRAPRVVDWIIELARRSGRRLMVRLVKGAYWDAEIKRA  
QVEGLAGYPVFTTRKLYTDVAYLACARQLLAARDVLYPQFATHNAHTLSAVFQLAGDDYAA  
GDYEFQCLHGMGEPLYDQVVGDTGSRRRVRIYAPVGSSETLLAYLVRRLLENGANS SFVN  
RIVDENVSIDALVADPVEEALPLAGAPHPRIPLPADLYGSERRNSAGHDLASEPVRQRIG  
AALQLSRSVRRAGPLLANGPASPASRDNLVVRNPADHSDVVGMMVHADEIDVERALAA  
ASGAAPGWAMRAAAARAACLERAAELIERDDELVALAVREAGKSWANVLAEVREAVDFC  
RYAARVRDFDNASHAALGPVLCISPWNFPLAIFTGQIAAALAAGNPVLAKPAEQTPLIA  
TAAVALFREAGVPAAVLQLLPGRGDIVGAALVADPRVRGVLTGTSVEVATRINRALARRG  
GDVPLIAETGGQAMIVDSTALAEQVVAIAASAFDSAGQRC SALRVLCQDDVADAVLA  
MLRGALDEMRLGDSSDVRNDIGPVIDADAQAALERHVAAMQASGARITRLALPQRCSRG  
FVAPTIIIEVGDIRDVGDEHFGPILHVLRYRAEELDRLLDAINATGYGLTMGVHSRIDETI  
DAVIAHARVGNLYVNRNMIGAVVGVPFGGEGSGTGPKAGGPLYVHRLRRSPGPALLEG  
RDRLPDGEAFGLVTWLDGAGRTLIDDAGRAFLHERIAACRATRLAGLRLALPGPTGEDN  
SLRFVPRGLVAGVATTTVGRHLQLLAALASGNRIVFTDDAAHRAFLDALPGPARKAVTLD  
TDWPGHPFGALLLDGTAAEADAWRVRLAERDGPVPLLPQEPEDYDAARLVHERTVSINTA  
AAGGNASLMALGA

>Ehrlichia Q3YS87 Q3YS87\_EHRCJ

MGDIGMISALQAPNEIRKRMQMLYRTEENSARYLTEKTEVSQDSKIRIYSVAKQIIIEKI  
RVDRNLGIIDAFMQEYGLSNEEGIALMCLAESLLRIPDDCTINDLIKDKIGNSMWSNHIG  
SSSSMFVNAATWGLFIGGIVLKESNDSAKWFGTINNLLKTMGEPIIRKAIQQAMCTLGKH  
FIKGRDITEALNNRKEGELYSFIDILGEAAKTRKDAERYFSEYMQAVDSIGKSKGSDDTGR  
LVYDEISVKISALHSRYEFSQIDDVLDIVDKLLQICRLAKEYNIRVCIDAEAEASRLIEI  
SLMILEKLRFESSLNGWEGLGLAVQAYQKRAFSVLDVFEDISVRSCHKMMVRLVKGAYWD  
YEIKNSQELGLSSYPVFTTRKVTYTDVSYLACANKILSKPNTFYPCFATHNAYTLAAILEMA  
NKDHPGFEFQRLHGMGASLYEYVTQELAANIKCRVYAPVGGYQDLLPYLIRRLLENGANS  
SFINQLNDSNISLEQLIQDPLEKAKELEYLPHPNIPKIDIFGPERLNSSGIDITDSVTL  
ANFNDEMKNYQNCFKKASSIVNGEEFDGDFIEILSPSNSEDLVGEVLFASSTQALSALDI  
AYSAFKDWSNVPVSTRASILEKAANLIEENKAKLIMLLIREGGKVISDAIAEIREAVDFL  
RYAVLGRQELEGSNRLPGPVGEDNYLYFRSRGVFVCISPWNFPLAIFIGPIAAALVTGN  
TVIAKPAEQTSIIAYEAVKLLYDAGIPKGVHLHLLGDGKELGEVLLKNEKIGGVAFTGST  
ETARIINQSIAEKEGGIIPFIAETGGLNTMITDTSALVEQVTNDVITSAFKSAGQRC SAL  
RVLFVQEEVADKQIEMICGAMEDLVIGDPMLLKTDIGPVIDKASQEMLIAHADRMSEQGK  
LLCQVKLGEECQKGYFFAPCAYEIQNISQLQREVFGPILHIIRYKKGDLHKILSEINDTG  
YGLTFAVQSRVQSNIDNIIDNINVGNVYVNRNQVGAVVGVPFGGQGLSGTGPKAGGPYY  
LHRFLTEKVVSINTTALGGNTSLMCLTDQ

>Agrobacterium Q44334 Q44334\_9R

MADGASKADVNPQQTVNGIFQNFAPPVREQSPLRKAITAAYRRPEEECLAPLIDAATVTP  
EQAAAIRTTATKLI EALRAKTKGTGVEGLVQEYSLSSHEGVALMCLAEALLRIPDTATRD  
ALIRDKIARGDWKSHIGGGRSLFVNAATWGLVITGKLTSTVND SGLSAAITKLIARAGEP  
VIRRGVDMAMRMMDQFVTGETIGEAIKRSKPLEEQGFQYSYDMLGEAATTAKDAERYK  
DYENAIHAIGKASAGRGIIYGGPGISIKLSALHPRYARVQAERVMAELLPRVKSMLLSKK  
YDIGLNIDAEADRLELSLDLLEALDKDLAGWNGLGFWVQAYGRRCPFVLDYIIDLAQ  
RAGRRIMVRLVKGAYWDAEIKRAQVDGLEDVFTTRKVHTDVSYIACARKLLAADVVF  
QFATHNAQSMATIIYHLAGPDFKLGDYEFQCLHGMGEPLYSEVVGKKKLDPRCFYAPVGT  
HETLLAYLVRRLLENGANS SFVNRIADPAVPVASLLEDVPTVVKAYPVPGARHDRIAAPA  
GLFGPERANSAGLDLSNETALAALDNVLKAGATTEWKAAPHAGGKTRPVLNPGDHNDVV  
GYVTEPTAEADVEAAMQRAASNWSSTPVEERAACLERAAARMQAEMPALLGLIMREAGKS  
MPNAIAEVREAIIDFLRYAAEARKTFKANETPLGPVVCISPWNFPLAIFIGQVTAALVAG  
NPVLAKPAEETPLIAAQGVRLLEAGVPQDAVQLLPDGDKTGAALVGSALTAGVMFTGST  
EVARLIQGLAGRVLANGQPVPLIAETGGQAMIVDSSALAEQVVAIVASAFDSAGQRC  
SALRILCLQEDVADRTLTMLKGALHELRIGRDTSLSVDVGPVITAEAKGIIIEKHVDSMRA

LGHRIEQISLAGETGKGTVPPTIIEMKSLADLKKEVFGPVLHVIRFKRDNLDRLIDEIN  
 ATGYGLTFGLHTRLDDTIQHVLRSVAAGNLYVNRNIIIGAVVGVQPFGGRLSGTGPKAGG  
 PLYLGRVTQTAPKIDRVASQQDQAAVDLARWLDENGQSVAAEAARQAAALSGLGFELELA  
 GPVGERNVYALHPRGKVLLIPATEQGLYRQLAAALATGNSVVIDNASGLEKSIYGLPATV  
 TSRTIWADSWEKSAPFAGALIEGDAERVVAINKKIPALPGPLVLVQAATTEALDRETQPY  
 NLDWLVEEVSVSNTTAAGGNASLMSIG  
 >Nitrosospira Q2Y8S2 Q2Y8S2\_NIT  
 MGKTAACPRFLRSAITHAYRHNETESVNGLLRQIDWPPCSRARAEELARKLVTSMRGKYS  
 HRGGVDALMHEFSLSSQEGVALMCLAEALLRIPDRETADRLIRDKISKGDWRVHVGHSPS  
 LFNAAAAGLLISRKLVSSTHREDGLSAALSGLMEKGGEPLIRKGMDLAMRMLGHQFVIGE  
 TIEEALERSREREMRGYRYSYDMLGEAAITEADAQRYWTSYASAIHAIGKSRGKGKIKSG  
 IYRGPGISVKLSALHPRYVRSQRERVMSSELLPRLKSLLLAKHYDMGFNMDAEEADRLDL  
 SLDLLLEALVFDPLAGWDGIGFVVQAYQKRCPFVVDWLIDLARRSGHRLMVRLVKGAYWD  
 GEIKRAQVEGLDGYVPVYTRKIHTDICYMVCAQKLLRAAEAVFPQFATHNAHTLSAVYQIA  
 QDADIEDYEFQYLHGMGETLYDQVELLKEDRFVKPCRIYAPVGSYETLLAYLARLLLENG  
 ANSSFVNRIILDDDIVVEELVADPVSQIEQEGVHPHPAIPPLPGDLYGHKRRNSAGLDFSDE  
 QALAALSAELTEMERREWRARPVLAAGGNAGNAGSRVLNPADRNDASAGTVVEATEHDVED  
 AIAVAHAFVAEWQSVSHEARAAMLERAADALEAHRTELMGLAIREAGKSLPDAVAEVREA  
 VDFCRYYGQQIRDWPNMSPSSALGPVVCISPWNFPLAIFIGQVSAALAAGNPVLAKPAEQ  
 TPLIAAVAVRLLHAAGIPRAALQLLPQGERVGEQLVKDVRVRGVIFTGSTEVAQLICRT  
 LALRAQKSEILFIAETGGQNAMIVDSSARIEQVVQDALTSAFDSAGQRCSALRVLCLOED  
 IAEQVLEVLRGAMGELTVGDPRELATDVGPVIDADAQHALLDHIKEMRAAGHTVQAAALP  
 SVCANGTFVAPTLEIDHIDELEREVFGPVLHVVRFARERVDELVGQINATGYGLTHGHIH  
 SRVDETIDFITKRVHAGNIYVNRNMIGAVVGVQPFGGEGKSGTGPKAGGPLYLHRLMPQT  
 PLLLADNGGLRVNSPPVELQVLAAWARQAGRDVLASLCEDYAMRTPFAFSIPLPGPTGES  
 NTLKFAPRRAVACIAVDEDDALLEQMAAALATGNQIILADNPPLRALLDKLPSQVRNRLRI  
 EREWIHAPVSAVLYSGPEDEAYRLRNELAGREGALVAFITASGTDFPLYRLTAERVVSVN  
 TTAAGGNPGLMGLDFNGSSTH  
 >Acidiphilium Q2D8X7 Q2D8X7\_ACI  
 MAVSTMGVKLLDDQVRARLRALAEREGRTTHHLAKQLILAGLERLERGEALDAAVTAEDDA  
 PAAVPFLEFVQDVQPQTVLRAAITAAYRIPETDAVAGLIEGATLPAAAAKQARATATNLV  
 TALRARRNAGLVETLLQEYALSSHEGIALMCLAEALLRIPDAATRDALIRDKIGAGDWQS  
 HLGGNKSVFINAATWGLLLTGRNLNATASEAGLSSALTRLLARGGEPVVRGVNIAMRLMG  
 EQFVMGRTIGEALANARKREAKGFAYSYDMLGEAALTAADAARYYRDYEQAIHAIGAAAG  
 GKGIYRGPGISVKLSALHPRYCRAQRARVMEELAPRLKALALLARRYDIGINIDAEADR  
 LDLSLDLLEGLCFEPGLAGWNGIGFVVQAYQKRARSVIEFLIDLARRSRHRLMVRLVKGA  
 YWDSEIKRAQLDGLGFPVFTRKIHTDLSYLACARAMLAARTEIFPQFATHNALTSLASIH  
 ALAGPAFEVGDYEFQCLHGMGEPLYEEVVGPPQKLDRPCRIYAPVGTHETLLAYLVRRLL  
 NGANTSFVNRLADRRVPVEALIEDPVAAARKIEPLGAPHPKIALPGAILGTRNSAGFDL  
 TSEQRLASLSGALLASLEQDWRAAPPDADPAAPGRTVVNPANIADRVGTVIEPDAGAVGA  
 ALARAAAMAPIWQATPAAERAAILLRAADLLEHRMTALVGLIVREAGKSLPAAIGEVREA  
 VDFMRYIYAGQLQDGFNDNETHRPLGVVAAISPWNFPLAIFTGQVVAALAAGNVVLAKPAEE  
 TPLIAAQGVRIHEAGVPADALQLLPDGDRGTGAALVGDARVGGVVFTGSTAVARLIQATL  
 ARRLDADGMPVPLIAETGGQNAMLVDSSALLEQAVGDIVTSAFDSAGQRCSALRILLVQD  
 DIADPLLAMLRGAMEELAVGATDRLSSDVGPVITREARDNIRAHVETMEGRGHKVFVSAL  
 PPETEGGWVAPTMIIEIDHPSALEREVFGPVLHVVRVYRREERNAMVAAVNALGYALTFGV  
 HSRIDETIAQAVGKAEAGNIYVNRNIVGAVVGVQPFGGHGLSGTGPKAGGPFLYLRLLAR  
 RPMPHGEGEPAFTKLVGWMREQGIETAPALRYAAASAFRDAELPGPVGEQNTLRLKPK  
 GLVLRCRAASPEGMWRQVAACLATGNAPLVLCDAEAEIARMPAEIRPAIAPADAVARAEF  
 SAVLFEGHRDALIALQMALAERDGPVIVVHALPAEDHSEWDYPLEFLLEEQSISVNTAAA  
 GGNASLMSIG  
 >Nitrosococcus Q3JAG9 Q3JAG9\_NI  
 MVMISDIELPSLDSPRAAISAAYLADETVMVKSLLRETELAPENVNERVKRRASQWVQLVR  
 EKRRWHGGDLAFLHEYNLSSQEGVVLMLCLAEALLRIPDDENADRLIHDKLLKGEWDRHLG  
 HSHSLFVNASTWGLMLTGRLMRLETPLIDDGKGVIKRLVKRGGEPLVRLALRQAMRIIGG  
 QFIMAPRIEQALTQCRENERYSFDMLEVALTQARVEQYYSYGRHAIRVLGETDSGEHNR  
 EATGISVKLSALHPRYTFSQRRRVQAEVLPRVLALAREACAADIGLTLDAEEADRLELML

DVFEAVFRDPSLRRWQGFGLALQAYQKRALPVLNYLRDLAQKEGRCIPVRLVKGAYWDTE  
IKRAQEQGLAGYPVFTRKVN TDVSFLALARRLLSARDVFYPQFASHNAHTVAVVLETAGE  
QQGFEFQRLYGMGELLYSALREQGISVPCRVPYAPVGGYADLLPYLVRRLLENGANTS FVN  
RIEDEEVPIEQIVADPSEYVRSLSKSHPNIP LPLRLY GKVRNSLGINLNDPTSLERLM  
AELGRAMEKQRQALPLVS GEAGKGT VQVVRDPSDRRRVLGT VVEADQEAIAEALSEADAV  
AAGWEATS VLGRAECLEQAADLFEERQVELMALCIREGGKTVADSLAEVREAVDACRYYA  
AEARRLFAMPKMLPGPTGEHNELTLHGRGVFVCISPWNFPLAIFTGQVAAALVAGNTVIA  
KPAGQTP LIAALVVQWFHEAGIPPRVLHFLPGRGSRVGQALVADYRISGVAFTGSTRTAA  
VINQVLAERKGPIVPLIAETGGQNAMIVDSSALPEQVVVDVMTSAFNSAGQRCSALRVLF  
LQEEVAEP ILEMLIGAMEELRLGEPGRLDTDIGPLIDGEARARLETHCQRMNREARLLCR  
LSLPEATQNGYFFAPRVYELENLAELTYEVFGPVLHVIRYSSKHLNKVIASINRTGYGLT  
LGIHSRVDET VRYI QNRVHAGNIYVNRNMIGAVVGVPFGGERLSGTGPKAGGPHYLLRF  
ATERSTSINMAAVGGNTDLLSLGE

>Anaplasma Q5PAT8 Q5PAT8\_ANAMM

MMISPLQSPDELKRMQGLYNADEKSYVRYLTERTEVSQESKVRIYSLAKQIIIEKVRANK  
NTTIIDAFMQYGLSTEEGLALMCLAESLLRIPDDCTIDDMIRDKIARTTWNKHIGRSTS  
IFVNVSTLALSIGAHMLREVDDSRWYGILGNLLKDMGEPVIRKAALQAMQVLGKHYVCGR  
TIEEAIARSYDAGHVCSFDVLGEAAKTRADADKYFAAYMGALETLSNAQAVDDLGSRHG  
ISVKLSSLHPRYEFGQADYVLKDISSKLELCQVAKKYNVKT TVDAEEARRLELSLMILD  
TVFSDSSLNGWEGLGFVIQAYQKRALAIDFVEDIAIRANRKMIIRLVKGAYWDYEIRNA  
QEMGLDGYPVFTRKVYTDVS YFACVQKLLSKPGTFYPVFGTHNAHSVSFILEMTDKDHPG  
FEFQRLHGMADLYDYVTKEVAPNVCCRVYTPIGQHQELLPYLMRRLIENGANVS FVNMI  
NDS DIPAECLCADPLEKAQSFEYAPHPIPLPADMFPDGRVNSAGVNTSDSLTMLALSEE  
VSFNDTHWKAYPIIGGQDITEGELYEVFFPASLSTKVGEVL FATAEHAAQSIEAARSSF  
YRWSNTPVGERAAILEHAADLLEKERGKFFSLLVREGGKVISDVIAEIREAVDFLRYAM  
LARDQLTDPIKLPGPAGEENLYFESRGTFVCISPWNFPLAIFLGPIAAALVTGNTVIAK  
PAEQTS LVAYEAVKLLYEAGVPTDVLHFVPGRGEVLGNALLSSANIAGVAFTGSTETANI  
INQAIAGRGRDIIPLIAETGGINAMVVDSSALPEQVVEDVITSAFKSAGQRCSLRLVFL  
QEEIADKTIEMLLGAVAELRLGNPMALSTDIGPVIDQQSFDMLTSYVEEMRKKKIKLLCK  
ADISYLSGEEEGYFFPPHIFELESMSQLSREVFGPVLHVIRYKKS DLPSILDDINSTGYG  
LTFAIQSRIQSSIDITDRIGAGNVYVNRNQVGAVVGVPFGGRLSGTGPKAGGPHYLH  
RFLTEKTVTVNTAALGGSVSLTCLDE

>Bradyrhizobium Q89E26 gi|27355

MPNIPPPFTAPYAPDDAEIAARLLPASHLSPPQEARIHRTATRLIEAIRKRDDR LGGVEDMLREFALSTK  
EGLALMVLAEALLRVPDARTADQFIEDKLGE GDFIHHE TKSTAF LVNASAWALGLSARVIQGETPDGTI  
GRLVKRLGAPAVRTATRQAMRLMGNHFVLGETIEQALERGKPRSGQKTRYSFDMLGEGARTAADARRYFD  
AYASAIETIGKAAGNHALPDRPGISVKLSALHPRFEAISRARVMVELVPQLLDLAQRAKADLNFTVDAE  
EADRLELSLDVIAATLADPSLKGWDGFLAIQAYQKRASAVIDYVDALARAHDRKLMVRLVKGAYWDTEI  
KRAQERGLDGYPVFTRKAMTD LNYVACASKLLALRPRIFPQFATHNALT VATVLEMAEGSSGF EFQRLHG  
MGEALYEQ LAKDHADIA YRTYAPVGS HRDLLAYLVRRLLENGANS SFVAQAADYRVPVPALLQRPADAIV  
RPQAAAHPRIP LPCDLFAPERRNSRGVEFGARTALDQLLTDVKAETGDLKPIADATPDQAHAAVAAARAG  
FAGWSRTPAGIRAAALEQA AHLLESRS AHFIALLQREGGKTLDDALSELREAADFCRYAAQGRK LFGSE  
TAMPGP TGESNALTMRGRGVFAISPWNFPLAIFLGQVTAALMAGNSV VAKPAEQTPRIAREAVALLHEA  
GIPKSALYLVTGDGRIGAALTAHPDIAGVVFTGSTEVARSINRALAAKDGPVPLIAETGGINAMIADAT  
ALPEQVADDVVTSAFRSAGQRCSALRLLFVQEDVADRMIE MVAGAARELKIGDPSDVATHVGPVIDVEAK  
QRLDAHIARMKTEARLHFAGPAPEGCFVAPHIFELTEAGQLTEEVFGPILHVVRYPENLERVLRAIERT  
GYGLTLGVHSRIDDSIEAII DRVQVGNIYVNRNMIGAVVGVPFGGNLSGTGPKAGGPHYLARFATEQT  
VTINTAAAGGNAALLAGEE

>Bacteroides Q8A340 Q8A340\_BACT

MVQRPQDKKFLVKMLDESSQIRDRILAKRIKTL LDQYGVPEFLNKRDSFLFKMYQAFGH  
HFDFIAIPIIKKRLRMNTSQVIINEARPQLTKHLAIRAKEKIGQNVNLLGEVVLGNGEAD  
HRYHHY LKALES PDINYISVKISGIYAQTHALNYEESFPELISRMSALYQKAIDFPYTDE  
EGVRRSKFINLDMEEYKDTHFTLRLFKTVLSLPQFKNYSAGIVVQAYLPDAYDFQTELIE  
FAKARVAEGGAPIKMRLVKG CNLEMETV ISSLRGWPNIIRPSKEEVDANYLHLLERALMP  
ENARVLHLGVASHNLFSIAYAYLLAQKYGTAEYMTFEMLEGMANHLWRAQSMLGNRVILY  
TPVVKNEHFLNAVSYLVRRMDENTAPDNFLTHSFNLRPNTKEWDFLAKQFEDAYAMKDQL  
SHVSPRTQNRNL PYTPVPADVLKNEPDTDFDL PQNQEWRSIFSKWKKGTEQPEI IPL

QIGAETVVCESRYPYTDRQCDDDEVICICEMSQADSAQVEKIIIEIAEADPAGWRKTTLEERH  
RIMYEAANRLADMRGDLIGCMCAVTGKTVEIEGDVEVSEAVDYARFYTTAMKKFAALDDVE  
MKPKGTILVISPNFPCAIPVGGIVAGLAGGNTVILKPATVAAPVAMWFAKAFWDAGVPK  
EALQVIITRREALKVLTTAPAIKHIIILTGGTDTAQNIAKANPTTPLSAETGGKNVIIILTA  
SGDRDHAIMNIVTSAFGNAGQKCSACSLLLVERSVYEDENFRSKLKDAATSLKTGSVWNA  
GNIVGPMITNKNNDKLLQAFNLEPGESWLVPFRFIDRREYILAPTVMKWGVKPEFSFSRTEL  
FGPLLSVACIENLEEGIRLVNGLDYGLTSGLQSLDEKEQKLWKNNSVMAGNLYINRGITGA  
IVNRQPFPGMKLSAFGGGIKAGGPNYCTCFLEITDKPDSRTDYRQSYAKAYQEEFSKPRD  
VNRLYGEQNLFRYLPLKNMILRLFPKDTDEEATMIAHAARICRTPLTISFGPTDDRSSL  
AGLGCTLRKESLEDFLKELPEYERVRTCSPDIPDVMYERAAETNKYIATAPPVKQGRIEL  
IHYIKEQSI AFEYHRYGSISEVPPCE

>Corynebacterium Q8FUB9 Q8FUB9\_

MGFLRCAGSPPNPPEILSAESSTDWVNFGRFWEQELGVKAATVSGGASAPAPGTAGDRI  
STCQYVGGHNNRDNWCGSHDGRVSARSVVGSGPRWPTNTARDVTNPGEQGASTMTATTDH  
SMKLPIELATLTDRVVKVRDWLEYAQQESVPNPTAERLAAILQDPNGLEFTVGFVDRV  
RTEDIHAAARALNDLGSIA PSTMSFIDRAQIQAGSLVGRALPHVVVPAARARIRQMVGHM  
IVDARDKPFGRVAELQGDGNRLNINLLGEAVLGEKEALKHLEDARRLLGRMDVDYVSIK  
VSSVASQISLWGFDETVEAVVKRLTPLYKEAAAATGTPGGTKFINLDMEEYGDRLRTIEV  
FKRLMSLPGVENLEAGIVLQAYLPDALASLQELAEFGAHRVDNNGGAPIKIRLVKGANLPM  
EHVHAEIAGWPVATMPKQATDANYKRVLWWALRRENMTGLRLGVAGHNLFDI AFAHLLS  
IERGVAEKVEFEMLQGMASDQARAASRDVGQLLLYVPAVRPQEFDAAI SYLVRRLEENSA  
SENFMSVIFDLEADNPAFRREESRFRASIEDLAGLIDAPVPGPNDTQDRGAQEAEETLEAA  
GERARELEAARAPDQLPPFANEPTDNPALTANQQWARAAIKRSAGEGWLEQQTAPLSVEE  
EDIDALIEGTRAAAAEWAALPPMERARILYRTADILAARRGHLVSI AAAEVGKVVEQTD  
EISEAIDFARYYAHRALELEQVDNADFTPDRVAVITPPWNFP IAI PAGSTFAALAAGAGV  
IHKPSKPSQHCSAAVVEALWEAGVPRRVLHCVPANREAGRRLVSHPEVDRVILTGSSET  
AAMFASWRPDLQINAETSGKNAMVITPAADRDLAVADLVHSAFGHAGQKCSAASLGILVG  
TMYTSEFRSRLVDAASSLVVDWPTNMSATVGPLTEQPSDKLQHALTQLEPGERWLLPEK  
PLDDTGRWLWRPGIKEGVQPGSFFHLTEVFGPVLGLMKADDLEQAIEYQNAVEFGLTGGIQ  
SLDIDEVRTWDAVEVGNVYVNRGITGAIVERQSFGGWKSSVGLGSKAGGPNYVMLMGR  
WSDKPAKDAPVKSSPLINKWTHTLSPDDITWLEQANASDALAWTSEFGTPRDP SGLAEAA  
NIFRYRPAKVVLRIADDAEPREVARAVLAARRAGAQLTAMVGPVGGGVREVLADASTSV  
ETIDDAVFITRLLRGDYDDGTGARVRVIGTVTPFQRRERLAVRPEVAILDEPVTSSGRVEL  
RYWLKEQAVSMTLHRFGNRSEAFHKLAADLKRPL

>Geobacter Q746X3 Q746X3\_GEOSL

MLNSELNTKIVNRGKEFFGSISGEKPSLFNKGAWMGKAMDWSMQNEQFKIQMFRFVDVFP  
SLTTSKLLTEHIREYFGNEQDMPAFMSTGAKVAGMLGSFGGAVLNKVLTSNIEEMARQFI  
VGETTKEAVKNLEKLRKDGF AAVVDVLGEATLSEEEAEVYTN TYLELLEALKKEQGSWKG  
LPGKGGDPGLDWGHAPKVNI AVKPTALFCLANPQDFEGSVVAILDRMRRIFKKVMELNGF  
LCIDMESYRHK EII LEVFRRLKLEYRDYPHLGIVLQAYLKDNDKDLDDLAWAKEHKVQI  
SVRLVKGAYWDYETVKAKQNDWEVPVWTIKAESDAAYERQARKILENHQICHFACASHNI  
RTISAVMEMARELNVPEDRYEFQVLYGMAEPVRKGILKVAGRIRLYAPYGNMVPGMGYLV  
RRLLENTANESFLRQSFAEDAQIERLLEDPAVTVERERAARAAPKKKERKGLGGLPPFNN  
EAMVDFTRADHRAAFPKHIAQVRTQLGKTYPLFINGKEVRTNDLIPTVNPKNKPEVLGQI  
CQAGTTEVGDAIAA AKAAPAWRDTDPRTAEYLLKAAQAARKRLFELSAWQVLEIGKQW  
DQAYADVTEAIDFLEY YAREMIRLGQPQRVGHAPGELNHYFYEPKGVA AVIAPWNFLAI  
SMGMASAAIVTGNCVVFKPSGITSII GWHLVELFREAGLPEGVFNFTPGRGSVMGDYLV  
HPDISLIAFTGSMETGLRIIERAAKVHPGQANVKKII SEMGGKNAI I IDDDADLDEAVPH  
VLYSAFGFGQKCSACSRVIVLDAVYDKFIERLVSMAKATKVGPSDPANYPMGAVADDKA  
MKSKEYAEIGKREGHVLYESPVPAGEGYFVPMTIIGGIKPEHRIAQEEIFGPVLAVMRA  
KDFDQAI EWANSTQFALTGGIFSR SPEHLAKARREFRVGNLYINRNNTGALVERQPFGGA  
RMSGVGTAKAGPDYLLHFMDPRVVTENTMRRGFAPIEEDDDWVD

>Desulfovibrio Q725V6 Q725V6\_DE

MDQQHLDGKVVERGKEFFRSISGEAPSIFNKGWWTGKVMWAMQNEDFKVQLFRFVDVLP  
YLNTSESLLRHIREYFATEDADIPVVKWGAGKAGIGGALTAKLMGMTIRSNI EGMARQF  
IIGDNSKEAVKGLAKLRKDGF TFTVDLLGEATVSEEESEAYA QGYHEVVDIAIAREQEKWK  
ALPGNGPVEGFDWGATPKVNVSIKPSALYSQAKPVDVEGSRGILSRLVPIYRKVVAMGG

FLCIDMEQLKYKEMTLELFKRLRSDPEFRHYPHLSIVLQAYLRDTEKDLDDLLHWARSEK  
LPIGIRLVKGAYWDYETVIAKQNGWEIPVWTDKPESDIAYEKLAHRILENSDIVYFACAS  
HNVRTIAAVMETALALNVPEHRYEFQVLYGMAEPVRKGLKNVAGRVRLYCPYGELIPGMA  
YLVRRLLENTANESFLRQSFAEGAALERLLENPQKTLHRLLAARPEPRAVEPGPGGLPPF  
TNDAMIDFTVPDNRKAFVEALADVRSRFGQTVPLYIGGRDVTADLIPTTNPAPAEVVA  
SICQAGRPEIDDAIAAAKKAALTWRDTSPADRAAYLRRADICRKRIWELSAWQVVEVGK  
QWDQAYHDTVTEGIDFLEYAREMLRLGAPRRMGRAPGEHNHLYQPKGIAAVIAPWNFPF  
AIAIGMASAAIVTGNPVIFKPSSISSRIGYNLAEVFREAGLPEGVFNYCPGRSSIMGDYL  
VEHPDISLICFTGSMEVGLRIQEKAQVQPGQRQCKRVIAEMGGKNATIIDDDADLDEAV  
LQVLYSAFGFGQKCSACSRVIVLDAIYDRFIERLVKAASSIHIGPSEDPSNYMGPVADA  
TLQKNVSDYIRIAEEEGRVLLKRTDLPAGECYVPLTIVGDIRPEHRIAQEEIFGPVLAVM  
RAATFDEALSANGTRFALTGAVFSRSPHELDKARREFRVGNLYLNKGSTGALVERQPFPG  
GFAMSGVSKTGGPDYLLQFMDPRVVTENTMRRGFTPIDEDDDWIV

>Syntrophobacter Q3MY03 Q3MY03\_

MDSDLERRVQQTGLWLYELIEGESPSVFRKEFWTGKMLEWCMQNEAFKVMFRFVDVFPY  
LTRPESVARHVQYFYSRPGVNFPAVLQWGLRAVSPGSLTAKVIARSITHNLHNMARQFIV  
GNSNPSEALPNLERLRGQGMFTIDLLGEAVVSEKEAEEYVSRYLELFDILDEAQRKWPAI  
GGGAQQADWGHAPKVNVS IKASAMYSQMSARSFEDSVARSKEKLRPILRKALATGSFVNL  
DMERHALKDLTLALFRSLMEDEFRDYPHVGIVIQAYLKDSERDLEEILGWAKATGRHFT  
IRLVKGAYWDSEVIWARQSEWPVPVFTSKPETDANFEKLADLIMENHQWVSLACASHNMR  
SISYVMERARDLSVPAGRLEYQVLYGMGEPVRNALRKAGLPVRLYTPVGDMIQGMSTLVR  
RLLENTANESFLRKSFFQGVSRRELLLRNPMVDLAEERTAGPVPARDAPEYGDKGPFCEP  
CFDWTIPEHRAGFRDALDRVRATFPIKVPLTIGGSRFDTPVRLRSVNPRAEEMVGDVAG  
AGPLEADA AVEAAKAAFAAWRDTPPGERAEYLFKAAAAARRIRYDLAALQVYEVGKAWSE  
ADADVCEAIDFLEYYGREMIRLSRPKRMGHAPGEISHLFYEPRGVA AVIAPWNFPMAIST  
GMTSAALVTGNTVVYKPAQSPVVGSMVMNVFEEAGLPKGVL SFLPGPGAQIGDYL VHHHP  
DVAVIAFTGSKKVGLDIIAQANRDAERAGHVKTVAEMGGKNAIVVDADADLDEALAQIV  
HSAFGYQGQKCSACSRILVLEEIYDKLVERLKAAAESIH LGPPEDPKNLMGAVIEAGARK  
RIMEYIELGRKDGTVLVERTVPGNEGFFVPLTILADLPPDHLAREEIFGPVLVVFVKVD  
RAIAEIANDEYALTGGVFSRSPANIDLARREFRTGNLYINRGCTGAVVERHPFGGFKL  
SGIGSKAGGPDYLLQFMVPRNVVENTLRRGFAPADE

>Bdellovibrio Q6MNK1 Q6MNK1\_BDE

MNDIQSQIVSRGEEILKRMESQSKASIFSKDFWYGSIMEWSMKNEKFKTNMFRFVDVLP  
INSGDEVARHLKEYFSEDGGTLPPVFNVLGLGLSLAPGLMAGAIKKNVMGMAKMFITGES  
PDEALPVLKKARKNKMTFTVDILGEATLSEKEAQDYSNKYMELVTWLAKDAEKWDEVPQI  
DRDHEGALPKVNVSVKMTALYSQIKDAAWDESKKILKDRLRPVFRLGMEKGVFVNLDMEQ  
YSVKHLTLEVFTELINPEFKNYKFFGIVIQAYLRDSFEDVKSLEFAQKRGTPFWVRLV  
KGAYWDYETIEAEQRGWPVPVYTINKAESDANYELCAKYLLENIKFIRPAFASHNVRTLAA  
CMLYAEKLNIPKEALEFQMLYGMAEPIKKTIVDMGYRMREYAPVGELIPGMAYLVRRLLE  
NTSNESWLGRKFADNK SMAELLKDPAQGLTPTSPVIPKPKGKFYNEPLLDFAVKADREKM  
LKALAEAKASLPVNVNIVINNKEQSGKIFDRVNPSQSDQIVGKIQMATTEQAEQAMQAA  
QTAYKTWKNVPCEQRAALVDKLADIMTRDRFKLIATQVLEVGKPAEADGDIGEAIDFCR  
YYARHMRRELQKPLRVGGLPGELSHYIYKSRGVTAVIAPWNFPLAILAGMVTAAAVAGNTV  
VMKP AEQSTTVVAGLMKMIQEAGFPQGVINFLPGYGEVGEYIVNHKYTTTIAFTGSKAV  
GLHIMNRAAVVQPGQQHVKRCIIEMGGKNAVIDNDADLDEAVDGVYISAFGFSGQKCSA  
ASRVIVLDEVYDRFVDRVLVETAKSIEIHPAENPKAYMGPVVDKEAYDRILGTIAEAEKNH  
KLLFKGSVPGGGFFAPPTIFGDVPGDAKLAQAEIFGPVVAVIRAKNLDQALDIANSTEYA  
LTGGVFSRSPANINRVKEELEVGNLVNRGITGAMVDRHPFGGFKMSGIGSKTGGPDYLLK  
QYMEPACVTENTLRRGFAPAE

>Trichodesmium Q3HDN5 Q3HDN5\_TR

MVEQISHTNYETKTQEIAKQLLKATQEKNSFLAQLQNQMRWDDKLLDWAMASPLRVQL  
FRFIDCLPALRSKPEIAAHLQEYLTTQEVELPETLKKLLNFANPDSVPGQLAATTVAPAV  
ETLAHKYIAGENVKQIIKTLEKLRKDKMCFTVDLLGEAVITETEAQLYLDRYLELMTQLS  
QAANSWSSIPQIDEAEGEKLPRVQVSVKLTAFYSQFDPLDVKGSQERVSDHVRTLLRHAQ  
KLGVAHVHFDMEQYTYKDLTIDILKELLMEEFRNRNDIGVTIQAYLRDSEKDLQGIIEWA  
KIRGRPVTVRLVKGAYWDQETIKALQHDWPQPVFNDKPETDANFEKLT YMMLNHEYIYS  
AIGSHNVRSQARAIAIAETLKVPRRCFEMQVLYGMGDKIATILAEKGYRVRVYCPYGDLL

PGMAYLIRRLLENTANSSFLKQSLNRPLEELLAAPSINGKTTIHDVVKPVFPNAADSDY  
ANFQQRQQAALNTIGQIRLELGKTYLP I INGEYTNTAQIVDSLNPSSKEVVGKIGLISVE  
QAEQAIQAAKAAFPSWKKTTPVRERTRILRKAADLMEKRRHELAAWMVLEVKGKPLNQGNAE  
VSEAIIDFCRYADEMERLEQGYNYDVAGETDRYYYQPRGISLVISPWNFPLAIPGTGMTVS  
SLVTGNCTLLKPAAVSSVIAASKISEILLEAGFPKGVFQFVPGNGSTVGDFMVKHPSVNSI  
TFTGSMEVVGCHIYAQAQAVLQPRQKHLKRVIAEMGGKNAIIVDESADLDQAVAGVVYSAFG  
YSGQKCSACSRVVVLATIIDSFVNRLVEATRSLNIGDAEKPSTQVGPVIDEKAQKRIQEY  
IVKGKQEAQAEVAIEMSAPKDGYPVGFVIFKDVSPSATIAQEEIFGPVLAVMKADNFTQALE  
IANGTNFALTGGLYSRTPSHIEQAQAEFEVGNLYINRGITGAIVSRQPFGGFKLSGVGSK  
AGGPDYLLQFLEPRTITENIQRQGFAPIEGVDN  
>Anabaena Q8YZD7 Q8YZD7\_ANASP 1  
MVLQVQTSTYEAKTQEIAARQLLGATQENRSFFASLRDQMRWDDKLLAWAMSNPGLRVQLF  
RFIDTLPALHSAEIAAHLQEYLGDESVELPAALKGMLNFANPDSVPGQVAATTVSTAVE  
TLAHKYISGENIKQVIKTVERLRKEKMAFTIDLLGEAVITETEAQSYLERYLELIAQLTE  
ASKNWGTIAAIDEADGEQLAKVQVSVKLTAFYSQFDPLDAKGSEEKVS DRIRILLRRAKE  
LGAAIHFDMEQYAYKDLTLNILQKILLEDEFQRQTDIGITIQAYLRDSEQDARNAIAWLK  
QRGYPLTIRLVKGAYWDQETIKAAQKHWPQPVFNDKAATDANFEAITQLLLENHQYVYSA  
IGSHNVRSQALAMAI AETLNVPRRRFEMQVLYGMGDKLAKALVDRGYRVRVYCPYGDLLP  
GMAYLIRRLLENTANSSFLRQNLNRPVEELLAAPKVDLAQAKVHSPEAFPGKHFGVGA  
DTDYAEEDRTKAARAFVVRGELGKTYLPLINGEYVQTAEVIDSVNPSNFSEVIGKVL  
ISVEQAEQAMQAQAAAFPGWRRTSVKERAGILRRAGDLMEQRRRAELSAWIVLEVGPVKE  
ADGEVSEAIIDFCRYADEMERLHQGINYDVGGETNRYIYQPRGIVVISPWNFPLAIAAG  
MTVAALVTGNCTLLKPAETSSVITAKLTEILVEAGIPKGVFQYVPGKGSQVGAYLVSHPD  
THLIAFTGSQEVGCRIYAEAAATLKPQQRHMKRVIAEMGGKNAIIVDESADLDQAVVGVVQ  
SAFGYSGQKCSACSRVVVVEAIYDAFIHRVVEATKSLNIGEAELPSTQVGPVIDANARDR  
IREYIEKGKAEQVALELSAPNHGYFVGPVIFGEVPPHGTIAQEEIFGPVLAVIKAKDFA  
QALAIANDTDYALTGGLYSRTPSHIQQAQEEFEVGNLYINRNITGAIVARQPFGGFKLSG  
VGSKAGGPDYLLQFLEPRTITENIQRQGFAPIEGAE  
>Crocospaera Q4BWE2 Q4BWE2\_CRO  
MVVQLDSTTYEQRTQEIAKELIAQTREKRSLWSKLGDQMRLLDDKLLDFAMANPGLRVQLF  
HFIDTLPALQSNAEIAAHLQYLGDESVELPSSLKGI LNFTDYNLSLPAKVAAETISKAVQ  
TLAFKYISGETVPQVIKTVERLRKEKMGFTIDLLGEAVITESEAKAYLDSYLDLMEKLAT  
ESKKWSNVAQIDTAGDENLSKVQVSVKLTAFYSQFDPIDPQGSKEKVCTLIRILLRRAQE  
LGVAIHFDMEQYVYKDLTSLILRELLLEEFNRNSDIGVTLQAYLRDSKQDLHDLISWAK  
QRGTPITIRLVKGAYWDQETIKSEQNHWPQPVYNQKSATDVNYEEMTQLLLENHQYLYAA  
IGSHNVRSQARAIAIAETLKVPSRAFEMQVLYGMGDQLAKALVKTGHRVRVYAPYGNLLP  
GMAYLIRRLLENTANSSFLRQNLNLEERPIEDLIASPTLSGNTERIAQKESFVNVPD TDYSR  
EVL RDKA EKALAKVKDSL GKTYLPLINGEYVQTDVIVESVNPSKSSEVVGQIGLISVSQA  
EQALNAAREAFKDWKKTTPATERARIIRKAGDLMEERRHEL SAWICVEVGKVLQQADAEVS  
EAIDFCRYADEMERLDKGYNYDVAGETNRYHYQPRGIALVISPWNPFAISTGMTVAAL  
VTGNCTLLKPAETSTVIAAKIAEILVDAGIPKGVFQLVPGKGSKVGAYMVNHPDVHLIAF  
TGSREVGCRITYADAAAILQPGQKHLKRVIAEMGGKNAIIVDESSDL DQAVAGAVFSAFGYS  
GQKCSAASRIIVLDPVYDAFLERFVEATKSLNVGATDQ PSTQVGPVIDATAQKRILEYIE  
IAKQESTLALQMEAPDNGFYVGPTIFGDVLPNHTIAQEEIFGPVVAVMRVKSFAEALGVA  
NGTDYALTGGLYSRSPHEIEQAQKEFEVGNLYINRTITGAIVSRQPFGGFKLSGVGSKAG  
GPDYLLQFLEPRHISENIQRQGFAPIEGNE  
>Synechococcus Q2JNZ3 Q2JNZ3\_SY  
MVAQGAPTAYEAQTQALASLLASLWGEKRSLLAQWRDQLRWEDKLLAWAMENPHLRTQL  
FRLIDVLP SLKSKAEVARHLQEYLSDPAVELPGMLKSLNLFADPDSLPGQLAATTLTA AV  
EALARRYIAGETLQVSKTLEALHRQGMAFTLDLLGEAVITEAEAQSYLD RYLQVMEHLA  
KMVKTWPPQPVQVSVKLTAFYSQFDPIDPLGAKAKVGERIRILLRRAEALGVGIHFD M  
EQYRYKSLTLAILQELLLEPEFKSR TDVGLTLQAYLRDSYTDLQNLIAWAKERGSPVTVR  
LVKGAYWDQETILAAQKHWPQPVYNSKSATDANFERMTQLLLEHHTLHAAIASHNVRSQ  
AKAIAIAQALEVPQSAFELQVLYGMADPLAKALVQKGQRVRVYCPYGELLPGMAYLIRRL  
LENTANTSFLRQSVQGYTPEQLLAPPVLEEGSVFPAPSLSF AAAPD TDFSQPPQ RDPFFQ  
ALDEIRPQLGQRVPWIAGEYRPTQQAMLSLNPADPQQVVAEIGLTEPEQVEQALAAAQA  
SFPSWRRTPVAVRAGILRRVAEQIEAQRAELAAMVLEVGPPIAQADGEISEAIDFCRY



AQQMEALDRGRECNLPGETNHYHYQPRGVAVVIAPWNFPLSIPCGMTAAALVAGNCVLLK  
 PAEQSSLIAAKLAEFILKALAEAGIPEGVFQFLPGVGEAIGPLLVDQRRVHLIAFTGSQA  
 VGCQILAAQAQLQPGQHIIKRVIAEMGGKNAILIDESADLDQAVKGVVNSAFGYSGQKCS  
 ACSRAIVLQSIHDLFLGRLIEAVRSLNVGDPAPHPSTQVGPVIDAEAQARLQQAIIQSAKAD  
 ARLDLSLPVPEKGYFVGPTVFSQVDPQSELAQRELFGPVLAVISAPDFSSALQMANATPY  
 ALTGGLYSRTPSHIQQARRDFAVGONLYINREITGALVERQPFGGFKLSGVGSKAGGPDYL  
 LQFLEPRTVTENTQRQGFAPIEGS  
 >Gloeobacter Q7NGY2 Q7NGY2\_GLOV  
 MELPPFQETRVLTVDPIESETQRIGQSLAAPQQSRFSFFERSFWDEKLLEWAMADDEL  
 VQLFRFIDCLPALKTNREVASHLQEYLGSVKLPGLAKALDFADPGSPAAVATLGLRQG  
 ISQMARRFIGENLKTAVKTIIEKLRSQNMVSLDLLGEAVVSEAEAEVYQRRYLELLSDL  
 HAAQSRWPVIDQIDRADGQLLPRVHFALKLTSLYSQFDAIDPATTGRNVKARLRPILRKA  
 RELGAFVHIDMEQSQHKDLILQIFKEVMVEADFRDWIDTGICLQAYLRSaelDAANVIAW  
 SKERGYPVTVRLVKGAYWDGEVIRAAQQRWVPVPVTRKADTDQYEVKVLHLLMENHRSVH  
 IAVGSHNARTVALAIALARRNRVPRRAFEVQMLYGMADHLKAGVAQQGERLRVYAPYGEL  
 LPGMAYLIRRLLENTANTSFLRQSVRPGSDVVRLAPPASGEAAPSLMGSEFVNAPDRD  
 FAVAAEREKLAAGLAEVRTCFGQTYWPVVGKARRGLPTLSVPNPAEPGTVLGLGLADA  
 ELADEAVKVAHTAWLSWSKTTPEARARLLGRLAELMEQQRSALTAWIVYETGKPWRESDA  
 DVSEAIDFCRYGRQILKLTAAQHRDVPGETNGYHYRSRGVAAVIAPWNFPLAIIITGMT  
 TAALATGNTVIMKPAEQSSIVAAQLMRLCEQAGFAAGVVNYLPGRGEVVGAKLVAHPQVH  
 LIAFTGSLAVGQRILAEASMVRPGQRHLKRVIAELGGKNAIIVDSADLDQAVVGVVQSA  
 FGYSQKCSACSRLIVLEGIYDVFIERLVQATRSIVGNPAQPATYTGPIVIARDACERIR  
 GVIEDAKGRHRLVLEVDVSHLGEYFIGPTIFADVDPQSSLAQEEIFGPVLAVIKARDFE  
 HAIEIANGTSFALTGGLFSRSPRHIAEARERFEVGNLYINRKITAALVDRQPFGGFRLSG  
 VGSKAGGPDYLLQFVEPVTVTENIQRQGFAPLPGL  
 >Helicobacter Q9ZN12 Q9ZN12\_HEL  
 MQKIIEDSLELAKKLQDSISNHLSEQEKAHFHFKMQKLLNNPENKVMLIELMDRSFRCLDN  
 KARFEMIEHVLVDKYKSREIFSSFEEKWLLMGFLSFGKMLPDMSPVFFVNKIRSDTKAMVLD  
 QEESQLRERILKRKNEKIIILNVNFIGEEVLGEEEAARFEKYSQALKSNYIYISIKITT  
 IFSQINILDFEYSKKEIVKRLDALYALALEEEKKQGMKFINLDMEEFRDLELTVESFME  
 SIAKFDLNLNAGIVLQAYIPDSYEYLKLLHAFSKERVVKGLKPIKIRFVKGANMESEETIAS  
 MKDWALPTFSSKQDTSNYNKMLDFVLEGDNYKYIHIGAASHNIFEIAYVYTRIHALNDP  
 VVLEHFSFEMLEGMSLQASQELKEMHKLILYAPVCDEAHFNNAIAYLVRRLDENTSSDNF  
 MKAFFNLKVGTSSEWKDQEQRFNLNLKGIATLDNTTHTQDRNAKQTGHTTYPNHSFKNES  
 DTDFILKANREWAKKVRDKMHNAPILELYPEIDGRFEDPNLTPLEVFDRIHKKIASVHL  
 ADKEAILKALEVAKSDKSRSFSQKSFTIEHALLSQTALFRERRGDLIGISALEVGKTFAE  
 TDAEVSEAIDFLEFYPSLRVLQEQNKTKFTPKGVGVVVIAPWNFPVGISVGTIAAPLAA  
 GNRVIYKPSLSSTVGYKLCECFWDAGVPRDALIYLPSKGSIDSEHLLKDESIKFAITG  
 GEDTAYKMLKANPTLALSATGGKNATIVSKMADRDQAIIKNIHSAFSNSGQKCSATSLL  
 VLEKEVYEDENFKKTLIDATLSLVGDPDFDKNKIGALADKPNEKVIKAIDELKSYENYE  
 IPASFVDDNPYLMKPSIKYGTGGDFTHQTELFTPILSVMKAKDLDEAIEIVNSTGYGLT  
 SALESLLDEREWEEYLERIEAGNIYINKPTTGAIVLRQPFGGVKKSAVGFGKRVGIFNYIT  
 QFVNIHQEEDENALKNPLSEALEGLTQKGYDEHTELKRAIFMAKSYAYHYKHEFSQAK  
 DYVKIRGEDNLFSTYKVTSVGYRITEKDTLSMDLGLVALACLISQIPLTISIENERANKDL  
 TFFLECLKALQANAPIVYESLQKFSEKLNAFNVRVYLKSDLDLLEHQASRLGMVLATAKP  
 CLNGRFELLYYHLERSVSISYHRYGNLGSRVLRQPTCHKSCCAEK  
 >Campylobacter Q4HED6 Q4HED6\_CA  
 MIQKSLALAEELQKIEANISNSEKEFHAKMQKLLNNPENKVMLIELLDRSFRCKDKRAS  
 FELIEHTLNKYGIADFFSAFEKFLLSFNLFGKFAPNLSVPFFVKHLREDTKAMVLDANP  
 SVLEPHMRKRKDQDNITLNVNLIGEEVLGEAESKYRIQKYEEALKSSYITYISIKITTIF  
 SQINIIDFEYSKDEVVKRLDHLALALEEEKKQGVSKFINLDMEEFRDLELTVAAFMESV  
 SKFDIKAGIVLQAYIPDSYEYLKLLHAFSKERVVKGMKPIKIRFVKGANMESEETIASQR  
 GWELPTFYKKIDTDSNYNKMLDFVLEGDNYKYINVGIASHNIFEIAYAYTRISEAGALDS  
 FTFEMLEGMSLQCSYELSKMHDILYAPVCDEAHFNNAIAYLVRRLDENTSEDNFMRYFF  
 NLKVGDNWNVNQKELFLKSLEGIKTLDNSTHTQDRNKAPNIVSAYESGMFNNESDTDFI  
 LPQNRWAKVIRAKYENLENYDMPVIGDLEFDKNTLNILEVKDKIKDRMIGKAYLAGEN  
 EIKKALKVAKNSNFKNTSFDEIHAILAKAANLMRERRGDLIGLAALEVGTFLIDPEVS

EAIDFTEFYPHSLKVLREQNKNTQFSPKGIGVTIAPWNFPIGISVGTIAAPLAAGNVVIY  
 KPSSLSTLTGYMLCKCFWDAGISKDALIFLPSKGS DISKYL LVEAVKFSILTGGEDTAY  
 AMLKANPTLLLSAETGGKNATIVSKFADRDSA IKNIIHSAFSNSGQKCSATSLLVLEEEV  
 YEDEEFKKTLDVDAASMAVGNPF EFKNKLGTLADKPSAKVEKALNELAPYEEWALKPQFL  
 ENNPYLMTPGIKYGTGGDFTHMNELFVPILSVMKAKDLKEAIEIVNSTGYGLTAGFESL  
 DEREWEIFHTHIEAGNIYINKPTTGAI VLRQPF GG VKKSAIGFGRKVG IYNYITQFLDIS  
 TSEADENLLNNEFVK TLEKIDLG TNEENK KALNNAILMAKSYAYHYRNEFSVSKDYVNIR  
 GEDNLF SYTKIKNLAFRVCENDNLQDILGVIIAANILNIPLSVSYEENDKISLVKELCKA  
 INLNLEITNESKAQFVSRLKNFERIRYHGKVSVEDEIYQEA AKEAKII IREKPLLNGRFE  
 LLFYHNEKALSVSFHRYGNLGIRALNH  
 >Thermus Q72IB8 Q72IB8\_THET2 Pr  
 MNLDLAYRSFVLGVAGHPQVERLIKHRAGLVRRYVAGETLEEALKA AEALERE GVHAIL  
 DLLGEMVRTEEEARAFQ RGLLELVWALAGKPWKYI SLKLTQLGLDLS EDLALALLREVL  
 REAEPRGVFVR LDMEDSPRVEATLRLYRALREEGFSQVGIVLQSYLYRTEKD LLDLLPYR  
 PNLRLVKGAYREPKEVAF PDKRLIDAEYLHLGKLALKEGLYVAFATHDPRIIAELKRYTE  
 AMGIPRSRFEFQFLYGV RP EEQRRLAREGYTVRAYVPYGRDWYPYLTRRIAERPENLLL V  
 LRSLVSG  
 >Geobacillus Q5KVJ1 Q5KVJ1\_GEOK  
 MEQLMRDFFLFLSKNKT LTKWAKRYGLRFGASRFVAGETIEEAVRVIRQLNEKGLAVTV D  
 YLGEFVDNEQEANEMARHCLEAIEAISREKLNSQLSLKMTSMGLDISDELVMRNMRRILD  
 AAKQRGVFTIDMEDY SRCQKTLDIFKTLKKEYDNVGT V LQAYLYRTEQDIEDLKPYRPN  
 LRLVKGAYKEPPEVAF PDKKDV DENFKKI IKMHLLNGNYTAVATHDDAII EYTKQLVKEY  
 NIPNSQFEFQMLY GIRPERQVQLAREGYTMRVYVPYGT DWYGYFMRRLAERPANVAFVLK  
 GILRK  
 >Deinococcus Q9RW55 Q9RW55\_DEIR  
 MIDQLYRKAVLTVAERPQVEQLARQKMWNLAERFVAGESIESAIQAVQALERDGIAGNLD  
 LLGEFIDSPAKCTEFADDVIK LIEAAHAAGIKPYVSIKLSSVGQ GKDENGEDLGLTNARR  
 IIAKAKKEYGGFICLDMEDHTRVDVTLEQFRTL VG EFGAEHVGTVLQSYLYRSLGDRASLD  
 DLRPNIRMVKGAYLEPATVAYPDKADVDQNYRRLVFQHLKAGNYTNVATHDERIIDDVKR  
 FVLAHGIGKDAFEFQMLY GIRRDLQKQLAAEGYRVRVYLPYGRDWYAYFSRRIAETPRNA  
 AFVVQGM LKG  
 >Bacillus Q81XI4 Q81XI4\_BACAN P  
 MEQLMRNSFLFLSKNKALTKLAKKYGLRFGAGR FVAGETIELATAAIQALNKQGLCVTID  
 YLGEFVDNEAEANEMANQSIEAIRAIGREGLDSQLSLKMTSMGLDISDEIVMNMNRRIE  
 AAKENG VFTIDMEDYTRCGKTIDIFKQLKSEYDNIGTVI QAYLYRTEKDIEDLNAYNPN  
 LRLVKGAYKEPEEVAF PDKKDVDDNYKKI IKMHLLNGNYTAIASHDEAII EYTKKLAEH  
 NIPRDQFEFQMLY GIRNERQLELVKEGYKMRVYVPYGN DWYGYFMRRLAERPANVAFVLK  
 GMVKK  
 >Exiguobacterium Q41B01 Q41B01\_  
 MERVLRDGFIFLSQNKTLNGLAKRYGLKFGAGR FVAGDSLEASKRAIQDLNSKGLCVTMD  
 HLGEFISTVAEAEMMTQECIRAVEMIAEEKLDSQLSLKLTSLGLDISDELIRSNMERILT  
 RAKEVG VFTIDMEDEPRCKE TIQLFEELRQSFDNIGTVIQSYLYRSEDDIKRVGRFETN  
 LRIVKGAYKEPATVAFPEKEDVDHNYIKLVKLQLSLGNAAVATHDDAMIEQIIRYAKEN  
 GIGNDKFEFQMLY GIRVERQLELVKLGYKVRVYVPYGRDWYGYFMRRLAERPANVAFVLK  
 GMVKG  
 >Symbiobacterium Q67RR3 Q67RR3\_  
 MSSSLARKAILSLAGNRFVTRVMTRHGLKIGAGR FVAGVT LQDAVAVTRRLNDEGLAVTLD  
 LLGEGVTD RDGARAMAEGCAGILEAIGREKLDANLSVKLTQLGLAVDPEAAMENMVYLQD  
 IARQAGIFIRIDMESSDVTDTLDIVRRLYARERNVGTVIQAYLYRSPKDLEELARLG MN  
 VRLVKGAYLEPPSVAYPKKADVDAAFRRLIAQHLSAGCYTAVATHDDAIIAFTESFVKEK  
 GIPRDQFEFQMLY GIRPERQRELARAGYRTRVYVPFGSDWYPYFVRRLAERPANVWFVLA  
 NLMKP  
 >Solibacter Q43US3 Q43US3\_SOLUS  
 MVRAFFLFLSRQQLRRWMETSPVAQRLSKRFVAGETLEQALAVSRKLNKQGITVTLDHL  
 GESVTS LAEAREARDVYRRTLD AIHAGDIQGNVSLKLTQFGLDLSYEECLANVEQLVRRRA  
 AELGSFVRVDMESSEYVDR TLDLVRTLHARHGAVGVVIQSYLYRSKDDIAKLCAEKIRVR  
 LCKGAYLEPASLAF PQKSDVDRSYVELTQKLLTYGVYPAIATHDEAMIGQTQKFVSSKGI

GRECFEFQMLYGIRADLQRLVADGYRLRLYVPFGKAWYPYMRRLAERPANVLFILRNL  
FRT

>Acidothermus Q2DYK6 Q2DYK6\_ACI  
MLRRLILEAADSQTLRRLIATAPPTRAVVHRFVAGTEVADGLAVARQLVADGLLVSLDRL  
GEQVRDLSQARATAEAYRELAIAIEQAGLAAEVEISLKL SALGLGLAGNASVGSPEEPRR  
VALDLAREICAAAQAAGTMVTFDMEDHTTTDDTLAIVAELRREFPSVGCVIQAYLRRLSLA  
DCRELAEAGARVRLCKGAYREPAEVAFTRRHEVDRNFVRCLRILMRGSGYPMVATHDPRL  
IAIASVMATQAGRGKDTYEFQMLYGVRPDEQQLVRRGERVRVYVPYGGQWYPYLMRRLA  
ERPANVAFFLRALGSKK

>Kineococcus Q40WW1 Q40WW1\_KINR  
MFGQLLLGVAGNRGVRSLVTGSSLSRPVVARFVAGDDVDAATAAVRTLTDGIGIAATLDR  
GEDVTEEAQADETVAGYRDLVERLAAEGLAAGNEISIKLSALGQGLGRSGPQRATERAHD  
LAAHAREHGVDVTVMEDHTRVDDTLTTVAALRADFPRTGCVLQAMLRRTEGDARDLAVA  
GSRVRLVKGAYNEPPEVAYPAKADVDKAYVRCLRTLDDGGAYPMIATHDLRIVNLAEEEL  
RGRDAGTAEFQMLYGIRAPEQQLARAGHVVRVYVPYGTDWYGYFSRRLAERPANLAFFA  
RSLVAG

>Salinibacter Q2S542 Q2S542\_SAL  
MKLPFFLASRFVAGETLETSLPVDDLNDGLHVALDKLGEHVQNRSEAI AARDAYIDL  
RTMAERDDHGQRNRISIKLSMMGQLIDEDFCEENLRRLLEVA AEHDLFVRLDMEGSDLTQ  
STLDLFEAVYPDFPNHVG PVLQAMLRKTRDRVDRMCELGVSVRLCKGAYAEPTSLAYQDM  
SQIRERYLDYTERLLQHTDDSGIATHDELIEATKSFVDRRGIDRDDFEFQMLYGLRRTT  
QREMAADGYNMLVYVPYGTWFPYFSRRLREKKENVWFVLRSLFQG

>Nocardioide Q3GZ84 Q3GZ84\_9AC  
MSLLRQPLLLARSSLVKKVSGMPVSAGIVRSYVPGETTESAVGATAELVDGGLRVTL  
YLGEDTTDAEQADATVAAYLDVLQELSARGLTRNAEVSVKLSAIGQFLPDAVGFGGGEKI  
ALENARTICRAARNAGTAVTLDMEDHTTTDSTLSILRELKDFPETGAVLQAALHRTE  
CRALAYEGSRVRLCKGAYLEPESVAFQDRLEISKSYVRCLKVLLAGEGYPMIATHDPRMI  
EIASSLASRYGRAAGTYEYQMLYGIRPEEQRLVASGETMRVYVPYGTWYGYLMRRLAE  
RPQNL SFFVKSLVSKK

>Oceanobacillus Q8CXJ6 Q8CXJ6\_O  
MANLTRDFFIGLSNNKLLNTNAKKYGFR LGA EK FVAGTNFDSIIGI IKDLNSEGISCTLD  
NLGEFVTEKSEAIEARDDIIDMLYKIHQRLDCHVSVKLTQLGLDIGDDFCINNMHAILK  
VANRFEIFINIDMEKHIHYGKTLEILNELRKEYDNVGTVIQSYLYSAEDDLAALEDVRIR  
LVKGAYKEDASIAYP SKEDIDRNFME LAKKRL LGNTFTSIATHDHNIIEELKSFVDEHNI  
SRDIFEFQMLYGFRTEMHNELAQAGYHFCTYIPFGSDWFGYFMRRLAERPQININLVKDV  
FYTKGNKLLKKEPVIAGVAALSLMYVNKKRKK

>Nocardia Q5YX89 Q5YX89\_NOCFA P  
MSGFTRLLRPALLAAAASPRVERTVTS LRATRALVDRFVAGTTEADALGTVEALLASGRW  
ITVDHLGEHTTDPARARDTVAHYRLLAALAE LPAAGAPGTVRPLEVSVKLSALGQALPG  
DGAAIALDHAREICTAASAAGIGVTVD AEDHTTTDATLAVVRELRADFPGVGTVLQAYLR  
RTEGD CREFAGPGSRIRLCKGAYREPASVAFQRAAEVDDSYRRCLRILMSGRGYPMVASH  
DPAMLA EADRLAAETGRGPDDFEYQMLFGIRDAEQRLADAGHRMRVYVPYGDQWYGYFM  
RRLAERPANLAFFLRAAASRDRA

>Streptomyces Q9Z560 Q9Z560\_STR  
MLGPVILAAASRSDRMRLVSAAPVTKPVVDRFIPGETVDQIVPIVRDLTDQGLELTMDVV  
GEDITTPAQAEAAARDAYLELIDRLKPLELGTRAEMSVKLSMFGQALDGGHELALANVRPV  
VEAAAEIGTTVTLD AEDHTTLD SMFAIHEELRKDFPQTGCVIQAYLFRTEADARRLADSG  
SRVRLVKGAYKEPAEVAYQQRHEIDKAYVRILRTLMEGEGYPMIGSHDPRLISIGQELAR  
TAGRKLDEYEFQMLYGIRGDEHLRLAAEGHRMRVYTAYGTDWYGYFMRRLAEKPANLRFF  
ARSMVSKG

>Chlorobium Q4AI77 Q4AI77\_9CHLB  
MNMFNKLIASLTLPYMPQSLVWVFSKKYIAGKTLD SAIDISKELNKN GSVMTIDLLGEFIT  
KLDEARSNKNEYLG IIDNVQKQKIDGNYS LKPTMFGLLLDEEAC YRNIREIVKKAAS YNN  
FVRIDMEDSQCVDMEIKLFRRLKEEF PANVGLVLQAYLKRTYQDITDMLDLNSKQLPVNY  
RLCKGIYVEPESIA YKKYEEINEHYLADLEYMFQ QGIYPGIATHDFRLIEGAYK LIEKFN  
VPKDKFEFQMLYGVTPGLRQSIIDKGFRMRVYVPFGEKWFAYSTRRLKENPRMAQDI IKG  
IFIKG

>Burkholderia Q396J7 Q396J7\_BUR  
MRILNTMAARAIPLVPRSLIRKISRRIIAGETLCDARTRIRALHAAGFRTTVDVLGESAS  
SSEQAESMTREYLNLI DALGAEREPTELS IKLTALGLHLDKDACMTRVAAILQSAAHGI  
NACIDMEDIRFTAKTLDAFSKFADGYAIGIALQAYLKRTSDDLVP LLARKSSMRICKGI  
YAEANEHLVDGASRDRAAINAHFVRHVSTALEAGSFVGIATHDAPLIDVLTGWLQRAQID  
RSRFEFQMLLGVCEPMRDALRAQGFNVRIYVPYQGDWYGYSTRRIKENPRIAGYILAAMV  
RADMR

>Staphylococcus Q8CNU4 Q8CNU4\_S  
MSLFKDDFFIALSNHTYLNKI AKKMGPQMGANRVVAGNTI HQLIETIQYLNNDYNISVTVDS  
LGEFVNTREESIKAKEEILEIIDAIYNNNVKAHMSVKISQLGSEFDLNLAYENMREILLK  
ADKNGKMHINIDTEKYDSLKIQHIIERLKGFEKNGVTVVQAYLYEADDIIDKYPELRLR  
LVKGAYKEDASIAFQSKEEIDANYIRIIKKRLLNSKNFTSVATHDNEIINQVKQFMKENH  
ISKDKMEFQMLYGFRTELSQKIANEGYFFTVYVPYGNDFAYFMRRLAERPQNL SLAIKE  
FTKPKILKKATLGIGIFATLLTSLILGIKRHKK

>Frankia Q2J961 Q2J961\_FRASC Pr  
MIQKLMPPVSRHPLTRALVTRTPLARGIIDRFVAGPSDTDAIAAVAGLADLGLLATVDLL  
GEDITRAQDAADTLLAYLG LLDLADRAGIAAGLDVSVKLSALGQAVPRDGRKLSYENAAE  
LCARAAAANATVTLDMEDHTTTTDTLDTLVELRRDFPFVGA VLQAQLLRTETDCRDLATA  
GSRVRLCKGAYREPSAVAYQGRPAVAAAYARCLGILLTGSGYPMIATHDPALLNLAGRFA  
EHVGRLPATFEYQLLYGVRPGEQRRLASTGATVRVYVPYGADCVPYLTRRLVERPTNLLL  
AARALRSRA

>Mycobacterium Q73WR8 Q73WR8\_MY  
MAGLFAHTLRPAILAAGRRPGLRRAAEALPVTRRVVHRF IAGETIDSALDSVTALRDSGR  
CVSVDHLGEDVSDADDADA AVR VYLELVDR LGCLGDGA AVRPLEVSLKLSALGQSLDRDG  
EKIARENAWAICAAAQRAGVWTVDAEDHTTTTDTLRIVRDLRREFDWLGVALQAYLRRT  
LGDCEEFAAAGARVRLCKGAYDEPASLAYRDPAAVTDSYLRCLRVLMAGSGYPMVASHDP  
AIIEAAPSLARESGRGTGEFEYQMLYGIRDDEQRR LAEAGHTVRVYVPFGTQWYGYFMRR  
LAERPANLTFFLRALAARRH

>Thermobifida Q47SU5 Q47SU5\_THE  
MLRTL LLLLAARSPRCRDFVTRSP LTRGVVRRFVAGDTLDATLPVLRQLTADRHVTVDYLG  
EDITDAEQASRTVDAYTHLLTALGEHGLAPRAEVS VKLSALGLALPRDGAQLALDHARQI  
CAAAEAVGTTVTVDMEDHTTTTDTLTDIVHQLRVDFPRTGAVLQAYLR RTEADCRDLAVPG  
SRVRLCKGAYDEPATVAYRDRAEVDRSYVRCLRILMDGPGYPMVATHDPRLLR IAAFLAR  
SAGRSADSYEQMLYGVRTDLQAALADRGERVRVYVPYGEQWYGYFMRR LAERPANTAFF  
ARALFAGGAVR

>Halobacterium Q9HNG0 Q9HNG0\_HA  
MIPPIANRFVAGETPAEAI EYAADLNDRGVTA I LNLG EHYHERPPAEDAAAYRRLVAD  
VGSDVDACVSVKPSQIGLDVGPEVFAENLETIAAAAADHDVFAWVDMEDHETTDATMDT  
FESLARTHAGNMGLCVQANLKRTEQDLDR LADVPGKVRLVKGAYDEPDDVAYQDKPDVNE  
AYRTHLEFMFREFDDGVAVGSHDPAMISYAAELHEEYGT DYEVQMLMGIREDAQT ELAAT  
GVPTYQYVPYGGKWF SYFYRRAMERKENLVFALRAVLGR

## CHAPTER 3

### Mechanism-Based Inactivation of *Thermus thermophilus*

#### Proline Dehydrogenase by *N*-Propargylglycine

##### **INTRODUCTION**

Mechanism-based enzyme inactivators contain latent functional groups that upon catalysis are transformed into a chemically reactive species (FIGURE 3.1). The reactive species typically becomes covalently bound to the enzyme before being released from the active site, thereby irreversibly inactivating the enzyme (1,2). These inactivators show time-dependent, first order and irreversible loss of enzyme activity, and inactivation is typically diminished in the presence of substrate (1). Mechanism-based inactivators are also known as suicide inhibitors,  $k_{cat}$  inhibitors, suicide enzyme inactivators, and irreversible inhibitors. Mechanism-based inhibitors have proven useful in elucidating catalytic mechanisms for a variety of enzymes (1,2).

*N*-propargylglycine and related compounds have been reported to be mechanism-based inactivators of several enzymes, including flavoenzymes, since the late 1970s. For example, Walsh's group studied inactivation of D- and L-amino acid oxidases, L-alanine transaminase, gamma-cystathioninase, and methionine gamma-lyase by various propargylglycines (3-7). Kraus and Belleau reported mechanism-based inactivation of the flavoenzyme monomeric sarcosine oxidase by *N*-propargylglycine (8). The proposed reaction mechanism included abstraction of the  $\alpha$ -proton from the propargyl group, and consecutive

nucleophilic attack by enzyme (8). These studies also established that proton abstraction was the rate-limiting step of the reaction because of the reduced inactivation rate observed with the deuterated inactivator *N*-( $\alpha,\alpha$ -didueteriopropargyl)glycine. Various substituents added to the propargyl frame have allowed mechanism-based enzyme inactivation of other enzymes. For example, *N,N*-dimethylglycine oxidase is irreversibly inhibited by *N*-methyl-*N*-propargylglycine (1). And several inactivators of the flavoenzyme monoamine oxidase have been developed around the propargyl moiety, including rasagiline (9,10).

Although reversible inhibition of proline dehydrogenases (PRODHs) by compounds such as THFA, L-lactate, and acetate is well documented, there is only one report of mechanism-based inactivation of PRODH. Tritsch, et al, reported that 4-methylene-L-proline (FIGURE 1.2) is a mechanism-based inactivator of PRODH activity in rat liver mitochondrial suspensions (11). It was shown that this compound is oxidized by PRODH with a  $K_m$  of 10 mM. This inactivator showed pseudo-first order kinetics, and PRODH activity was protected upon addition of substrate, L-proline, or L-lactate. The reported Kitz and Wilson kinetic constants were  $K_i = 5$  mM and  $k_{inact} = 0.117 \text{ min}^{-1}$  at 30 °C. A proposed mechanism involves oxidation of the inactivator to  $\Delta^1$ -pyrroline-3-methylene-5-carboxylate and subsequent nucleophilic attack by the enzyme on the electrophilic methylene C atom, yielding the inactivation complex shown in FIGURE 3.2. The identity of the enzyme nucleophile is unknown.

We report here the first structure of a PRODH inactivation complex along

with characterization of inactivation kinetics and spectral changes caused by inactivation. The structure of *Thermus thermophilus* PRODH inactivated by *N*-propargylglycine shows that the  $\epsilon$ -amino group of Lys99 is covalently attached to the FAD N5 atom via a 3-carbon linkage. To our knowledge, this is the first report of this type of an inactivation complex for a flavoenzyme.

## **MATERIALS & METHODS**

### **Crystallization**

*N*-propargylglycine was kindly provided by Prof. Christian Whitman of the University of Texas-Austin. TtPRODH was expressed and purified as previously reported (12). Purified TtPRODH (3 mg/mL) was incubated with a 300 molar excess of *N*-propargylglycine (1mg of protein per 1 mg of inhibitor) for 30 minutes. The inactivated enzyme was pipetted (2  $\mu$ L) into sitting drop crystallization trays, mixed with an equal volume of reservoir solution, sealed with clear tape and placed in an incubator at room temperature. The optimal reservoir consisted of 100 mM imidazole pH = 7, 100 mM MgCl<sub>2</sub>, 14% 2-methyl-2,4-pentanediol and 5 mM fresh dithiothreitol. Thin football shaped crystals formed overnight and had dimensions of 0.4 mm x 0.2 mm x 0.1 mm (FIGURE 3.3). The crystals were pale yellow compared to oxidized TtPRODH crystals, which are vibrant yellow (12). Loss of yellow color implicates of reduction of the FAD. These crystals were cryoprotected with reservoir buffer containing 25% 2-methyl-2,4-pentanediol and inhibitor, picked up with mounting loops, and plunged into N<sub>2</sub> (1).

## X-ray Diffraction Data Collection, Processing, and Refinement

A 1.9 Å data set was collected at the Advanced Light Source Beamline 4.2.2 using a NOIR 1 detector. The data set used for structure determination consisted of 144 images with a crystal to detector distance of 130 mm, oscillation range of 1 degree per frame and exposure time of 20 s/frame. Data collection was performed at an X-ray wavelength of 1.0 Å at -180 °C. Integration and scaling were performed with d\*TREK (13)

The space group is  $P2_12_12_1$ , with unit cell dimensions  $a = 82.3$  Å,  $b = 90.2$  Å,  $c = 94.9$  Å. We note that the structure of oxidized TtPROD<sub>H</sub> was determined from crystals also having space group  $P2_12_12_1$  and similar unit cell lengths ( $a = 82.1$  Å,  $b = 89.6$  Å,  $c = 94.3$  Å (14). Data processing statistics are listed in TABLE 3.1. The data set used for refinement is 99.3% complete and 5.8-fold redundant.

The structure of inactivated TtPROD<sub>H</sub> was determined using molecular replacement as implemented in MOLREP (15). The search model consisted of residues 40-281 of oxidized TtPROD<sub>H</sub>. FAD and active site residues including Lys99 were omitted from the search model. A clear solution was identified with 2 molecules in the asymmetric unit, having a correlation coefficient of 0.644 and R-factor of 0.372. The model from molecular replacement was extended and improved with several rounds of model building in COOT and restrained refinement with TLS in REFMAC5. Ten optimal TLS domains were determined with TLSMD (16). The test set used for R-free calculations was based on the set used previously for refinement of oxidized TtPROD<sub>H</sub> owing to the similarity in the



crystal forms.

Special attention was required to model the modified lysine and reduced FAD. The modified lysine 99 was created using CCP4's monomer library. Lysine was found in the library (LYS.pdb) by searching for amino acids. Using CCP4's monomer sketcher, a 3-carbon modification was drawn on lysine's  $\epsilon$ -amine. The 3-carbon modification contained a double-bond between the  $\epsilon$ -amine and the C1, and another double bond between C2 and C3. Monomer sketcher was then used to create a library description for this molecule, which was named LYX. FAD was found in the CCP4 monomer sketcher library (FAD.pdb), and the isoalloxazine planar restraints were changed by manually editing the cif file. One planar restraint group contained the atoms in the pyrimidine portion of the isoalloxazine. The other planar restraint group contained the atoms in the dimethylbenzene portion of the isoalloxazine. Atoms N5 and N10 of the isoalloxazine were not contained in the planar restraints. The planar restraints for the adenine portion of FAD were left unchanged. This molecule was named FDH, and a library description was created using the monomer sketcher.

### **Kinetic and Spectroscopic Characterizations**

Inactivation parameters were determined using the Kitz and Wilson approach (17). The assay used for this study was the DCPIP-based assay described previously (14,18). Samples of TtPRODH (0.3 mg/mL) were incubated at 25°C with 0.5 mM, 1.0 mM, 2.5 mM, and 5.0 mM *N*-propargylglycine. Aliquots were removed at various time points over 30 minutes and assayed immediately with a constant proline concentration of 50 mM to determine remaining activity.

The initial linear parts of the Kitz and Wilson plot were used in the replot analysis. Using Origin 7.0, the normalized data were plotted and fit globally sharing parameters A and  $Y_0$  with the exponential decay equation

$$Y = Y_0 + Ae^{-x/t}$$

The half-lives were determined by calculating  $t$  and multiplying  $t$  by 0.693. The half-lives were plotted versus inverse of the *N*-propargylglycine concentrations to make the Kitz and Wilson Replot. The data in the replot were fit linearly and inactivation parameters,  $K_I$  and  $k_{inact}$ , were calculated from the equation of the line.

Absorption spectra of the bound FAD cofactor were acquired with a Cary 100 spectrophotometer. Spectral changes caused by inactivation were examined as follows. TtPROD<sub>H</sub> was added to a quartz cuvette at 0.2 mg/mL and spectra were acquired at 25 °C in the wavelength range 300–600 nm. A quartz cuvette with buffer was used as the reference. Inhibitor was added to a final concentration of 500  $\mu$ M, the solution was mixed and spectra were obtained every 30 s for 60 min.

An additional set of experiments was performed at 4 °C for use in estimating inactivation constants. For this study, the decrease in absorbance at 452 nm was monitored with *N*-propargylglycine present at 5–10 mM and an enzyme concentration of 0.25 mg/mL.

### **Mass Spectrometry**

TtPRODHD was dialyzed overnight into 100 mM ammonium acetate, and then inactivator was added at a 300 molar excess. The inactivated enzyme was analyzed using Nanospray QqTOF mass spectrometry by the University of Missouri Proteomics Core.

## **RESULTS**

### **Structure of TtPRODHD inactivated by *N*-propargylglycine**

Inactivation of the enzyme caused no noticeable change in the global structure of TtPRODHD (FIGURE 3.4 and FIGURE 3.5). Two major changes, however, were observed in the active site. First, electron density maps clearly indicated that the FAD isoalloxazine was no longer planar, as in the oxidized enzyme, but rather it appeared highly bent with the ring system bowed toward the proline binding pocket. Second, it was apparent that Lys99 had been covalently modified at the  $\epsilon$ -amino group. Electron density could be seen connecting the  $\epsilon$ -amino of Lys99 with the N5 atom of the isoalloxazine, suggesting that the two were linked by a covalent connection. These features were present in both TtPRODHD molecules in the asymmetric unit. A model consistent with these electron density features was built and refined.

The final refined structure shows that the FAD isoalloxazine is bent along the N5-N10 axis (FIGURES 3.6-3.9). This type of distortion from planarity is known as butterfly bending (19). The butterfly angle of inactivated TtPRODHD is approximately 25°. The planar isoalloxazine conformation is typically associated with the oxidized state of the flavin, whereas highly nonplanar isoalloxazine

conformations indicate reduced states. The butterfly angle of 25° observed here is rather large for flavoenzymes, and it suggests that the FAD of inactivated TtPRODHD is reduced.

Electron density between Lys99 and the FAD N5 was modeled as a 3-carbon covalent linkage that connects the  $\epsilon$ -amino group of Lys99 with the FAD N5 (FIGURE 3.6). The model is consistent with mass spectral data. Native TtPRODHD had a molecular mass of 37976 Da, which corresponds to the protein without FAD (FIGURE 3.10). The inactivated enzyme showed two mass spectral peaks, one at 37976 Da and another at 39797 Da (FIGURE 3.11), with the latter peak presumably representing the inactivated enzyme. The difference in mass between the apo and inactivated enzyme is 821 Da, which is approximately equal to the sum of the masses of reduced FAD (FADH<sup>-</sup>, 787 Da) and the modeled 3-carbon linker =CH-CH=CH- (39 Da).

Aside from the butterfly bend and covalent modification of N5, the conformation of the cofactor is identical to that of the oxidized enzyme. We do, however, observe that the cofactor shifts slightly in the active site toward Lys99 as shown in FIGURE 3.5.

Inactivation also causes conformational changes in active site residues other than Lys99 (FIGURE 3.12). Most notable is the movement of Arg184. In the oxidized enzyme, the guanidinium group of Arg184 donates a hydrogen bond to the flavin N5 (3.2 Å). This residue is universally conserved throughout the entire PRODHD family as discussed in Chapter 2 and in White, et al. (14). The Arg-N5 hydrogen bond is also present in PutA PRODHD domain structures

(20,21). Inactivation of TtPRODHD causes the guanidinium to move away from the flavin, so that closest distance between the Arg guanidinium and FAD N5 is 3.9 Å. Rupture of this hydrogen bond is consistent with the transfer of hydride to the FAD so that N5 is protonated.

Other changes are also observed in the active site. The hydrogen-bonding pair Asp133-Tyr275, which forms the ceiling of the active site, moves 0.5 Å away from the active site. This movement is probably due to steric clash with the flavin's dimethylbenzene, which has shifted toward Lys99. Also, movements of up to 0.4 Å are observed in the loop between  $\beta$ -strand 5. This loop movement starts at Tyr190 and ends at Lys201. Similar movements are present in chain B, although they are not as large. Lastly, we see movement of helix 8 away from the active site. Helix 8 contains conserved Arg residues that orient carboxylate-containing ligands, such as the substrate proline, in the active site (21). Helix 8 containing completely conserved Arg288 and Arg289 has much weaker density than the rest of the barrel. As compared to the oxidized structure, this helix in the inactivated structure moves away slightly from the active site. The B-factors and deviation from the oxidized structure both increase proceeding along the helix, reaching  $B = 50 \text{ Å}^2$  and 0.5 Å deviation at Arg289. With the exception of Arg288, this trend is also present in chain A although the deviations are not as large comparing oxidized and inactivated enzymes. In chain A, Arg288 has moved out of the active site and forms hydrogen bonds with Thr287. In chain B, Arg288 is oriented toward the active site, as seen in oxidized TtPRODHD.

A strong electron density feature that could not be assigned to the protein

or the modified cofactor was observed in the active site. As discussed below, our proposed mechanism predicts that glycine is a byproduct of the inactivation reaction. Thus, we considered the possibility that this electron density feature represents a bound glycine molecule. Although the inhibition constant for glycine has not yet been determined, initial assays show that glycine is an inhibitor. A glycine molecule was modeled into this density feature, but the average B-factor refined to the unacceptably high value of  $74 \text{ \AA}^2$  (FIGURE 3.13). We note that the surrounding residues have B-factors in the range 40-50  $\text{\AA}^2$ . Moreover, there are no hydrogen-bonding partners nearby, with the closest interactions occurring with Tyr190 at 4.8  $\text{\AA}$ , Y285 at 4.8  $\text{\AA}$ , isoalloxazine at 4.61  $\text{\AA}$  and R289 at 3.9  $\text{\AA}$ . Based on this information, it is likely that the occupancy of glycine in the active site is low or that this feature represents other bound solvent species such as water. Given these results, this electron density feature was left unmodeled.

### **Spectral changes caused by inactivation**

Oxidized TtPRODH showed a characteristic flavin absorption spectra with maxima at 452 nm and 381 nm (FIGURE 3.14). The spectrum changed significantly upon addition of *N*-propargylglycine. The peak at 452 nm disappears over time to baseline, which is similar to what was previously seen with electropotentiometric and proline titrations of TtPRODH. The peak at 381 nm first decreases and then gradually increases throughout the duration of the experiment. Note that the peak at 381 nm not only increases, but also shifts to a longer wavelength of 386 nm.

The absorbance values for  $\lambda = 382 \text{ nm}$  and 452 nm are plotted as functions

of time in FIGURE 3.15. We see that the rate of decrease of  $A_{452}$  is much faster than the rate of appearance of  $A_{382}$ . This indicates that the two spectral features are monitoring different steps of the inactivation reaction. The consistent decrease of  $A_{452}$  is very similar to the behavior observed during potentiometric and proline titrations of TtPRODH, which suggests that the cofactor is reduced during inactivation of the enzyme. In contrast, an increase in absorbance in the range  $\lambda=380-386$  is not observed during potentiometric and proline titrations of TtPRODH. This suggests that the spectral feature in this region arises from a new flavin species that is formed during inactivation. This new species is presumably the covalently modified FAD described in the previous section.

The reductant sodium dithionite was added after 60 minutes of incubation of the enzyme with *N*-propargylglycine. As shown in FIGURE 3.16, the strong absorbance at 386 nm remains, and there is no further decrease in absorbance near 452 nm. These results suggest that the cofactor is in an irreversibly reduced state, which is consistent with the bent flavin and covalent modification observed by crystallography.

### **Kinetics of inactivation**

Before describing our results, we present a brief summary of the kinetic framework used for analyzing mechanism-based inactivators because it differs somewhat from that used to analyze reversible inhibitors. Two kinetic constants describing rates of inactivation can be obtained for the mechanism-based inactivators (22). Referring to FIGURE 3.1, the inhibition constant,  $K_i$ , is the ratio of  $k_{-1}/k_1$ , when  $k_2$  is rate-limiting. The second kinetic constant,  $k_{\text{inact}}$ , is more

complex and comprises rate constants  $k_2$ ,  $k_3$  and  $k_4$ . Step 2 ( $k_2$ ) is most often the rate-limiting step, and assuming infinite concentration of inactivator the expression for  $k_{\text{inact}}$  is

$$k_{\text{inact}} = (k_2 * k_4) / (k_3 + k_4)$$

The rate constant of inactivation is sometimes incorrectly referred to as  $k_2$ . The rate constant  $k_3$  describes the escape of the inactivator from active site before covalent modification.  $k_4$  describes conversion of the inactivating species to the final inactivated enzyme.  $k_3$  and  $k_4$  are related by the partition ratio which describes the released product per inactivation event and is defined by  $k_3 / k_4$ .

To determine these kinetic constants,  $K_i$  and  $k_{\text{inact}}$ , one ideally utilizes a continuous assay. Enzyme and various concentrations of inactivator are incubated together. Aliquots are removed at various time points and assayed with substrate. The log of the percent of remaining enzyme activity is plotted versus time, a so-called Kitz and Wilson Plot (FIGURE 3.17) (17). Half-lives of inactivation are determined from the Kitz and Wilson plot for each value of the inactivator concentration, and these half-lives are plotted versus the inverse of inactivator concentration. The resulting plot is known as the Kitz and Wilson Replot and the curve, in theory, should be linear as shown in FIGURE 3.18.

The kinetics of inactivation for TtPRODHD was studied using a dye-coupled continuous activity assay. The Kitz and Wilson plot is shown in FIGURE 3.19. Interestingly, the initial parts of the curves are linear but the inactivation rate



flattens out at longer time, indicating a departure from pseudo first-order kinetics. This phenomenon, called non-pseudo first-order kinetics, can occur for various reasons, including high partition ratio ( $k_3/k_4$  or escape vs. turnover) and generation of a secondary metabolite that binds to the active site (23). In the present case, the second explanation may be reasonable because, as discussed below, *N*-propargylglycine is oxidized by TtPROD<sub>H</sub> and subsequently hydrolyzed to two metabolites, propynal and glycine. Moreover, electron density maps suggested that glycine may be bound in the active site, albeit weakly (FIGURE 3.13).

The inactivation constants estimated with these data are  $K_i = 838 \mu\text{M}$  and  $k_{\text{inact}} = 0.3 \text{ min}^{-1}$  (FIGURE 3.19). These data agree with the previously determined kinetic parameters determined with 4-methylene-L-proline using rat liver PROD<sub>H</sub> at 30°C (11). Spectroscopic data were also used to estimate inactivation constants. Kitz and Wilson plot and replot were also obtained when using  $A_{452}$  to follow the reaction (FIGURE 3.20). These data were collected at 4°C in order to slow the inactivation rate. This analysis resulted in estimated inactivation constants of  $K_i = 206 \text{ mM}$  and  $k_{\text{inact}} = 6.6 \text{ min}^{-1}$ .

## **DISCUSSION**

### **Inactivation of monoamine oxidase by propargylglycine compounds**

Maycock and colleagues performed pioneering studies of inactivation of monoamine oxidase (MAO) by propargyl-based compounds. This work has inspired our thinking about the mechanism of inactivation of TtPROD<sub>H</sub> by *N*-

propargylglycine, we briefly summarize their results in this section.

MAO is a tightly bound outer mitochondrial membrane enzyme that oxidizes biogenic amines to their corresponding imines (24). Two isoforms, A and B, have been characterized. The different isoforms are localized together in some organs like liver, although only MAO A is found in placenta, and only MAO B is found in platelets (25). MAO plays roles in metabolism of neurotransmitters, like dopamine and serotonin, and is a target for treatment of depression, dementia, and early stages of Parkinson's disease. MAO inhibitors are currently used for treatments of various neurological disorders.

Maycock and Abeles studied inactivation of MAO by propargyl-containing compounds such as dimethylpropargylamine (1,26). Upon flavoenzyme catalysis of a mechanism-based inactivator, the flavin itself becomes modified (FIGURE 3.21). Based on the chemical and spectral properties of the isolated flavin-adduct (27), Maycock determined that flavin N5 was modified and proposed three likely reaction mechanisms (27). The proposed reaction mechanisms included carbanion formation, radical pair complex, or Michael addition of flavin nucleophile to the acetylenic moiety (FIGURE 3.22).

In the carbanion-based mechanism, the enzyme catalyzes the removal of the  $\alpha$ -proton from the inactivator to yield carbanion (1,27) (FIGURE 3.22B), which can subsequently react with the oxidized flavin N5 to form a modified flavin (1,27). In this proposed mechanism, a reduced inactivator reacts with an oxidized flavin (27). The most likely scenario for this reaction mechanism to occur is using  $\alpha$ -amino or  $\alpha$ -hydroxy acids where an activating group is adjacent to the site of

proton removal (27).

The radical pair-based mechanism involves reaction of a partially reduced flavin and partially oxidized inactivator (27) (FIGURE 3.22C). The enzyme could catalyze the removal of the  $\alpha$ -proton to the flavin or could catalyze electron transfer from an initially formed substrate carbanion to the oxidized flavin. Radical pair collapse and subsequent protonation leads to formation of the adduct (27).

Complete oxidation of the inactivator generates reduced flavin and the highly reactive species dimethylpropargylimine (27) (FIGURE 3.22D). Upon Michael addition, a reduced flavin would be reacting with an oxidized inactivator. The reduced flavin has been shown to act as a nucleophile, utilizing both the N5 and C4a positions to perform this reaction (27). Williams studied free dihydrolumiflavin and its anionic N1 form on reactions with various carbonyl-containing pyruvate derivatives and found that indeed, reduced flavin could act as a nucleophile occurring by the proposed carbanion mechanism (28). Confirmation of a nucleophilic enzyme-bound flavin was demonstrated in UDP-galactopyranose mutase (29). Addition of the reduced flavin N5 across the  $\gamma$ -carbon acetylene of dimethylpropargylimine by Michael addition would give rise to the monoamine oxidase flavin adduct that Maycock isolated (27) (FIGURE 3.21D).

Crystal structures have been determined for MAO inactivated by propargyl-containing compounds have been determined (PDBIDs 2C64, 2C65, 2C66 1S2Q, 1S2Y, 1S3B, 1S3E) (9,10,30)). These studies are important because they

definitively established the structure of the flavin adduct of the inactivated enzyme. Significantly, the structures for the enzyme inactivated by rasagiline reveals that the flavin is modified at the isoalloxazine N5 position, as in TtPRODH (FIGURE 3.23).

### **Proposed mechanism of inactivation of TtPRODH by *N*-propargylglycine**

The structural, spectroscopic and mass spectral data presented here shows that the cofactor of TtPRODH is reduced and that the flavin N5 is covalently attached to the  $\epsilon$ -amino group of Lys99 by a 3-carbon linkage. The mechanism proposed in FIGURES 3.24-3.26 is consistent with these data and previous studies of MAO inactivation by propargyl compounds.

In the first step of the proposed mechanism, *N*-propargylglycine is oxidized to *N*-propargyliminoglycine with concomitant reduction of FAD. In step 2, *N*-propargyliminoglycine is nonenzymatically hydrolyzed to propynal and glycine. Note that these two steps are analogous to oxidation of the substrate proline to glutamic semialdehyde. The third and fourth steps are (3) formation of a Schiff base between Lys99 and the propynal aldehyde group and (4) Michael addition of the reduced flavin to the acetylene group.

Considering the reaction of propynal with Lys99, the general reaction for typical Schiff base formation involves attack of a lone pair from the  $\epsilon$ -amino of lysine at an aldehyde or ketone group (FIGURE 3.27). A carbinolamine intermediate is formed, and finally the imine is produced with the exclusion of water. Lys99 must be in the neutral ionization state ( $-\text{NH}_2$ ) to form a Schiff base. The  $\text{pK}_a$  of Lys is typically 10-11 (depending on reference used), we expect that

Lys99 to be positively charged at the pH used in these studies (pH=8). The structure of oxidized, uninhibited TtPRODHD shows that Lys99 forms hydrogen bonds with water molecules in the active site. Structures of the *E. coli* PutA PRODHD domain complexed with reversible inhibitors show that Lys99 interacts with the carboxyl groups of Asp370 (3.1 Å) and the inhibitor (2.7 Å). Based on the inhibited EcPutA PRODHD, it appears that a general base is required for deprotonation of Lys99 during inactivation by *N*-propargylglycine. The identity of this base is unknown, but possible candidates are Asp133 or Glu135.

It is proposed that the cofactor is in a reduced state, based on the bleaching of the crystal, decrease of absorbance at 425 nm, and large butterfly bending of the isoalloxazine. In other flavoenzymes, isoalloxazine bending is associated with reduction (19,31). This bending is due to a change in hybridization of N5 from  $sp^2$  to  $sp^3$  upon reduction. The isoalloxazine is planar in structures of oxidized TtPRODHD and the PutA PRODHD domain. The recent structure of the *E. coli* PutA PRODHD domain reduced by dithionite shows that reduction of the flavin induces a butterfly angle of  $22^\circ$  (31), which is similar to the isoalloxazine of inactivated TtPRODHD (FIGURE 3.28). Comparing the isoalloxazines of inactivated TtPRODHD and reduced PutA PRODHD reveals a similar butterfly conformation, but the ring system of reduced PutA is more symmetric than that of TtPRODHD due to twisting of the isoalloxazine in inactivated TtPRODHD (FIGURE 3.28 and FIGURE 3.29). The asymmetry in inactivated TtPRODHD presumably results from strain due to covalent linkage to Lys99.

Following Maycock's work, we propose that the reduced FAD attacks the

acetylene group of the hydrolyzed inhibitor. Previous reports of nucleophilic flavins suggest that the flavin is most likely in the anionic form ( $\text{FADH}^-$ ), with a negative charge on N1. Negative charge on N1 enhances nucleophilicity of N5 by increasing the electron density in the isoalloxazine (29). Soltero-Higgin measured the  $\text{pK}_a$  of anionic flavin using fluorescence, and the value of 6.7 indicates that a majority of the flavin is in the anionic form at physiological pH (29). In addition, the ribityl 2'-OH of TtPRODHDH is positioned to donate a hydrogen bond to the N1, which may further stabilize the anionic reduced FAD.

As described in the previous section, Maycock envisioned three possible mechanisms by which propynal reacts with the FAD: carbanion formation, radical pair complex, or Michael addition of nucleophile across the acetylenic moiety (27). A radical mechanism is the least likely scenario for TtPRODHDH inactivation because no stabilization of flavin semiquinone was observed under potentiometric titrations (14). Furthermore, sulfite reactivity, an indicator of radical formation, was not observed (14). The carbanion mechanism is more likely, since this reaction is favored for  $\alpha$ -amino acids due to the activating group next to the site of proton abstraction (1). The activating group is normally a carbonyl or carboxylate, but in the case of proline and *N*-propargylglycine, the carboxylate is 3-4 atoms away. Most carbanions need stabilization from an electronegative group, such as amino acid residue like glutamate and aspartate. In the active site, Asp133 is close to the site of proton abstraction. Based on the available data, we favor Michael addition of the anionic flavin N5 to propynal  $\gamma$ -carbon. Nucleophilic flavins have been investigated in free solution and

proposed for flavoenzymes (27,32). Soltero-Higgin, et al. reported convincingly that UDP-galactopyranose mutase utilizes a nucleophilic FADH<sup>-</sup> (29). Also, the imine formed by the Schiff base reaction is highly reactive and a good Michael acceptor.

### **Comparison to structures of other inactivated flavoenzymes**

Mechanism-based inactivation has been observed for numerous flavoenzymes (33). These include monoamine oxidase, monomeric sarcosine oxidase, dimethylglycine oxidase, lactate dehydrogenase and cytochrome c (1). Inactivators that have been used include *N*-propargylglycine, dimethylpropargylamine amine, vinylglycine, 2-hydroxy-3-butynoate and rasagiline. Interestingly, X-ray crystallographic data is sparse for these mechanism-based inactivated covalently-modified flavins. Binda, et al. determined structures of inactivated monoamine oxidase A and B with various propargyl inactivators, such as rasagiline(9,10). The flavin is modified at the N5 atom as in *N*-propargylglycine inactivated TtPRODH (FIGURE 3.23). The structure reported here is different from rasagiline-inactivated MAO in that the FAD is covalently connected to a protein side chain. To our knowledge, this is the first report of such a modified flavoenzyme.

### **Potential applications of mechanism-based inactivators of PRODH**

#### *Stress response*

Organisms accumulate proline in response to various stresses, including oxidative stress. Since PRODH degrades proline, specific mechanism-based inactivators of PRODH could enhance protection by proline. Plants, for example,

accumulate proline in response to extreme temperatures, salinity, drought, and heavy metals such as Cd, Cu, Zn (34-38). Proline concentrations as high as 1 M have been measured in plant tissues subjected to osmotic stress due to high salinity (34). Yeast and fungi also utilize proline accumulation upon exposure to stress (39).

The basis for protection is that proline can serve as an osmolyte, radical scavenger, electron sink, macromolecule stabilizer and component of cell walls (34). As an osmolyte, proline has been shown to prevent freezing by stabilizing membranes (40). Proline binds to head groups of membrane phospholipids, replacing water and preventing cell shrinkage upon freezing (41). As an antioxidant, proline scavenges reactive oxygen species like hydroxyl radical (42). It has been proposed that the hydroxyl radical either removes a proton from proline on the C5 to form water or can react to form proline-nitroxyl radical (43,44). Proline has also been shown to quench singlet oxygen ( $^1\text{O}_2$ ) by forming an electron charge-transfer complex (45).

#### *Pesticide Development*

Proline is a major fuel for the flight muscles in *Glossinia morsitans* (46). *Glossinia* is a major vector for transmission of parasitic African trypanosomes, which cause trypanosomiasis (African Sleeping Sickness) and Chagas disease. Upon uptake by *Glossinia*, trypanosomes utilize L-proline as the respiratory substrate (47). If proline is the major fuel for *Glossinia* during flight and is important for trypanosome respiration, PRODHs from these organisms are attractive targets for pesticide and anti-trypanosome development. In fact, the



only other reported mechanism-based inactivator of PRODH, 4-methylene-L-proline, and was lethal to *Glossinia* within 12 hours at a concentration of 250 µg, although flight was not impaired (11).

#### *Manipulation of proline catabolism in eukaryotic cells*

Specific mechanism-based inactivators of human PRODH may be useful reagents for modulating PRODH activity in eukaryotic cells. One potential application is the study of the function of PRODH in cancer and apoptosis. As discussed in the introduction to this thesis, PRODH (specifically PRODH2) is a pro-apoptotic protein that helps reduce carcinogenesis in humans by serving as a superoxide generator. The PRODH2 gene is induced by the cell proliferation regulator p53. Many cancers are due to mutations in p53, or inactivation of p53-mediated apoptosis. More than half of colorectal cancer cell lines show inactivation of p53. Overexpression of PRODH (also called proline oxidase or POX in this context) in colorectal cancer cell lines and various carcinomas induces p53-mediated apoptosis (48-51). The mechanism by which this happens is currently being investigated, although there is evidence it happens by both intrinsic and extrinsic pathways (52). Further research shows that PRODH induces apoptosis in a proline-dependent manner by superoxide generation, even without utilizing p53-mediated pathways (48). This is currently being investigated as a potential cancer treatment, although it is unclear whether proline-dependent superoxide generation is specific to cancerous cells. Mechanism-based inhibitors of human PRODH offer an alternative to gene inactivation and RNAi for studying the connection between proline metabolism

and apoptosis in the setting of cancer cells.

*Biophysical and structural studies of reduced PRODH and PutA*

Mechanism-based inactivators of PRODH lock the enzyme in the reduced state under aerobic conditions. Thus, these inactivators could prove useful for biophysical and structural studies of PRODHs and PutAs because the reduced enzyme can be studied outside of an anaerobic chamber. Potential uses include crystallization, NMR and ligand binding studies. This should be especially useful for PutAs, which are thought to exhibit large conformational changes upon reduction of the FAD.

## REFERENCES

1. Maycock, A. L. (1980) *Methods Enzymol* **66**, 294-302
2. Bugg, T. D. (2001) *Nat Prod Rep* **18**, 465-493
3. Marcotte, P., and Walsh, C. (1976) *Biochemistry* **15**, 3070-3076
4. Soper, T. S., Manning, J. M., Marcotte, P. A., and Walsh, C. T. (1977) *J Biol Chem* **252**, 1571-1575
5. Abeles, R. H., and Walsh, C. T. (1973) *J Am Chem Soc* **95**, 6124-6125
6. Johnston, M., Jankowski, D., Marcotte, P., Tanaka, H., Esaki, N., Soda, K., and Walsh, C. (1979) *Biochemistry* **18**, 4690-4701
7. Johnston, M., Marcotte, P., Donovan, J., and Walsh, C. (1979) *Biochemistry* **18**, 1729-1738
8. Kraus, J.-L., and Belleau, B. (1975) *Canadian Journal of Chemistry* **53**
9. Binda, C., Hubalek, F., Li, M., Herzig, Y., Sterling, J., Edmondson, D. E., and Mattevi, A. (2004) *J Med Chem* **47**, 1767-1774
10. Binda, C., Hubalek, F., Li, M., Herzig, Y., Sterling, J., Edmondson, D. E., and Mattevi, A. (2005) *J Med Chem* **48**, 8148-8154
11. Tritsch, D., Mawlawi, H., and Biellmann, J. F. (1993) *Biochim Biophys Acta* **1202**, 77-81
12. White, T. A., and Tanner, J. J. (2005) *Acta Crystallography* **F61**, 737-739
13. Pflugrath, J. (1999) *Acta Crystallography* **D55**, 1718-1725
14. White, T. A., Krishnan, N., Becker, D. F., and Tanner, J. J. (2007) *J Biol Chem*
15. Vagin, A., and Teplyakov, A. (1997) *Journal of Applied Crystallography* **30**, 1022-1025
16. Painter, J., and Merritt, E. A. (2006) *Acta Crystallogr D Biol Crystallogr* **62**, 439-450
17. Kitz, R., and Wilson, I. B. (1962) *J Biol Chem* **237**, 3245-3249
18. Abrahamson, J., Baker, L., Stephenson, J., and Wood, J. (1983) *European Journal of Biochemistry* **134**, 77-82
19. Lennon, B. W., Williams, C. H., Jr., and Ludwig, M. L. (1999) *Protein Sci* **8**, 2366-2379
20. Lee, Y. H., Nadaraia, S., Gu, D., Becker, D. F., and Tanner, J. J. (2003) *Nature Structural Biology* **10**, 109-114
21. Zhang, M., White, T. A., Schuermann, J., Baban, B. A., Becker, D. F., and Tanner, J. J. (2004) *Biochemistry* **43**
22. Silverman, R. B. (1988) *J Enzyme Inhib* **2**, 73-90
23. Silverman, R. B. (1995) *Methods Enzymol* **249**, 240-283
24. Silverman, R. B. (2002) *The Organic Chemistry of Enzyme-Catalyzed Reactions*, Revised Ed., Academic Press
25. Muller, F. (2000) *Chemistry and Biochemistry of Flavoenzymes* (CRC, Ed.), CRC Press
26. Abeles, R. H., and Maycock, A. L. (1976) *Accounts of Chemical Research* **9**, 313-319
27. Maycock, A. L., Abeles, R. H., Salach, J. I., and Singer, T. P. (1976) *Biochemistry* **15**, 114-125

28. Williams, R. F., and Bruice, T. C. (1976) *J Am Chem Soc* **98**, 7752-7767
29. Soltero-Higgin, M., Carlson, E. E., Gruber, T. D., and Kiessling, L. L. (2004) *Nat Struct Mol Biol* **11**, 539-543
30. Binda, C., Li, M., Hubalek, F., Restelli, N., Edmondson, D. E., and Mattevi, A. (2003) *Proc Natl Acad Sci U S A* **100**, 9750-9755
31. Zhang, W., Zhang, M., Zhu, W., Zhou, Y., Wanduragala, S., Rewinkel, D., Tanner, J. J., and Becker, D. F. (2007) *Biochemistry* **46**, 483-491
32. Ghisla, S., Hartmann, U., Hemmerich, P., and Muller, F. (1973) *Justus Liebegs Ann. Chem*, 1338
33. Abeles, R. H., and Tashjian, A. H., Jr. (1974) *Biochem Pharmacol* **23**, 2205-2207
34. Sharma, S. S., and Dietz, K. J. (2006) *J Exp Bot* **57**, 711-726
35. Aspinall, D., and Paleg, L. G. (1981) in *The physiology and biochemistry of drought resistance in plants*, pp. 205-240, Australia
36. Ashraf, M., and Harris, P. J. C. (2003) *Plant Science* **166**, 3-16
37. Naidu, B. P., Paleg, L. G., Aspinall, D., Jennings, A. C., and Jones, G. P. (1991) *Phytochemistry* **30**, 407-409
38. Schat, H., Sharma, S. S., and Vooijs, R. (1997) *Physiologia Plantarum* **101**, 477-482
39. Chen, C., and Dickman, M. B. (2005) *Proc Natl Acad Sci U S A* **102**, 3459-3464
40. Yancey, P. H. (2005) *J Exp Biol* **208**, 2819-2830
41. Rudolph, A. S., and Crowe, J. H. (1985) *Cryobiology* **22**, 367-377
42. Smirnoff, N., and Cumbes, Q. (1989) *Phytochemistry* **29**, 1057-1060
43. Rutgsi, S., Joshi, A., Moss, H., and Riesz, P. (1977) *International Journal of Radiation Biology and Related Studies of Physics, Chemistry and Medicine* **31**, 415-440
44. Floyd, R. A., and Nagy, Z. S. (1984) *Biochemica et Biophysica Acta* **790**, 94-97
45. Alia, Mohanty, P., and Matysik, J. (2001) *Amino Acids* **21**, 195-200
46. Bursell, E. (1963) *Bull World Health Organ* **28**, 703-709
47. Vickerman, K., Tetley, L., Hendry, K. A. K., and Turner, M. R. (1988) *Biology of the Cell* **64**, 109-119
48. Donald, S. P., Sun, X. Y., Hu, C. A., Yu, J., Mei, J. M., Valle, D., and Phang, J. M. (2001) *Cancer Res* **61**, 1810-1815
49. Maxwell, S. A., and Rivera, A. (2003) *J Biol Chem* **278**, 9784-9789
50. Rivera, A., and Maxwell, S. A. (2005) *J Biol Chem* **280**, 29346-29354
51. Maxwell, S. A., and Davis, G. E. (2000) *PNAS* **97**, 13009-13014
52. Liu, Y., Borchert, G. L., Surazynski, A., Hu, C. A., and Phang, J. M. (2006) *Oncogene* **25**, 5640-5647

FIGURE 3.1. Kinetic scheme for mechanism-based enzyme inactivation.

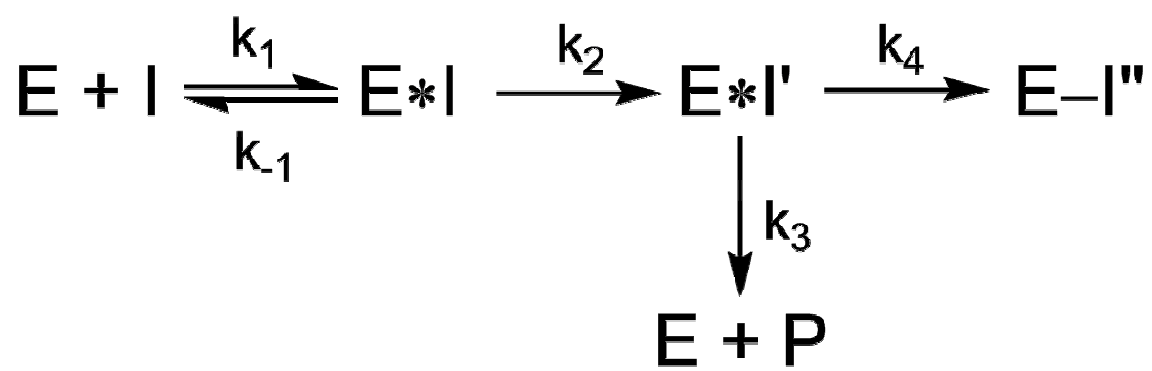


FIGURE 3.2. Proposed action of PRODH mechanism-based inactivator, 4-methylene-L-proline (adapted from Tritsch, 1993).

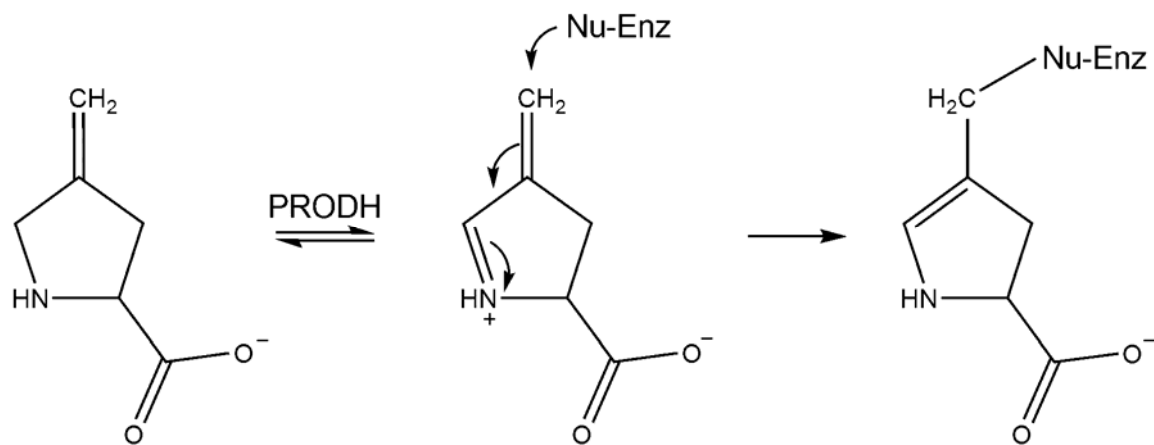


FIGURE 3.3. Crystals of *Thermus thermophilus* proline dehydrogenase inactivated by *N*-propargylglycine.



FIGURE 3.4. *Thermus thermophilus* proline dehydrogenase monomer inactivated with *N*-propargylglycine. The  $(\beta\alpha)_8$  barrel is shown in cartoon rainbow coloring, covalently-modified flavin adenine dinucleotide is shown in white CPK sticks.





FIGURE 3.5. Superposition of oxidized TtPROD<sub>H</sub> (white) and *N*-propargylglycine inactivated TtPROD<sub>H</sub> (rainbow). Oxidized FAD is shown in white sticks and inactivated TtPROD<sub>H</sub> flavocyanine shown in green sticks.

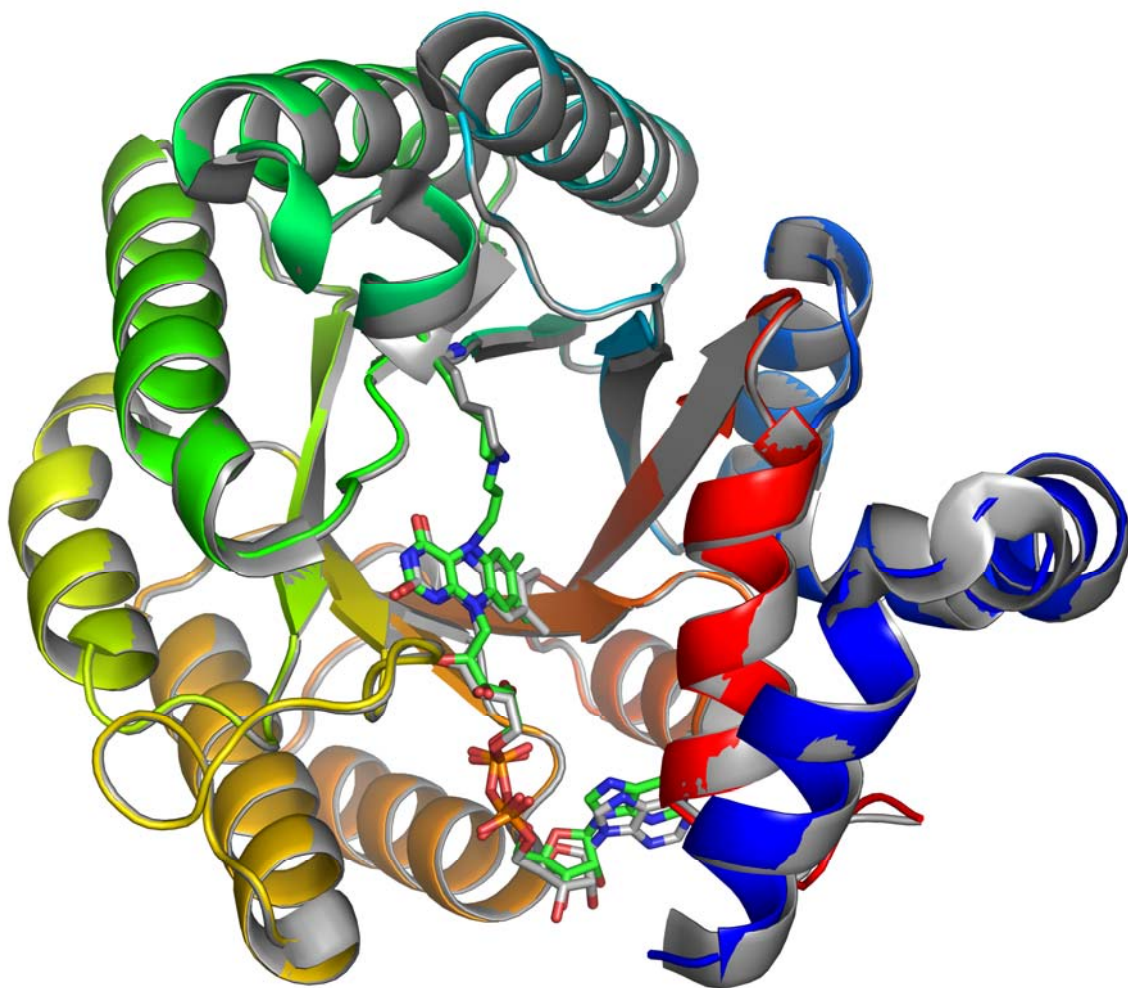


FIGURE 3.6. Two views of the modified flavin of inactivated TtPROD<sub>H</sub> (chain A) covered by an electron density map ( $2.5\ \sigma$ ). The map is a simulated annealing  $F_o - F_c$  omit map using. The modified lysine is shown in cyan sticks and the flavin shown in yellow sticks.

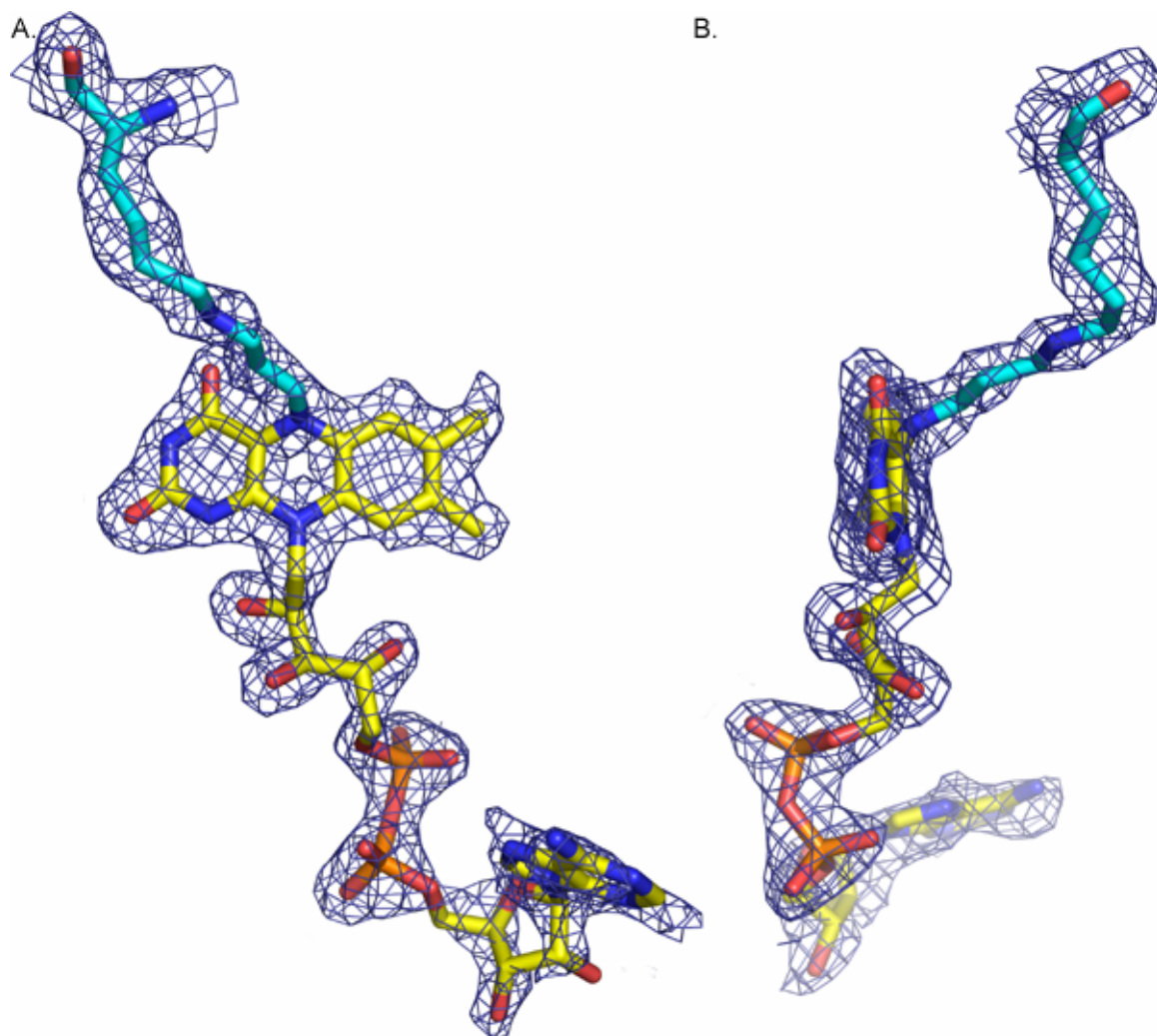


FIGURE 3.7. Side view of the *N*-propargylglycine-inactivated flavin of TtPRODH. FAD is shown in yellow, Lys99 in green.

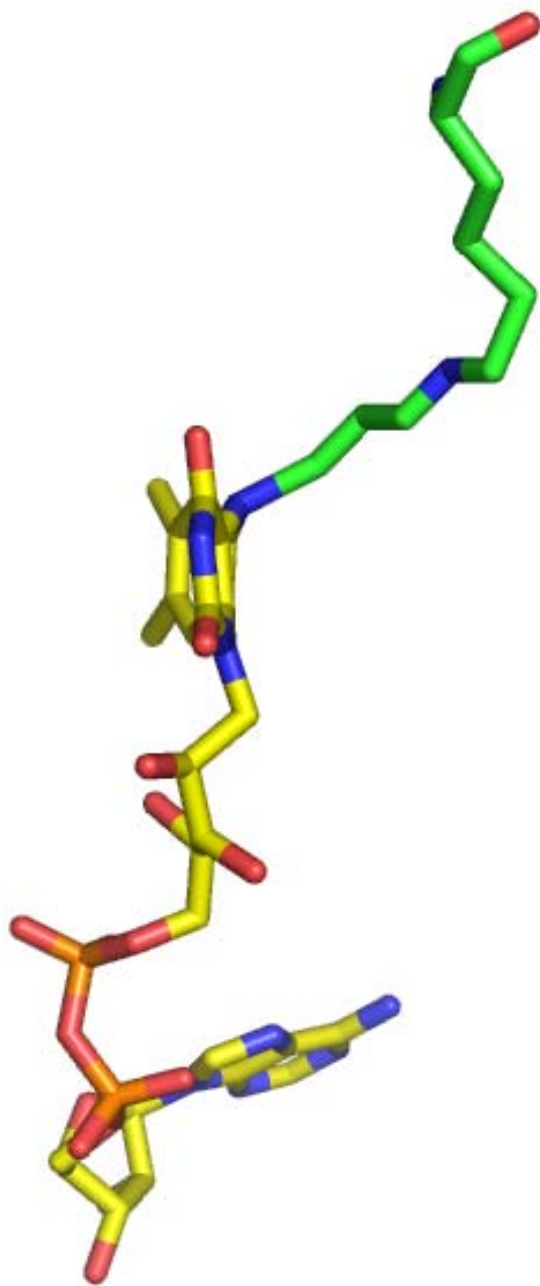


FIGURE 3.8. Views of the FAD isoalloxazine from TtPRODHS. A) isoalloxazine of *N*-propargylglycine inactivated TtPRODHD B) isoalloxazine of inactivated TtPRODHD with electron density from a simulated annealing  $F_o - F_c$  omit map ( $2.5 \sigma$ ). The isoalloxazine is oriented so that the plane of the dimethyl benzene ring is perpendicular to the page, which allows one to see the twisting of the isoalloxazine. C) Same as in (B) but the isoalloxazine is oriented so that the plane of the pyrimidine ring is perpendicular to the page. D) Superposition of isoalloxazines from oxidized (magenta) and inactivated (yellow) TtPRODHDs.

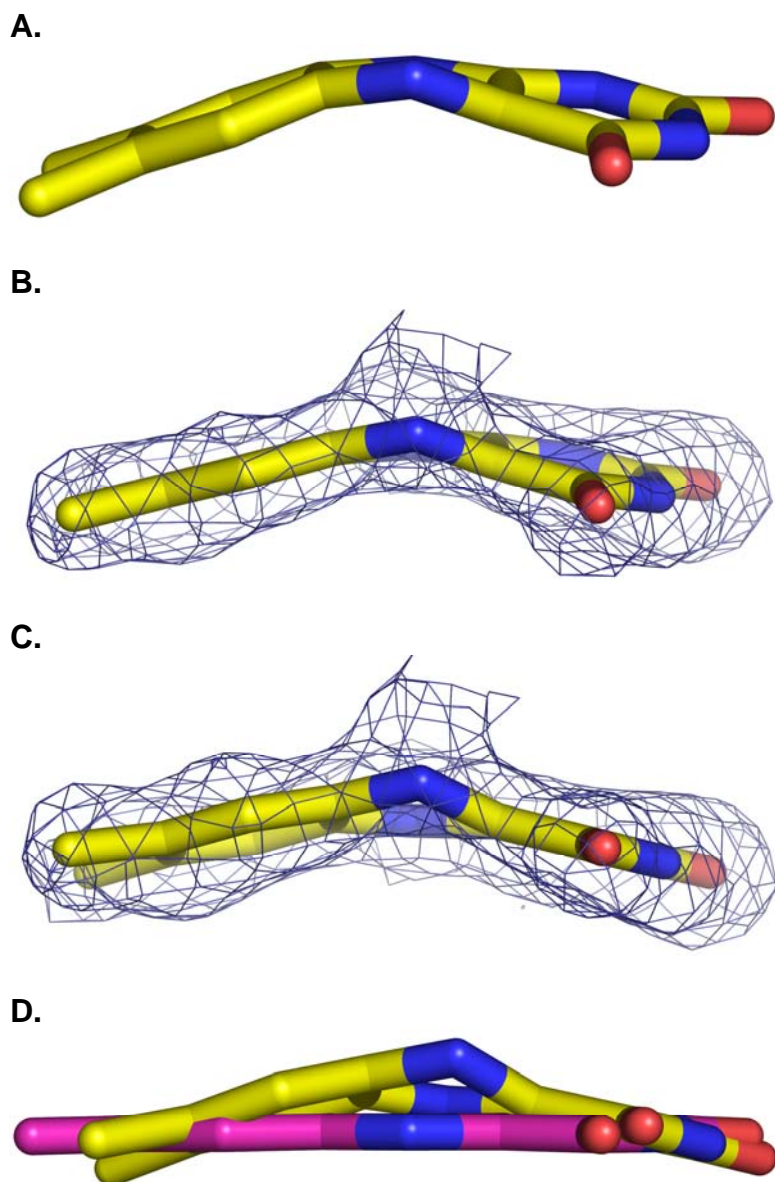


FIGURE 3.9. Four views of *N*-propargylglycine covalently-modified FAD of TtPROD<sub>H</sub>.

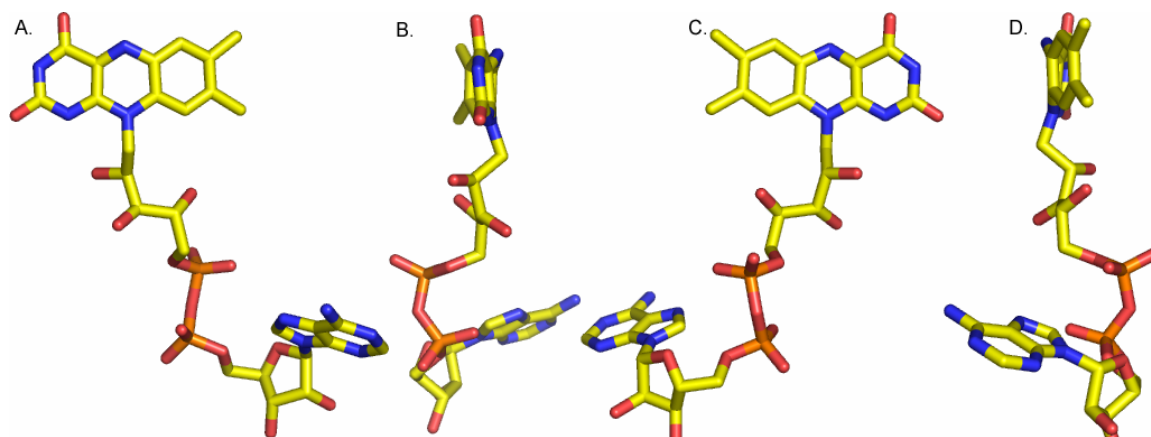
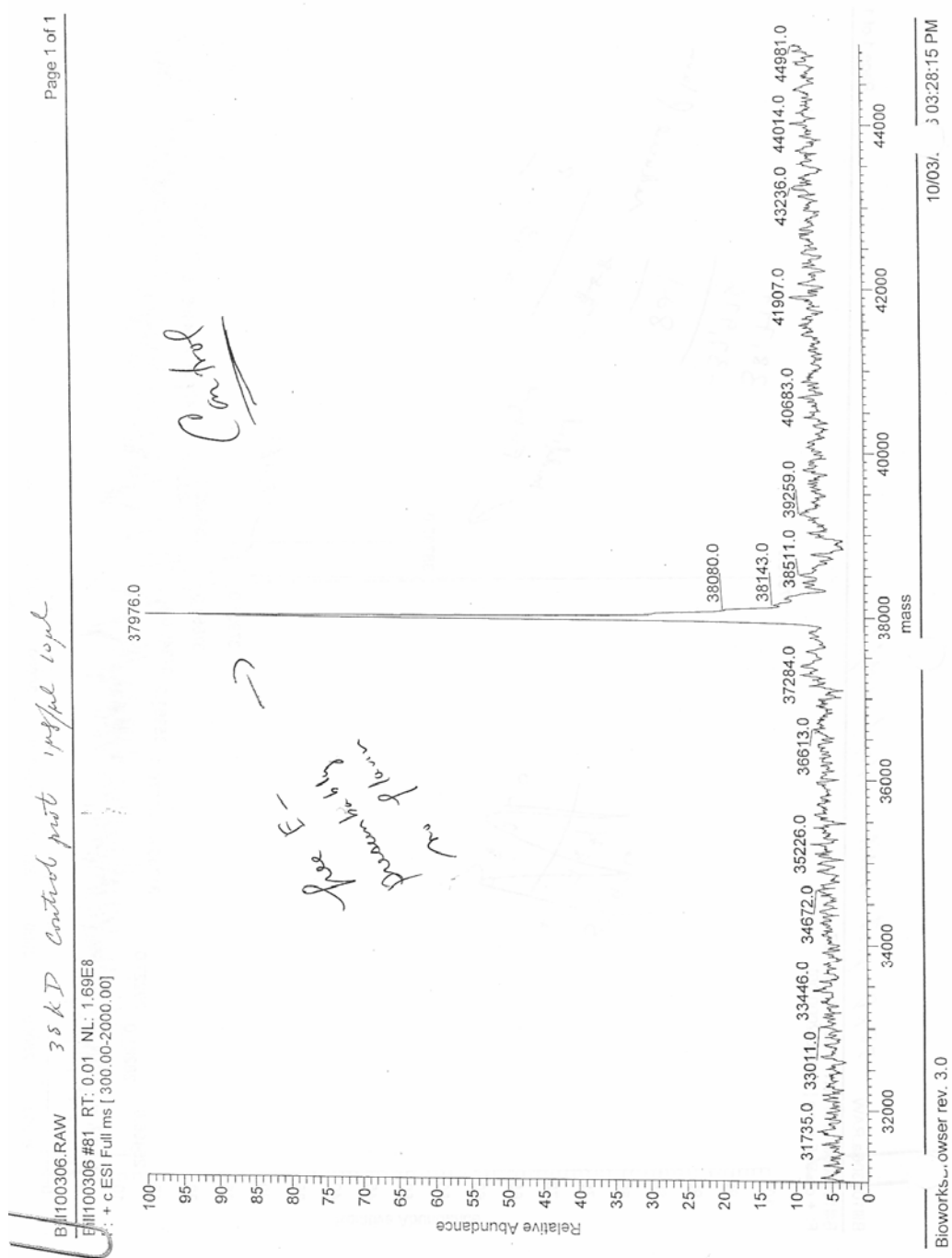


FIGURE 3.10. Electrospray Ionization – time of flight mass spectrometry of TtPROD. The peak at 37976 corresponds to the molecular weight of the apo enzyme.



Bill101301a RAW 38 kD prot + AA 100% 100%  
 Bill101301a #101 RT: 0.00 NL: 8.57E7  
 F: + C-50 Full ms [ 300.00-2000.00]

38,797  
 -37,976  
 821  
 858  
 433  
 reduced  
 molecular  
 Every  
 38,468

25406.0 28281.0 29227.0 31735.0 33976.0 35361.0 37245.0 37905.0 38797.0 39332.0 39361.0 42431.0 44983.0 45930.0 47624.0 48713.0

Relative Abundance  
 mass

Page 1 of 1



FIGURE 3.12. Active site changes beyond the flavocyanine adduct. Arg184 is shown in orange, Asp133 is shown in green and Tyr275 shown in cyan. Hydrogen bonds are shown by black dotted lines. Flavocyanine shown in white CPK sticks. Strands are shown in light pink cartoons and helices are shown in light cyan cartoons

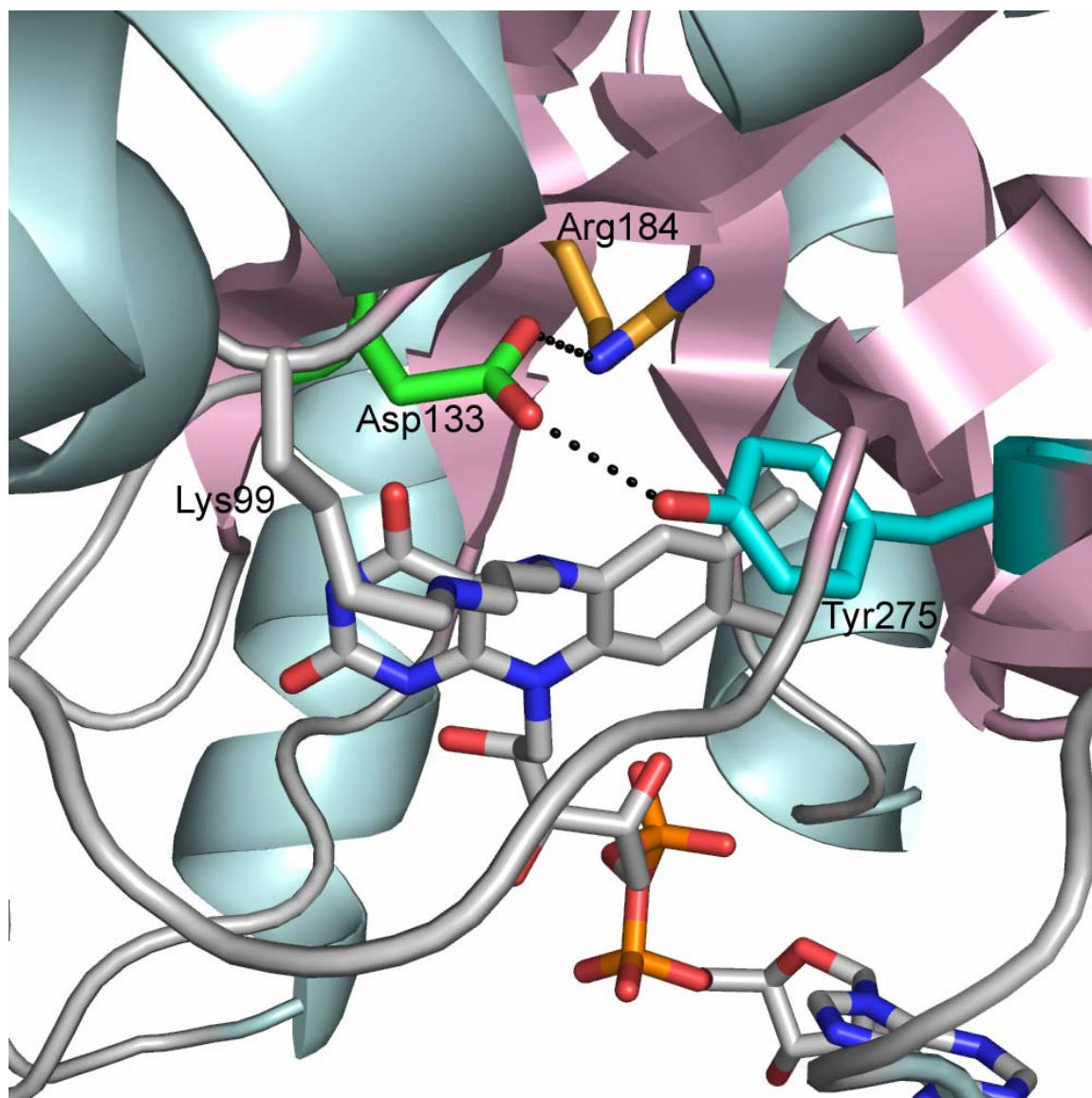




FIGURE 3.13. Residual active site electron density. The map is a simulated annealing  $F_o - F_c$  omit map ( $2.5\ \sigma$ ) in which the modeled glycine molecule was omitted prior to simulated annealing. Note that the density is quite weak and suggests low occupancy for glycine. Glycine was omitted from the final model.

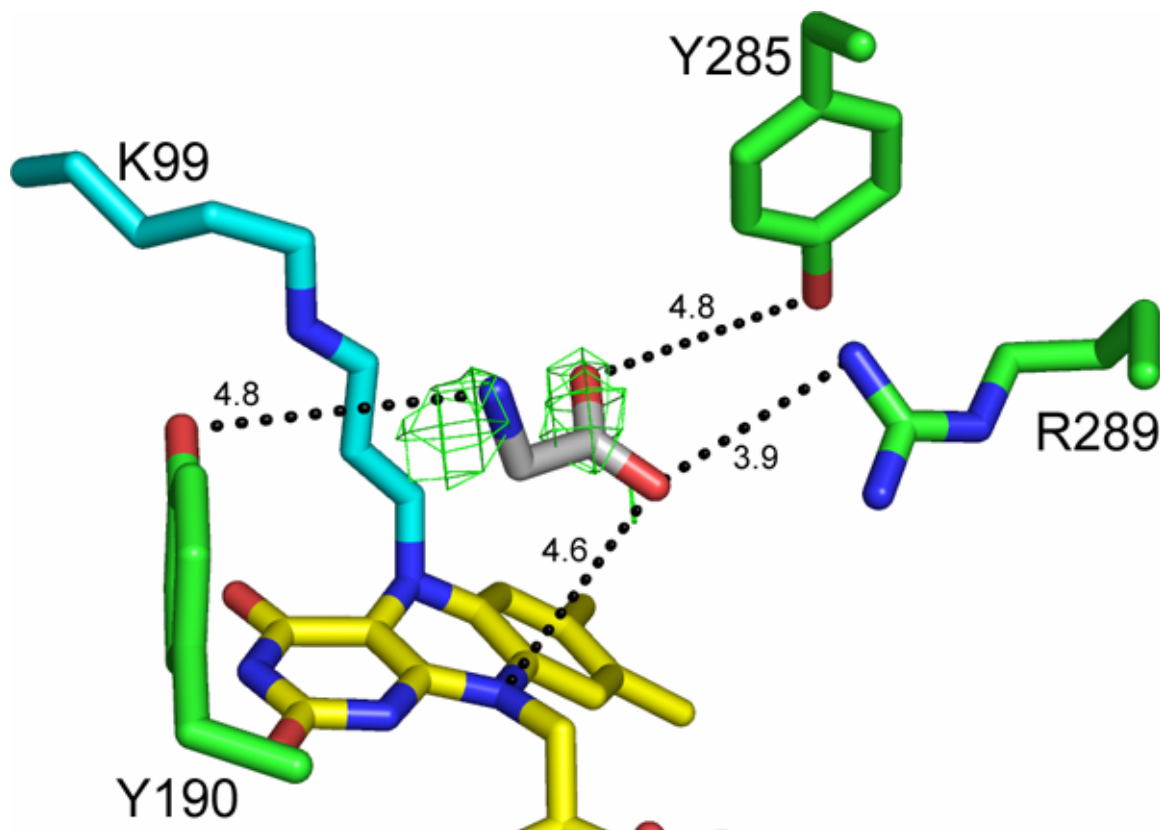


FIGURE 3.14. Spectral changes caused by inactivation of TtPRODH by *N*-propargylglycine. The flavin spectrum of oxidized TtPRODH is shown in red and displays characteristic peaks at 452 and 382 nm. The other curves correspond to various time points up to 60 minutes. Note that the peak at 452 nm disappears and a new peak centered at 386 nm appears as time advances.

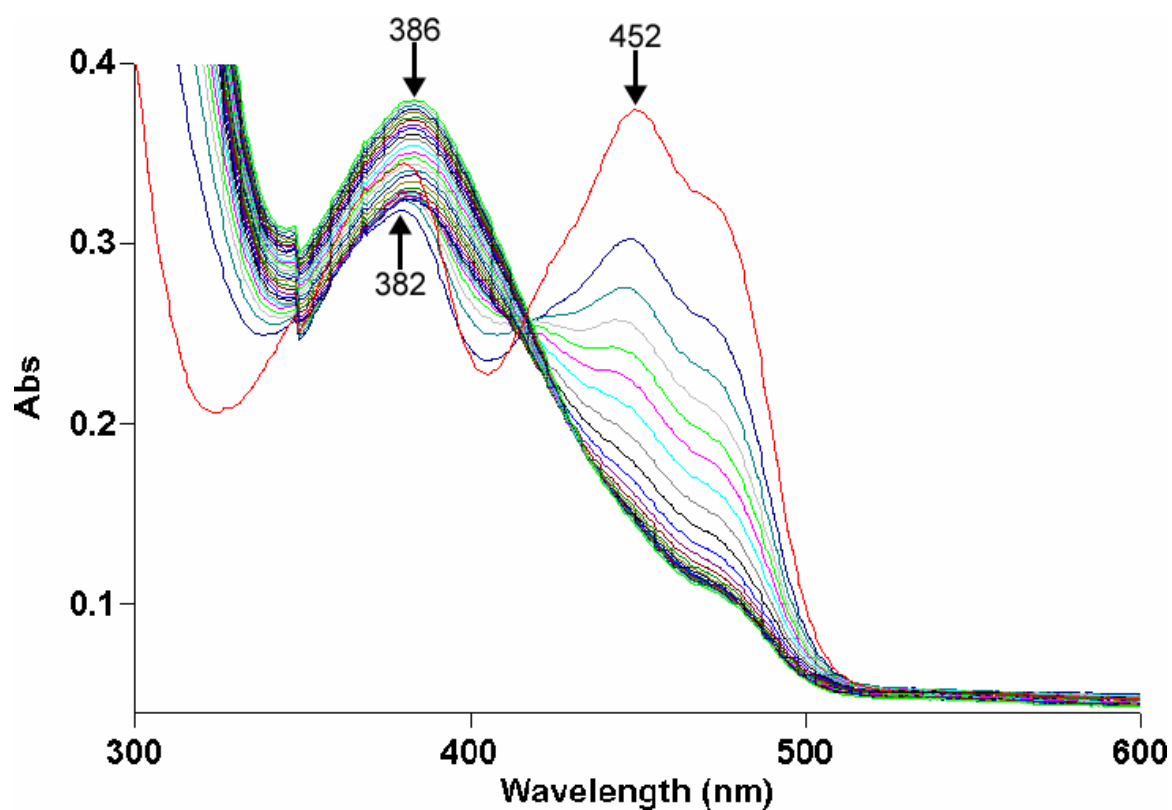


FIGURE 3.15. Time course of inactivation of TtPROD<sub>H</sub> by *N*-propargylglycine monitoring 452 nm, 382 nm and enzyme activity.

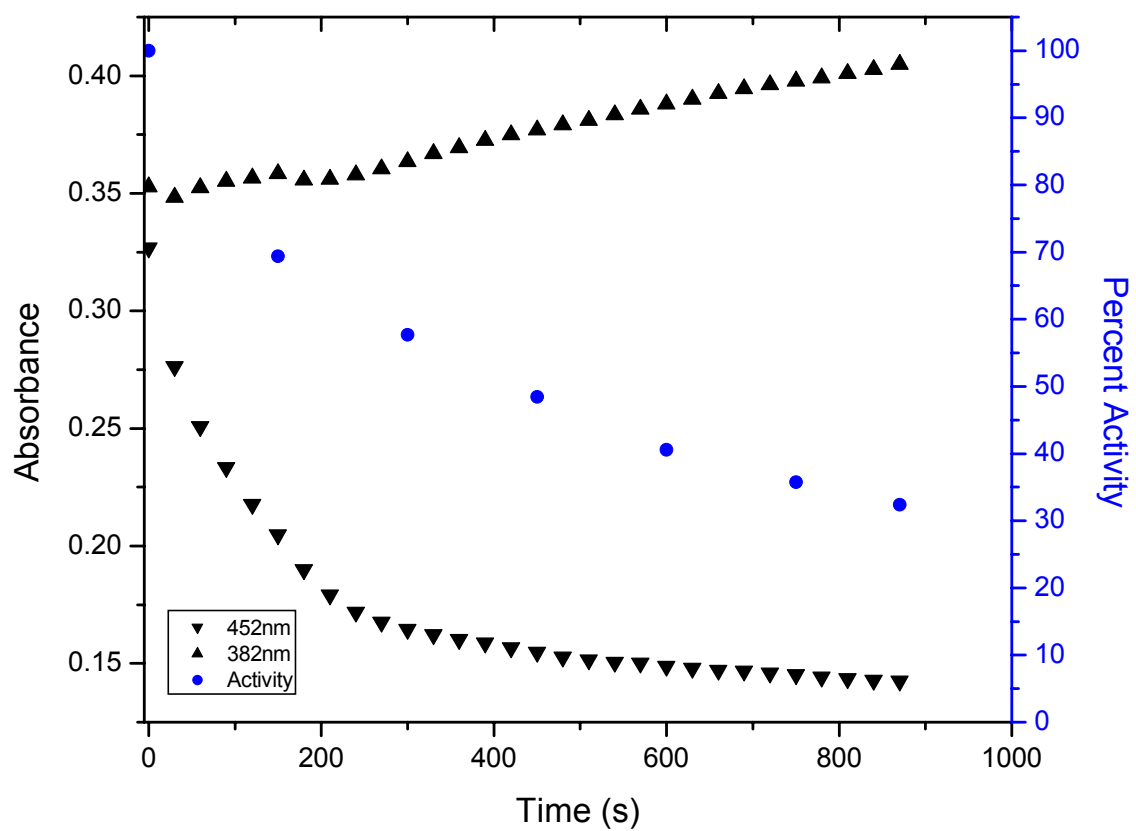


FIGURE 3.16. Effect of adding sodium dithionite to a sample of TtPROD<sub>H</sub> that had been inactivated by *N*-propargylglycine. Spectra are labeled as: oxidized enzyme ( $E_{ox}$ ), dithionite reduced enzyme ( $E_{red}$ ), *N*-propargylglycine inactivated ( $EI''$ ), and dithionite-reduced inactivated ( $EI''red$ ).

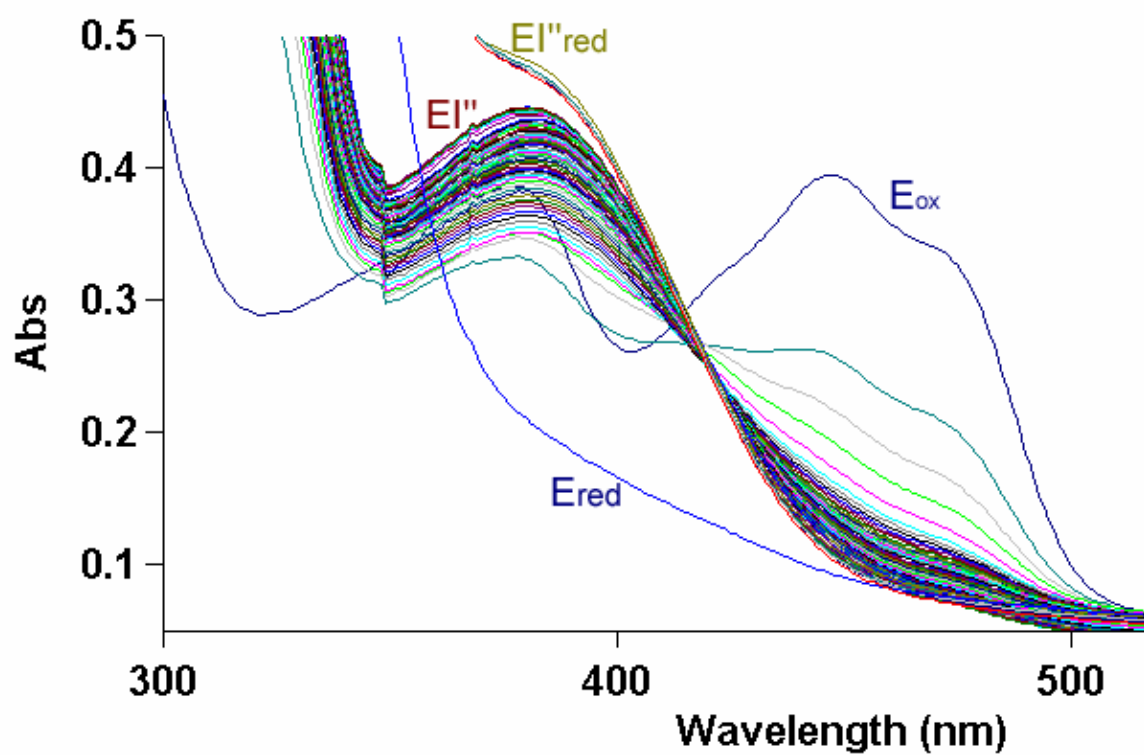


FIGURE 3.17. Theoretical Kitz and Wilson plot (adapted from Silverman, 2002).

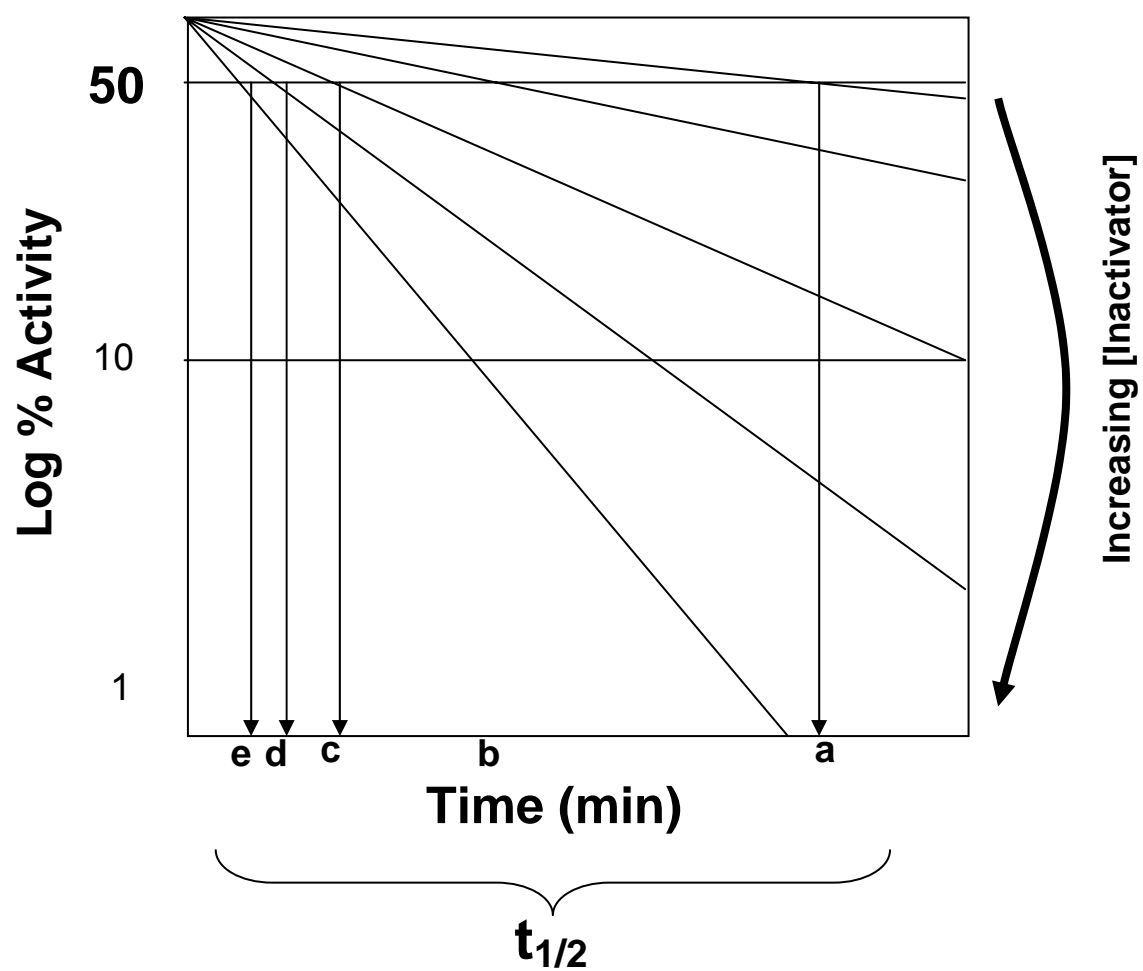


FIGURE 3.18. Theoretical Kitz and Wilson replot (adapted from Silverman, 2002).

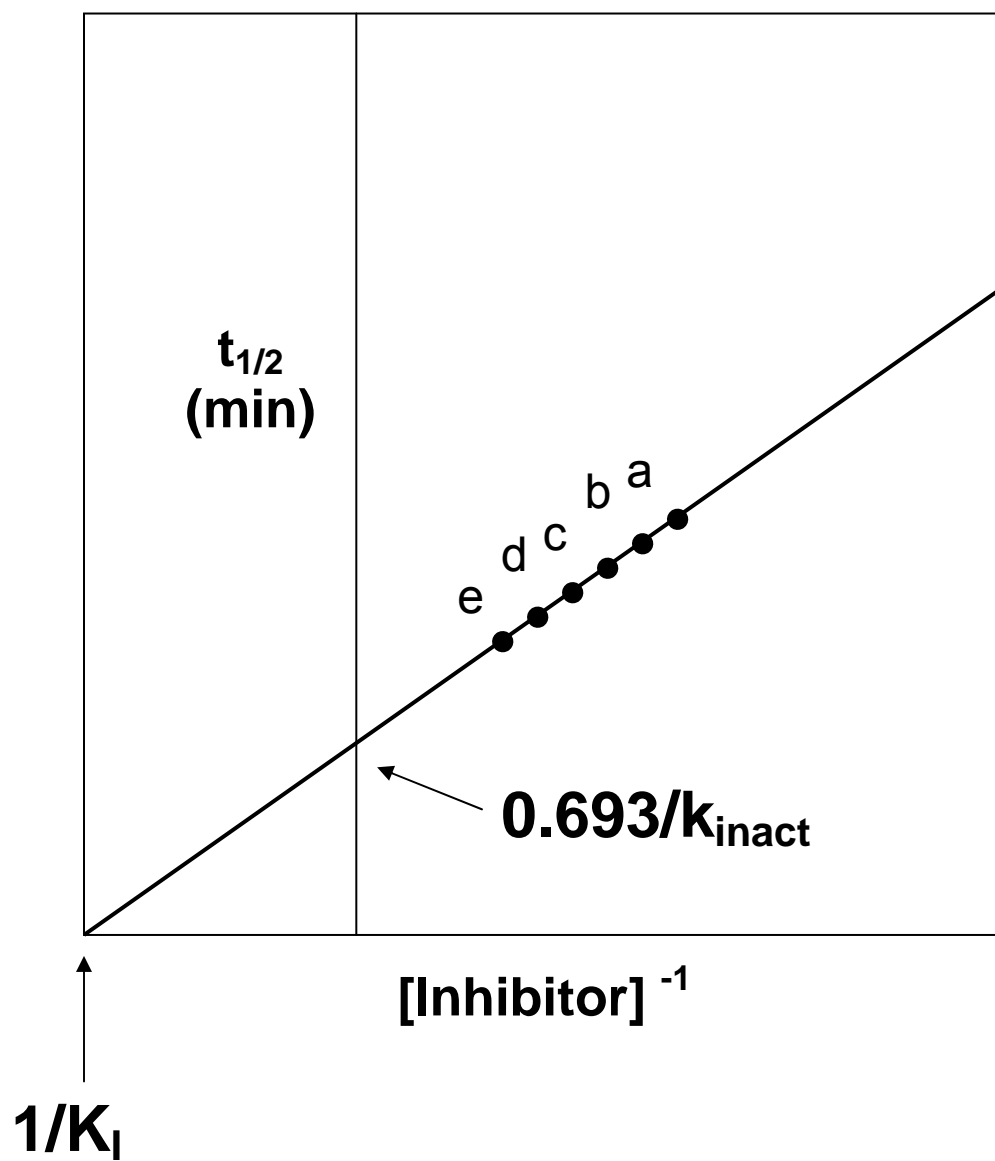


FIGURE 3.19. Kitz and Wilson plot (top) and replot (bottom) for TtPRODH inactivation by *N*-propargylglycine at 25 °C. The legend lists *N*-propargylglycine concentrations.

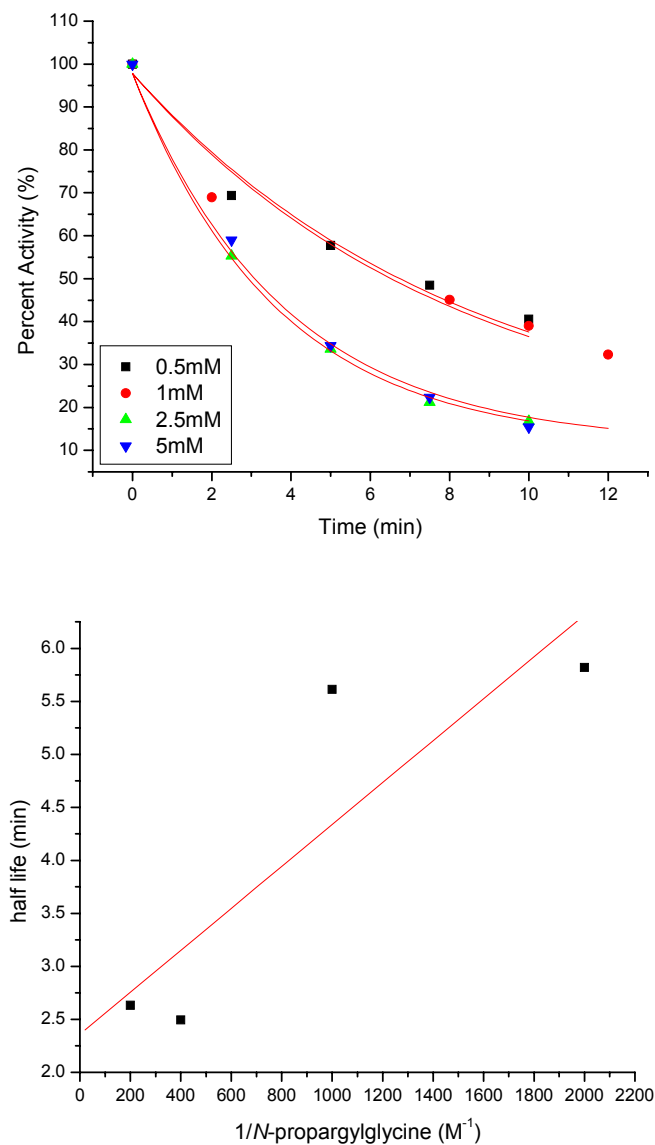


FIGURE 3.20. Kitz and Wilson plot (top) and replot (bottom) of TtPRODH inactivation with *N*-propargylglycine at 4 °C.

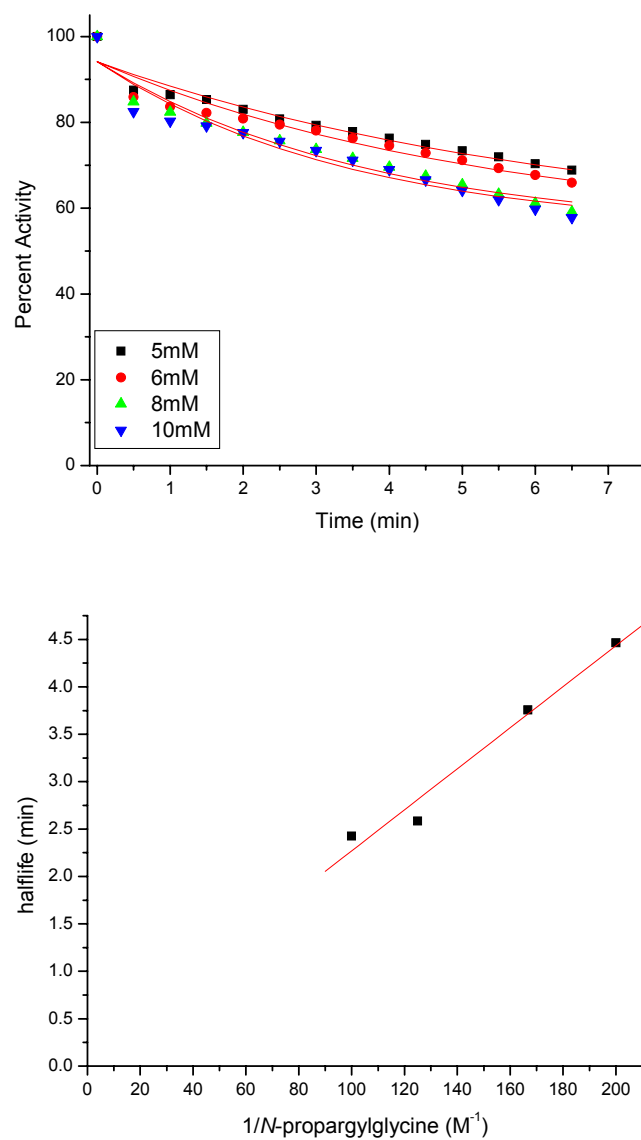




FIGURE 3.21. Possible flavin adducts formed by mechanism-based inactivation. The sites of modification include N5 (A), C4a (B), both N5 and C4a (C). (D) The modified flavin observed by Maycock and colleagues. (E) The modified flavin observed in TtPRODHD inactivated by *N*-propargylglycine.

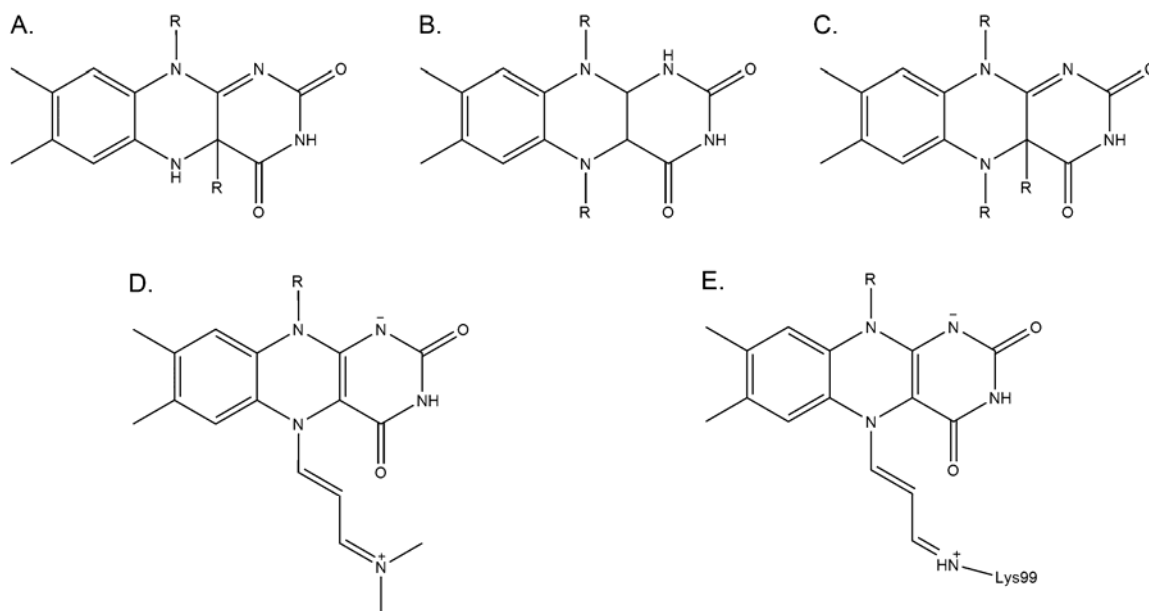


FIGURE 3.22. Maycock's proposed reaction mechanisms for flavin adduction by mechanism-based inactivators with an acetylenic group. A) Theoretical acetylenic mechanism based inactivator. B) Carbanion mechanism. C) Radical pair complex. D) Michael addition (note the isoalloxazine has truncated in these drawings).

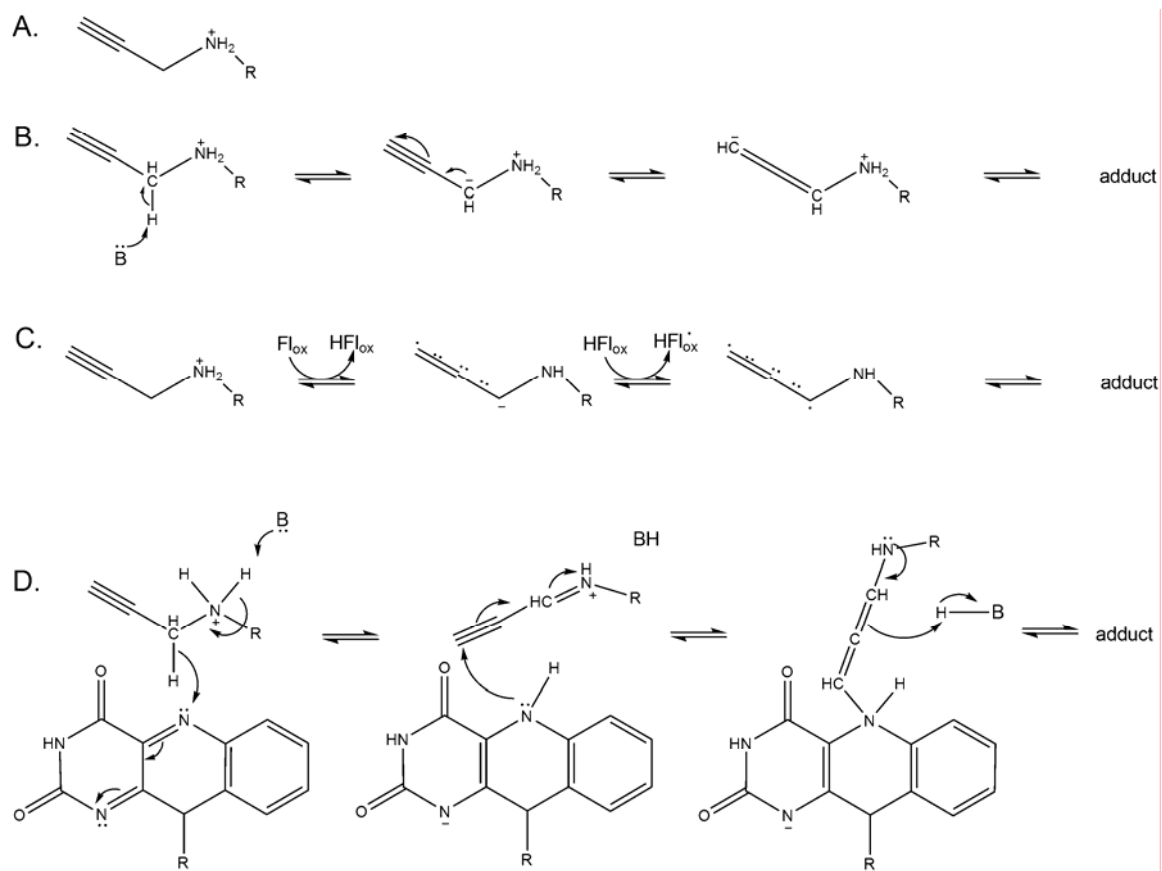


FIGURE 3.23. Structure of monoamine oxidase inactivated with rasagiline. A) Monoamine oxidase B shown in rainbow cartoon with black arrow head indicating the flavocyanyne adduct (PDBID 1S2Q). B) Monoamine oxidase B flavocyanyne adduct with FAD in yellow and rasagiline adduct in cyan. C) Monoamine oxidase A shown in rainbow cartoon with black arrow head indicating the flavocyanyne adduct (PDBID 2BK4). D) Monoamine oxidase A flavocyanyne adduct with FAD in yellow and rasagiline adduct in cyan.

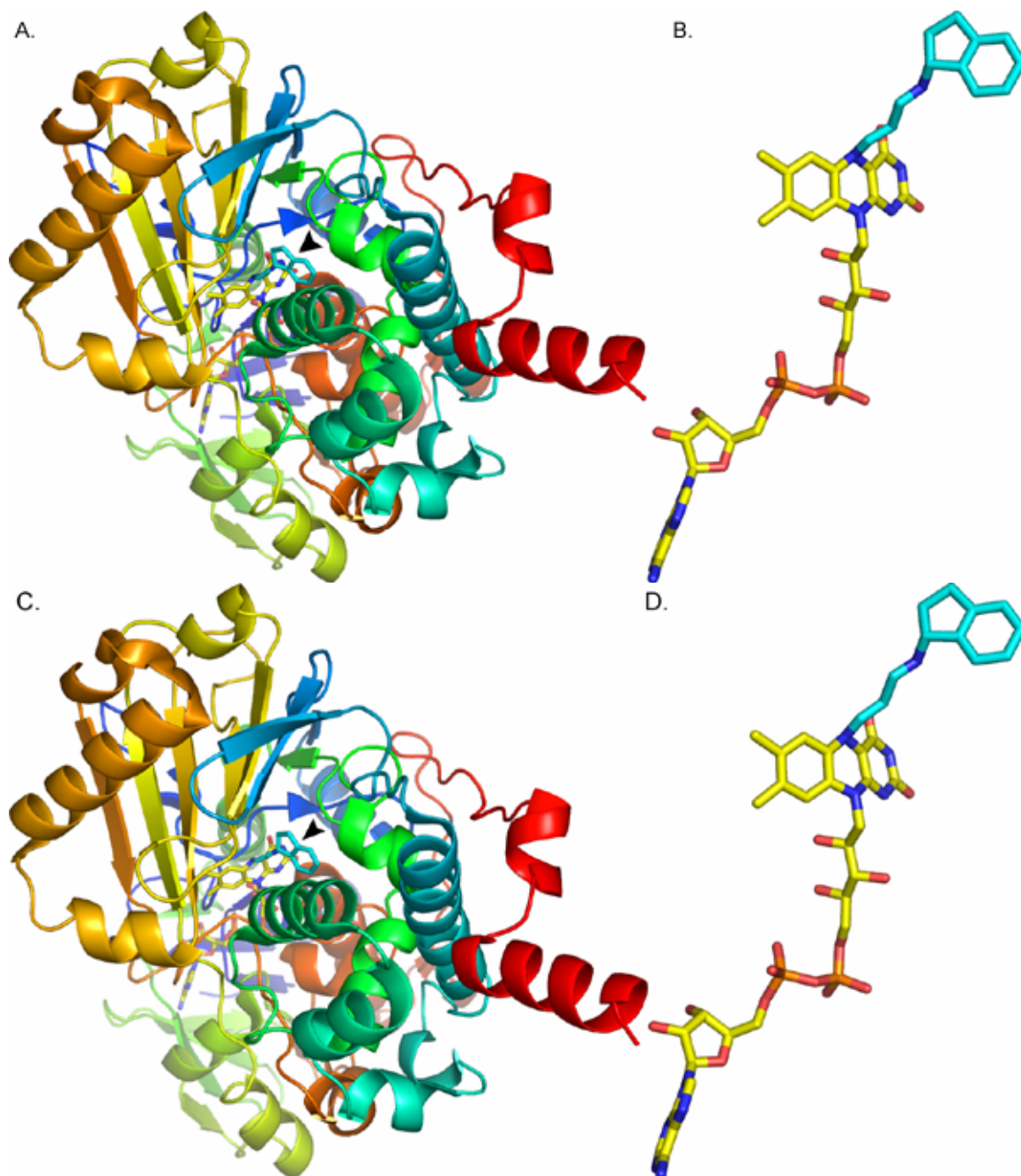


FIGURE 3.24. Steps 1 and 2 of the proposed mechanism of inactivation of TtPROD H by *N*-propargylglycine.

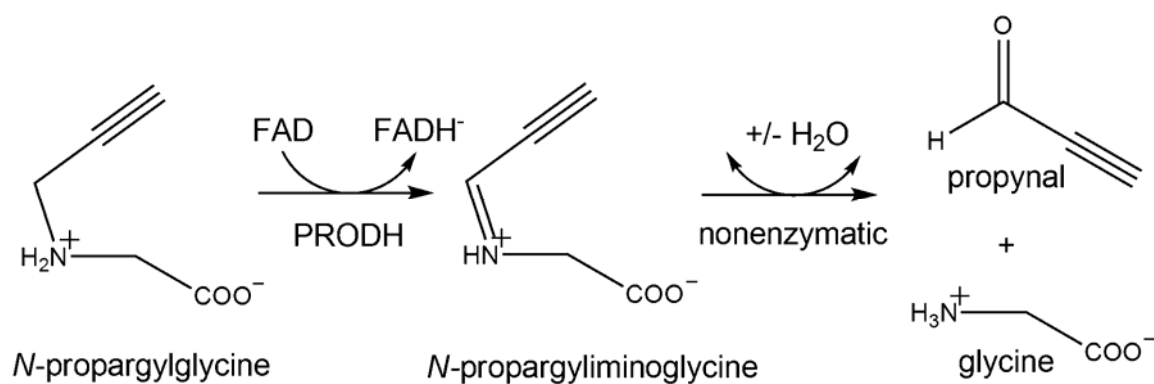


FIGURE 3.25. Proposed Schiff base formation with propynal and K99. There is a strategically placed active site H<sub>2</sub>O to form the carbinolamine intermediate.

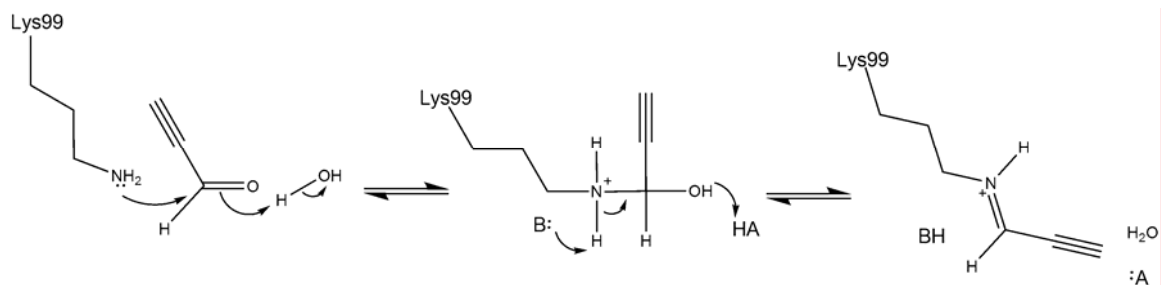


FIGURE 3.26. Last step of the proposed mechanism of inactivation of TtPRODHD by *N*-propargylglycine. The reaction is a Michael addition of reduced flavin to propynal-modified lysine 99.

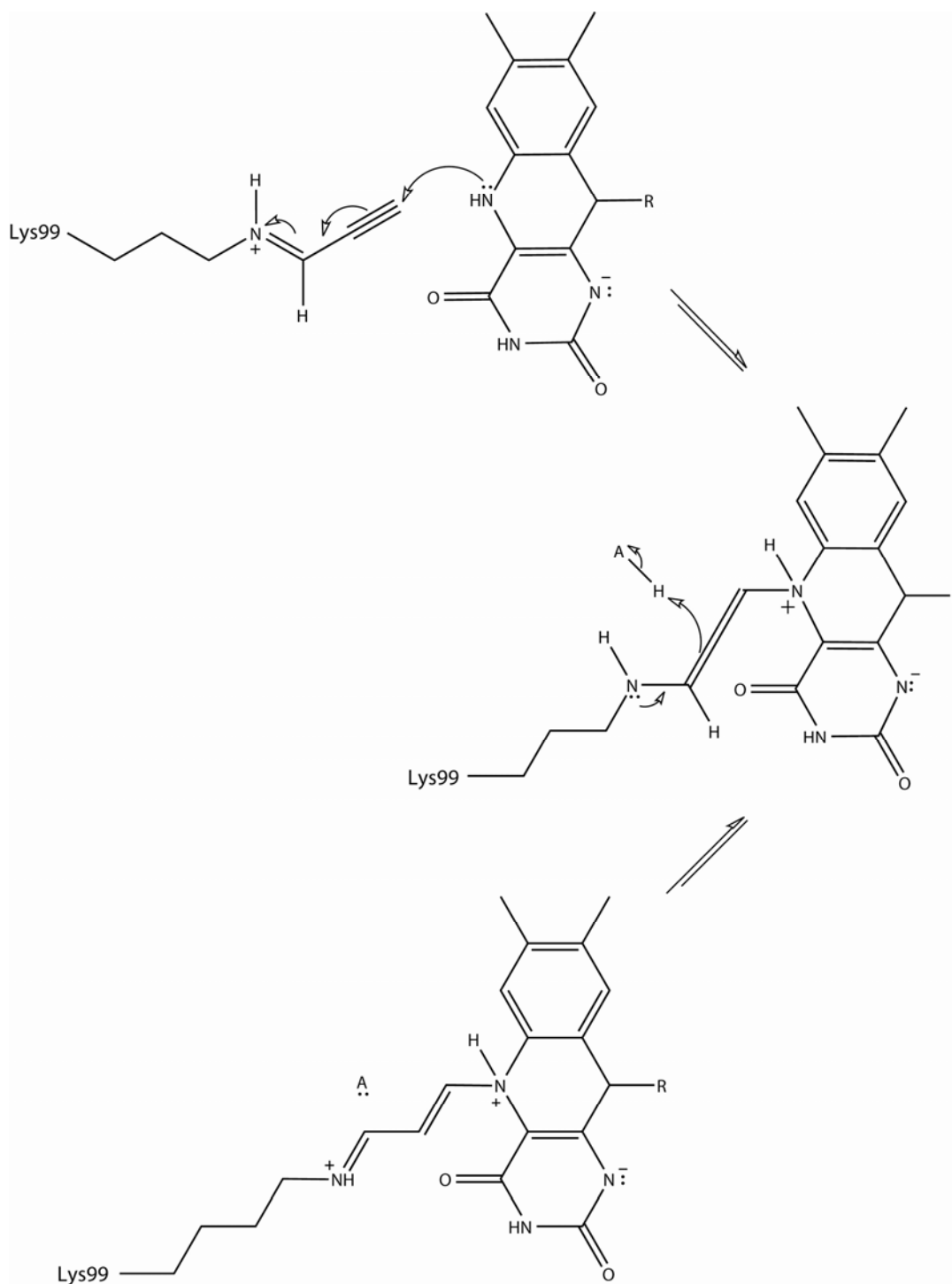


FIGURE 3.27. Generic Schiff base reaction between an amine and an aldehyde or ketone to form the carbinolamine intermediate and finally the imine and water.

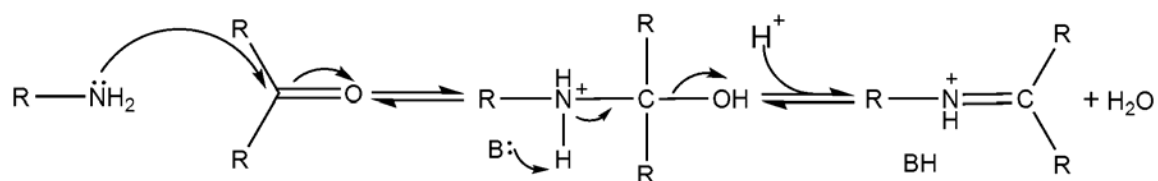


FIGURE 3.28. Comparison of isoalloxazines from inactivated TtPRODHD (yellow) and dithionite-reduced *E. coli* PutA PRODHD domain (green).

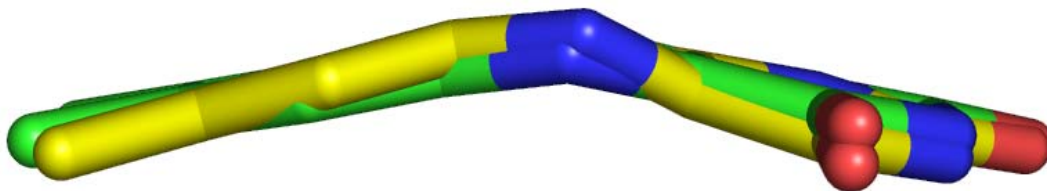




FIGURE 3.29. Comparison of FAD from inactivated TtPRODH (yellow) and dithionite-reduced *E. coli* PutA PRODH domain (green).

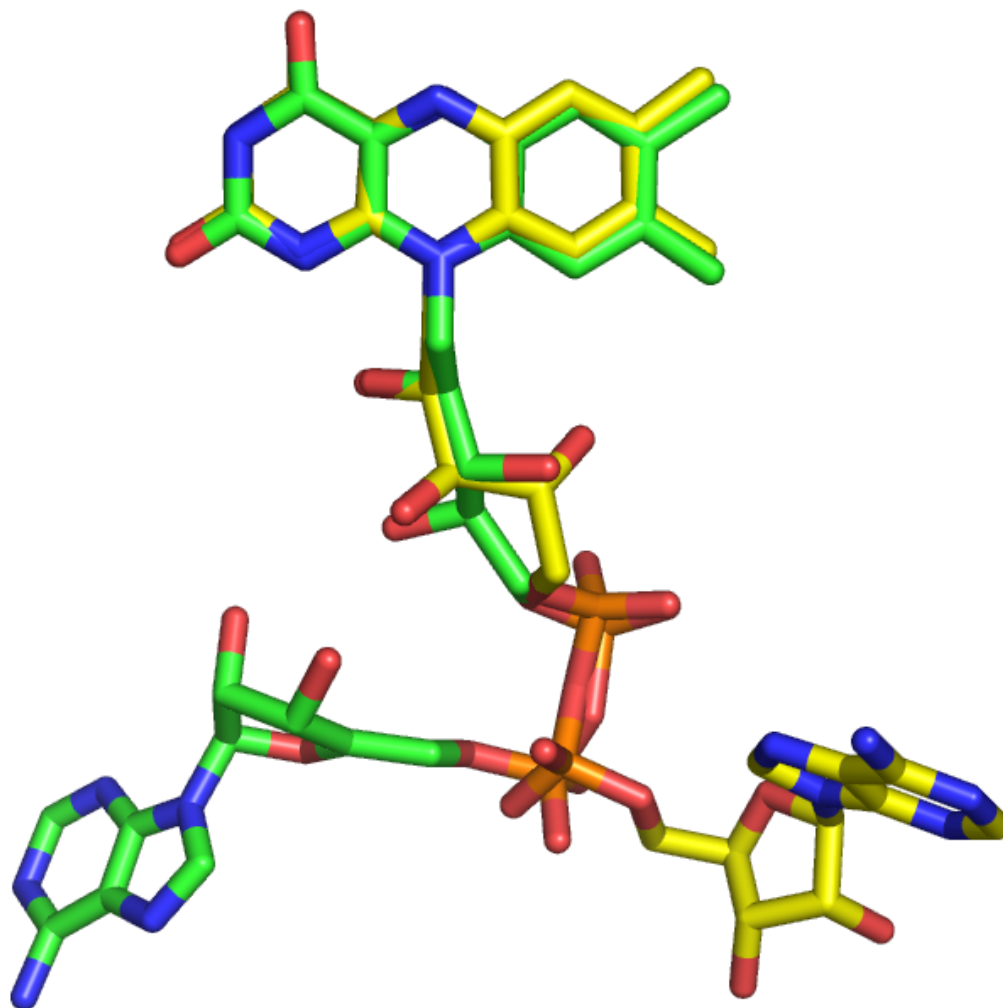


TABLE 3.1. Data Collection and Refinement Statistics for TtPROD<sub>H</sub> inactivated by *N*-propargylglycine<sup>a</sup>

Wavelength (Å)	1.00
Diffraction resolution (Å)	1.9
No. of observations	325777
No. of unique reflections	55959
Redundancy	5.82 (5.78)
Completeness (%)	99.3 (100)
R <sub>merge</sub>	0.059 (0.356)
Average I/σ	12.5 (3.3)
Wilson B-factor (Å <sup>2</sup> )	33
No. of protein chains	2
No. of protein residues	589
No. of protein atoms	5221
No. of water molecules	462
R <sub>cryst</sub>	0.193 (0.238)
R <sub>free</sub> <sup>b</sup>	0.220 (0.299)
RMSD <sup>c</sup>	
Bond lengths (Å)	0.012
Bond angles (deg.)	1.296
Ramachandran plot <sup>d</sup>	
Favored (%)	95
Allowed (%)	5
Average B-factors (Å <sup>2</sup> )	
Protein	33.3
FAD	36.4
Modified Lysine	36.6
MPD	50.0
Water	38.1

<sup>a</sup>Values for the outer resolution shell of data are given in parenthesis.

<sup>b</sup>5% random R<sub>free</sub> test set.

<sup>c</sup>Compared to the Engh and Huber force field (51).

<sup>d</sup>The Ramachandran plot was generated with PROCHECK

## CHAPTER 4

### Preliminary Studies of Interactions Between *T. thermophilus* Proline Dehydrogenase and $\Delta^1$ -Pyrroline-5-Carboxylate Dehydrogenase

#### INTRODUCTION

Channeling is the direct transfer of intermediate between the active sites of enzymes that catalyze sequential reactions (1). This can occur in multifunctional enzymes, tightly-associated multienzyme complexes or transiently associating enzymes. Channeling of intermediates of many metabolic pathways has been reported, including enzymes involved in nucleotide biosynthesis, amino acid metabolism, lipid metabolism, glycolysis, TCA cycle, DNA replication, RNA synthesis and protein biosynthesis (2). Benefits of channeling intermediates include decreased transit time, prevention of intermediate entry into competing metabolic pathways, and protection of reactive, toxic or labile intermediate (1).

Tryptophan synthase (TrpS) is perhaps the best characterized system for intermediate channeling (3). TrpS catalyzes the last two steps of tryptophan biosynthesis (3). In bacteria and higher plants, the enzymes form a tightly associated heterotetramer  $(\alpha\beta)_2$  enzyme complex, whereas in mold and yeast, TrpS is a bifunctional enzyme with fused  $\alpha$  and  $\beta$  domains (2). The  $\alpha$ -subunit catalyzes breakdown of indole 3-glycerol phosphate to form indole and D-glyceraldehyde 3-phosphate. The  $\beta$ -subunit utilizes cofactor PLP, the indole formed from the  $\alpha$ -subunit, and serine to catalyze the formation of tryptophan (2). The intermediate indole is channeled from the  $\alpha$ -subunit to the  $\beta$ -subunit. The

crystal structure of *S.typhimurium* TrpS revealed a 25 Å tunnel leading from the  $\alpha$ -subunit to the  $\beta$ -subunit (3) which can hold up to 4 indole molecules (2). Kinetic studies confirmed channeling for TrpS. Steady state kinetics failed to trap the indole intermediate indicating that it was not released from the protein. And introducing a bulky aromatic residue in the proposed channel by mutagenesis made catalysis less efficient (3).

Yeast TrpS is an example of what Eisenberg and colleagues refer to as a Rosetta Stone protein because it deciphers protein-protein interactions (4). For TrpS, the Rosetta Stone hypothesis predicts that monofunctional  $\alpha$  and  $\beta$  enzymes interact, which, of course, is true. The Rosetta Stone hypothesis makes a similar prediction about monofunctional proline catabolic enzymes proline dehydrogenase (PRODH) and  $\Delta^1$ -pyrroline-5-carboxylate dehydrogenase (P5CDH) based on the observation that these enzymes are fused in some organisms into the bifunctional enzyme Proline utilization A (PutA).

Other considerations also argue in favor of interactions between monofunctional PRODH and P5CDH as well as channeling between the two enzyme active sites. PRODH and P5CDH catalyze the oxidation of L-proline to L-glutamate via the intermediates pyrroline-5-carboxylate (P5C) and glutamic semialdehyde (GSA). Evidence is mounting for the toxicity of the proline catabolic intermediate P5C/GSA. Yeast deficient in P5CDH ( $\Delta put2$ ) have been reported to generate reactive oxygen species (ROS) upon proline treatment (5,6). P5C (1 mM) treatment of mutant *A.thaliana* having hypersensitivity to proline results in visible damage within 9 hours and death within 3 days, whereas

treatment of hypersensitive mutant plants with L-proline (100 mM) weakly affected the whole plant after 3 days (6). Upon treatment with exogenous proline, P5CDH-deficient *A.thaliana* display sensitivity to proline resulting in apoptosis, callous deposition, and ROS generation (7).

Besides toxicity issues, P5C and GSA are reactive intermediates. The aldehyde moiety of glutamic semialdehyde is especially prone to nucleophilic attack. Other competing metabolic pathways share P5C and GSA as intermediates. For example, GSA enters the urea cycle by ornithine aminotransferase, and P5C can be converted back to proline by P5C reductase. The toxicity, reactivity, and metabolic utility of P5C and GSA make them ideal candidates for channeling.

Another argument in favor of interactions between PRODH and P5CDH is that kinetic data suggest that channeling occurs in PutAs. Maloy's group reported data showing that *S.typhimurium* PutA channels the intermediate P5C/GSA (8). Upon examination of substrate preference by measuring NADH formation as a function of P5C concentration, they found that PutA had a greater preference (14-fold) for P5C from PRODH catalysis rather than exogenously supplied P5C. When measuring NADH formation as a function of time, P5CDH oxidized endogenous P5C more efficiently (8-fold) then compared to exogenous P5C. Also, they found that, in the absence of  $\text{NAD}^+$ , PRODH was active with concomitant release of P5C and that exogenous P5C can be oxidized by P5CDH. Based on these data, Maloy and coworkers termed this mechanism of intermediate transport a "leaky" channel (8). More recently, kinetic data in

support of channeling of has been obtained by Prof. Donald Becker's group for PutAs from *B. japonicum* and *E. coli* (unpublished data).

Based on the Rosetta stone hypothesis, the reactivity of P5C/GSA, and the observation of channeling in PutAs, we have begun to examine the possibility that monofunctional PRODH and P5CDH from *Thermus thermophilus* interact and engage in intermolecular substrate channeling.

## **MATERIALS AND METHODS**

### **Cloning**

The genes encoding PRODH and P5CDH from *T. thermophilus* HB27 were cloned from genomic DNA by the University of Missouri DNA core into plasmid pKA8H. The resulting plasmids encode proteins having N-terminal 8x His tags that are cleavable with TEV protease. TtPRODH was cloned as previously described (9) and TtP5CDH was cloned into pKA8H using the following primers:

Forward 5' – CCTTGATCATATGACGGTGGAAACCTTTCCGGAACG – 3'

Reverse 5' – TTTGGATCCCTAGAAGCGCTCGGCCACCGCC – 3'

Correct sequences were confirmed using T7 forward and reverse primers.

Coexpression vector pET-Duet1 containing two multi-cloning sites (MCS1, MCS2) was purchased from Novagen. Various pET-Duet1 constructs containing one or both genes were created using PCR primers listed in Table 4.1. The genes were subcloned from pKA8H. First, two plasmids corresponding to pET-Duet1 with either the TtPRODH or TtP5CDH gene in MCS2 were created. NdeI

and EcoRV restriction sites were used for these two constructs. Presence of the TtPRODH and TtP5CDH genes in MCS2 were confirmed with sequencing. Next the P5CDH gene with DNA encoding a TEV-cleavable 8x-histag was subcloned into MCS1 of the pET-Duet1 vector containing the TtPRODH gene in MCS2. XbaI and EcoRI restriction sites were used. Presence of the TtP5CDH gene in MCS1 was confirmed by sequencing.

### **Expression and Purification**

TtPRODH and TtP5CDH were separately expressed from the pKA8H vector using *E. coli* strain, BL21(DE3)pLysS. An 10 mL overnight culture was used to inoculate 1.5 L of LB broth. When the  $OD_{600} = 0.6$ , protein was induced using 0.5 mM IPTG for 3 hours at 37 °C. Cells were harvested and frozen in 10 mL 50 mM  $NaH_2PO_4$  pH 8, 300 mM NaCl, 10 mM imidazole and 5 % glycerol. Upon thawing, protease inhibitors were added (AEBSF, TPCK, E64, Pepstatin and Leupeptin) and cells were lysed by French press at 16,000 psi. TtPRODH is pure after Ni-NTA affinity chromatography (Qiagen), whereas TtP5CDH requires an extra step of anion exchange using a HiTrap Q column. Both enzymes were separately dialyzed into 50 mM Tris pH 8, 50 mM NaCl, 0.5 mM EDTA, 0.5 mM DTT, and 5 % glycerol.

Coexpression of TtPRODH and TtP5CDH using pET-Duet1 resulted in production of TtP5CDH with cleavable 8x His tag and TtPRODH without a His tag. From freshly transformed BL21(DE3)pLysS cells containing the pET-Duet1 vector (clones 173181, 173182, and 173192), an overnight culture was used to inoculate 700 mL of LB broth. When  $OD_{600} = 0.6$ , protein was expressed using

0.5 mM IPTG for 3 hours at 37 °C. Cells were harvested and frozen in 10 mL 50 mM NaH<sub>2</sub>PO<sub>4</sub> pH 8, 300 mM NaCl, 10 mM imidazole and 5 % glycerol. Upon thawing, protease inhibitors were added (AEBSF, TPCK, E64, Pepstatin and Leupeptin) and cells were lysed by French press at 16,000 psi. Using 2.5 mL Ni-NTA affinity resin, gravity flow purification was used to isolate His tagged TtP5CDH and potential partner TtPRODH by elution with 250 mM imidazole. FAD (50 μM) was added to the eluted protein and it was dialyzed into 4L of 50 mM Tris pH 8, 50 mM NaCl, 0.5 mM EDTA, 0.5 mM DTT, and 5 % glycerol. Total protein concentration was determined using the Comassie Plus reagent (Pierce). The purity was analyzed by SDS-PAGE and activity assays.

#### **TtPRODH and TtP5CDH activity**

TtPRODH activity was analyzed using the DCPIP assay with proline (30 mM) as the substrate (10). TtP5CDH was assayed by monitoring NADH formation at 340 nm using 0.2 mM NAD<sup>+</sup> and 0.5 mM P5C in 20 mM MOPS pH 7.5.

#### **Assessment of Intermediate P5C/GSA Channeling**

Channeling was assessed by appearance of the intermediate P5C. P5C was detected as the yellow dihydroquinazolinium complex with *o*-aminobenzaldehyde (*o*-AB) by monitoring absorbance at  $\lambda = 443$  nm ( $\epsilon = 2900$  M<sup>-1</sup>cm<sup>-1</sup>, (11)). The assay mixture included 50 mM potassium phosphate buffer pH=7.5, 200 μg of *o*-AB, 300 mM proline and 0.2 mM NAD<sup>+</sup>. For some of the assays, membranes from *E. coli* (250 μg) or *T. thermophilus* (140 μg) were added as electron acceptors. Channeling assessment was also performed by



monitoring NADH formation upon addition of 300 mM proline as the substrate and 0.2 mM NAD<sup>+</sup>. These assays were likewise performed in the presence and absence of membranes from *T. thermophilus* (140 µg) or *E. coli* (250 µg).

### **Gel Filtration**

Gel filtration was used to assess association between TtPRODH and TtP5CDH. A Superdex 200 column was used with a buffer of 50 mM Tris pH 8, 50 mM NaCl, 0.5 mM EDTA, 0.5 mM DTT, and 5 % glycerol.

The separately expressed and coexpressed enzymes were analyzed. For the separately expressed enzymes, many variations of mixing and incubating the two enzymes were attempted and gel filtration conducted. The enzymes were mixed at an apparent 1:1 molar ratio and 300 µL of 0.2 mg/mL protein solution was injected on the column. In a separate experiment the separately expressed enzymes were mixed in a 1:1 molar ratio and incubated at 75 °C for 60 min before gel filtration. Similar studies were performed for the proteins after the His tags were removed.

For the enzymes coexpressed from pET-Duet1, gel filtration was performed after Ni-NTA affinity purification and a subsequent dialysis step. After determining total protein concentration using Comassie Plus (Pierce), 300 µL of 0.25 mg/mL protein solution was injected on the gel filtration column. A standard consisting of β-amylase (200,000 Da) was analyzed using the same buffer as the samples. The sample volume was 300 µL and the protein concentration was 0.25 mg/mL.

## **RESULTS**

### **Analysis of separately expressed TtPRODH and TtP5CDH**

The gel filtration profile of TtPRODH (38 kDa) showed a broad peak with  $V_e = 10.49$  (FIGURE 4.2, green). Upon addition of 20 mM n-octyl  $\beta$ -D-glucopyranoside this peak narrowed and shifted to  $V_e = 12.2$  mL (FIGURE 4.2, brown) which indicates a species larger than bovine serum albumin (66 kDa, data not shown). This result suggested that TtPRODH forms an apparent homodimer in the presence of detergent. TtP5CDH (59.5 kDa) displayed a fairly sharp elution peak at  $V_e = 10.0$  mL (FIGURE 4.2, blue), which is larger than the elution volume of  $\beta$ -amylase (200 kDa, data not shown). This result is consistent with TtP5CDH forming an apparent homotetramer under these conditions (TAW unpublished result).

The enzymes were mixed at a molar ratio of 1:1 and then analyzed by gel filtration. The chromatogram had a large peak at  $V_e = 10$  mL (FIGURE 4.3, blue) and a significant peak at the void volume of 7 mL. There was also a shoulder peak near  $V_e = 8.0$ -8.5 mL, which was not present in the chromatograms of the individual enzymes. Heating the mixed proteins at 75 °C resulted in almost complete disappearance of the  $V_e = 10$  mL peak and enhancement of the  $V_e = 8.0$ -8.5 mL shoulder (FIGURE 4.3, green). The effect of removing the His tags from both enzymes (without heating) was investigated. As with heating, removal of the His tags resulted decreased the  $V_e = 10$  mL peak and enhanced the  $V_e = 8.0$ -8.5 mL shoulder (FIGURE 4.3, red). His tag removal also resulted in a large peak at the void volume. The profile obtained after His tag removal and heating

(FIGURE 4.3, brown) was similar to that obtained by His tag removal alone (compare brown and red curves in FIGURE 4.3).

It appeared that His tag removal caused the disappearance of the  $V_e = 10$  mL peak associated with TtP5CDH and appearance of a new peak at  $V_e = 8.0-8.5$  that was not observed when either enzyme was analyzed separately. We followed up on this observation by examining protein mixtures in which only one of the His tags was removed by proteolysis (FIGURE 4.4). The result for a 1:1 mixture of His-TtPRODH and untagged TtP5CDH is shown in blue in FIGURE 4.4. The peak at  $V_e = 10$  is present and there is large void volume peak. Heating the sample produced a similar chromatogram except that the peak at  $V_e = 10$  mL was decreased (FIGURE 4.4, red). Experiments corresponding to mixtures of untagged TtPRODH and His-TtP5CDH are shown in green and brown in FIGURE 4.4. In the absence of heating, this mixture resulted in a gel filtration profile with a prominent peak at  $V_e = 8.3$  mL and a peak at the void volume (FIGURE 4.4, green). The heated sample also resulted in a similar chromatogram but the peak at  $V_e = 10$  mL was larger (FIGURE 4.4, brown). These results show that the peak at  $V_e = 8.3$  is associated with removal of the His tag from PRODH (FIGURE 4.4, green and brown) and that removal of the tag from P5CDH results in a large peak at the void volume (FIGURE 4.4, blue and red).

Another set of gel filtration studies was performed using enzymes that were expressed separately, but the cells from two expression experiments were combined, lysed in the same vessel and purified using Ni-NTA chromatography.

Gel filtration profiles are shown in FIGURE 4.5. The resulting profile is very similar to that obtained when the proteins were purified separately (compare blue curves of FIGURE 4.5 and FIGURE 4.3). Heating produced a broad peak at  $V_e = 8.4$  mL (FIGURE 4.5 green). Removal of the His tags had minimal effects, which was unexpected (FIGURE 4.5 red). In particular, the peak at  $V_e = 8.3$  was absent in this chromatogram. Removing the His tags and heating decreased the  $V_e = 10$  mL peak and increased the void volume peak, but did not cause appearance of the  $V_e = 8.3$  mL peak, which was unexpected.

These studies were inconclusive, due perhaps to problems involving self-association of TtPRODHD. We note that addition of detergent was necessary to obtain crystals of TtPRODHD, as described previously (9).

### **Coexpression of TtPRODHD and TtP5CDH**

Coexpression of the two enzymes was pursued using a pET-Duet1 construct with the P5CDH gene in MCS1 and the PRODHD gene in MCS2. P5CDH is expressed with a His tag while PRODHD does not have an affinity tag. SDS-PAGE analysis of the protein sample after elution from a gravity flow Ni-NTA affinity column showed two major bands having the molecular weights expected for TtP5CDH and TtPRODHD (FIGURE 4.6). This result suggests that TtPRODHD copurified with TtP5CDH.

There was also a substantial amount of apparent TtP5CDH in the wash fraction (FIGURE 4.6). We note that in our experience the enzyme encoded by MCS1 is always expressed at a much higher level than the enzyme encoded by MCS2. The cause is unknown.

### Enzymatic activities of coexpressed TtPRODH and TtP5CDH

The eluted protein sample displayed both PRODH and P5CDH activities. Utilizing the DCPIP assay(10), PRODH activity was detected at a level 10-fold above background when using 30 mM L-proline and 100  $\mu$ L of eluted and dialyzed enzyme sample (FIGURE 4.7). P5CDH activity was also detected by measuring increasing production of NADH at 340 nm upon addition of neutralized P5C (0.5 mM),  $\text{NAD}^+$  (0.2 mM) and increasing enzymes concentration (FIGURE 4.8).

The presence of P5C released into solution was tested using the *o*-AB assay. Using a proline concentration of 300 mM proline as substrate, the P5C-*o*AB complex was not detected under any condition tested (FIGURE 4.10; FIGURE 4.11; FIGURE 4.12; FIGURE 4.13). Several assays were performed: without  $\text{NAD}^+$  and membranes (FIGURE 4.10), no  $\text{NAD}^+$  and 140  $\mu$ g of *T. thermophilus* membranes (FIGURE 4.11), 0.2 mM  $\text{NAD}^+$  and no membranes (FIGURE 4.12), and 0.2 mM  $\text{NAD}^+$  and 140  $\mu$ g *T. thermophilus* membranes (FIGURE 4.13).

The sample was also assayed for P5CDH activity by monitoring NADH production at 340 nm using 300 mM proline and 0.2 mM  $\text{NAD}^+$  (0.2 mM). No activity was detected. The assay was repeated in the presence of membranes isolated from *T. thermophilus* and *E. coli* which could act as the electron acceptor for the reduced flavin. An increase at 340 nm was observed but the same increase was observed in the absence of enzyme indicating that production of NADH was likely due to activity of enzymes associated with the membranes,

such as NAD<sup>+</sup> dehydrogenase. We note that Maloy's group used membranes from a NAD<sup>+</sup> dehydrogenase-deficient (*ndh*<sup>-</sup>) *E. coli* strain MWC215 (8).

### **Gel filtration studies of coexpressed TtPRODH and TtP5CDH**

Gel filtration analysis was also conducted on protein sample purified from coexpression of the two enzymes (FIGURE 4.9). Major peaks were observed at  $V_e = 9.7$  mL, 13.9 mL and 17.6 mL. The  $V_e = 13.9$  peak represents a contaminant that appears on SDS-PAGE near 20 kDa and the peak at  $V_e = 17.6$  results from excess FAD added during purification. The peak at  $V_e = 9.7$  mL has a pronounced shoulder. Recall that the profile for separately expressed TtP5CDH has a sharp peak at  $V_e = 10.0$  mL (FIGURE 4.2 blue) and that the profile for TtPRODH has a broad peak at  $V_e = 10.5$  mL (FIGURE 4.2 green). It is tempting to speculate that the peak at  $V_e = 9.7$  mL in the chromatogram for the coexpressed enzymes represents a species not present in the individual protein samples.

## **DISCUSSION**

Purification of TtPRODH and TtP5CDH separately and mixing the two proteins did not yield definitive identification of a functional complex. Highly aggregated species were observed in gel filtration with elution volumes similar to the void volume. This is logical since the N-terminally His tagged TtPRODH displays significant self-association and aggregation in the absence of detergent.

Coexpression of the two enzymes yielded promising preliminary results. SDS-PAGE and PRODH activity assays suggested that TtPRODH copurifies with

TtP5CDH. And gel filtration chromatography revealed a new peak that was not present in profiles of the individually purified proteins.

The P5C trapping experiments were less encouraging. Based on previous results with PutA, we expected that P5C would be produced when the enzyme pair is incubated with proline and membranes in the absence of  $\text{NAD}^+$ . P5C, however, was not detected in such an assay for the coexpressed enzymes. P5CDH activity was not detected when proline was used as the substrate, although the method for detecting P5CDH activity is not optimal. Perhaps NADH was consumed by NAD dehydrogenase isolated with membranes. This may imply lack of a functional channel, but a better method of determining NADH formation is necessary. Measuring the product, glutamate, instead may provide a better analysis of P5CDH activity.

Future studies will focus on performing a larger scale purification of the coexpressed enzymes for analysis with mass spectrometry, analytical ultracentrifugation, and additional enzyme assays.

## REFERENCES

1. Miles, E. W., Rhee, S., and Davies, D. R. (1999) *J Biol Chem* 274, 12193-12196
2. Huang, X., Holden, H. M., and Raushel, F. M. (2001) *Annu Rev Biochem* 70, 149-180
3. Schlichting, I., Yang, X. J., Miles, E. W., Kim, A. Y., and Anderson, K. S. (1994) *J Biol Chem* 269, 26591-26593
4. Marcotte, E. M., Pellegrini, M., Ng, H. L., Rice, D. W., Yeates, T. O., and Eisenberg, D. (1999) *Science* 285, 751-753
5. Deuschle, K., Funck, D., Hellmann, H., Daschner, K., Binder, S., and Frommer, W. B. (2001) *Plant J* 27, 345-356
6. Hellmann, H., Funck, D., Rentsch, D., and Frommer, W. B. (2000) *Plant Physiol* 123, 779-789
7. Deuschle, K., Funck, D., Forlani, G., Stransky, H., Biehl, A., Leister, D., van der Graaff, E., Kunze, R., and Frommer, W. B. (2004) *Plant Cell* 16, 3413-3425
8. Surber, M. W., and Maloy, S. (1998) *Arch Biochem Biophys* 354, 281-287
9. White, T. A., and Tanner, J. J. (2005) *Acta Crystallography* F61, 737-739
10. Abrahamson, J., Baker, L., Stephenson, J., and Wood, J. (1983) *European Journal of Biochemistry* 134, 77-82
11. Mezl, V. A., and Knox, W. E. (1976) *Anal Biochem* 74, 430-440



FIGURE 4.1. Schematic diagram of proline catabolic enzymes from *E. coli*, *B. japonicum*, and *T. thermophilus*.

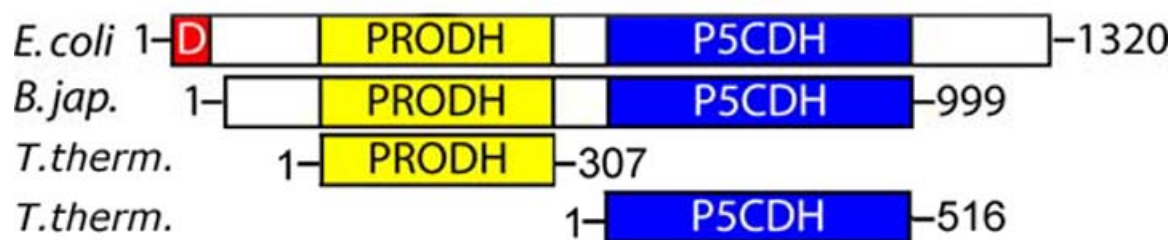


FIGURE 4.2. Gel filtration profiles for TtPROD<sub>H</sub> and TtP5CD<sub>H</sub>. The enzymes were expressed separately from pKA8H and purified by Ni-NTA affinity chromatography. Profiles for TtPROD<sub>H</sub> are shown in green (no BOG) and brown (20 mM BOG). The profile for TtP5CD<sub>H</sub> is shown in blue. The void volume is approximately 7 mL.

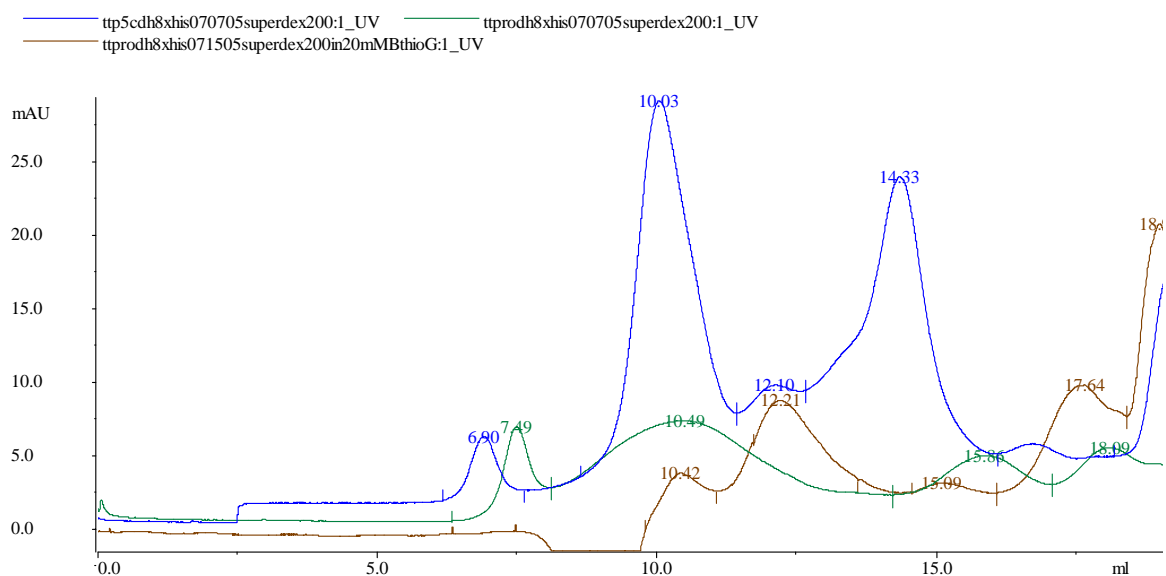


FIGURE 4.3. Gel filtration profiles for mixtures of TtPRODH and TtP5CDH. Each protein was separately expressed, lysed and purified. The purified proteins were mixed in a 1:1 molar ratio. The profile for the mixture with no further manipulation is shown in blue. The green curve corresponds to heating the mixture at 75 °C for 60 min. The red profile corresponds to the mixture after cleavage of the His tags with TEVP. The brown curve results from His tag cleavage and heating at 75 °C for 60 min. Void volume is approximately 7 mL.

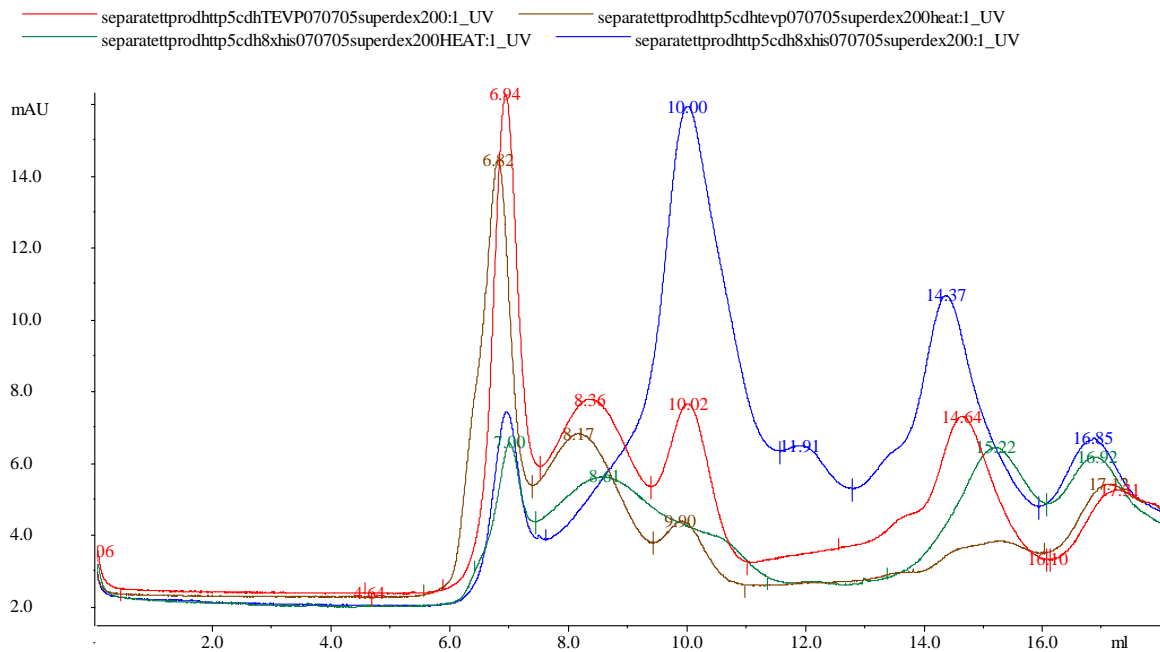


FIGURE 4.4. Gel filtration profiles for mixtures of TtPRODH and TtP5CDH in which the His tag of one protein had been cleaved. Each protein was separately expressed, lysed and purified. The proteins were mixed in 1:1 molar ratios. The blue curve represents a mixture of His-TtPRODH and cleaved TtP5CDH. The red curve represents a mixture of His-TtPRODH and cleaved TtP5CDH incubated together at 75 °C for 60 min. The green curve represents a mixture of His-TtP5CDH and cleaved TtPRODH. The brown curve represents a mixture of His-TtP5CDH and cleaved TtPRODH incubated together at 75 °C for 60 min. Void volume is approximately 7 mL.

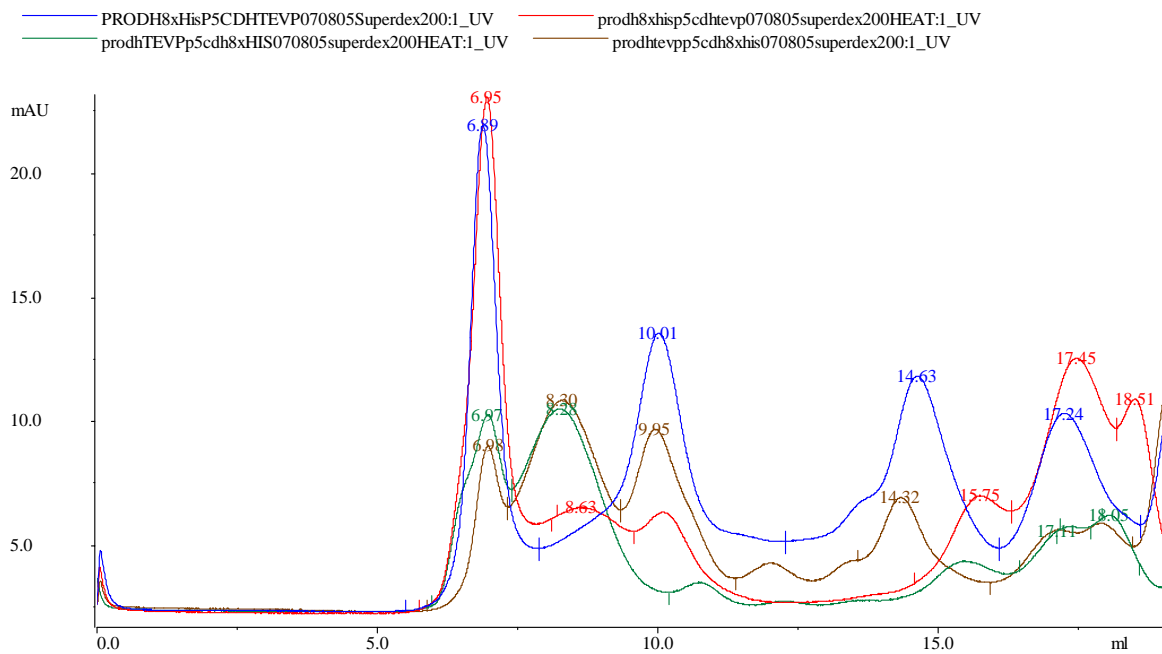


FIGURE 4.5. Gel filtration profiles for separately expressed, but copurified samples of TtPRODHD and TtP5CDH. The His-tagged enzymes were expressed separately, combined as whole cells, lysed in the same vessel and purified with Ni-affinity chromatography. The blue curve represents the purified protein sample with no further manipulation. The green curve represents the sample incubated at 75 °C for 60 min. The red curve represents the sample after cleavage with TEVP. The brown curve represents the sample after cleavage with TEVP and heating at 75 °C for 60 min. Void volume is approximately 7 mL.

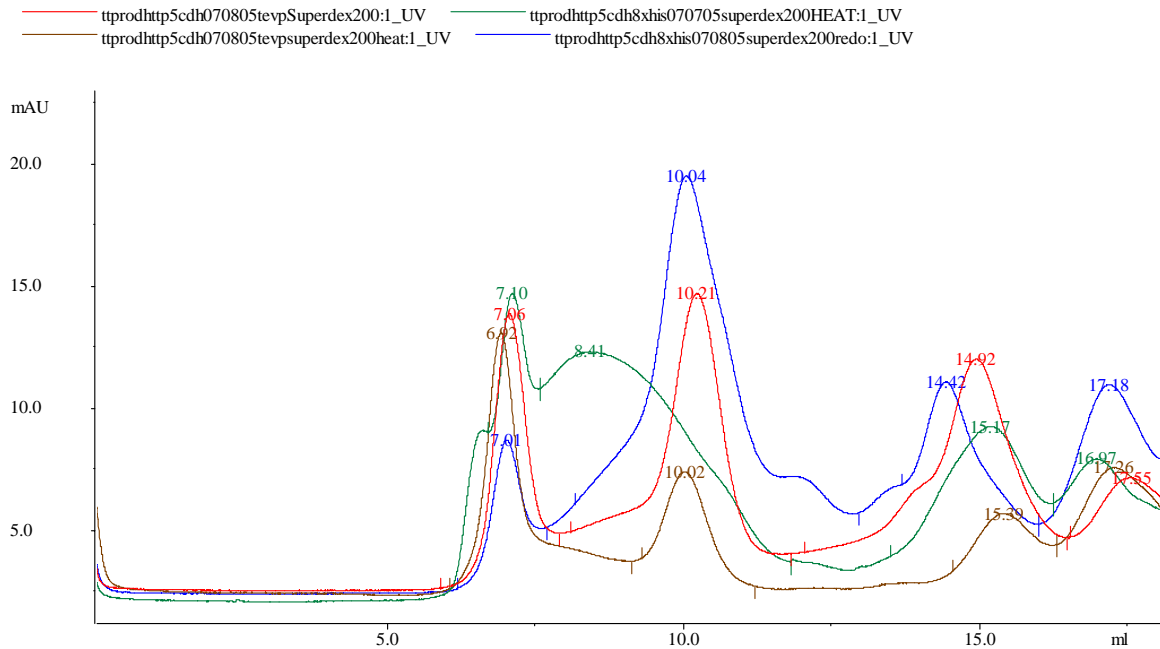


FIGURE 4.6. SDS-PAGE analysis of coexpressed His-TtP5CDH and untagged TtPRODH. The sample was purified using gravity-flow Ni-NTA affinity chromatography.

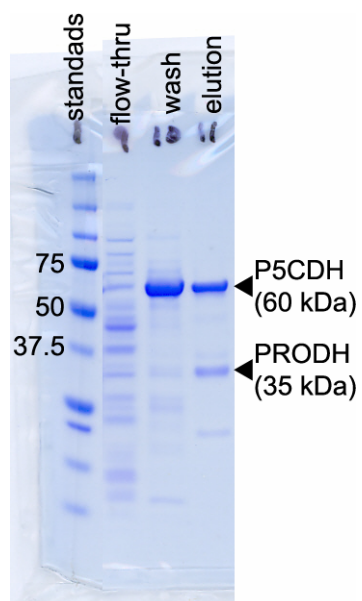


FIGURE 4.7. PRODH activity assay of coexpressed His-TtP5CDH and TtPRODH after Ni-NTA chromatography. The slope from a control assay performed without enzyme -0.0026.

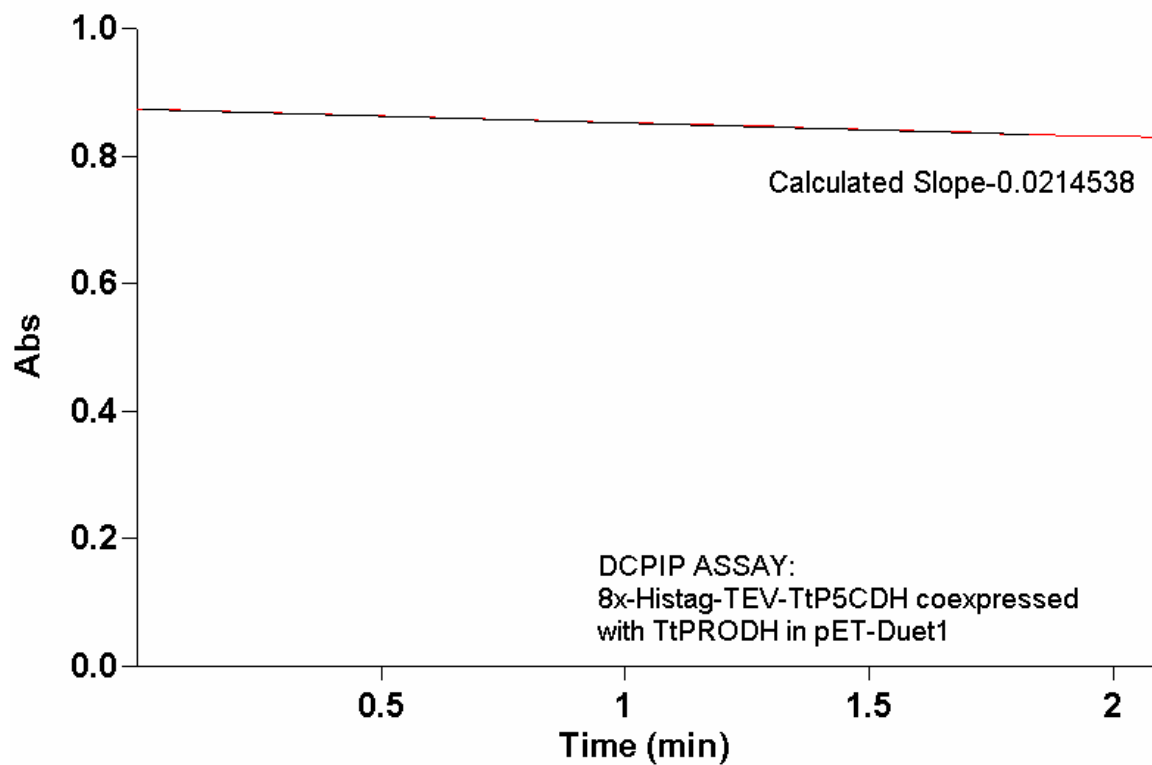


FIGURE 4.8. TtP5CDH activity assay of coexpressed His-TtP5CDH and TtPRODHD after Ni-NTA chromatography using exogenous P5C as the substrate. NADH was monitored as absorbance at 340 nm. The panels correspond to different amounts of enzyme added. The assay contained P5C (0.5 mM, pH 7), and  $\text{NAD}^+$  (0.2 mM) in MOPS (20 mM pH 7.5).

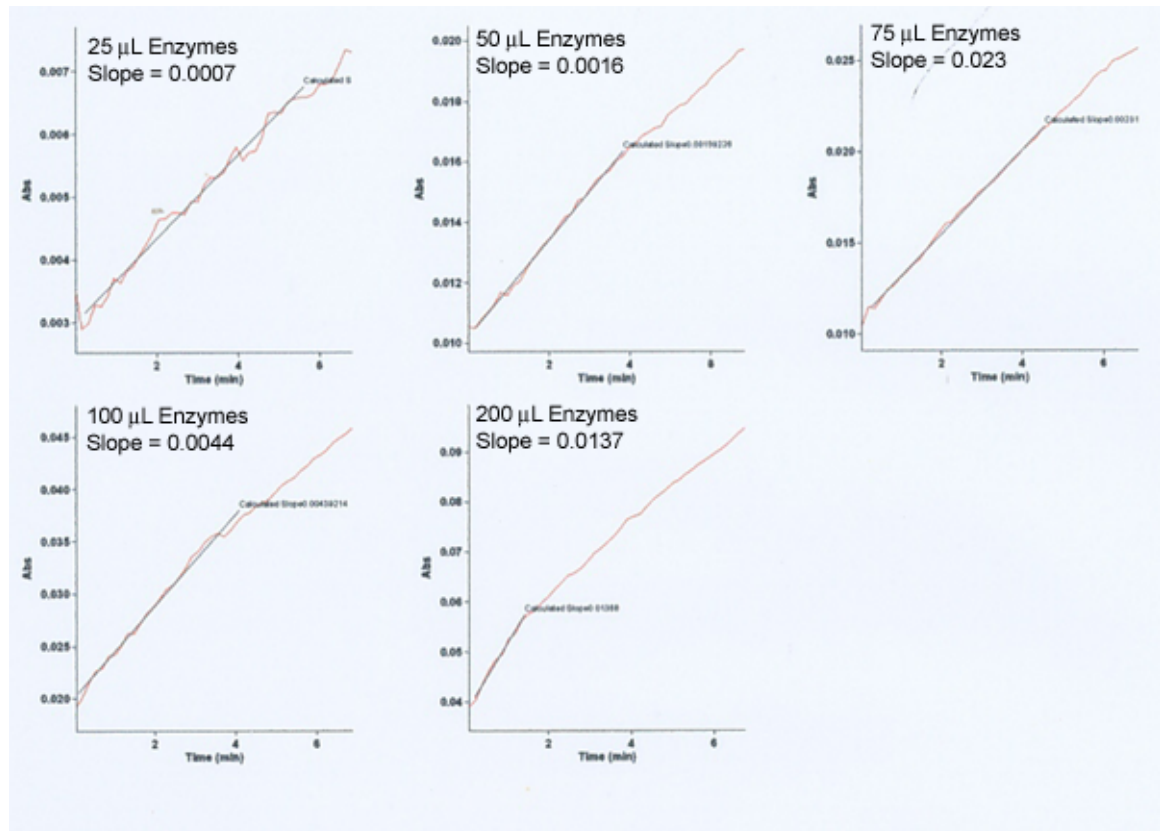




FIGURE 4.9. Gel filtration chromatogram of coexpressed His-TtP5CDH and TtPRODHD after Ni-NTA chromatography. A) Chromatogram for the enzyme sample. Note the peak at 17.6 mL is most likely due to excess flavin added during dialysis. B)  $\beta$ -amylase standard (200 kDa) run on the same day.

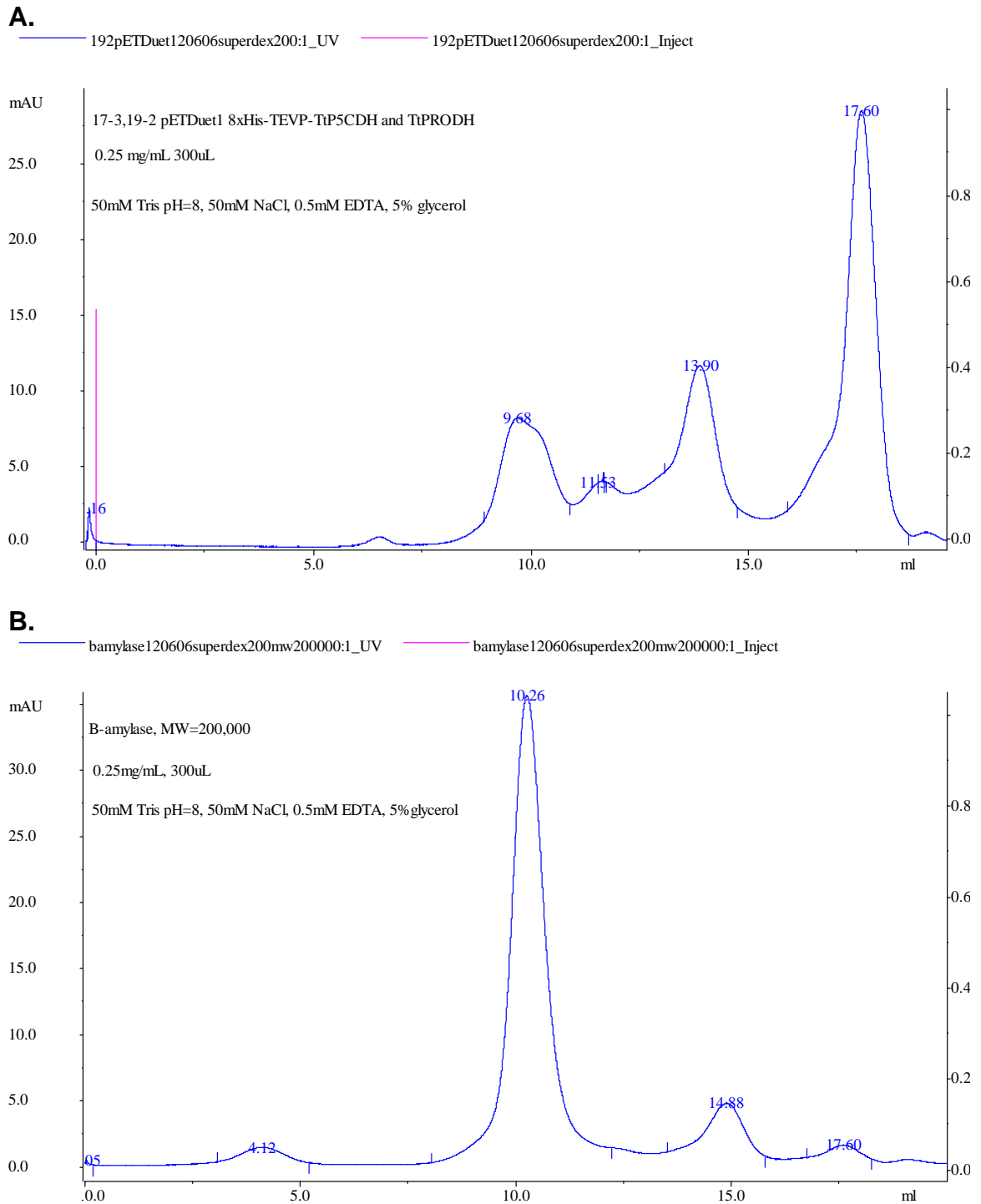


FIGURE 4.10. Detection of P5C using the o-AB assay with coexpressed His-TtP5CDH and TtPRODHD after Ni-NTA chromatography. Increasing volumes of the purified enzymes were assayed for P5C:o-AB complex formation. No NAD<sup>+</sup> or *T. thermophilus* membranes containing electron acceptors were added to these experiments. Purified 8x-histagged-TEV-TtPRODHD (20 µg) assayed with proline (30 mM) was used as a positive control (last graph).

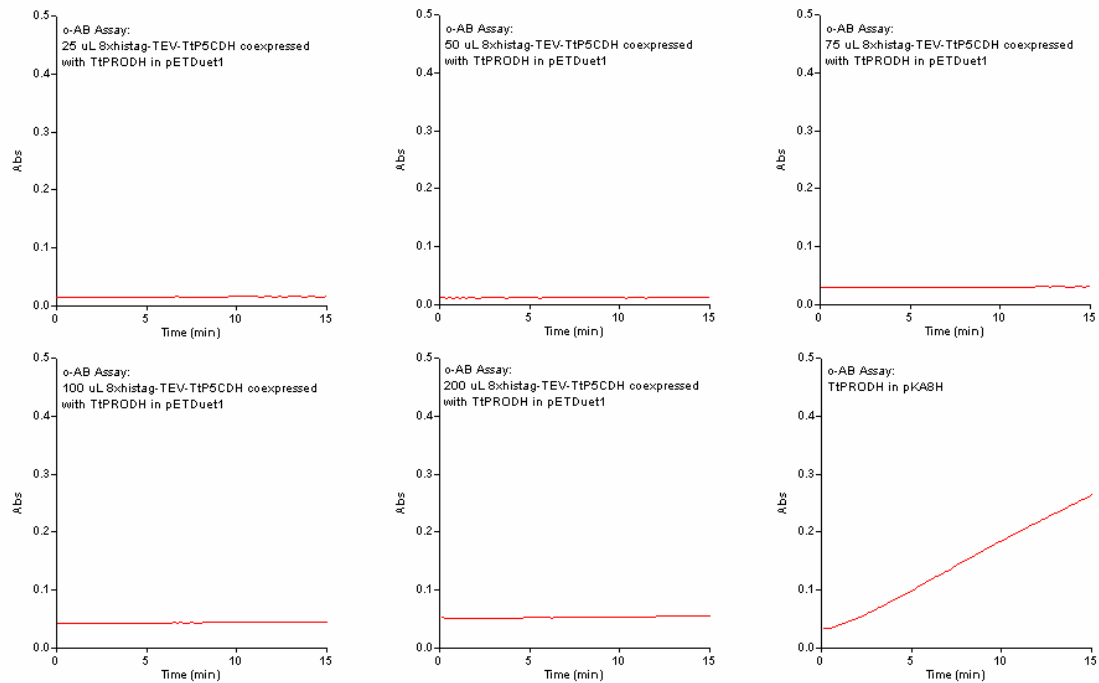


FIGURE 4.11. Detection of P5C using the o-AB assay with coexpressed His-TtP5CDH and TtPRODHD after Ni-NTA chromatography. Increasing volumes of the purified enzymes were assayed for P5C:o-AB complex formation. Proline (300 mM) and *T. thermophilus* membranes (140  $\mu$ g) containing electron acceptors were added. No NAD<sup>+</sup> was added to these experiments.

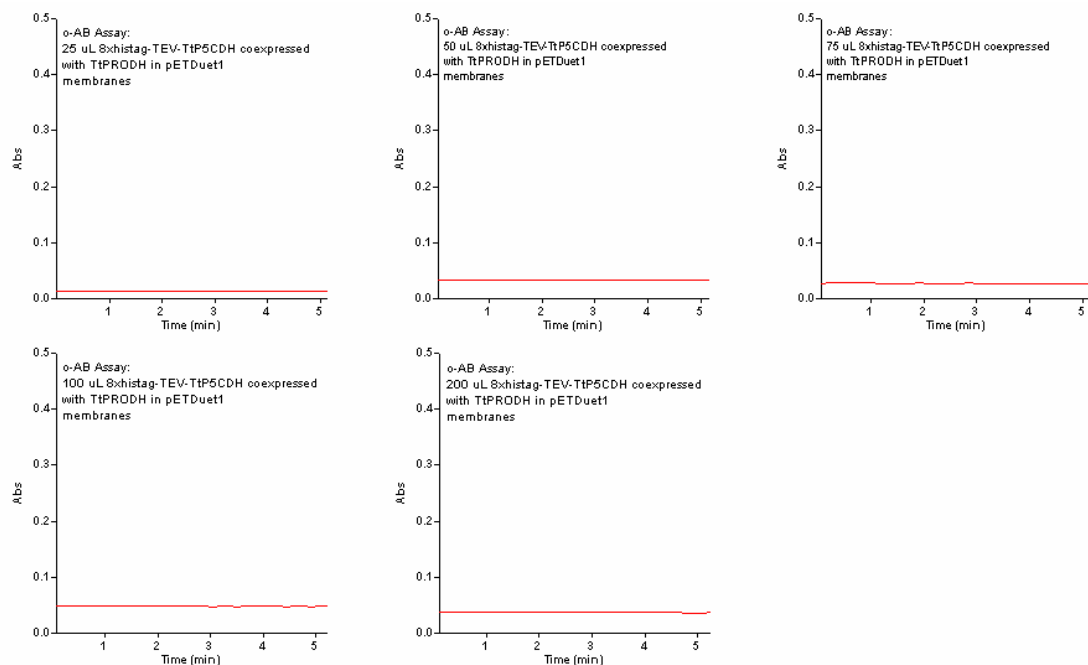


FIGURE 4.12. Detection of P5C using the *o*-AB assay with coexpressed His-TtP5CDH and TtPRODHD after Ni-NTA chromatography. Increasing volumes of the purified enzymes were assayed for P5C:*o*-AB complex formation. Proline (300 mM) and NAD<sup>+</sup> (0.2 mM) were added to these experiments. No *T. thermophilus* membranes containing electron acceptors were added. Purified 8x-histagged-TEV-TtPRODHD (20 μg) assayed with proline (30 mM) was used as a positive control (last graph).

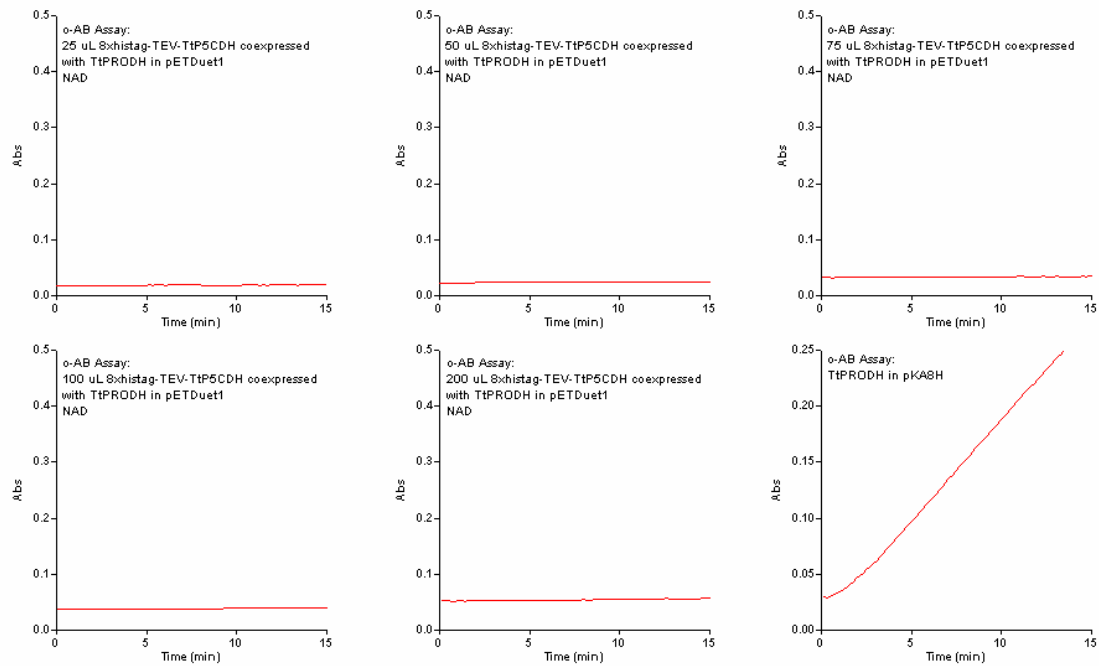


FIGURE 4.13. Detection of P5C using the o-AB assay with coexpressed His-TtP5CDH and TtPRODHD after Ni-NTA chromatography. Increasing volumes of the purified enzymes were assayed for P5C:o-AB complex formation. Both NAD<sup>+</sup> (0.2 mM) and *T. thermophilus* membranes (140 µg) containing electron acceptors were added to these experiments. Purified 8x-histagged-TEV-TtPRODHD (20 µg) assayed with proline (30 mM) was used as a positive control (last graph).

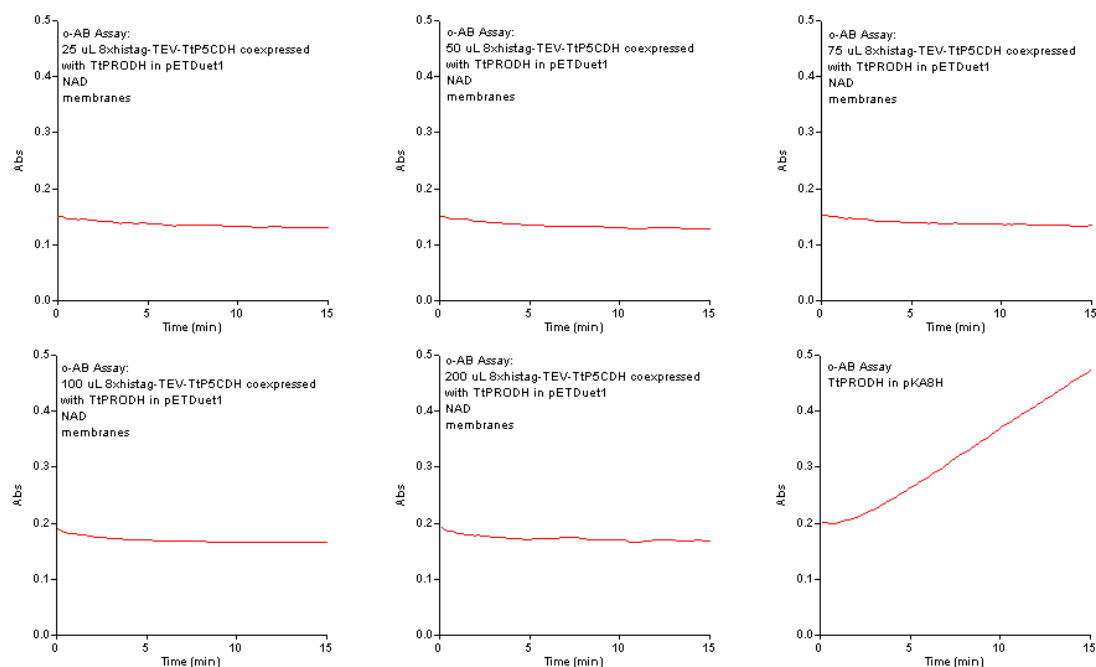


TABLE 4.1. PCR primers used for subcloning TtP5CDH and TtPRODH into pET-Duet1.

<b>TtPRODH – MCS 1</b>	
Forward	5' – TAATACGACTCACTATAGGG - 3'
Reverse	5' - TGCAGTGAATTCGGATCCCTAGCCGAAACCAGGCT - 3'

<b>TtP5CDH – MCS 1</b>	
Forward	5' – TAATACGACTCACTATAGGG - 3'
Reverse	5' - TGCAGTGAATTCGGATCCCTAGCCGAAACCAGGCT - 3'

<b>TtPRODH – MCS 2</b>	
Forward	5' - TAATACGACTCACTATAGGG - 3'
Reverse	5' - TGTTTGACAGCTTATCATCG - 3'

<b>TtP5CDH – MCS 2</b>	
Forward	5' - TAATACGACTCACTATAGGG - 3'
Reverse	5' - TGTTTGACAGCTTATCATCG - 3'

## CHAPTER 5

### Attempted Structure Determination of *Bradyrhizobium japonicum* PutA: Inherent Crystallographic Pathology

#### INTRODUCTION

Research described in this chapter continues work started by J.P. Schuermann on structure determination of *Bradyrhizobium japonicum* PutA (BjPutA). Initial structure determination was performed by JPS using crystals with hexagonal bipyramidal shape and apparent space group  $P6_222$ . Models were built using MAD and SAD phases from a selenomethionyl derivative (JPS, dissertation). Electron density was quite strong for residues 362-989 (?) and a nearly complete model in this part of the protein could be built. Density in parts of the PRODH domain was much weaker, particularly for the FAD isoalloxazine and strands near the isoalloxazine. These best model had  $R=0.26$   $R_{\text{free}}=0.36$  for data to 2.6 Å resolution. This model included 943 residues and 7142 atoms. Although the R-values is acceptable for a large protein at moderate resolution, the high value of  $R_{\text{free}}$  and the large difference between  $R_{\text{free}}$  and R indicated potential problems with the data and/or model.

A second crystal having a diamond shape was obtained in the same crystallization conditions as the hexagonal bipyramids. These crystals had apparent space group  $P4_32_12$  and the diffraction was weaker than that of the hexagonal form. Refinements against data collected from the tetragonal form also produced unacceptable statistics.

Data from both crystal forms displayed unusual intensity statistics

indicating inherent pathologies such as twinning, anisotropy and pseudosymmetry. This chapter discusses my attempts to identify these pathologies and to account for them during refinement. In the rest of this section, I discuss these various pathologies and methods of diagnosing them. I apply these techniques to the hexagonal and tetragonal crystal forms in the remainder of this chapter.

### **Crystal Pathology: Twinning, Pseudosymmetry, and Anisotropy**

Hemihedral twinning in protein crystals occurs when two crystal domains are oriented differently (1). These different domain orientations can be described by whether or not they overlap in all dimensions (2). These different orientations are related by a transformation that does not correspond to the crystal's point group symmetry, but is related to the crystal lattice (FIGURE 5.1) (1,2).

Merohedral twinning refers to crystals having a higher lattice symmetry than point group (class) symmetry (1). Merohedral twin domains overlap in all three dimensions (2). The transformation that describes the symmetry element contributing to twinning is known as the twinning operator. This is classic twinning, and is possible in higher symmetry spacegroups of trigonal, tetragonal, hexagonal or cubic (1). In the case of hemihedry, each observed intensity ( $I_{\text{obs}}$ ) is the weighted sum of the intensities of the two reflections,  $h_1$  and  $h_2$ . These reflections are not related by crystallographic symmetry, but by a twinning operation (TABLE 5.1) (2). The twin domains may contribute equally to the observed diffraction intensities (perfect twinning) or unequally (partial twinning), and is defined by the twin fraction,  $\alpha$ . For perfectly twinned crystals, the twin



fraction is 0.5 and for partial twinning the twin fraction ranges from  $0 < \alpha < 0.5$ . The following equations describe the relationships between the twin-related reflections.

$$I_{\text{obs}}(h_1) = (1 - \alpha)I(h_1) + \alpha I(h_2)$$

$$I_{\text{obs}}(h_2) = \alpha I(h_1) + (1 - \alpha)I(h_2)$$

Pseudomerohedral twinning occurs when, by chance, the crystal metric corresponds to a higher symmetry system (1). The twin domains of pseudomerohedrally twinned crystals overlap approximately, but not exactly, in 3-dimensions (2). Although pseudomerohedry is commonly unreported, this can occur in centered-orthorhombic, tetragonal, and hexagonal (3,4). Some pseudomerohedral twins may be recognized at higher resolution since the spot profiles start to split (1). Most pseudomerohedral twins have identical characteristics to merohedral twins.

Non-merohedral twinning occurs when only a subset of reflections overlap (in less than 3-dimensions), which can be seen upon inspection of the diffraction image (1,2). Inspecting diffraction intensities from twinned crystals can be useful for diagnosing non-merohedral twinning.

Besides twinning, another potential pathology is the occurrence of pseudosymmetry due to a rotation. Rotational pseudosymmetry (RPS) occurs when the rotational component of the non-crystallographic symmetry operator is approximately equal to the twinning operator in a potentially twinned crystal.

Lebedev, 2006 discusses cases of RPS, effects on these cases on the perfect twinning test, and identification (3). When a crystal is twinned, it is common that RPS exists resulting in ambiguous twinning test results.

Translational non-crystallographic symmetry (TNCS) occurs if multiple molecules occur in the asymmetric unit and are related by a parallel translation by a vector close to a fraction of one unit cell dimension. This pathology will cause some classes of reflections will have abnormally weak intensities, shifting the overall intensity distribution toward a centrosymmetric character. TNCS can occur for both twinned and non-twinned crystals. Pseudocentering is a special type of translational non-crystallographic symmetry (1).

Anisotropy is another pathology which may affect refinement (5). Anisotropic correction may be necessary if a crystal diffracts less in one dimension of reciprocal space than in the others. Anisotropically-diffracting crystals have reflections with unusual intensity distributions, similar to what is seen with translational non-crystallographic symmetry.

With the many potential crystal pathologies that can be present, it is necessary for the crystallographer to be aware of potential problems that can arise. Detection of these pathologies by careful inspection of intensities during data collection and later during refinement will facilitate speed structure determination. Methods for detecting twinning and the above pathologies are be discussed below.

### **Detection of Crystal Pathology**

Howells first introduced cumulative intensity distribution  $N(z)$  plots to

differentiate between centrosymmetric and non-centrosymmetric crystals (1,6). The variable  $z$  is the local average intensity calculated in small resolution bins and  $N(z)$  is the fraction of reflections that have intensities lower than the average. For non-centrosymmetric crystals, the fraction of reflections with lower than average intensity is less than for centrosymmetric crystals. For a twinned crystal, the fraction of the non-centrosymmetric reflections with lower than average intensities are even less. A plot can be constructed and plotting  $z$  versus  $N(z)$  results in two lines for centric and acentric reflections, known as a cumulative intensity distribution. Plotting intensity statistics for normal crystals results in exponential curves, although with a twinned crystal, a sigmoidal shape is observed for acentric reflections. Although qualitative, the cumulative intensity distribution can provide insights into unusual intensities, which may be indicative of inherent crystal pathology. For an example of a plot of cumulative intensity distributions for non-centrosymmetric reflections see FIGURE 5.2.

Normalized within resolution shells, observed intensities can be sampled in one-dimension and assigned the variable  $Z$ . The perfect twin test plots resolution versus the ratio of the average of the squared intensities over the average intensity squared,  $\langle I^2 \rangle / \langle I \rangle^2$ , also known as the second moment of  $Z$ , or  $Z^2$  (FIGURE 5.3). To perform these tests, higher resolution data should be removed where  $R_{\text{standard}}, \langle \sigma(F) \rangle / \langle F \rangle$ , increases.  $R_{\text{standard}}$  can be obtained from the program SFCHECK (7). As a function of resolution, these values should fall around 2 for an untwinned crystal. With a perfect merohedrally twinned crystal, the value of the perfect twin test will be around 1.5 (TABLE 5.2, FIGURE

5.3).

Estimation of the twin fraction is necessary for properly dealing with intensities from twinned crystals. There are multiple tests for estimating twin fraction. The most popular tests are the Britton plot, Murray Rust Plot, Yeates S(H) plot (2), Rees N(z) plot, and more recently the L-function (1,8-12). Dauter (2003) provides a good overview of each of these methods championing the Yeates S(H) plot to determine twin fraction(1). Calculation of the ratio of difference to sum of twin-related diffraction intensities ( $I_1$  and  $I_2$ ) allows one to accurately determine twinning fraction, this term is named H and is represented by the following equation.

$$H = | I_1 - I_2 | / | I_1 + I_2 |$$

Plotting H of non-centrosymmetric reflections versus the dependence of the cumulative distribution of H, known as S(H), leads to straight lines with a slope of  $1 / (1 - 2\alpha)$ . Twin fraction can be estimated from the slope of this line, which can be performed with SFCHECK, only if the program detects twinning and the spacegroup allows merohedral twinning.

Various methods of dealing with hemihedral twinning have been described. One approach is to detwin data. This results in a loss of reflections resulting in loss of completeness. This can be done with CCP4i DETWIN or CNS partial/perfect detwin scripts (13,14). Another method is to take twinning into account during refinement was described by Herbst-Irmer & Sheldrick and

implemented in SHELXL and CNS(15). During refinement, one enters the twinning operator and twin fraction.

Translational NCS or pseudocentering has the opposite effect on the perfect twin test displaying values much greater than 2, although this deviation from 2 will decrease with increasing symmetry. Although the perfect twin test may indicate twinning, it doesn't mean that the twinning will be merohedral.

For crystals displaying anisotropy and pseudocentering (TNCS), Padilla and Yeates introduced the Local Intensity function, or L-function to compare intensities that may vary systematically within crystals exhibiting these abnormalities (1,12). The L-function is based on the idea of the H-function, which was discussed earlier with merohedral twinning (1,12). The H-function which identifies twin fraction  $\alpha$ , subtracts twin-related intensities and divides this by their sum (2). Instead of using twin-related intensities, the L-function uses reflections in reciprocal space that are proximally located (1,12).

$$L = \{I(h_1) - I(h_2)\} / \{I(h_1) + I(h_2)\}$$

Using the local intensity function, anisotropic crystals that had unusual intensity statistics indicating twinning now display values that indicated these crystals were not twinned (12). Other crystals that were highly merohedrally twinned and pseudocentered displaying normal intensity statistics, utilizing L-function analysis displayed the twinned values which were indicative of the crystal's pathology. TABLE 5.1 shows expected values for normal and twinned crystals.

Examination of the self-rotation function as calculated by GLRF can help identify extra symmetry elements that are not described by the point symmetry (16). This test identifies symmetry that is related by rotation around a certain axis. Also defined as rotational pseudosymmetry, extra peaks arise in the calculated rotation functions. From these peaks, it can be determined if there are extra elements of symmetry not described by the point group.

Translational pseudosymmetry can be identified by viewing a native Patterson map at 4 Å resolution. Off-origin peaks with peak heights of 15-20% of the origin peak height indicate translational non-crystallographic symmetry. Translational non-crystallographic symmetry (TNCS) can also be detected in the perfect twin test (3). A perfect twin test having a value above much greater than 2 at moderate resolution is indicative of translational non-crystallographic symmetry. It is essential that a moderate resolution cutoff for the data is utilized to examine TNCS due to increased error of high resolution data which twinning tests do not take into account (3). Another test that can be utilized for detection of pseudocentering is the parity test (17). Systematically weak reflections are indicative of pseudocentering, a specific type of TNCS, and can be determined by calculating the average intensity ratios for even and odd reflections. A crystal displaying no pseudocentering will result in a parity test ratio of one since the intensities will be equivalent. A pseudocentered crystal will have systematically weak absences, resulting in a ratio less than one. For example, a crystal with C-face pseudocentering will have the H+K reflections odd/even less than 0.5. The weak class of reflections indicates which face is pseudocentered. Different high

resolution cutoffs should be employed to detect pseudocentering, which is more likely to show up at lower resolution cutoffs. Weak average intensity ratios can be examined with DATAMAN using the parity test (17).

Regular refinement programs such as Refmac and CNS can scale mild or moderate anisotropy. When it becomes strong or severe, other strategies for handling anisotropy are needed. Anisotropy affects R-factor in two ways. Considerable quantities of poorly measured weak reflections ( $F/\sigma < 3$ ) increases the R-factor in anisotropic diffracting crystals. The features of electron density maps are also degraded with anisotropic diffraction. This is because refinement programs scale up the weaker diffraction and scale down the stronger diffraction. Strong, et al. suggest using an ellipsoidal cutoff to remove these weak, poorly measured reflections and has designed a server to complete these calculations (5).

## **MATERIALS AND METHODS**

### **Crystals and Soaks**

Crystals used for these experiments were grown by J.P. Schuermann or D. Karr. Mutant BjPutA A310V was characterized as described previously (18). Most of the work described here is focused on crystals of native BjPutA. Some work on the A310V mutant is also described. This mutant was characterized previously by Becker's group (18).

For radical scavenging experiments, crystals were cryoprotected with the final solution containing 250 mM ascorbic acid, looped and plunged into liquid N<sub>2</sub>.

For reduction of crystals, crystals were cryoprotected with the final solution containing 25 mM L-proline and 25 mM sodium dithionite. When the yellow crystals were bleached upon reduction, they were plunged into N<sub>2</sub> (*l*).

### **Data Collection and Processing**

Several data sets were collected at APS and ALS (APPENDIX 5.1). I was responsible for data sets collected in Jan. 2005 and beyond. Jon Schuermann collected the other data sets. Although many data sets were collected and analyzed, I will focus only on a few representative ones in this thesis. Unless otherwise indicated, the representative data sets discussed here are the d8x5 data set collected from a hexagonal crystal reduced with 25 mM dithionite and 25 mM L-proline (ALS 4.2.2, September 2006), and the d3\_04\_2 data collected from a tetragonal crystal (ALS 4.2.2, May 2006). Indexing logs for these data sets are provided in APPENDIX 5.2 for d8x5 and APPENDIX 5.3 for d3\_04\_02. Data processing statistics are summarized in APPENDIX 5.4 for d8x5 and APPENDIX 5.5 for d3\_04\_02. Resolution cutoffs were determined by analyzing the high resolution bin values for  $R_{\text{merge}}$  (less than 0.4) and  $I/\sigma$  unaveraged (greater than 2).

### **Molecular Replacement**

Molecular replacement was conducted using with CCP4 MOLREP when the spacegroup was known and PHASER when exploring alternate choices of spacegroup (19,20). Models used for were initially built by J.P. Schuermann and J.J Tanner For model 104nofad.pdb 943 residues and 7142 atoms and was built using Se-Met SAD data that had been locally scaled by RESOLVE. The



refinement R-factors are  $R = 0.2968$  and  $R_{\text{free}} = 0.3859$ . From this model, another model (d8x5\_1\_001\_refmac12.pdb) was generated from multiple refinements alternating between CNS simulated annealing and Refmac5 maximum likelihood refinements utilizing TLS using the d8x5 data processed with MOSFLM in  $P6_222$  (14,21,22). This model contained chain breaks where density was lacking, especially in loops, but consisted of residues 31-992. This model has 764 residues and 5040 atoms.

### **Refinement**

Refinement (without twinning taken into account) was performed with CNS simulated annealing and Refmac5 maximum-likelihood restrained refinement utilizing TLS (14,22). Refinement with merohedral twinning was performed with CNS (14). COOT was used for viewing maps and model building (23).

### **Crystal Pathology Detection**

Several tests and programs were used to detect crystal pathologies. Inspection of cumulative intensity distributions were viewed using the CCP4i import module log graphs output (13,24). Perfect twin tests were generated using CCP4 SFCHECK utilizing all data (shown) and data truncated to 3.5 Å (not shown). L-function tests were performed using moderate resolution data (8-3.5 Å) using the web server at <http://nihserver.mbi.ucla.edu/pystats/> (12). Parity tests were conducted with DATAMAN using various values of the high resolution cut-off in the range 3 Å - 11 Å (17). Native Patterson maps were generated using the CCP4i Generate Patterson maps module using data to 4 Å resolution (13). Self rotation function maps were generated using CCP4i MOLREP using data to

4 Å resolution (19). Anisotropy was detected and resolution cutoffs made using the web server at <http://www.doe-mbi.ucla.edu/~sawaya/anisotomax/> (5).

### **Merohedral Twinning**

Merohedral twinning refinements for the hexagonal crystal form were conducted using CNS least-squares twinning refinements in all possible space groups and using various twin fractions (TABLE 5.2) (14). For the tetragonal form, the twin fraction was obtained using SFCHECK and twin operator used was provided by CNS.

## **RESULTS**

### **BjPutA Mutant A310V**

BjPutA Mutant A310V was utilized for crystallographic experiments since this mutant can be reduced fully with the substrate L-proline. Hexagonal bipyramids were grown in similar conditions as wildtype (D.Karr, personal communication). Data sets collected at ALS beamline 4.2.2 had high resolution limit of only 3 Å. A minimal model having ~63% of the residues modeled (residues 362-989) was used for refinement in REFMAC5 using space group P6<sub>2</sub>22. Typical statistics from refinement were R=0.43-0.5 and R<sub>free</sub> > 0.5. These crystals were not pursued further due to the weak resolution and poor refinement statistics.

### **Crystal Reduction, Radical Scavenging and Merging Initial Data**

On ALS beamline 8.3.1, it became apparent that the portion of the BjPutA hexagonal bipyramid crystal illuminated by the X-ray beam was being bleached

(JP Schuermann, personal communication). Radical scavenging experiments using crystals soaked in ascorbate (250 mM) and merging the initial 5° of data from several crystals (TABLE 5.3) were attempted to prevent possible conformational changes upon this potential reduction. Data was collected and processed assuming P6<sub>2</sub>22 spacegroup. Molecular replacement using MOLREP was conducted (19) with both the P5CDH domain and the entire 104nofad.pdb structure (TABLE 5.4). Refinements were conducted using CNS rigid body and simulated annealing refinement (14). The best R-factor was obtained with initial 5° merged data set had value of 0.3908 with an R<sub>free</sub> of 0.494, which was obtained by refinement of 104nofad.pdb against ALS beamline 4.2.2 May 2006 datasets 1, 2, 5, 6 and 7 (see TABLE 5.3 and TABLE 5.4 for the actual dataset names). The best R<sub>free</sub> that was obtained with any single data set had a value of 0.4875 with an R-factor of 0.3935. This was obtained by refinement of 104nofad.pdb against the single dataset ALS beamline 4.2.2 May 2006 dataset b12\_05.

### **Proline and Dithionite Reduction of BjPutA**

To lock-in conformational changes that may occur upon BjPutA reduction in the X-ray beam, the hexagonal bipyramidal crystals were reduced. Before looping, these crystals were soaked 25 mM each dithionite and L-proline until bleached indicating that these crystals were reduced (FIGURE 5.4 A-C shows diamond form). The dataset d8x5 was collected at ALS beamline 4.2.2 in September 2006. Data were processed to 2.6 Å with MOSFLM with in an apparent spacegroup of P6<sub>2</sub>22 (21). MOLREP found one molecule in the

asymmetric unit using the P5CDH domain (residues 546-992) from 104nofad.pdb as the search model. The R-factor was 0.4571 and  $R_{\text{free}}$  was 0.4894. Using both programs iteratively, after 24 rounds of refinement in CNS utilizing simulated annealing then REFMAC5 with TLS (12 rounds of each), a model (d8x5\_1\_001\_refmac12.pdb) consisting of residues 31-992 (5040 atoms) was constructed which was missing disordered loops throughout the PRODH domain and between the PRODH domain and P5CDH domain. The R-factor was 0.3529 and  $R_{\text{free}}$  was 0.4204 after REFMAC5 refinement using two TLS domains consisting of residues 31-535 and 542-992.

### **Oxidized Diamonds**

Data from diamond crystals were collected assuming spacegroup of  $P4_32_12$ . These crystals diffracted to 2.6 Å. Molecular replacement using MOLREP provided a suitable solution with two molecules in the asymmetric unit using 104nofad.pdb as the search model with an R of 0.506 and a correlation coefficient of 0.225 (19). Restrained REFMAC5 refinement (no TLS) resulted in an R-factor of 0.4176 and  $R_{\text{free}}$  of 0.489 (22).

### **Spacegroup investigation for the Hexagonal Bipyramidal form**

Alternative choices for the spacegroup were investigated for the hexagonal bipyramids. PHASER was utilized to investigate alternate choices of spacegroup using d8x5\_1\_001\_refmac12.pdb (20). The spacegroups with the highest log-likelihood gain were  $P6_222$ ,  $P6_2$ ,  $P3_221$ , and  $P32$ . CNS simulated annealing refinements of the molecular replacement solutions obtained with PHASER are listed in TABLE 5.5 (14,20). The best solution was obtained with

P3<sub>2</sub> (best R-factor of 0.3652) and P6<sub>2</sub> (best R<sub>free</sub> of 0.4165). This result is also reflected in those obtained using REFMAC5 refinement calculations post-simulated annealing in CNS, with P3<sub>2</sub> (best R-factor of 0.3399) and P6<sub>2</sub> (best R<sub>free</sub> of 0.3906) (not shown), giving the best results.

## **Analysis of Pathology Indicators**

### *Cumulative Intensity Distribution*

Upon analysis of the cumulative intensity distributions, it was observed that the data from the hexagonal bipyramids have acentric reflections with centric character (FIGURE 5.5). This indicates TNCS or pseudocentering. The diamond data sets had acentric reflections which had sigmoidal curvature, indicating twinning (FIGURE 5.6).

### *Perfect Twin Test*

A value of 2 is expected for nontwinned data and 1.5 indicates perfect twinning. Hexagonal bipyramids had a value much greater than 2 (FIGURE 5.7B, last panel). This value much greater than two indicates TNCS or pseudocentering. The perfect twin test for the diamonds had a value lower than 2, indicating twinning (FIGURE 5.8B, last panel).

### *Partial Twin test*

The partial twin test will only be reported in SFCHECK if the spacegroup allows and cumulative intensity distributions suggests twinning. For the diamonds, the partial twin test indicated a twin fraction of 0.363 (FIGURE 5.8A and FIGURE 5.8B, middle right panel.)

### *L-function*

This test is more reliable at detecting twinning when it may be masked by other pathologies. The L-function for the hexagonal bipyramids did not track along the theoretical twinned or the theoretical untwinned line (FIGURE 5.9). Although not specifically mentioned in the algorithm documentation, this indicates TNCS and pseudocentering. The diamond data track between the theoretical twinned and the untwinned curves, indicating twinning (FIGURE 5.10).

#### *Native Patterson*

Translational pseudosymmetry can be detected by the native Patterson map calculated to 4 Å. Native Patterson maps calculated for both hexagonal bipyramids (FIGURE 5.11) and diamonds (FIGURE 5.12) showed no large, off origin peaks with heights greater than 10% of the origin.

#### *Parity Tests*

Pursuing the idea of pseudocentering for the hexagonal bipyramids further, the parity test is an indicator of pseudocentering (17). Parity tests were conducted on the d8x5 data using many different resolution cutoffs. The parity test ratios obtained never indicated pseudocentering, with all ratios at or above 0.9 (not shown).

#### *Self Rotation Functions*

Rotation pseudosymmetry can be detected in the self rotation function. No extra symmetry elements were detectable in the  $\chi = 180^\circ$  for hexagonal bipyramids (FIGURE 5.13) or diamonds (FIGURE 5.14).

#### *Anisotropy Detection*

Anisotropic data can cause refinements to stall (5). Data from the

hexagonal bipyramids have strong anisotropy. Diffraction drops off quickly in the  $a^*$  and  $b^*$  dimensions (FIGURE 5.15). The diamond crystal data are much less anisotropic, displaying mild anisotropy (FIGURE 5.16). Anisotropic corrections for data can be obtained through the web-based server. Refinements in CNS against the anisotropic-corrected data did help R-factor and  $R_{\text{free}}$ , although the split between the two was not reduced.

### **Merohedral Twinning Refinements**

PHASER determined molecular replacement solutions in  $P6_2$ ,  $P3_221$ , and  $P32$  using `d8x5_1_001_refmac12.pdb` for the hexagonal bipyramids. Entering various twin fractions and twin operators (TABLE 5.6), least-squares merohedral twinning refinements were conducted using CNS (14). The statistical indicators revealed  $R_{\text{free}}$  greater than or equal to 0.40. Using the diamond data and `104nofad.pdb` as the search model,  $P4_3$  was determined by PHASER to be the best spacegroup and found 4 molecules in the asymmetric unit. Merohedral twinning refinements were conducted in this spacegroup with operator  $h, -k, -l$  utilizing a twinning fraction of 0.4. Since these crystals indicated twinning it was anticipated that this would provide the drop in R-factor and  $R_{\text{free}}$  expected. Unfortunately, the  $R_{\text{free}}$  did not drop below 0.42.

## **DISCUSSION**

### **Exploration of BjPutA oxidation and reduction**

#### *B.japonicum PutA A310V Mutant*

BjPutA has a thermodynamic barrier to become fully reduced with L-

proline due to an extremely negative reduction potential of -132 mV (18). A mutant was found that could be fully reduced with L-proline BjPutA A310V. Based on homologous structures, the proposed location of this alanine to valine mutation occurs behind the C4 and C4a portion of the isoalloxazine (FIGURE 5.17). Most other PutA proteins have valine in this position. This mutant BjPutA was utilized for crystallization trials. Unfortunately this mutated BjPutA did not resolve the issues with statistical indicators, R and  $R_{\text{free}}$ , with value of these staying above 0.4.

#### *Radical Scavenging and Merging Wedges of Initially-Collected Data*

During data collection, it was observed that the distinct yellow color of the flavin-containing BjPutA crystals was fading. This change of color is similar to what happens upon reduction of FAD with L-proline or sodium dithionite (18). It was thought that perhaps the intense X-ray beam at the synchrotron was reducing the FAD cofactor. Examples reported in the literature of reduction of enzymes by X-rays include the photolyase from *A.nidulans* and horseradish peroxidase. These enzymes contain redox sensitive sites of deazaflavin and haeme (25,26).

Synchrotron radiation-induced damage to various proteins has been reported previously (27). There are two types of radiation damage, primary and secondary (28). Ionization of an atom through photo-electric absorption or Compton scattering comprises primary radiation damage. Secondary damage is caused by formation of secondary electrons, such as free-radicals, which cause further ionization events (28). Also, photoreactive molecules may have



superexcited states which result in relaxation with damage to the enzyme their contained in or reaction with molecular oxygen to create reactive oxygen species (26,29). Dose-rate effects of radiation damage have been studied and Leiros, et al. proposes that at high dose-rates, the damage may be related to steady state free-radicals generated upon X-ray exposure (30). The total free-radical population is composed of the formation, recombination and diffusion of free-radicals and at the highest dose rates recombination may not be fast enough leading to free-radical diffusion to reduce sensitive sites (30).

It has been reported that soaking crystals with free-radical scavengers reduces the ability of radiation to reduce sensitive sites (28). Examples of scavengers are ascorbate, 1, 4-benzoquinone, 2, 2, 6, 6,-tetramethyl-4-piperidone (TEMP), and dithiothreitol (FIGURE 5.18). The effectiveness of these scavengers was investigated and varies upon the type of system utilized, but ascorbate and quinone were effective on two reduction-sensitive models (disulfide-containing protein and lipoic acids) (28) (FIGURE 5.18).

Using hexagonal bipyramidal crystals of BjPutA soaked in 250 mM ascorbate, data were collected for P6<sub>2</sub>22 spacegroup. The best data sets from ALS 4.2.2 May 2006 were identified by low merging statistics and high resolution (TABLE 5.3). To catch the oxidized enzyme before changes from radiation damage and flavin reduction occurred, merging of the first 5° of data from many crystals was attempted. TABLE 5.3 displays the data collection statistics for the merged datasets. TABLE 5.4 contains the R and R<sub>free</sub> values after CNS simulated annealing refinement with 104nofad.pdb. The drop in R and R<sub>free</sub> was

not large as anticipated with the values staying in the 0.40s.

#### *Proline & Dithionite soaks*

Since it was suspected that BjPutA changed conformation during data collection, the crystals were reduced with proline and sodium dithionite prior to data collection. If these crystals were no longer able to undergo conformational changes in the beam, it was suspected that data collection statistics and resulting maps would be better thus allowing better models to be built ultimately reflected in the statistical indicators, R and  $R_{\text{free}}$ . Once reduced, these crystals were looped and plunged into N<sub>2</sub> (l) to preserve this reduced state.

Data collection on proline/dithionite reduced crystals seemed to result in better resolution and better density maps than similar oxidized crystals. Comparing maps provided insights into the quality of structure determination. These maps were compared by viewing the unmodeled flavin density and the  $\beta$ -strands behind the flavin isoalloxazine which seemed blurred in some maps. In the case of the proline/dithionite reduced hexagonal bipyramids, the flavin density looked better with the exception of the isoalloxazine ring for which density was weak. The blurring of the density for the strands was still evident although not as much perhaps due to higher resolution data. Unfortunately, the resulting  $R/R_{\text{free}}$  statistics did not improve greatly as anticipated, with the R factor at 0.36 and  $R_{\text{free}}$  at .42 using REFMAC 5 refinement with TLS.

#### **Spacegroup Investigation for the Hexagonal Bipyramidal Form**

Initial spacegroup determination was P6<sub>2</sub>22, but upon  $R/R_{\text{free}}$  lagging with further model building, assignment of space group was revisited (APPENDIX 5.1

& 5.2). PHASER was utilized to test all spacegroups during molecular replacement (20). Hexagonal and trigonal spacegroups were used in refinements to see if drops in  $R/R_{\text{free}}$  occurred (TABLE 5.5). One caveat to consider when making these comparisons is to include the number of atoms used in the refinement (indicated by mol/ASU in TABLE 5.5). The more atoms in the model, the more likely that artificial decreases in R-factor are seen. Another consideration is the completeness of the data utilized. The R-factor and  $R_{\text{free}}$  can be artificially decreased by using less complete data, which can occur from attempting to decrease point group symmetry when only enough data was collected for the higher symmetry point group,. Data utilized in CNS refinements is indicated by percent of total reflections included in the refinement (indicated by % reflections in TABLE 5.5).  $R/R_{\text{free}}$  statistics were only decreasing slightly, most likely to the increasing number of atoms in the asymmetric unit. To no avail, this investigation did not shed light on an alternative space group.

### **Examination of Intensity Distributions, Anisotropy and Twinning**

#### *Hexagonal Bipyramids*

After much crystal manipulation, literature review of various pathological cases proved fruitful. Examining at the various pathology indicators described above, provided new insights about BjPutA hexagonal bipyramidal crystals.

Cumulative intensity distributions  $N(z)$  plots created with CCP4 did not show the signature sigmoidal curves of a twinned crystal (FIGURE 5.5) (13). Although, on closer inspection it revealed that the acentric reflections had a very centric character, with the observed acentric reflections tracking just above of the

centric theoretical reflections. According to Dauter, this is indicative of a crystal with translational non-crystallographic symmetry, whether it is twinned or untwinned (1). Using SFCHECK to analyze the data, the second moment of Z displayed a much higher value than 2 (FIGURE 5.7B, last panel) (7). Although Dauter would argue that for proper analysis only lower resolution data (less than 3.5 Å) should be utilized for the perfect twin test, cutting off data at 3.5 Å still gave an average second moment of Z higher than 2 (not shown). These two tests are indicating that perhaps we have translational non-crystallographic symmetry.

To investigate further this idea of translational non-crystallographic symmetry, a native Patterson map with data truncated to 4 Å was generated using CCP4i (FIGURE 5.11A) (13). As stated earlier, if TNCS is present, a peak in the map with 15-20 % of the origin peak height will appear. Peaks with this height were never encountered upon calculation of the native Patterson (FIGURE 5.11 A & 5.12 B), although some smaller peaks were present in the native Patterson however. SFCHECK confirms the lack of TNCS in the output report stating that there is no translational pseudosymmetry detected (FIGURE 5.7A).

The L-function, which has been shown to be a robust way to analyze intensities, displayed an unusual feature not described by the Padilla and Yeates paper (12). Analyzing our moderate resolution data and with the L-function server showed our data tracking below the line for untwinned data (FIGURE 5.9). This result most likely indicates pseudocentering.

The possibility that the crystal is pseudocentered was investigated. From

P6<sub>2</sub>22, symmetry allows for C-centered orthorhombic to be a potential space group. The indexing of d8x5 from ALS May 2006 is shown in APPENDIX 5.2. This shows a least squares residual of 0.094 for selection of a centered orthorhombic space group as compared to 0.156 for P6<sub>2</sub>22. Although perfect twin tests, the L-test and cumulative intensity distributions indicated pseudocentering, parity tests did not indicate pseudocentering (not shown). Refinements were conducted against 2.6 Å C222 d\*TREK-processed data (APPENDIX 4). With only 83.8% of the data used for CNS simulated-annealing refinements, statistical indicators did not drop significantly, with R-factor = 0.36 and R<sub>free</sub> = 0.42.

Rotational pseudosymmetry was examined using a resolution cut-off of 4 Å using MOLREP (19). The P6<sub>2</sub>22 d8x5 ALS September data  $\chi = 180$  section of the self rotation function shows a 6-fold symmetry (FIGURE 5.13A). When processed in P3 (FIGURE 5.13B, the  $\chi = 180$  still shows a 6-fold symmetry, although the self rotation function looks a little different but the features are not strong. These maps indicate no rotational pseudosymmetry.

Anisotropy, which can cause refinement to stall, was also investigated. Indeed d8x5 showed strong anisotropy as indicated by the Diffraction Anisotropy Server (5). FIGURE 5.15A and FIGURE 5.15B displays the results from analysis of our data for anisotropy. FIGURE 5.15A shows much higher diffraction in the c\* direction and diffraction in the a\* and b\* directions. Ellipsoidal truncation of the data to 2.7 Å was applied (FIGURE 5.15B) and used in refinement. Although we did see better statistics, truncation did not significantly improve our refinement values.

Twinning was investigated utilizing CNS least-squares twin simulated annealing refinement. Various space groups with merohedral twin operators and various twin fractions were used. Using  $P6_2$ ,  $P3_221$ ,  $P3_2$  space groups, refinement taking twinning into account dropped the R-factor to 0.30-0.32 depending on space group and twin fraction, but the  $R_{\text{free}}$  never dropped below 0.40 (TABLE 5.6).

### *Diamonds*

Diamond-shaped crystals would sometime occur in the same crystallization drops as the hexagonal bipyramidal crystals. The best diffraction obtained with these crystals was 2.7 Å. Originally, the Laue group was thought to be 4/mmm and data were collected accordingly at the Advanced Light Source, beamline 4.2.2. Indexing of these crystals is shown in APPENDIX 5.3. Further investigation of systematic absences with dtcell showed the most likely spacegroup was  $P4_32_12$  (24). Molecular replacement provided a suitable solution, although upon refinement, the  $R/R_{\text{free}}$  still remained high.

After looking at cumulative intensity distributions, the observed acentric reflections showed a sigmoidal curvature, indicating twinning (FIGURE 5.6). The perfect twinning test  $\langle I^2 \rangle / \langle I \rangle^2$  was  $\sim 1.7$  with this being displayed in the SFCHECK output (FIGURE 5.8B last panel). Utilizing the L-function analysis to analyze local intensities, the d3\_04\_2 data tracked between the theoretically untwinned and perfectly twinned curves (FIGURE 5.10) indicating twinning. Peak heights with 15-20% of the origin peak height were not detected in 4 Å native Patterson map (FIGURE 5.12). Pseudo translations were not detected by

SFHECK (FIGURE 5.8A). Self-rotation functions of data processed in P4 indicated a four-fold symmetry at  $\chi = 180^\circ$  (FIGURE 5.14), although no other strong rotational pseudosymmetry was seen. Anisotropy was checked and these crystals had mild anisotropy (FIGURE 5.16A). Slight ellipsoidal truncation was not performed since refinement programs can handle mild anisotropy (FIGURE 5.16B).

Pursuing the idea of twinning further, least-squares merohedral twinning refinements were conducted. The Yeates S(H) plot and the partial twinning test estimated a partial twin fraction of 0.36-0.4 (2) (FIGURE 5.8A & 9B middle right panel). Upon reindexing the data choosing P4 with unit cell dimensions of  $a=138.17 \text{ \AA}$   $c= 267.3 \text{ \AA}$ , PHASER was utilized to find a proper molecular replacement solution, with the best log-likelihood gain occurring in  $P4_3$  (20). Although twinning was suspected, least-squares twinning refinement utilizing the P4 merohedral twinning operator and calculated twin fraction 0.4 resulted in 81% data used in refinement, with a  $R = 0.27$  and  $R_{\text{free}} = 0.40$ .

### **Pseudomerohedral twinning**

Interestingly, Parsons discusses pseudomerohedrally twinned crystals that emulate tetragonal symmetry which are actually orthorhombic ( $\beta \sim 90^\circ$ ) (4). These are related by a two-fold rotation around the longer dimension's (usually  $c^*$ ) axis or around the diagonal along the  $a^*-b^*$  axis.

Parsons also discusses a similar case for pseudomerohedrally twinned monoclinic crystals that emulate hexagonal crystals ( $\beta \sim 120^\circ$ ), although there are more than two twin domains that occur (4). A three-domain twinning case was

recently described for the aclacinomycin oxidoreductases where they utilized a three-domain twin operator to describe the symmetry (31).

Studies of BjPutA and the d3\_04\_2 datasets are currently being investigated for the occurrence of pseudomerothedral twinning. Since the diamond crystals may be emulating a tetragonal spacegroup, it is suspected that the twin operator will be a two-fold around the  $c^*$  axis described by  $-k, h, l$  or a diagonal in the  $a^*-b^*$  plane  $k, h, -l$ . Current difficulties include finding datasets to merge together to obtain a complete dataset to perform refinements. Only two programs are currently available to handle refinements of data with pseudomerothedral twinning; SHELX and PHENIX (15,32).

A new program from the PHENIX program suite (PHENIX.xtriage) was also used to analyze data collected from the diamond-shaped crystals (apparent tetragonal form). This analysis was performed on a d3\_04 data set that had been processed in  $P2_12_12_1$ . The data set was 90 % complete to 2.8 Å. The analysis indicated pseudomerothedral twinning with twin operator  $-k, -h, -l$ . Thus, refinement assuming pseudomerothedral twinning was investigated.

Using a search model created from d8x5\_1\_001\_refmac12.pdb (04.pdb obtained from JJ Tanner), a suitable molecular replacement solution was identified using MOLREP with 4 molecules in the asymmetric unit. PHENIX.refine was used for refinement since it is the only program currently available that properly treats pseudomerothedral twinning at moderate resolution. The least squares twinning refinements previously described by Herbst-Irmer and Sheldrick (15) has been implemented in PHENIX.refine. (We note that SHELX



also treats pseudomerohedral twinning but it is not recommended at moderate resolution.)

Non-crystallographic symmetry restraints were utilized for refinements with or without twinning. The untwinned refinement resulted in  $R = 0.4093$  and  $R_{\text{free}} = 0.4491$ . The analogous refinement taking twinning into account resulted in significantly lower R-factors of  $R = 0.3089$  and  $R_{\text{free}} = 0.3554$ . After 7 rounds of PHENIX least squares twin refinement the current model has 844 residues and  $R = 0.2691$  and  $R_{\text{free}} = 0.3132$ . These twinning refinements have revealed previously unobserved density for the N-terminal domain which in previously modeled structures had been incorrectly modeled or not modeled at all.

### **Strategies for Structure Completion**

The current crystal forms of BjPutA have an inherent pathology which could be described by pseudomerohedral twinning and current refinements have lowered both R-factor and  $R_{\text{free}}$  substantially with anticipation of structure completion. Other strategies that are currently being pursued are finding a new crystal form of BjPutA and homolog screening.

One way other crystal forms could be obtained is by cleaving off the TEV-protease cleavable 8x-Histidine affinity tag. Removal of the histidine tag may allow the enzyme to pack differently in the crystal lattices resulting in a new crystal form. Another strategy is lysine methylation, which has been shown to be an effective strategy for obtaining crystals (33). Lysine methylation targets the primary amine of surface lysines and converts the primary amine to a tertiary amine by methylation. Lysine methylation is a better alternative to surface

mutagenesis since the modifications only happen on the surface of a folded protein. The result is a change in the overall surface charge, and disruption of salt bridges formed on the surface. As discussed in Chapter 3, *N*-propargylglycine has been shown to inhibit PutA (D Srivastava and JD Larson, unpublished results). Inactivation of BjPutA may be an effective way to obtain the reduced crystal form without reoxidation and may provide a new crystal form.

Homolog screening is yet another method for obtaining a bifunctional PutA structure. *Legionella pneumophila* and *Pseudomonas aeruginosa* are two bifunctional PutA enzymes that are cloned and show promise with expression of monodisperse, soluble protein. Moreover, small crystals of LpPutA have been obtained (JD Larson and D Srivastava, unpublished results). LpPutA also has a TEV-protease cleavable 6x-Histidine tag and cleavage could aid in crystallization trials. There are more PutA homologs to be examined, some of which include *Shewanella* sp., *Wolbachia* sp., *Xanthomonas* sp., and *Rhodopseudomonas* sp.

Improvements in detecting crystal pathology during data collection and refinement should aid in structure determination. Outlined in this chapter are the various pathologies that have been detected in the literature, methods for their remedy and application to pathological crystals of BjPutA.

## REFERENCES

1. Dauter, Z. (2003) *Acta Crystallogr D Biol Crystallogr* **59**, 2004-2016
2. Yeates, T. O. (1997) *Methods Enzymol* **276**, 344-358
3. Lebedev, A. A., Vagin, A. A., and Murshudov, G. N. (2006) *Acta Crystallogr D Biol Crystallogr* **62**, 83-95
4. Parsons, S. (2003) *Acta Crystallogr D Biol Crystallogr* **59**, 1995-2003
5. Strong, M., Sawaya, M. R., Wang, S., Phillips, M., Cascio, D., and Eisenberg, D. (2006) *Proc Natl Acad Sci U S A* **103**, 8060-8065
6. Howells, E., DC, P., and D, R. (1950) *Acta Crystallography D* **3**, 210-214
7. Vaguine, A. A., Richelle, J., and Wodak, S. J. (1999) *Acta Crystallogr D Biol Crystallogr* **55**, 191-205
8. Britton, D. (1972) *Acta Crystallography A* **28**
9. Murray Rust, P. (1973) *Acta Crystallogr B* **29**, 2559-2566
10. Yeates, T. O. (1988) *Acta Crystallography A* **44**, 142-144
11. Rees, D. C. (1980) *Acta Crystallographica A* **36**, 578-581
12. Padilla, J. E., and Yeates, T. O. (2003) *Acta Crystallogr D Biol Crystallogr* **59**, 1124-1130
13. 4, C. C. P. N. (1994) *Acta Crystallography D* **50**, 760-763
14. Brunger, A. T., Adams, P. D., Clore, G. M., DeLano, W. L., Gros, P., Grosse-Kunstleve, R. W., Jiang, J. S., Kuszewski, J., Nilges, M., Pannu, N. S., Read, R. J., Rice, L. M., Simonson, T., and Warren, G. L. (1998) *Acta Crystallogr D Biol Crystallogr* **54**, 905-921
15. Herbst-Irmer, R., and Sheldrick, G. M. (2002) *Acta Crystallogr B* **58**, 477-481
16. Tong, L., and Rossmann, M. G. (1997) *Methods Enzymol* **276**, 594-611
17. Kleywegt, G. J., and Jones, T. A. (1996) *Acta Crystallogr D Biol Crystallogr* **52**, 826-828
18. Krishnan, N., and Becker, D. F. (2005) *Biochemistry* **44**, 9130-9139
19. Vagin, A., and Teplyakov, A. (1997) *Journal of Applied Crystallography* **30**, 1022-1025
20. Storoni, L. C., McCoy, A. J., and Read, R. J. (2004) *Acta Crystallogr D Biol Crystallogr* **60**, 432-438
21. Leslie, A. G. (2006) *Acta Crystallogr D Biol Crystallogr* **62**, 48-57
22. Murshudov, G. N., Vagin, A. A., and Dodson, E. J. (1997) *Acta Crystallogr D Biol Crystallogr* **53**, 240-255
23. Emsley, P., and Cowtan, K. (2004) *Acta Crystallogr D Biol Crystallogr* **60**, 2126-2132
24. Pflugrath, J. (1999) *Acta Crystallography D* **55**, 1718-1725
25. Berglund, G. I., Carlsson, G. H., Smith, A. T., Szoke, H., Henriksen, A., and Hajdu, J. (2002) *Nature* **417**, 463-468
26. Kort, R., Komori, H., Adachi, S., Miki, K., and Eker, A. (2004) *Acta Crystallogr D Biol Crystallogr* **60**, 1205-1213
27. Banumathi, S., Zwart, P. H., Ramagopal, U. A., Dauter, M., and Dauter, Z. (2004) *Acta Crystallogr D Biol Crystallogr* **60**, 1085-1093

28. Southworth-Davies, R. J., and Garman, E. F. (2007) *J Synchrotron Radiat* **14**, 73-83
29. Wondrak, G. T., Jacobson, M. K., and Jacobson, E. L. (2005) *J Pharmacol Exp Ther* **312**, 482-491
30. Leiros, H. K., Timmins, J., Ravelli, R. B., and McSweeney, S. M. (2006) *Acta Crystallogr D Biol Crystallogr* **62**, 125-132
31. Sultana, A., Alexeev, I., Kursula, I., Mantsala, P., Niemi, J., and Schneider, G. (2007) *Acta Crystallogr D Biol Crystallogr* **63**, 149-159
32. Adams, P. D., Grosse-Kunstleve, R. W., Hung, L. W., Ioerger, T. R., McCoy, A. J., Moriarty, N. W., Read, R. J., Sacchettini, J. C., Sauter, N. K., and Terwilliger, T. C. (2002) *Acta Crystallogr D Biol Crystallogr* **58**, 1948-1954
33. Walter, T. S., Meier, C., Assenberg, R., Au, K. F., Ren, J., Verma, A., Nettleship, J. E., Owens, R. J., Stuart, D. I., and Grimes, J. M. (2006) *Structure* **14**, 1617-1622

FIGURE 5.1. An example of a twinned diffraction pattern from a hexagonal crystal in the P6 space group. The two upper figures represent different orientations of diffraction patterns from a P6 spacegroup, but the patterns are oriented within the hexagonal P622 symmetry. They are related by a two-fold rotation around the  $a^*$  axis. In the upper figures, the selected reflections have varying intensities when in P6. In a perfect twin (bottom), the two upper orientations superimpose, the diffraction pattern acquires a P622 symmetry and the intensities average together. Taken from Dauter "Twinned Crystals and anomalous phasing" 2003 (1).

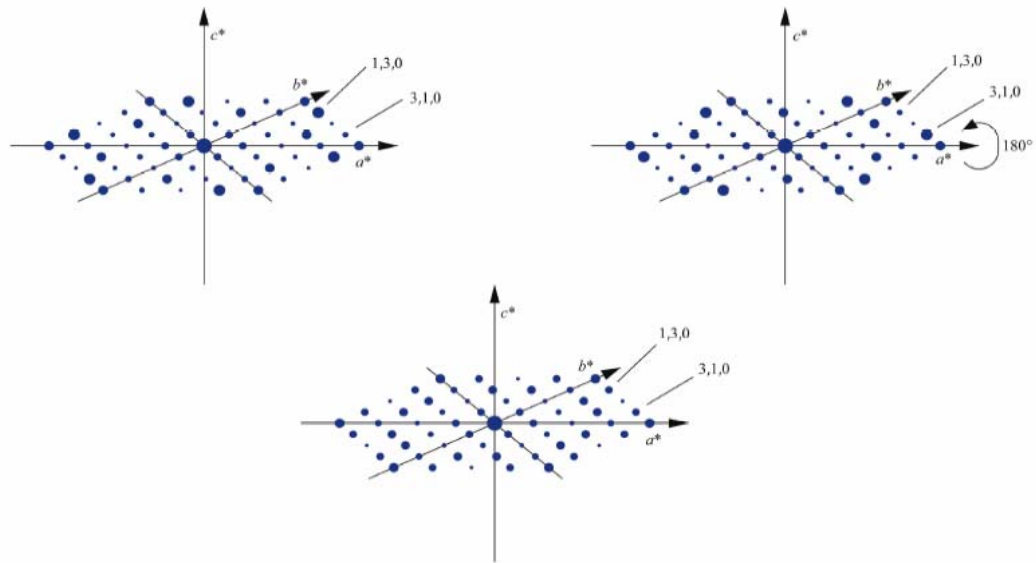


FIGURE 5.2. Example of expected cumulative intensity distribution for an untwinned crystal (upper exponential curve) and purely twinned crystal (sigmoidal curve). Dotted lines represent pathological crystals from gpD (blue dots) and IL- $\beta$  (red dots). Taken from Dauter “Twinned Crystals and anomalous phasing” 2003(1).

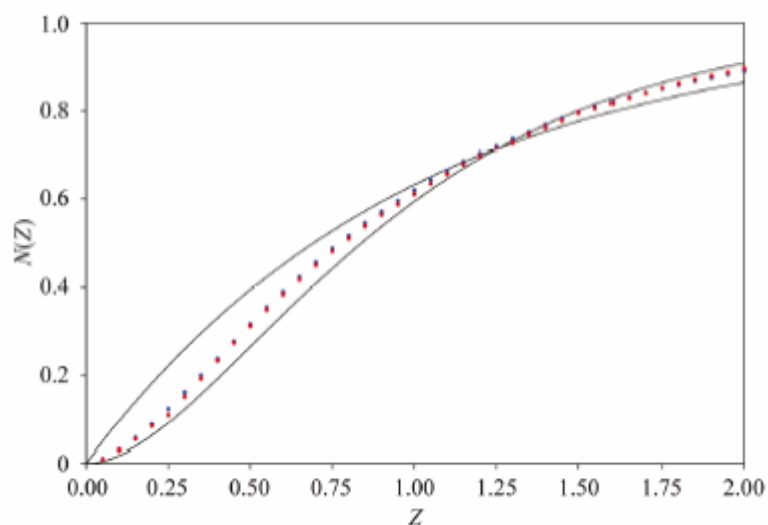


FIGURE 5.3. Example of the Perfect Twin Test and sample data (taken from Dauter, 2003). The green curve indicates a untwinned data and the blue and red curves indicate twinning (1).

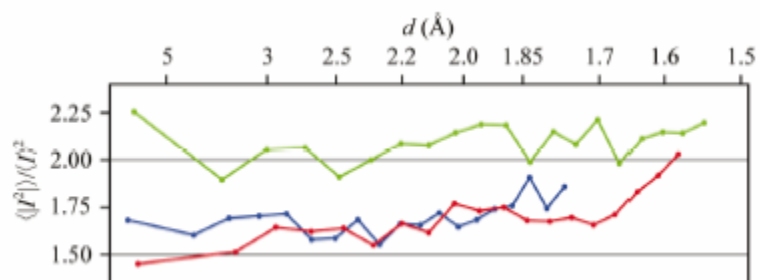


FIGURE 5.4. Redution of BjPutA with 25 mM sodium dithionite. A) BjPutA fully oxidized. B) BjPutA after addition of sodium dithionite. C) Fully reduced BjPutA.

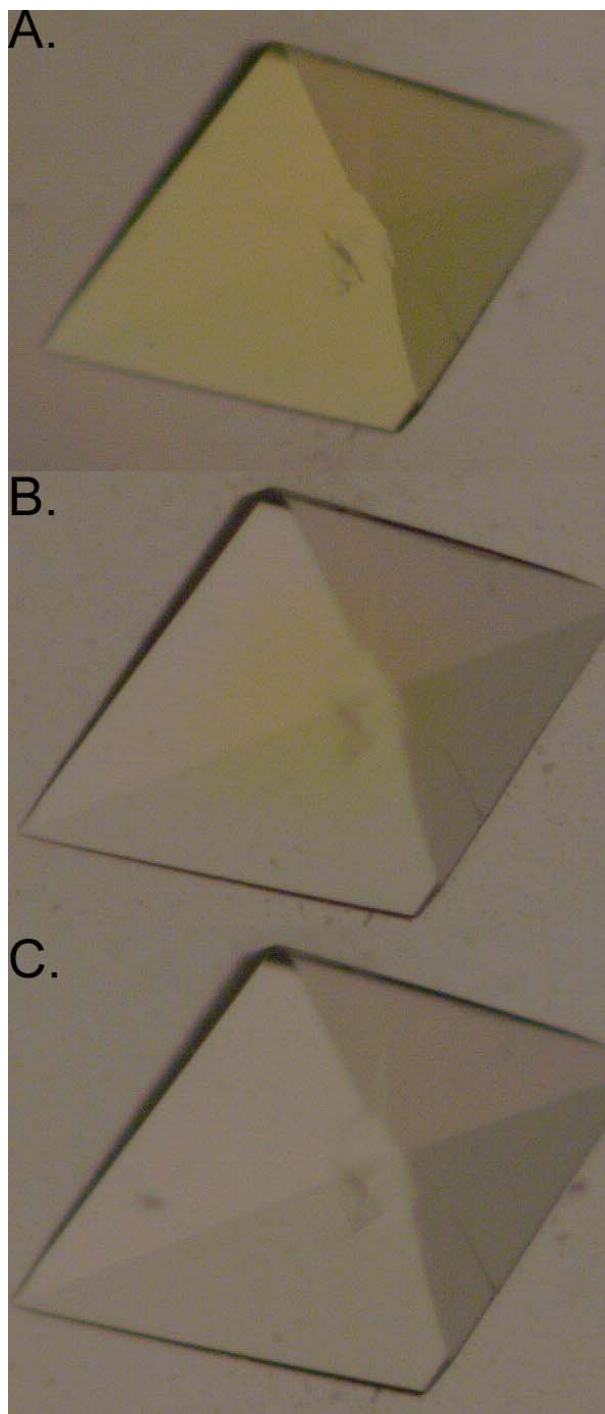




FIGURE 5.5. Cumulative intensity distribution created upon import of scaled data into CCP4 using MOSFLM-processed ALS May 2006 d8x5 to 2.6 Å. Green and red lines track normal theoretical intensity distributions for centric and acentric reflections, respectively. Black and blue lines track our experimentally determined intensity distributions for centric and acentric reflections, respectively.

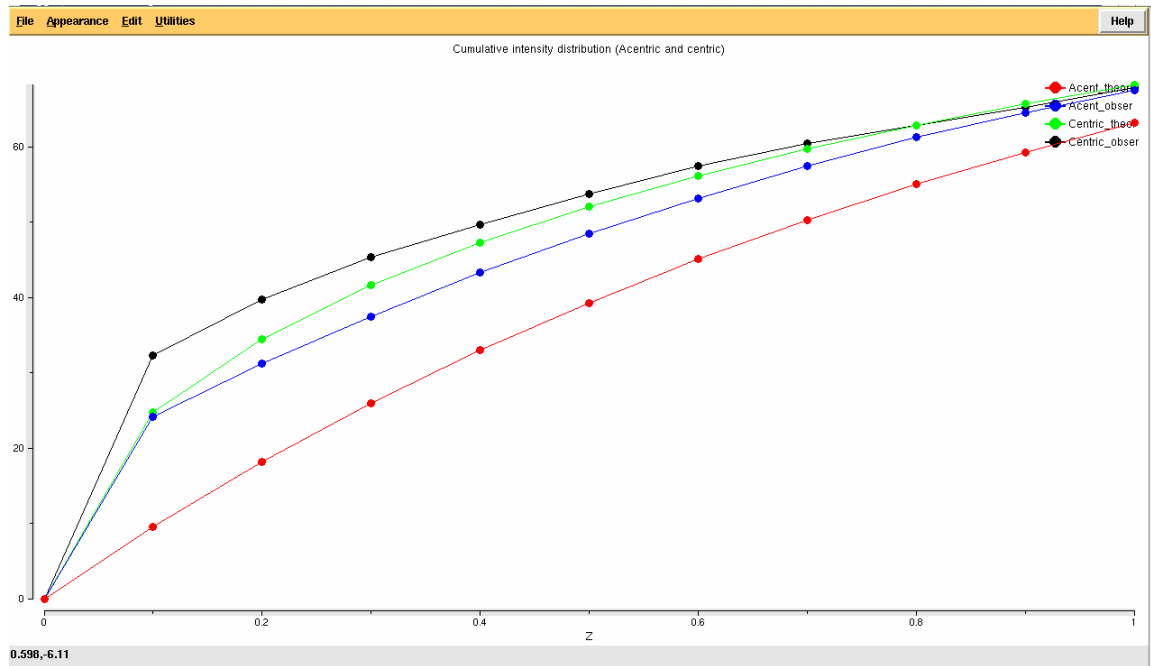


FIGURE 5.6. Cumulative intensity distribution created upon import of scaled data into CCP4. Using d\*TREK-processed ALS May 2006 d3\_04\_2 to 2.8 Å. Green and red lines track normal theoretical intensity distributions for centric and acentric reflections, respectively. Black and blue lines track our experimentally determined intensity distributions for centric and acentric reflections, respectively.

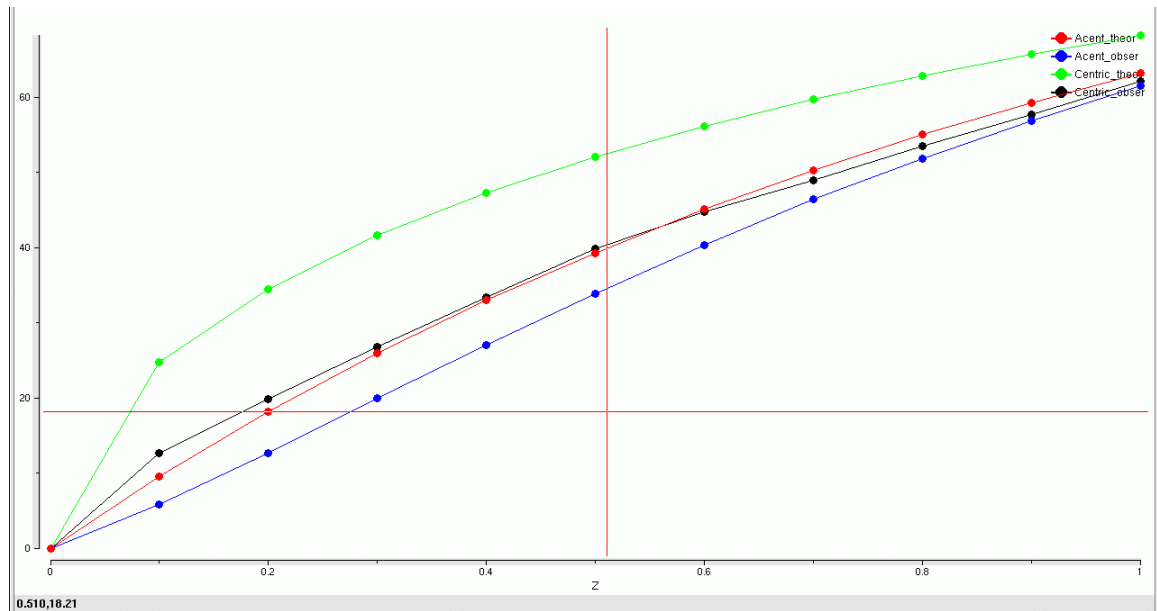


FIGURE 5.7A. SFCHECK output for ALS September 2006 d8x5 MOSFLM-processed data to 2.6 Å showing the data statistics, pseudotranslations, Wilson Plot, completeness and Rstandard, optical resolution, coordinate errors and the perfect twinning test.

"Judge not, that you be not judged" Bible, Matthew, ch.7

## Structure Factor Check

### XXXX

Title:  
Date:  
PDB code: XXXX

Crystal	Structure Factors
<p>Cell parameters:  a: 145.25 Å    b: 145.25 Å    c: 185.42 Å  α: 90.00°    β: 90.00°    γ: 120.00°  Space group: P 62 2 2</p>	<p>Input  Nominal resolution range: 43.50 – 2.65 Å  Reflections in file: 33744  Unique reflections above 0: 33744  above 1σ: 33077  above 3σ: 21143</p> <p><b>SFCHECK</b>  Nominal resolution range: 43.50 – 2.65 Å  (max. from input data, min. from author)  Used reflections: 33744  Completeness: 98.8 %  R<sub>std</sub>(F) = <math>\langle \sigma(F) \rangle / \langle F \rangle</math> : 0.052  Anisotropic distribution of Structure Factors  ratio of eigen values: 1.0000 1.0000 0.4855  B<sub>overall</sub> (by Patterson): 45.5 Å<sup>2</sup>  Optical resolution: 2.02 Å  Expected opt. resol. for complete data set: 2.02 Å  Estimated initial error: 0.052 Å  Pseudo-translation is not detected</p>

BIO-RAPID v. 2.2

FIGURE 5.7B. Continued SFCHECK output for ALS September 2006 d8x5 MOSFLM-processed data to 2.6 Å showing the data statistics, pseudotranslations, Wilson Plot, completeness and  $R_{\text{standard}}$ , optical resolution, coordinate errors and the perfect twinning test.

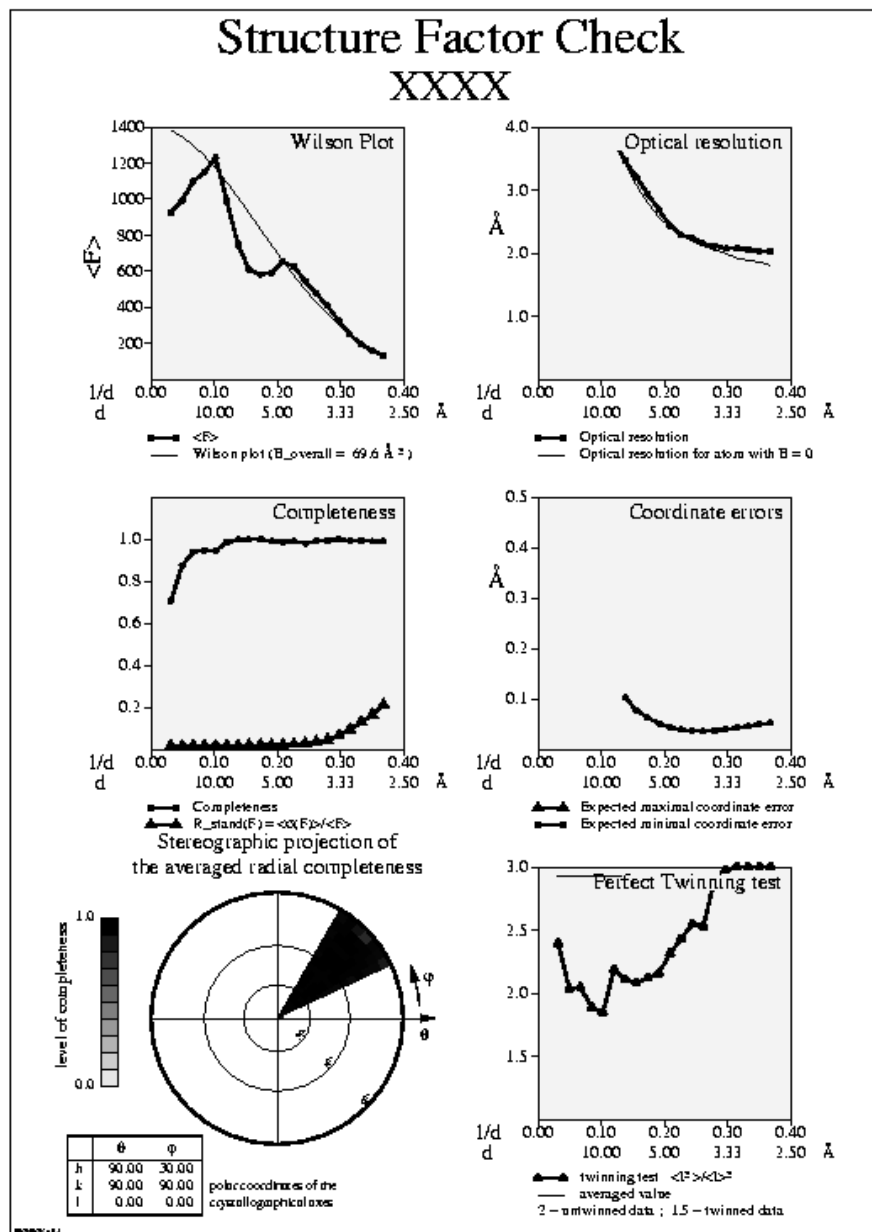


FIGURE 5.8A. Output from SFCHECK utilizing d\*TREK-processed ALS May 2006 d3\_04\_2 data.

<p><small>*Judge not, that you be not judged* Bible, Matthew, ch.7</small></p> <h1>Structure Factor Check</h1> <h2>XXXX</h2>	
<div> <div> <p>Title:</p> <p>Date:</p> <p>PDB code: XXXX</p> </div> <div> <h3>Crystal</h3> <p>Cell parameters:</p> <p>a: 138.03 Å    b: 138.03 Å    c: 267.04 Å</p> <p>α: 90.00°    β: 90.00°    γ: 90.00°</p> <p>Space group: P 43</p> </div> </div>	
<div> <h3>Structure Factors</h3> <p>Input</p> <p>Notation resolution range: 46.01 – 2.80 Å</p> <p>Reflections in file: 107060</p> <p>Unique reflections above 0: 107060</p> <p>                          above 1σ: 106874</p> <p>                          above 3σ: 75353</p> <p>SFCHECK</p> <p>Notation resolution range: 46.01 – 2.80 Å</p> <p>                          (max. from input data, min. from author)</p> <p>Used reflections: 107059</p> <p>Reflections out of resolution: 1</p> <p>Completeness: 97.6%</p> <p>R<sub>stnd</sub>(F) = &lt;σ(F)&gt;/&lt;F&gt; : 0.099</p> <p>Anisotropic distribution of Structure Factors</p> <p>          ratio of eigen values: 0.7773 0.7773 1.0000</p> <p>B<sub>ovetall</sub> (by Patterson): 42.4 Å<sup>2</sup></p> <p>Optical resolution: 2.04 Å</p> <p>Expected opt. resol. for complete data set: 2.04 Å</p> <p>Estimated minimal error: 0.061 Å</p> <p>Pseudo-translation is not detected</p> <p>Probably crystal is twinned</p> <p>Twinning fraction: 0.363</p> </div>	

FIGURE 5.8B. Output from SFCHECK utilizing d\*TREK-processed ALS May 2006 d3\_04\_2 data.

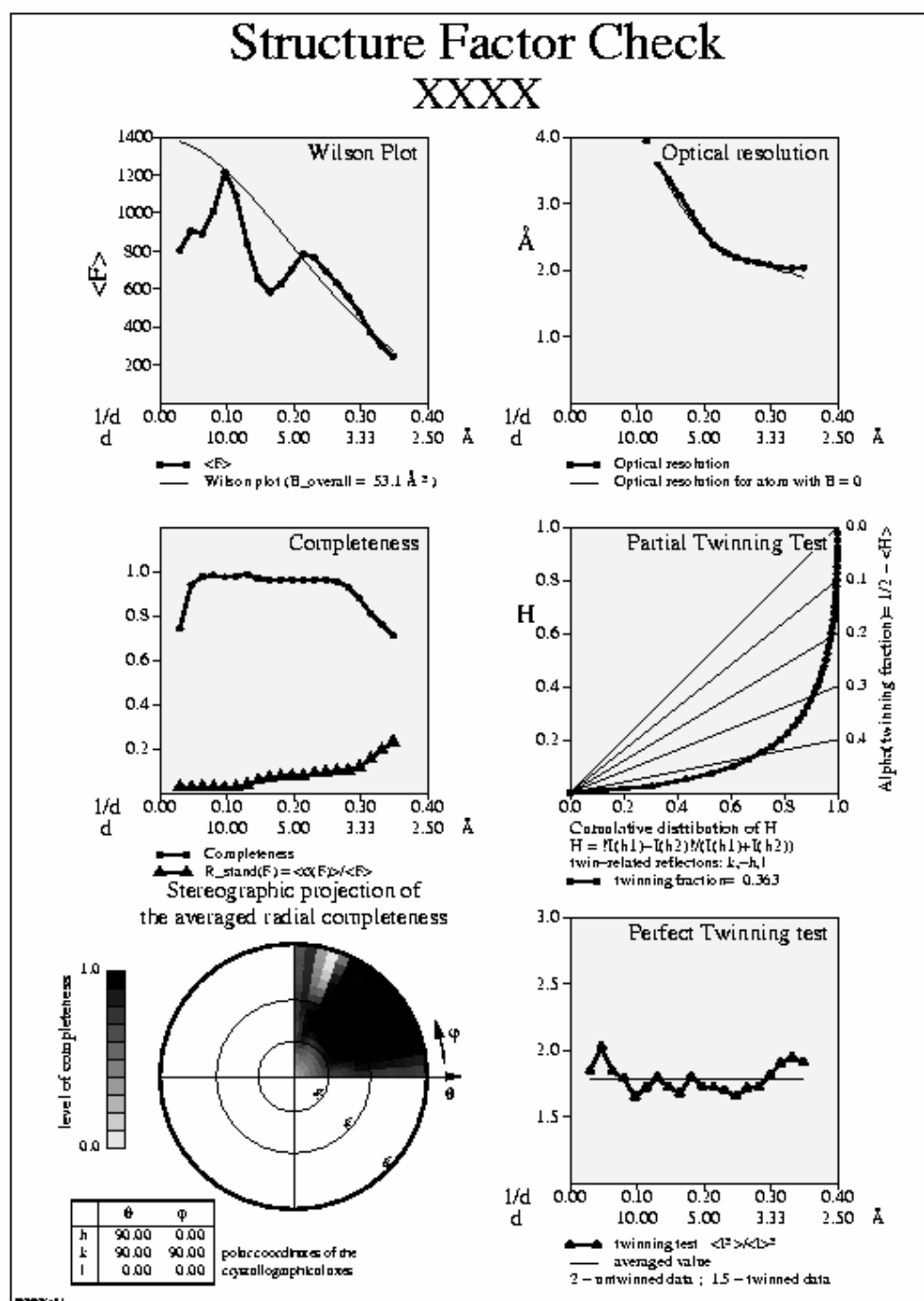


FIGURE 5.9. L-function output of ALS May 2006 d8x5 truncated to 8 - 3.5 Å shown in blue. The red line displays results of L-function on untwinned crystals and upper red curve is the result for perfectly twinned crystals.

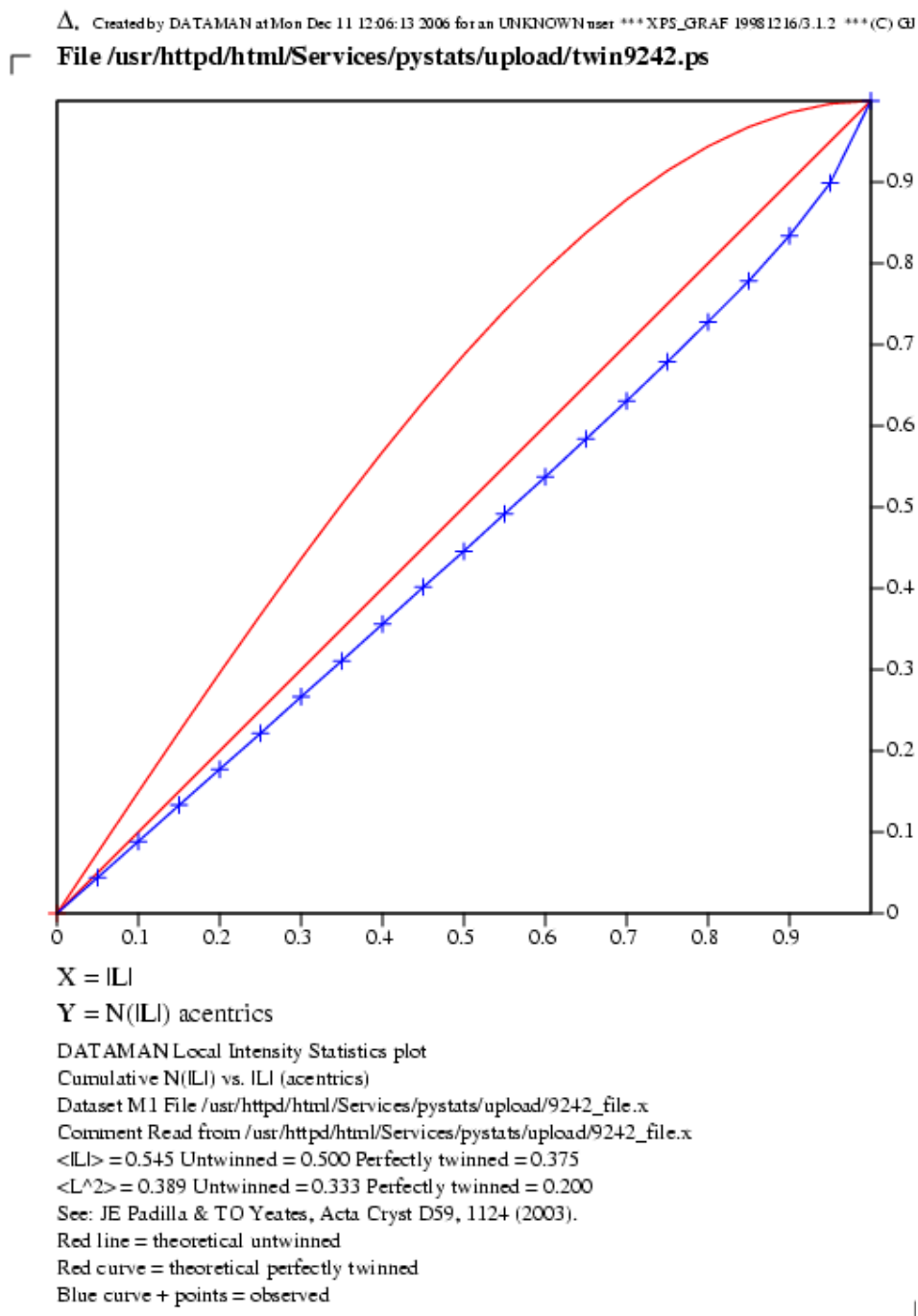


FIGURE 5.10. Using the L-function to analyze proximal reflection intensities of ALS May 2006 d3\_04\_2 data truncated from 8 - 3.5 Å shown in blue. The linear red line displays results of L-function on untwinned crystals and the upper red curve is the result for perfectly twinned crystals.

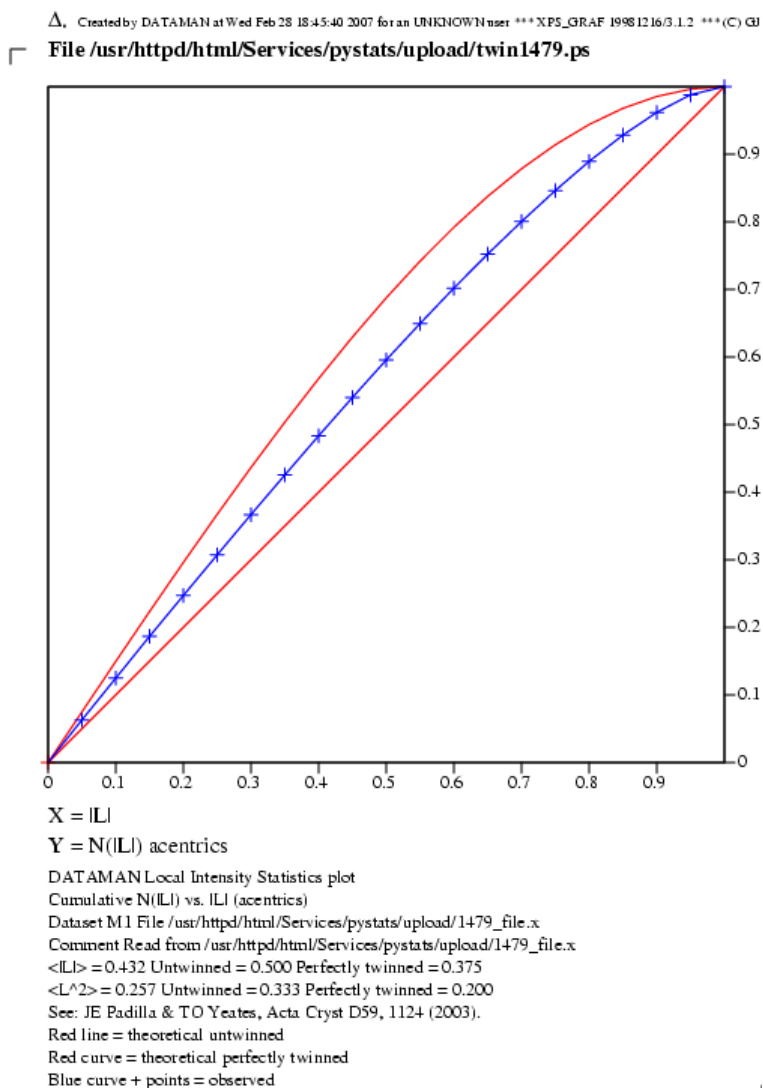




FIGURE 5.11 A. Native Patterson results from the ALS May 2006 d8x5 dataset truncated to 4 Å resolution. These native pattersons were calculated for data processed in P6<sub>2</sub>22. Shown here are the x vs w and the u vs w Patterson maps.

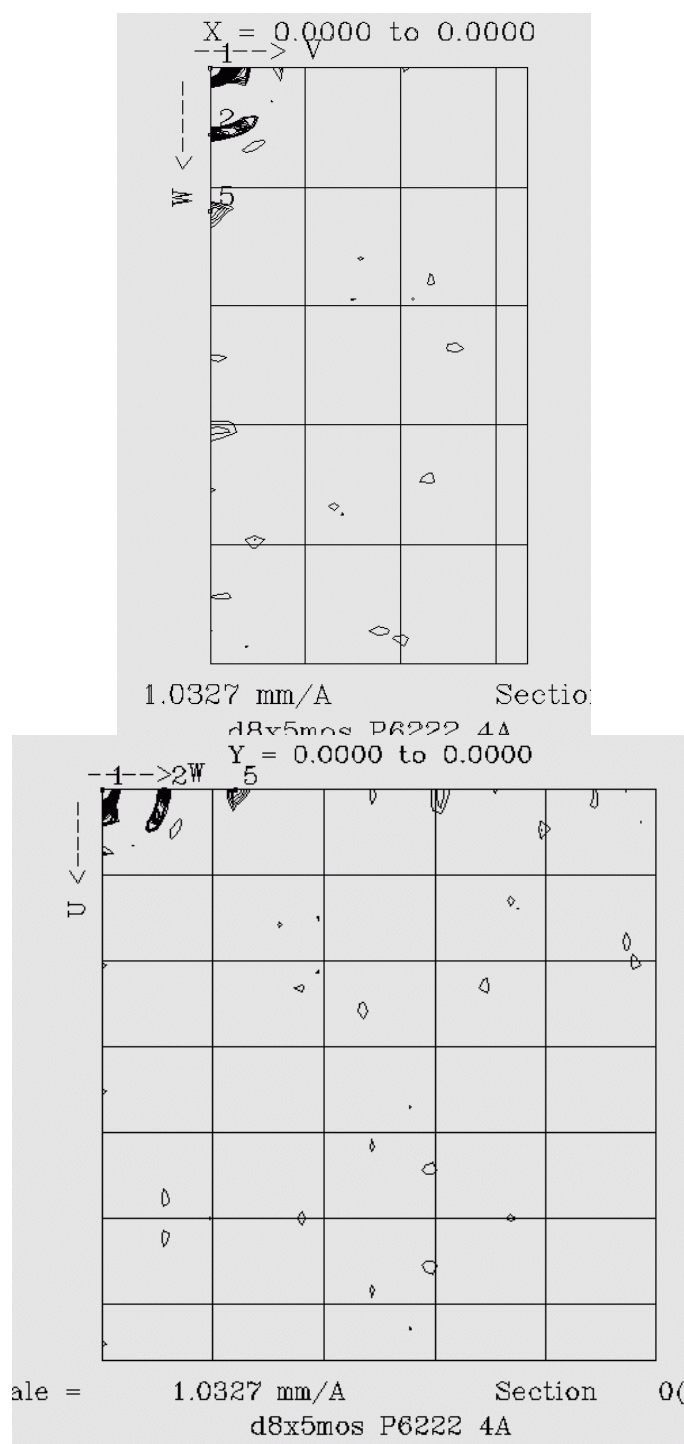


FIGURE 5.11B. Native Patterson results from the ALS May 2006 d8x5 dataset truncated to 4 Å resolution. These native pattersons were calculated for data processed in P6<sub>2</sub>22. Shown here are two u vs v Patterson at Z = 0 and Z = 0.3.

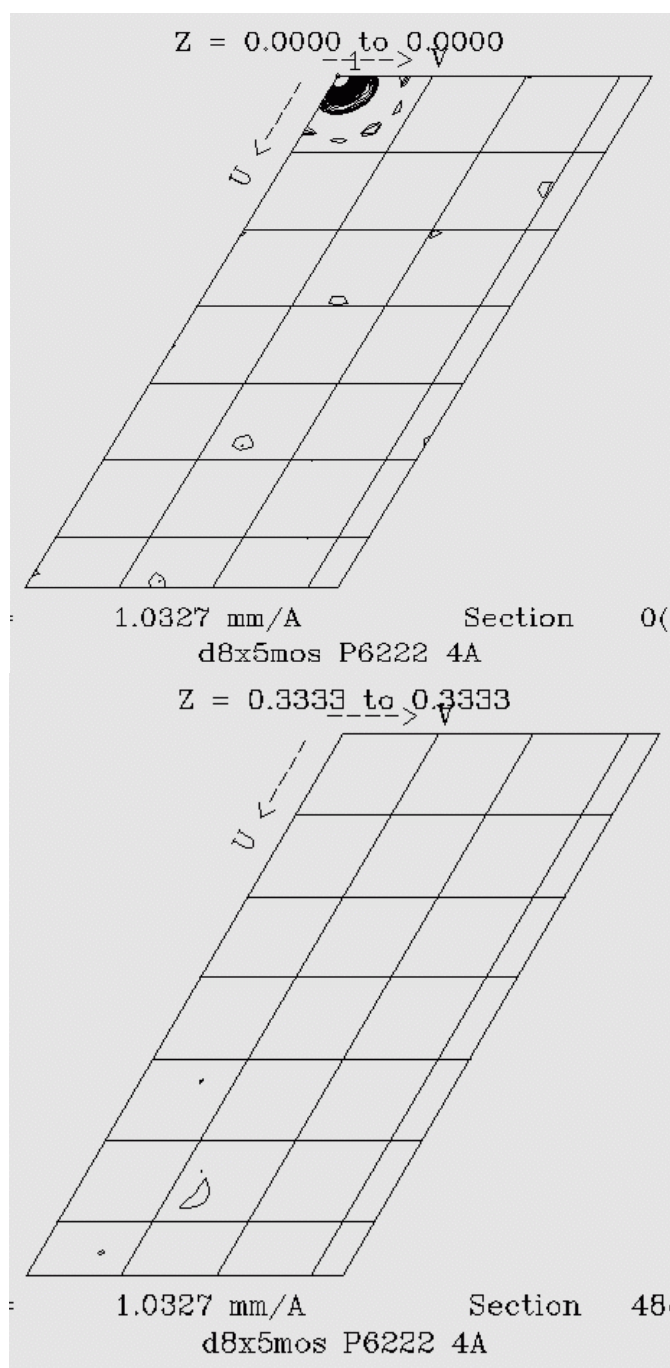


FIGURE 5.12. Native Patterson calculated to 4 Å using ALS May 2006 d3\_04\_2 d\*TREK processed data.

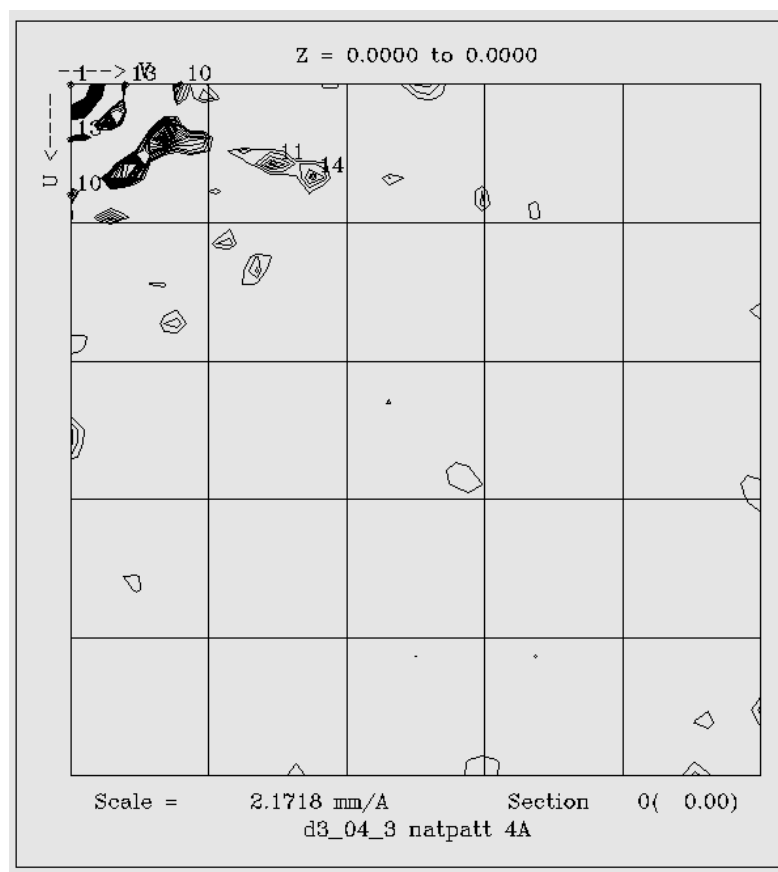


FIGURE 5.13A. Self Rotation function of P6<sub>2</sub>22 MOSFLM processed d8x5 ALS September 2006 data

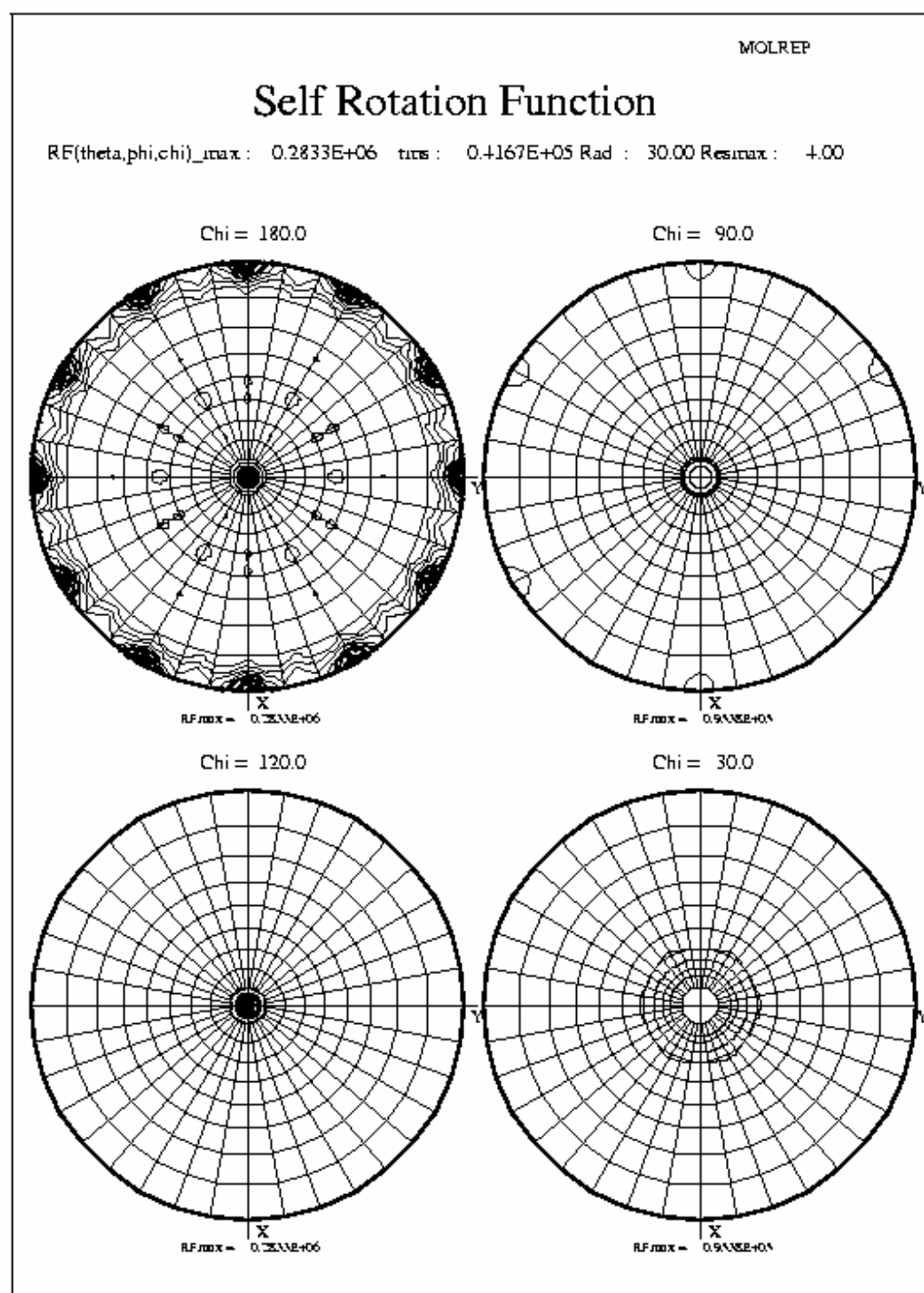


FIGURE 5.13B. Self Rotation function of P3 MOSFLM processed d8x5 ALS September 2006 data

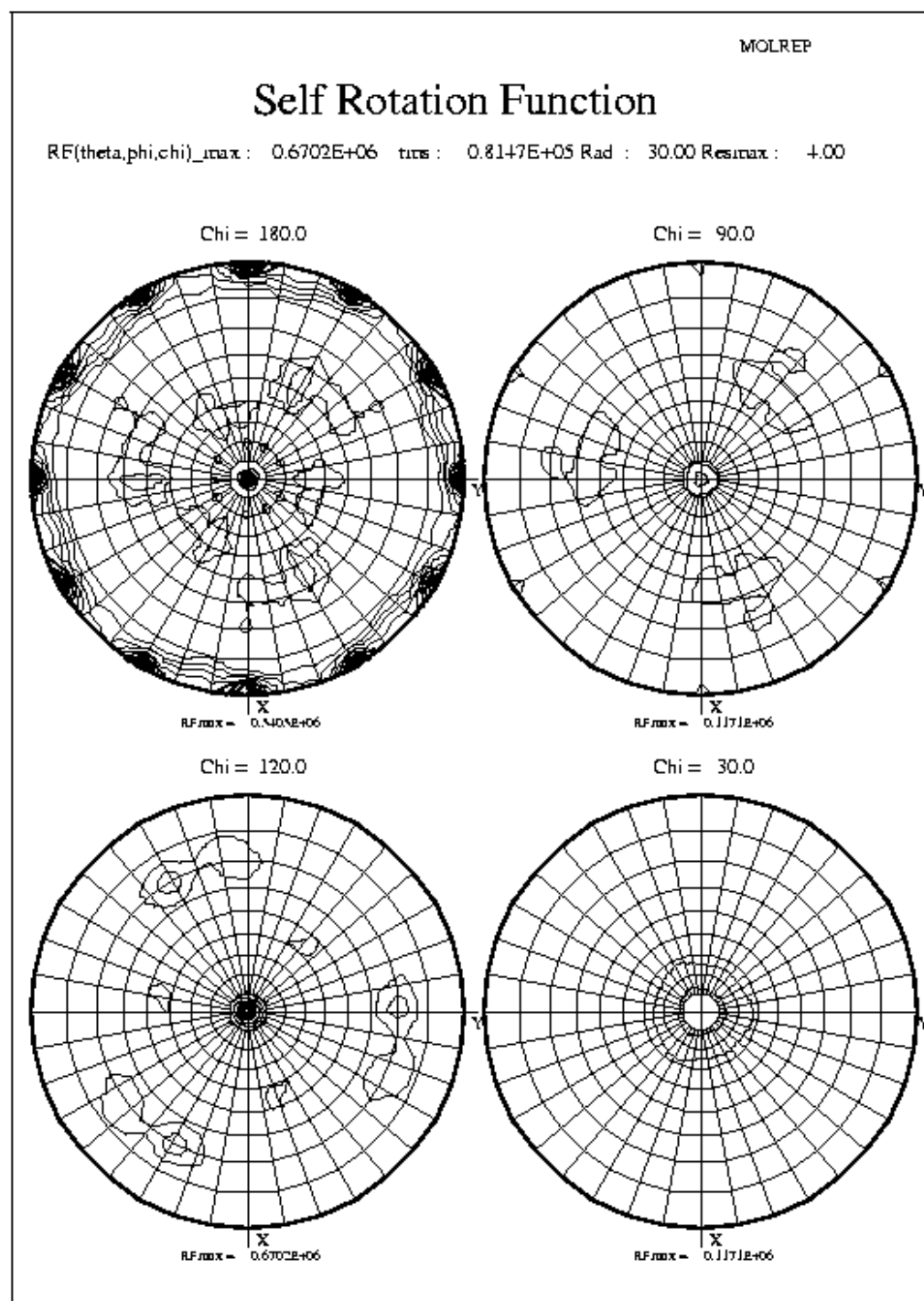


FIGURE 5.14. Self rotation function calculated for P4 d\*TREK processed d3\_04\_2 ALS May 2006

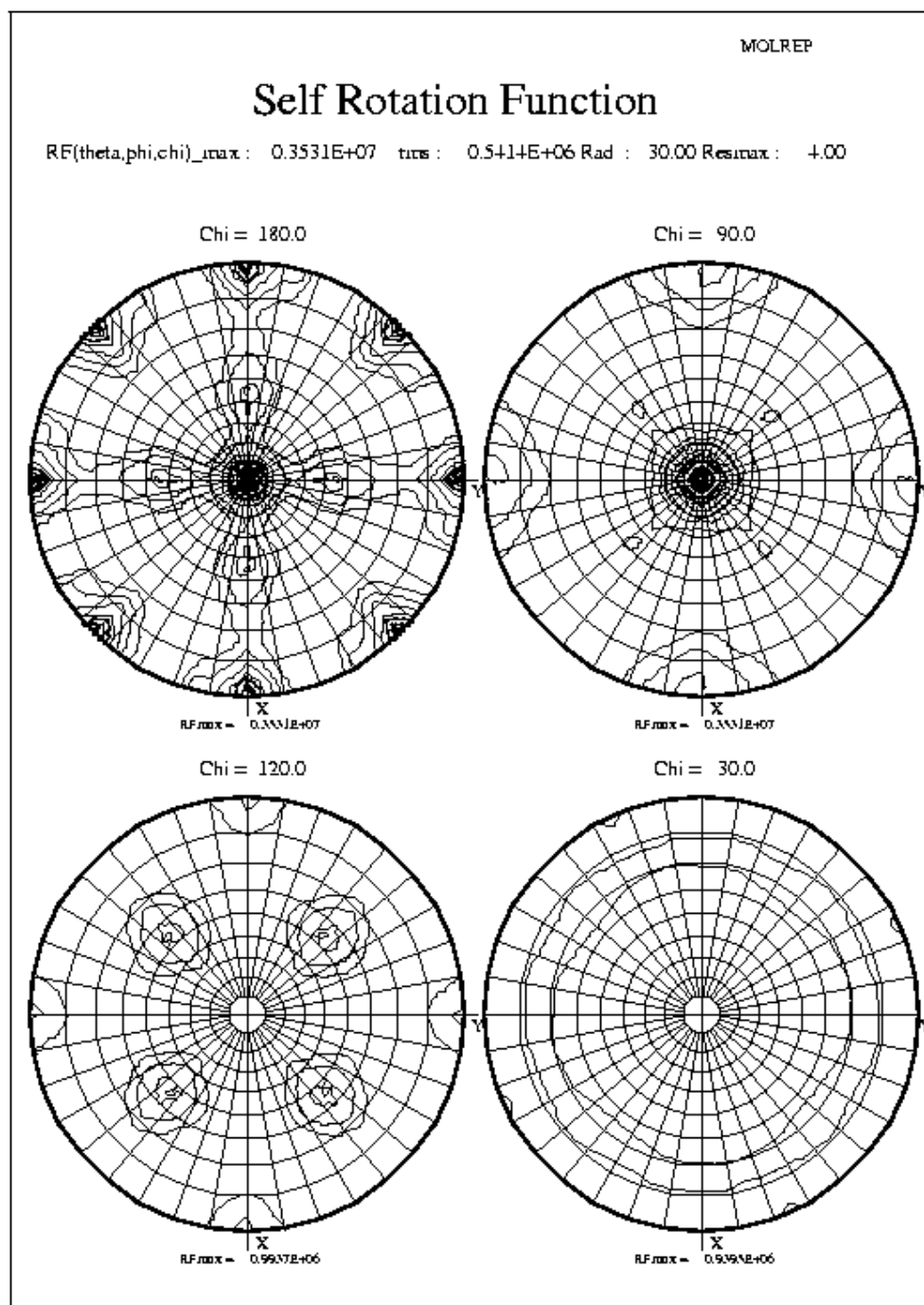
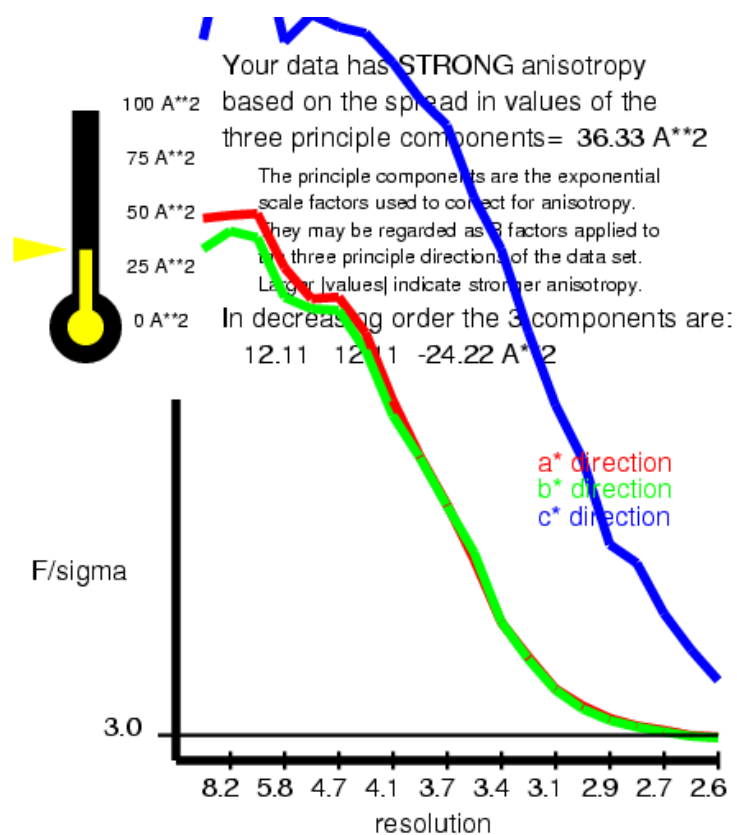


FIGURE 5.15A. Results from the Diffraction Anisotropy Server using d8x5 from ALS May 2006.



The recommended resolution limits along a\*,b\*,c\* are

2.7 Ang 2.7 Ang 2.6 Ang

These are the resolutions at which F/sigma drops below an arbitrary cutoff of 3.0



FIGURE 5.15B. Results from the Diffraction Anisotropy Server using d8x5 from ALS May 2006. Ellipsoidal Data Truncation to remove weakly diffracting spots.

35707 reflections were in the initial data set. 1744 were discarded because they fell outside the specified ellipsoid with dimensions  $1/2.7, 1/2.7, 1/2.6 \text{ \AA}^{-1}$  along  $a^*, b^*, c^*$ , respectively. These discarded reflections had an average  $F/\sigma$  of 3.67.

33963 reflections remain after ellipsoidal truncation. Anisotropic scale factors were then applied to remove anisotropy from the data set. Lastly, an isotropic B of  $-12.58 \text{ \AA}^2$  was applied to restore the magnitude of the high resolution reflections diminished by anisotropic scaling. The following pseudo precession images illustrate the individual steps.

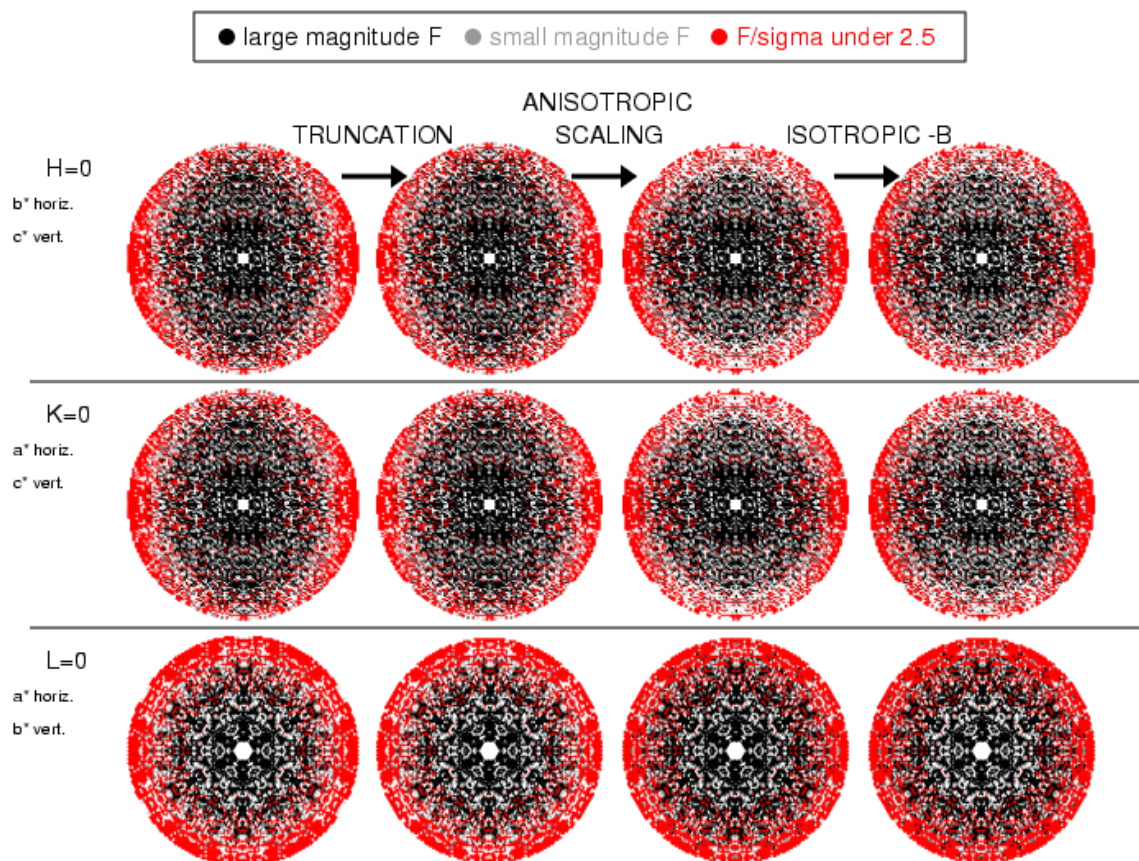




FIGURE 5.16A. Results from the Anisotropy Diffraction server for ALS May 2006 d\*TREK-processed d3\_04\_2 data.

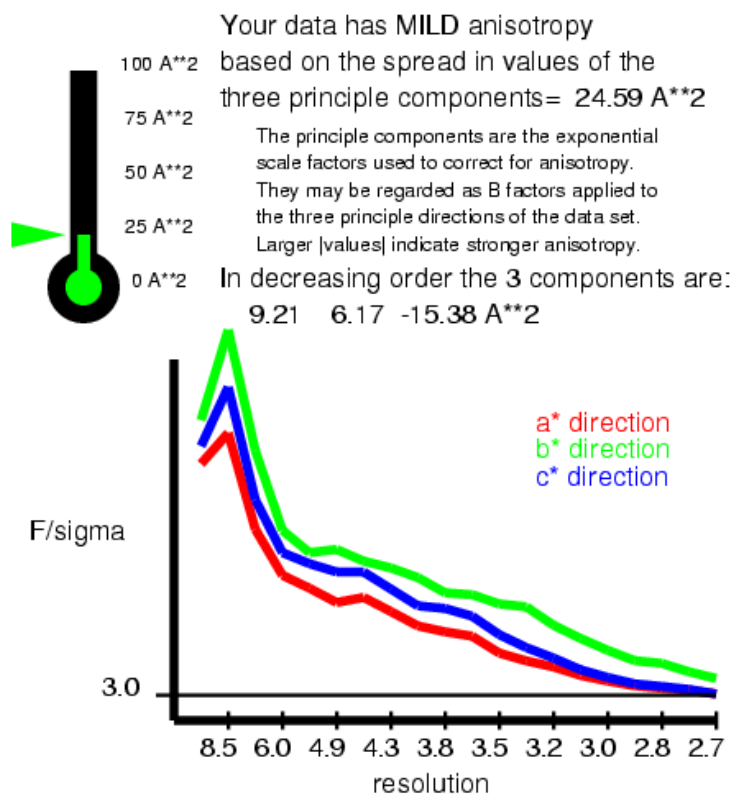


FIGURE 5.16B. Ellipsoidal truncation results from ALS May 2006 d\*TREK-processed d3\_04\_2 data.

171 043 reflections were in the initial data set. 0 were discarded because they fell outside the specified ellipsoid with dimensions  $1/2.7, 1/2.7, 1/2.7 \text{ \AA}^{-1}$  along  $a^*, b^*, c^*$ , respectively. These discarded reflections had an average  $F/\sigma$  of 0.00.

171 043 reflections remain after ellipsoidal truncation. Anisotropic scale factors were then applied to remove anisotropy from the data set. Lastly, an isotropic  $B$  of  $-7.68 \text{ \AA}^2$  was applied to restore the magnitude of the high resolution reflections diminished by anisotropic scaling. The following pseudo precession images illustrate the individual steps.

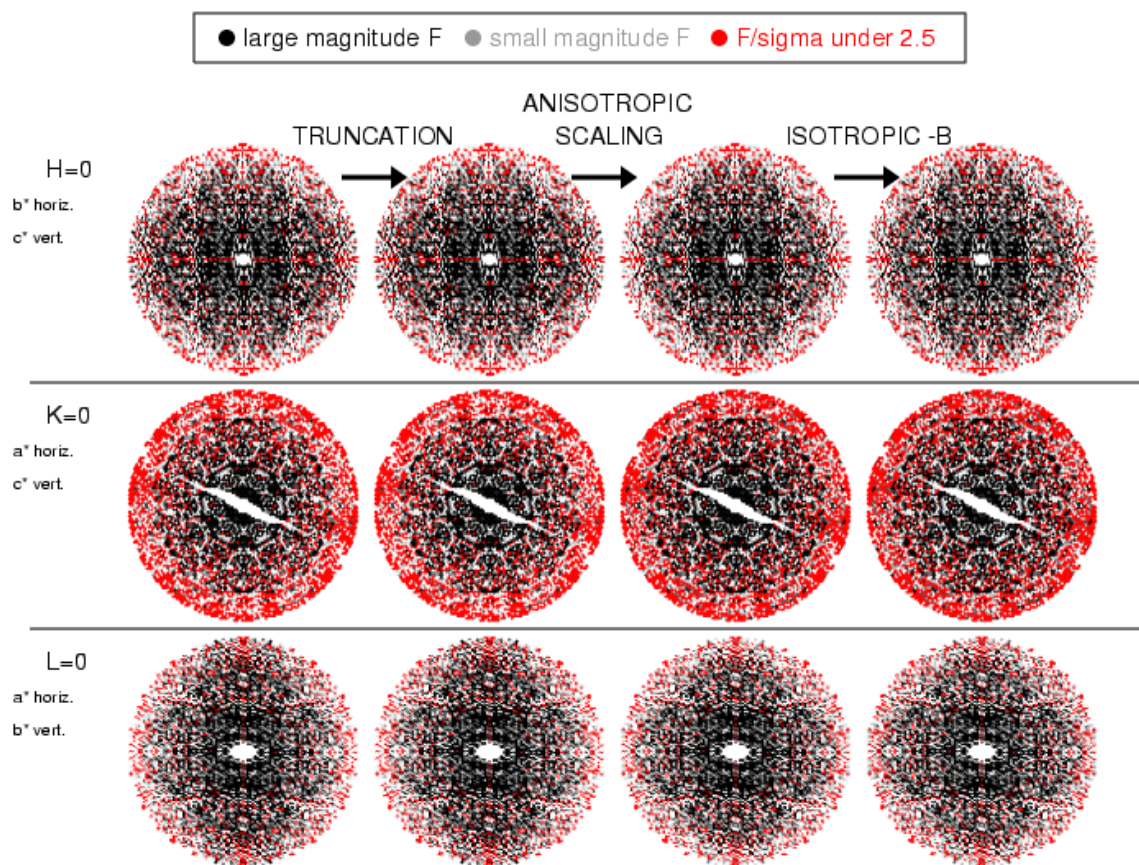


FIGURE 5.17. Location of the BjPutA A310V mutation (pink). A) EcPutA PRODH domain B) TtPRODH

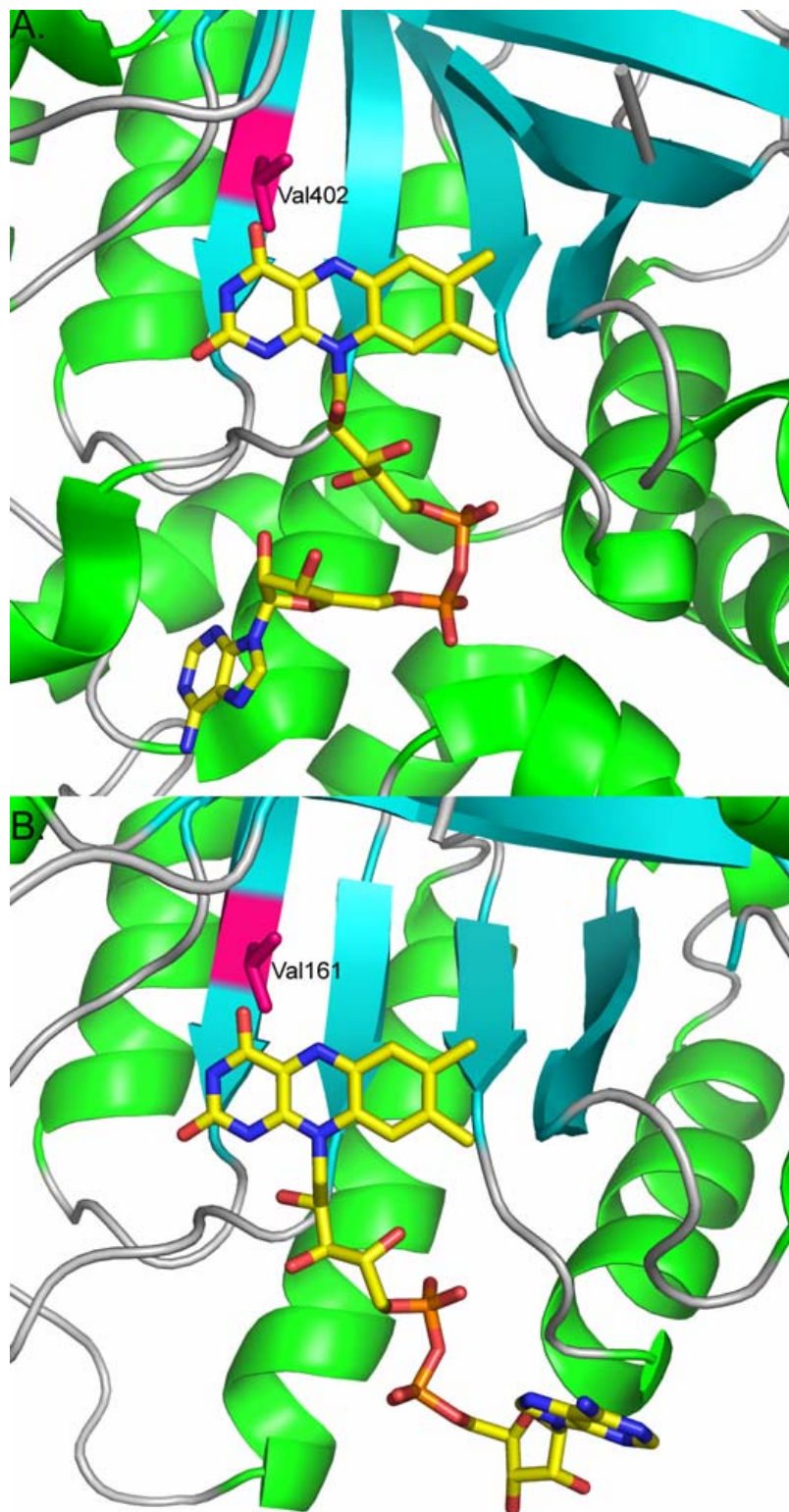
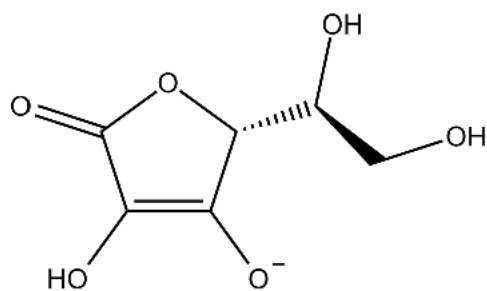
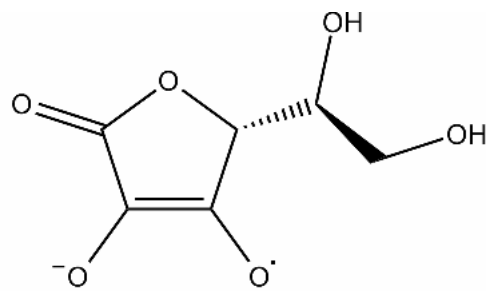


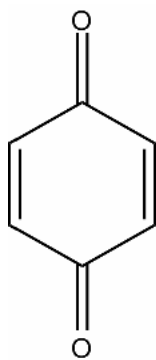
FIGURE 5.18. Radical scavengers A) oxidized ascorbate B) reduced ascorbate and C) oxidized quinone D) reduced quinone.



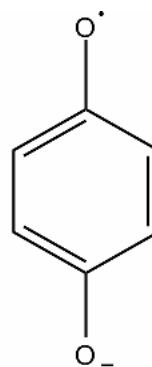
A.



B.



C.



D.

TABLE 5.1. Expected intensity distributions values for normal and twinned crystals (taken from Dauter, 2003).(1)

Cumulative intensity distributions	
Non-centrosymmetric reflections	
Untwinned	${}_1N(z) = 1 - \exp(-z)$
50% twinned	${}_1N(z, 0.5) = 1 - (1 + 2z)\exp(-2z)$
$\alpha$ twinned	${}_1N(z, \alpha) = (\alpha[\exp(-z/\alpha) - 1] - (1 - \alpha)[\exp(-z/(1 - \alpha)) - 1]) / (1 - 2\alpha)$
Centrosymmetric reflections	
Untwinned	$_{-1}N(z) = \text{erf}(z/2)^{1/2}$
50% twinned	$_{-1}N(z, 0.5) = 1 - \exp(-z)$
Cumulative $S(H)$ distributions	
Non-centrosymmetric reflections	$S(H) = H/(1 - 2\alpha)$
Centrosymmetric reflections	$S(H) = \cos^{-1}[H/(2\alpha - 1)/\pi]$

(b) Moments of  $I$  and  $H$ .

	$\langle I^2 \rangle / \langle I \rangle^2$	$\langle F \rangle^2 / \langle I \rangle$ (Wilson ratio)	$\langle H \rangle$	$\langle H^2 \rangle$
Non-centrosymmetric				
Untwinned	2.0	0.785 ( $= \pi/4$ )	$\frac{1}{2} - \alpha$	$(1 - 2\alpha)^2/3$
50% twinned	1.5	0.885	0.5	0.333
Centrosymmetric				
Untwinned	3.0	0.637 ( $= 2/\pi$ )	$2(1 - 2\alpha)/\pi$	$(1 - 2\alpha)^2/2$
50% twinned	2.0	0.785	0.637	0.5
			0.0	0.0

(c) Moments of  $L$  and cumulative  $N(|L|)$  distributions.

	$\langle  L  \rangle$	$\langle L^2 \rangle$	$N(L)$	$N( L )$
Non-centrosymmetric				
Untwinned	1/2	1/3	$(L + 1)/2$	$ L $
Twinned	3/8	1/5	$(L + 1)^2(2 - L)/4$	$ L (3 - L^2)/2$
Centrosymmetric untwinned				
	$2/\pi$	1/2	$\arccos(-L)/\pi$	$(2/\pi)\arcsin( L )$

TABLE 5.2. Merohedral Twinning operations for various point groups.

True Point Group	Twin Operation	<i>hkl</i> related to
3	2 along a,b 2 along a*,b* 2 along c	<i>h</i> , - <i>h</i> - <i>k</i> , - <i>l</i> <i>h</i> + <i>k</i> , - <i>k</i> , - <i>l</i> - <i>h</i> , - <i>k</i> , <i>l</i>
4	2 along a,b,a*,b*	<i>h</i> , - <i>k</i> , - <i>l</i>
6	2 along a,, a*,b*	<i>h</i> , - <i>h</i> - <i>k</i> , - <i>l</i>
321	2 along a*,b*,c	- <i>h</i> , - <i>k</i> , <i>l</i>
312	2 along a,b,c	- <i>h</i> , - <i>k</i> , <i>l</i>
23	4 along a,b,c	<i>k</i> , - <i>h</i> , <i>l</i>

TABLE 5.3. Data collection statistics processed with d\*TREK sets used in ascorbate soaks and statistics of merging of initial data from hexagonal bipyramids. The data set labels correspond to the following:

- 1) b12\_05 – 2.7 Å
- 2) b2\_04 – 2.55 Å
- 3) b7\_05 – 2.6 Å
- 4) b7\_03 – 2.6 Å
- 5) b7\_02 – 2.6 Å
- 6) b2\_03 – 2.9 Å
- 7) b3\_04 – 2.8Å
- 8) b7\_03 – 5-2.5Å

**7 data sets**

	<b>R<sub>merge</sub></b>	<b>R<sub>merge</sub> low</b>	<b>R<sub>merge</sub> high</b>	<b>% Complete</b>	<b>Multiplicity</b>
1234567	0.106	0.073	0.372	91.9	3.82
1235678	0.105	0.072	0.072	91.9	3.83

**6 data sets**

	<b>R<sub>merge</sub></b>	<b>R<sub>merge</sub> low</b>	<b>R<sub>merge</sub> high</b>	<b>% Complete</b>	<b>Multiplicity</b>
123456	0.100	0.068	0.367	90.0	3.43
123567	0.101	0.063	0.373	90.8	3.28
123568	0.100	0.068	0.371	90.0	3.44

**5 data sets**

	<b>R<sub>merge</sub></b>	<b>R<sub>merge</sub> low</b>	<b>R<sub>merge</sub> high</b>	<b>% Complete</b>	<b>Multiplicity</b>
12356	0.095	0.059	0.373	88.8	2.88
12456	0.096	0.065	0.348	85.6	2.96
12567	0.098	0.062	0.357	86.8	2.80
12568	0.095	0.065	0.350	85.6	2.97
12578	0.101	0.101	0.354	82.6	3.13

**4 data sets**

	<b>R<sub>merge</sub></b>	<b>R<sub>merge</sub> low</b>	<b>R<sub>merge</sub> high</b>	<b>% Complete</b>	<b>Multiplicity</b>
1256	0.089	0.053	0.350	83.9	2.39
1257	0.096	0.096	0.353	80.5	2.54
1258	0.093	0.093	0.348	77.1	2.80

TABLE 5.4. CNS simulated annealing refinements of 104nofad.pdb P5CDH (542-992) or PutA (2-992) against the first 5° of various data sets. The data set labels correspond to the following:

- 1) b12\_05 – 2.7 Å
- 2) b2\_04 – 2.55 Å
- 3) b7\_05 – 2.6 Å
- 4) b7\_03 – 2.6 Å
- 5) b7\_02 – 2.6 Å
- 6) b2\_03 – 2.9 Å
- 7) b3\_04 – 2.8Å
- 8) b7\_03 – 5-2.5Å

<b>P5CDH refine.pdb</b>	<b>R</b>	<b>R<sub>free</sub></b>
dm1234567	0.4693	0.5174
dm123456	0.4662	0.513
dm1235678	0.4688	0.5215
dm123567	0.464	0.5227
dm123568	0.4667	0.5139
dm12356	0.4661	0.5158
dm12456	0.4693	0.5206
dm12567	0.4651	0.5232
dm12568	0.4657	0.5109
dm12578	0.4661	0.5304
dmb12_05	0.4651	0.516
dmb2_04	0.4992	0.5418
dmb7_02	0.4943	0.531
dmb7_03	0.4867	0.5165
dmb7_05	0.4891	0.5295

<b>PutA refine.pdb</b>	<b>R</b>	<b>R<sub>free</sub></b>
dm123456b	0.3999	0.5012
dm1234567b	0.3974	0.4998
dm12356b	0.3963	0.4934
dm123567b	0.3957	0.4879
dm1235678b	0.3991	0.4883
dm123568b	0.3944	0.4951
dm12456b	0.4055	0.5096
dm12567b	0.3908	0.494
dm12568b	0.3989	0.5182
dm12578b	0.4003	0.5154
dmb12_05b	0.3935	0.4875
dmb2_04b	0.4239	0.4967
dmb7_02b	0.4272	0.5164
dmb7_03b	0.4221	0.4942
dmb7_05b	0.426	0.5125



TABLE 5.5. Spacegroup investigation. Using model d8x5\_1\_001\_refmac12.pdb, CNS simulated annealing refinements after 3 rounds of rigid body refinements using data set d8x5 processed with MOSFLM. Percent of reflections utilized for this refinement is indicated by % reflections and number of molecules in the asymmetric unit are listed as mol/ASU.

<b>Spacegroup</b>	<b>R</b>	<b>R<sub>free</sub></b>	<b>% reflections</b>	<b>mol/ASU</b>
P6 <sub>2</sub> 22	0.3748	0.4446	93.6	1
P6 <sub>2</sub>	0.3665	0.4165	99.0	2
P3 <sub>2</sub> 21	0.3695	0.4233	99.0	2
P3 <sub>2</sub>	0.3652	0.4232	97.6	4

TABLE 5.6. Utilizing CNS least squares merohedral twinning refinements for various space groups and twinning fractions with ALS May 2006 d8x5 data. Note,  $P3_2$  has three twinning operators, the results for only one is shown in this table. The other two  $P3_2$  twinning operators are the same operators used for  $P6_2$  and  $P3_221$ ,  $h, -h-k, -l$  and  $-h, -k, l$ , respectively.

Spacegroup	twin operator	twin fraction	R	R <sub>free</sub>
$P6_2$	$h, -h-k, -l$	0.00	0.3445	0.4337
		0.25	0.3128	0.4228
		0.35	0.3039	0.4134
		0.45	0.2987	0.4061
		0.50	0.2979	0.4060
$P3_221$	$-h, -k, l$	0.00	0.3482	0.4384
		0.25	0.3164	0.4203
		0.35	0.3061	0.4199
		0.45	0.2996	0.4147
		0.50	0.2960	0.4127
$P3_2$	$h+k, -k, -l$	0.00	0.3360	0.4371
		0.25	0.3023	0.4181
		0.35	0.2919	0.4142
		0.45	0.2859	0.4114
		0.50	0.2859	0.4065

## APPENDIX 5.1. Data Set Summary of BjPutA

### Advanced Photon Source 19-BM

- MARCH 17-19th, 2004 (BjPutA native and HA soaks)

### Advanced Photon Source 19ID

- NOVEMBER 14-16th, 2003 (BjPutA I90, w1-47)
- JUNE 15-16th, 2003
- AUGUST 11-12, 2004 (BjPutA SMPProaps1, SMPProAPS6)

### Advanced Light Source

- DECEMBER 7-8th, 2004 (BjPutA SeMet BH4, Pro+dithio)
- JANUARY 22-23rd, 2005 (BjPutA SeMet)
- AUGUST 27-28th, 2005 (A310V Pro)
- OCTOBER 11-12th, 2006 (A310V crosslink, A310V THFA & A310V oxidized)
- MAY 12-13th 2006 (ascorbate hexagonal P6222, ascorbate diamond P422)
- SEPTEMBER 11-12th (hexagonal P6222 oxidized and dithionite/proline reduced)

## APPENDIX 5.2. Indexing from ALS May 2006 d8x5 utilizing d\*TREK.

Least-squares fit of reduced primitive cell to 44 lattice characters  
sorted on decreasing (highest to lowest) symmetry.  
Only solutions with residuals <= 55.\_\_\_\_0 are listed.

Soln num	LeastSq residual	Spgrp num*	Cent type	Bravais type Cell volume	a alpha	b beta	c gamma
1	47.215	195	P	cubic 4057935	159.503 90.000	159.503 90.000	159.503 90.000
2	49.668	197	I	cubic 4632563	166.702 90.000	166.702 90.000	166.702 90.000
4	37.499	146	R rhomb/hexagonal	14155210	158.662 90.000	158.662 90.000	649.292 120.000
5	0.156	143	P trig/hexagonal	3372911	145.024 90.000	145.024 90.000	185.181 120.000
6	35.936	79	I tetragonal	4091247	186.601 90.000	186.601 90.000	117.497 90.000
7	41.941	75	P tetragonal	3891714	144.968 90.000	144.968 90.000	185.181 90.000
8	34.273	23	I orthorhombic	10073163	144.907 90.000	167.466 90.000	415.096 90.000
9	0.094	21	C orthorhombic	6746040	144.907 90.000	251.398 90.000	185.181 90.000
10	18.868	22	F orthorhombic	7979092	91.719 90.000	242.443 90.000	358.825 90.000
11	41.941	16	P orthorhombic	3891712	144.907 90.000	145.029 90.000	185.181 90.000
12	0.047	5	C monoclinic	6751327	144.964 90.000	251.496 128.091	235.290 90.000
13	0.123	3	P monoclinic	3373019	144.907 90.000	185.181 119.920	145.029 90.000
14	0.000	1	P triclinic	3373017	144.907 89.964	145.029 89.939	185.181 60.080

\*Suggested spacegroup number until systematic absences are examined.

To view least-squares fits to other lattices,  
enter a new residual between 55 and 100 at the following prompt.

### APPENDIX 5.3. Indexing from ALS May 2006 d3\_04\_2 utilizing d\*TREK.

Least-squares fit of reduced primitive cell to 44 lattice characters  
sorted on decreasing (highest to lowest) symmetry.  
Only solutions with residuals <= 3.0 are listed.

```
=====
```

Soln	LeastSq	Spgrp	Cent	Bravais type	a	b	c
num	residual	num*	type	Cell volume	alpha	beta	gamma
=====							
7	1.875	75	P	tetragonal	138.601	138.601	266.580
				5121070	90.000	90.000	90.000
9	1.870	21	C	orthorhombic	195.762	196.261	266.580
				10242108	90.000	90.000	90.000
11	1.859	16	P	orthorhombic	138.135	139.065	266.580
				5120955	90.000	90.000	90.000
12	0.513	5	C	monoclinic	196.261	195.762	266.580
				10240716	90.000	90.945	90.000
13	0.368	3	P	monoclinic	139.065	138.135	266.580
				5120088	90.000	91.055	90.000
14	0.000	1	P	triclinic	138.135	139.065	266.580
				5120011	88.945	89.720	89.854

```
=====
```

\*Suggested spacegroup number until systematic absences are examined.

To view least-squares fits to other lattices,  
enter a new residual between 15 and 100 at the following prompt.

# APPENDIX 5.4. Data processing statistics using various spacegroups for ALS May 2006 d8x5 processed with MOSFLM.

P6222

=====

Summary data for Project: ProDithio Crystal: d8x5\_1 Dataset: d8x5\_1

	Overall	OuterShell
Low resolution limit	47.56	2.74
High resolution limit	2.60	2.60
Rmerge	0.076	0.698
Rmeas (within I+/I-)	0.080	0.733
Rmeas (all I+ & I-)	0.080	0.733
Fractional partial bias	-0.024	-0.040
Total number of observations	375060	53088
Total number unique	36104	5187
Mean(I)/sd(I)	20.0	2.3
Completeness	99.9	100.0
Multiplicity	10.4	10.2

=====

P62

=====

Summary data for Project: ProDithio Crystal: d8x5\_1 Dataset: d8x5\_1

	Overall	OuterShell
Low resolution limit	47.56	2.74
High resolution limit	2.60	2.60
Rmerge	0.074	0.671
Rmeas (within I+/I-)	0.081	0.741
Rmeas (all I+ & I-)	0.081	0.741
Fractional partial bias	-0.021	-0.043
Total number of observations	375101	53093
Total number unique	67882	9940
Mean(I)/sd(I)	14.5	1.6
Completeness	99.8	100.0
Multiplicity	5.5	5.3

=====

# APPENDIX 5.4. Data processing statistics for ALS May 2006 d8x5 processed with MOSFLM in various spacegroups (continued).

P32

=====

Summary data for Project: ProDithio Crystal: d8x5\_1 Dataset: d8x5\_1

	Overall	OuterShell
Low resolution limit	47.56	2.74
High resolution limit	2.60	2.60
Rmerge	0.067	0.581
Rmeas (within I+/I-)	0.080	0.693
Rmeas (all I+ & I-)	0.080	0.693
Fractional partial bias	-0.020	-0.039
Total number of observations	375179	53098
Total number unique	132057	19381
Mean(I)/sd(I)	10.4	1.2
Completeness	98.1	98.2
Multiplicity	2.8	2.7

=====

P3221

=====

Summary data for Project: ProDithio Crystal: d8x5\_1 Dataset: d8x5\_1

	Overall	OuterShell
Low resolution limit	47.56	2.74
High resolution limit	2.60	2.60
Rmerge	0.073	0.668
Rmeas (within I+/I-)	0.081	0.738
Rmeas (all I+ & I-)	0.081	0.738
Fractional partial bias	-0.021	-0.049
Total number of observations	375096	53093
Total number unique	69849	10143
Mean(I)/sd(I)	14.3	1.6
Completeness	99.8	100.0
Multiplicity	5.4	5.2

=====

## APPENDIX 5.4. C222 d\*TREK processing of ALS September 2006 d8x5 data.

Rmerge vs Resolution

Resolution range	Average counts	Num rejs	Num mults	I/sig unavg	I/sig avg	Rducd ChiSq	Model Eadd*	Rmerge shell	Rmerge cumul
57.03 - 5.38	13870	409	10241	13.9	26.9	0.64	0.06	0.028	0.028
5.38 - 4.27	8327	292	10279	8.8	17.9	0.64	0.08	0.041	0.033
4.27 - 3.73	5625	359	10280	6.1	12.6	0.74	0.11	0.057	0.038
3.73 - 3.39	3226	329	10311	4.4	8.9	0.84	0.15	0.081	0.042
3.39 - 3.15	1440	287	10384	2.7	5.5	0.97	0.21	0.129	0.046
3.15 - 2.96	778	234	10497	2.0	4.1	1.03	0.26	0.172	0.049
2.96 - 2.82	422	292	10507	1.6	3.0	1.13	0.32	0.246	0.052
2.82 - 2.69	284	240	10524	1.3	2.3	1.21	0.36	0.315	0.055
2.69 - 2.59	185	372	10584	1.1	1.8	1.35	0.42	0.425	0.057
2.59 - 2.50	150	418	10517	1.0	1.5	1.41	0.48	0.512	0.059
57.03 - 2.50	3451	3232	104124	4.3	8.5	0.99	0.10	0.059	0.059

I/sig unavg is the mean I/sig for the unaveraged reflections in the input file.

I/sig avg is the mean I/sig for the unique reflections in the output file.

\* When EMul == 1.41

### Summary of data collection statistics

Spacegroup	C222		
Unit cell dimensions	144.87	251.36	185.01
	90.00	90.00	90.00
Resolution range	57.03 - 2.50		(2.59 - 2.50)
Total number of reflections	427543		
Number of unique reflections	113474		
Average redundancy	3.77		(3.65)
% completeness	97.6		(98.7)
Rmerge	0.059		(0.512)
Reduced ChiSquared	0.99		(1.41)
Output <I/sigI>	8.5		(1.5)

Note: Values in ( ) are for the last resolution shell



## APPENDIX 5.5. Processing statistics of ALS May 2006 d3\_04\_2 data in various spacegroups utilizing d\*TREK.

### Summary of data collection statistics

```
-----
Spacegroup                P43
Unit cell dimensions      138.03   138.03   267.04
                          90.00   90.00   90.00
Resolution range         46.01 - 2.80   (2.90 - 2.80)
Total number of reflections 209861
Number of unique reflections 107065
Average redundancy        1.96           (1.55)
% completeness            87.6           (70.3)
Rmerge                    0.092          (0.241)
Reduced ChiSquared        0.97           (0.96)
Output <I/sigI>           6.7            (2.4)
-----
```

Note: Values in ( ) are for the last resolution shell.

### Rmerge vs Resolution

```
-----
Resolution   Average   Num   Num   I/sig   I/sig   Rducd   Model   Rmerge   Rmerge
  range      counts    rejs  mults unavg  avg    ChiSq  Eadd*   shell   cumul
-----
46.01 - 6.03   1234    597  11293   8.7   14.7   0.89   0.09   0.058   0.058
6.03 - 4.79    705    233  10288   4.7    6.9   1.01   0.17   0.099   0.070
4.79 - 4.18    965    219   9809   4.5    6.3   1.03   0.18   0.101   0.078
4.18 - 3.80    752    167   9539   4.1    5.5   1.06   0.20   0.108   0.083
3.80 - 3.53    569    223   8552   4.2    5.4   1.02   0.20   0.107   0.085
3.53 - 3.32    419     65   7113   4.2    5.3   0.93   0.20   0.107   0.086
3.32 - 3.15    275     35   6040   3.4    4.3   0.92   0.22   0.131   0.087
3.15 - 3.02    192     14   5525   2.7    3.4   0.97   0.27   0.171   0.089
3.02 - 2.90    135     18   5049   2.2    2.7   0.98   0.32   0.213   0.090
2.90 - 2.80    108     15   4739   1.9    2.4   0.96   0.34   0.241   0.092
-----
46.01 - 2.80    649   1586  77947   4.6    6.7   0.97   0.17   0.092   0.092
-----
```

I/sig unavg is the mean I/sig for the unaveraged reflections in the input file.

I/sig avg is the mean I/sig for the unique reflections in the output file.

\* When EMul == 2.18

# APPENDIX 5.5 (continued). Processing statistics of ALS May 2006 d3\_04\_2 data in various spacegroups utilizing d\*TREK.

## Summary of data collection statistics

Spacegroup	P422		
Unit cell dimensions	138.17	138.17	267.30
	90.00	90.00	90.00
Resolution range	46.06 - 2.80	(2.90 - 2.80)	
Total number of reflections	210980		
Number of unique reflections	59993		
Average redundancy	3.52	(2.70)	
% completeness	93.0	(78.0)	
Rmerge	0.111	(0.296)	
Reduced ChiSquared	0.92	(1.01)	
Output <I/sigI>	8.0	(2.9)	

Note: Values in ( ) are for the last resolution shell.

## Rmerge vs Resolution

Resolution range	Average counts	Num rejs	Num mults	I/sig unavg	I/sig avg	Rducd ChiSq	Model Eadd*	Rmerge shell	Rmerge cumul
46.06 - 6.03	1220	523	6736	7.2	16.4	0.80	0.10	0.070	0.070
6.03 - 4.79	707	283	6482	4.5	8.9	0.90	0.17	0.108	0.082
4.79 - 4.18	964	207	6393	4.3	8.0	0.97	0.18	0.116	0.091
4.18 - 3.80	749	184	6378	3.8	6.7	0.96	0.21	0.128	0.097
3.80 - 3.53	564	232	6111	3.8	6.4	0.93	0.20	0.129	0.100
3.53 - 3.32	416	63	5713	3.8	6.2	0.91	0.20	0.135	0.103
3.32 - 3.15	270	32	5185	3.1	4.9	0.92	0.24	0.169	0.105
3.15 - 3.02	189	32	4815	2.7	4.3	1.05	0.25	0.211	0.107
3.02 - 2.90	133	24	4508	2.2	3.4	1.01	0.30	0.259	0.109
2.90 - 2.80	106	16	4260	1.9	2.9	1.01	0.32	0.296	0.111
46.06 - 2.80	644	1596	56581	4.2	8.0	0.92	0.17	0.111	0.111

I/sig unavg is the mean I/sig for the unaveraged reflections in the input file.

I/sig avg is the mean I/sig for the unique reflections in the output file.

\* When EMul == 2.50

## VITA

Tommi Anna White is the daughter of Calvin and Margaret White and grew up in St. Peters, Missouri. She attended University of Missouri-Columbia as an undergraduate and graduated with a Bachelors of Science in Biochemistry in December of 2000. After employment conducting research at both Pharmacia and at University of Missouri-Columbia, she was accepted into the University of Missouri-Columbia Ph.D. program in Biochemistry. Tommi joined Jack Tanner's group to pursue crystallographic studies of proline catabolic enzymes. She completed her Ph.D. in Biochemistry in April 2007. In July 2007, Tommi will start her post-doctoral fellowship at the National Cancer Institute under Jacqueline Milne, studying pyruvate dehydrogenase complex using cryo-electron microscopy and electron tomography.